Charles University

Faculty of Science

Study program: Developmental and Cell Biology

Mgr. Michal Dibus

Identification of novel substrates of PKN3 kinase and characterization of the role of phosphorylation in the regulation of Rho GAP activity

Identifikace nových substrátů kinázy PKN3 a charakterizace úlohy fosforylace v regulaci aktivity Rho GAP proteinů

Doctoral thesis

Supervisor: doc. RNDr. Daniel Rösel, PhD.

Advisor: doc. RNDr. Jan Brábek, PhD.

Prague, 2021

Prohlášení:

Prohlašuji, že jsem závěrečnou práci zpracoval samostatně a že jsem uvedl všechny použité informační zdroje a literaturu. Tato práce ani její podstatná část nebyla předložena k získání jiného nebo stejného akademického titulu.

V Praze, 4. 3. 2021

Poďakovanie

Na tomto mieste by som rád poďakoval všetkým, ktorí sa zaslúžili o vznik tejto práce. V prvom rade by som chcel poďakovať doc. RNDr. Danielovi Röselovi, Ph.D. a doc. RNDr. Janovi Brábkovi, Ph.D, za odborné vedenie a diskusie vedecké i nevedecké, za veľkú voľnosť pri riešení projektov, ktorá ma (snáď) naučila kriticky myslieť a plánovať viac ako jeden pokus dopredu, za prejavenú dôveru a férový prístup.

Ďalej by som rád poďakoval všetkým súčasným i bývalým členom Laboratória invazivity nádorových buniek za cenné rady a nápady, za skúsenosti pozitívne i negatívne, za kamarátstva i priateľstvá a za to, že boli, sú a budú pre mňa tak trochu rodinou. Menovite by som chcel poďakovať Maruške Charvátovej, ktorá sa o nás stará ako o vlastné deti a je tu vždy pre nás v otázkach pracovných i osobných.

Špeciálna vďaka patrí Nikol Baloghovej, v blízkej budúcnosti Dibusovej, ktorá počas celého štúdia statočne znášala moje Ph.D. nálady, bola mi oporou v časoch dobrých i tých horších a vďaka ktorej som pri písaní článku či tejto práce nemusel pohnúť takmer ani prstom.

V neposlednom rade by som rád poďakoval rodičom a sestre, za finančnú, materiálnu i psychickú podporu počas celého môjho predošlého štúdia, bez čoho by som sa na doktorát nikdy ani nedostal.

Nakoniec ďakujem všetkým kamarátom a priateľom za podporu, fandenie a občasné odreagovanie od laborkového života, ktoré je tak potrebné.

Abstrakt

Proteínová fosforylácia predstavuje jednu z najdôležitejších posttranslačných modifikácií v signálnom prenose a zohráva kľúčovú úlohu v regulácii väčšiny bunkových procesov, vrátane bunkového cyklu, komunikácie s extracelulárnym prostredím, bunkovej migrácie, alebo apoptózy. Fosforylácia je sprostredkovaná kinázami, deregulácia ktorých často negatívne ovplyvňuje vývoj a celkovú homeostázu a vedie k vzniku viacerých druhov ochorení, vrátane rakoviny. V tejto práci sme sa zamerali na identifikáciu nových substrátov kinázy PKN3, ktorá je známym regulátorom organizácie cytoskeletu a pro-malígneho rastu nádorov. Za použitia analóg-senzitívnej mutácie PKN3 sme urobili fosfoproteomický screen a identifikovali sme 281 proteínov, ktoré by potenciálne mohli byť fosforylované kinázou PKN3. Spomedzi týchto proteínov sme pre ďalší výskum vybrali ARHGAP18 z rodiny Rho GAP proteínov. Potvrdili sme, že PKN3 je schopná fosforylovať ARHGAP18 na Thr154, Ser156 a Thr158, a že tieto proteíny sú schopné vzájomnej interakcie v závislosti na izoforme ARHGAP18. Ďalej sme ukázali, že zámena týchto troch miest za fosfomimikujúci aspartát viedla k aktivácii GAP domény ARHGAP18, výsledkom čoho došlo k zníženiu hladiny aktívneho RhoA naznačujúc možnú existenciu negatívnej spätnej väzby v regulácii RhoA signalizácie. V druhej štúdii sme popísali intramolekulárne regulačné mechanizmy ďalšieho Rho GAP proteínu, ARHGAP42, a charakterizovali sme funkciu jeho jednotlivých proteínových domén. Ukázali sme, že fosforylácia Tyr376 kinázou Src bola dostačujúca k rozrušeniu autoinhibičnej konformácie ARHGAP42 a k aktivácii jeho GAP domény. Aktivácia ARHGAP42 viedla k zníženiu celkového množstva aktívneho RhoA, výsledkom čoho došlo k zvýšeniu dynamiky fokálnych spojov a lamelipodiálnych výbežkov a k zvýšeniu bunkovej migrácie.

Táto práca prináša nové fosfoproteomické dáta, ktoré by mohli byť cenným zdrojom pre budúce štúdium signalizácie kinázy PKN3, a zdôrazňuje dôležitosť proteínovej fosforylácie ako jedného z kľúčových regulátorov aktivity proteínov.

Kľúčové slová: fosforylácia, PKN3, Rho GTPázy, ARHGAP18, ARHGAP42

Abstract

Protein phosphorylation represents one of the most important posttranslational modifications in signal transduction and plays a crucial role in regulation of most of the cellular processes including cell cycle, communication with extracellular environment, cell migration or apoptosis. Phosphorylation is mediated by protein kinases, deregulation of which often negatively affects development and overall homeostasis and leads to development of several diseases, including cancer. In the first part of this work we focused on identification of new substrates of PKN3 kinase, which is a known player in regulation of cytoskeletal organization and pro-malignant tumor growth. Using an analog-sensitive mutant of PKN3 we performed a phosphoproteomic screen and identified 281 proteins that could potentially be phosphorylated by PKN3. Among these, we selected ARHGAP18, a protein from Rho GAP family, for further study. We confirmed PKN3 is able to phosphorylate ARHGAP18 on Thr154, Ser156 and Thr158 and that the two proteins are able to interact with one another in an ARHGAP18 isoform-specific manner. We further showed that substitution of the three candidate sites for phosphomimicking aspartate led to the activation of ARHGAP18 GAP domain which resulted in decreased levels of active RhoA, suggesting the existence of a negative feedback loop in regulation of RhoA signaling. In the second study we described the intramolecular regulatory mechanism of another Rho GAP protein, ARHGAP42, and characterized the function of individual ARHGAP42 domains. We showed that phosphorylation of Tyr376 by Src kinase was sufficient to disrupt the autoinhibitory conformation of ARHGAP42 and to activate its GAP domain. Activation of ARHGAP42 led to a decrease in the levels of active RhoA resulting in increased focal adhesion dynamics, lamellipodial protrusion velocity and cell migration.

Taken together, this work presents novel phosphoproteomic data that could be valuable for the future studies of PKN3 signaling and highlights the importance of protein phosphorylation as one of the key regulators of protein activity.

Key words: phosphorylation, PKN3, Rho GTPases, ARHGAP18, ARHGAP42

List of abbreviations

AGC	protein kinase A, protein kinase G and protein kinase C related
ARF	ADP-ribosylation factor
Arp2/3	actin related protein 2/3
AS	analog-sensitive
ATP	adenosine triphosphate
BAR	Bin/ amphiphysin/Rvs
BIG2	brefeldin A-inhibited guanine nucleotide-exchange protein 2
Cdk1	cyclin-dependent kinase 1
CML	chronic myeloid leukemia
DAPK	death-associated protein kinase
DLC1	Deleted in liver cancer 1
FAK	focal adhesion kinase
GAP	GTPase-activating protein
GDI	guanine nucleotide dissociation inhibitor
GDP	guanosine diphosphate
GEF	guanine nucleotide exchange factor
GRAF	GTPase regulator associated with FAK
GTP	guanosine triphosphate
HR1	protein kinase C related kinase homology region 1
IMAC	immobilized metal affinity chromatography
iTRAQ	isobaric tags for relative and absolute quantitation
LC MS/MS	liquid chromatography-coupled tandem mass spectrometry
LIMK	LIM kinase
LRRC16A	F-actin-uncapping protein LRRC16A
MLC	myosin light chain
MLCP	myosin light chain phosphatase
MOAC	metal oxide affinity chromatography
NPC	nasopharyngeal carcinoma
OPHN1	oligophrenin-1
p130Cas	Crk-associated substrate
PAK	p21 activated kinase
PDK1	3-phosphoinositide-dependent protein kinase-1
PH	pleckstrin homology
PI3K	phosphatidyl-inositol 3 kinase
PKC	protein kinase C
PKN	protein kinase N

PNBM	p nitrobenzyl mesylate
PTM	posttranslational modification
PTP1B	protein tyrosine phosphatase 1B
Rho	Ras homolog
ROCK	Rho associated protein kinase
SH2	Src-homology 2 domain
SH3	Src-homology 3
SILAC	stable isotope labeling with amino acids in cell culture
SMC	smooth muscle cell
TMT	isobaric tandem mass tags
WASH	Wiskott-Aldrich syndrome protein and SCAR homolog
WASP	Wiskott-Aldrich syndrome protein
WAVE	WASP family Verprolin-homologous protein
YAP	Yes associated protein

Table of contents

1. Introduction

Posttranslational modifications (PTMs) represent one of the most important regulatory mechanisms in signal transduction. They are mediated by specialized enzymes catalyzing the attachment of specific chemical groups or small proteins to target amino acids of their substrates. One of the most important PTMs is protein phosphorylation which is regulated mainly by the opposing action of two groups of proteins. One of them are protein kinases that catalyze the transfer of the phosphate group from the molecule of ATP to the phosphoacceptor site, and the second group is represented by protein phosphatases which are catalyzing the removal of phosphate moieties from phosphorylated proteins. Together, kinases, phosphatases and their substrates form a dynamic phosphorylation network which must be tightly regulated on several levels to specifically transmit the response to stimuli emerging form the cellular microenvironment. To date, however, the corresponding kinase was identified for only about 5 % of the known phosphosites with almost insignificant functional assignments (Needham et al., 2019). The identification of protein kinase substrates thus represents one of the essential tools to characterize the complex phosphorylation network and to understand its regulation and function.

In this work we aimed to identify new substrates of a largely understudied serine/threonine kinase PKN3 which is strongly implicated in cancer progression and has been characterized as a promising therapeutic target. Among various phosphoproteomic approaches currently used to screen for the kinase substrates we decided to use an analog-sensitive mutant of PKN3. The phosphoproteomic methods based on the analog-sensitive kinases represent an important chemical genetic tool to identify direct substrates of the studied kinase. Indeed, we identified 218 new putative substrates of PKN3 in our screen, which will hopefully serve as a valuable resource for future study of PKN3 signaling.

We further studied the effect of phosphorylation on the regulation of two Rho GAP proteins, ARHGAP18 and ARHGAP42. We identified ARHGAP18 as one of the PKN3 substrates in our phosphoproteomic data and showed that its phosphorylation by PKN3 led to activation of its GAP domain, resulting in decrease of the cellular levels of active RhoA. Similarly, we characterized the effect of ARHGAP42 phosphorylation by tyrosine kinase Src on the regulation of its conformation and activity. Our results highlight the importance of phosphorylation in regulation of signaling and uncover add a new knowledge into the complex phosphorylation network.

In the following chapters of literature review, the most commonly used phosphoproteomic approaches will be described, followed by a brief description of the structure, function and regulation of small Rho GTPases and Rho GAP proteins ARHGAP18 and ARHGAP42. Finally, a brief review on PKN kinases focused mainly on signaling of PKN3 will be presented.

2. Literature review

2.1. Kinases and phosphorylation

There are 518 kinases encoded in human genome and, as such, kinases form one of the largest groups of proteins in eukaryotes constituting about 1,7 % of all human genes (Manning et al., 2002). The vast majority of the kinases are catalytically active and catalyze the transfer of the γ-phosphate from ATP (*adenosine triphosphate*) to the hydroxyl group of serine, threonine or tyrosine residues, however, phosphorylation of other residues such as histidine, arginine or lysine has also been getting attention recently (Adam and Hunter, 2018; Fu et al., 2020). Based on the kinase domain evolutionary relationships and sequence similarity, the human kinases are clustered into eight main groups (Figure 1.): TK (*tyrosine kinases*), TKL (*tyrosine kinase-like*), STE (*kinases related to STE20, STE11 and STE7*), CK1 (*casein kinase 1*), AGC (*protein kinase A, protein kinase G and protein kinase C related*), CAMK (*Ca^{2+}/calmodulin-dependent kinases*), CMGC (*Cdk, MAPK, GSK and Cdk-like related*) and other kinases (Duong-Ly and Peterson, 2013).

The early autoradiographic experiments showed that the ratio of serine, threonine and tyrosine phosphorylation in cells is far from being balanced (Hunter and Sefton, 1980). Indeed, the substantial part of phosphorylation events occurs on serine residues, about 10-15 % on threonines and only about less than 1 % of all phosphosites are tyrosines (Hunter and Sefton, 1980; Sharma et al., 2014). The main reasons for this are, that unlike Ser/Thr phosphorylation, phosphorylation of tyrosine residues in the proteins plays rather regulatory than a structural role and is characterized by a fast turnover unless protected by phospho-tyrosine binding domains. Moreover, most of the tyrosine kinases are tightly regulated and activated only under specific circumstances (Hunter, 2009; Hunter and Sefton, 1980). Also, from an evolutionary point of view, tyrosine phosphorylation is considered relatively modern and it became essential mainly in the metazoan evolution (Lim and Pawson, 2010).

It was estimated that more than 90% of expressed proteome would exhibit detectable phosphorylation when using ultra-deep identification methods with sufficient coverage (Sharma et al., 2014). There is a vast number of possible functional outcomes of phosphorylation, such as induction of conformational changes leading to enzyme activation or inhibition, regulation of protein-protein interactions, stability, etc. Thus, it is not surprising that phosphorylation is involved in the majority of the signal transduction events and plays a role in regulation of processes such as development, cell cycle, cell migration and reorganization of cytoskeleton, apoptosis, and others (Jurcik et al., 2020; Manning et al., 2002).

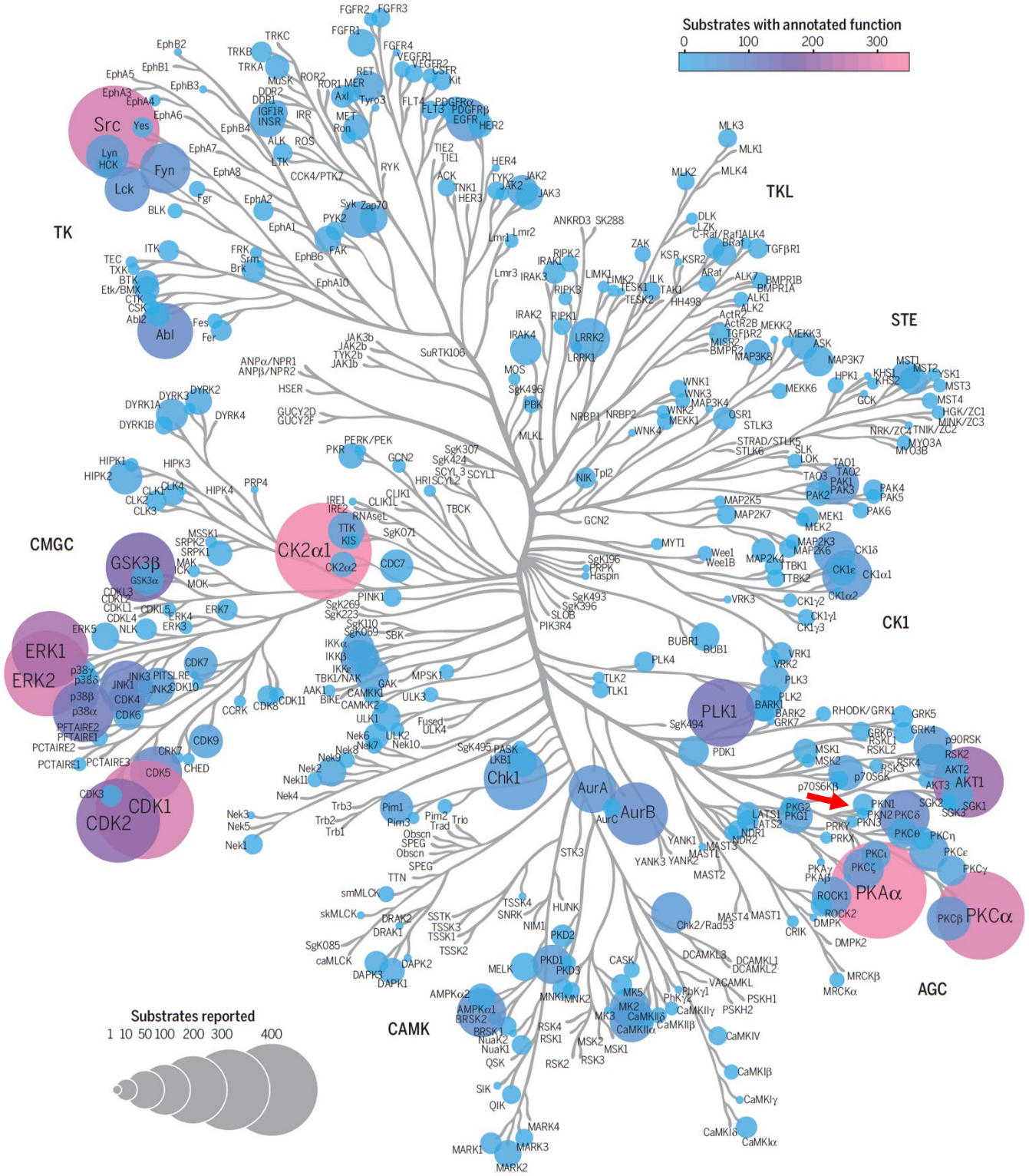

Figure 1. The dendrogram tree of human kinome depicting the individual kinases and their respective kinase families. Number of substrates recorded for each kinase corresponds to the area of the circle. The color of individual circles indicates the number of kinase substrates with annotated function. TK (*tyrosine kinases*), TKL (*tyrosine kinase-like*), STE (*kinases related to STE20, STE11 and STE7*), CK1 (*casein kinase 1*), AGC (*protein kinase A, protein kinase G and protein kinase C related*), CAMK (*Ca^{2+}/calmodulin-dependent kinases*), CMGC (*Cdk, MAPK, GSK and Cdk-like related*). The red arrow marks the PKN family of kinases present in the AGC branch. Figure edited from Needham et al., 2019.

2.2. Phosphoproteomic approaches in kinase research

Mass spectrometry-based (*liquid chromatography-coupled tandem mass spectrometry*, LC-MS/MS) phosphoproteomic approaches represent one of the essential tools to study kinase signaling. Most of the approaches follow a similar workflow based on protein extraction and denaturation, followed by enzymatic digestion, enrichment of the phosphopeptides, LC-MS/MS with or without prior fractionation and, finally, bioinformatic analysis (Figure 2.).

Given the low stoichiometry of phosphorylation events, enrichment steps are usually essential prior to LC-MS/MS analysis and are performed either at the protein or at the peptide level. At the protein level, the most common enrichment method is the affinity purification using either a phosphospecific antibody targeting a specific motif (Rikova et al., 2007), or, alternatively, using full-length proteins or protein domains that are known to bind phosphorylated motifs, such as 14-3-3 proteins for serine/threonine phosphorylation (Nishioka et al., 2012) or SH2 (*Src-homology 2*) domains for phosphorylated tyrosines (Ke et al., 2017). Much better and consistent results, however, are obtained using enrichment at the phosphopeptide level, mainly when interested in serine and threonine phosphorylation. For phosphopeptide enrichment, IMAC (*immobilized metal affinity chromatography*) and MOAC (*metal oxide affinity chromatography*) based on interaction of the phosphopeptides with chelated metal ions (e.g. Fe^{3+}) or covalent metal oxides (e.g. TiO_2), respectively, are the most specific and widely used (Leitner, 2016).

In general, LC-MS/MS-based methods currently used to study the kinase signaling can be classified as *indirect* or *direct* (Jurcik et al., 2020), the main differences will be discussed in the following chapters.

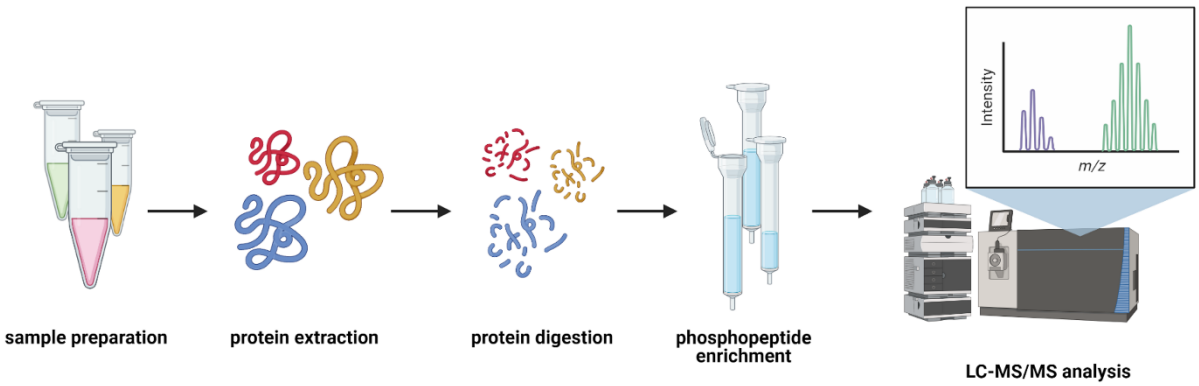

Figure 2. Basic phosphoproteomic workflows are usually based on protein extraction from the samples followed protein digestion using proteases, such as trypsin, or chymotrypsin. Subsequently, phosphopeptides are usually enriched using IMAC or MOAC approaches and subjected to LC-MS/MS analysis. The figure was created using BioRender.com.

2.2.1. Indirect LC-MS/MS methods

Indirect LC-MS/MS methods are generally based on quantitative large-scale phosphoproteomics and rely on identification of several thousands of phosphosites with a subsequent quantitative comparison of phosphorylation levels between the control and treated samples. Most often, a selective kinase inhibitor in combination with phosphatase inhibitors is used to inhibit downstream signaling of the studied kinase providing a general picture of phosphorylation changes upon the kinase inhibition as a result, however, to discern the direct substrates from phosphorylation changes induced further downstream may be rather challenging. Moreover, when using kinase inhibitors, the specificity might always represent an issue and inhibition of possible off-targets should be taken into account when analyzing the data (Browne et al., 2019; Byrne et al., 2020; Polat et al., 2015; Rimel et al., 2020).

In order to compare the changes between two or more studied samples, especially when using indirect LC-MS/MS phosphoproteomic approaches, several labeling strategies are currently used. One of the most common and most used labeling methods is SILAC (*stable isotope labeling with amino acids in cell culture*). SILAC is based on metabolic labeling of the whole proteome using stable isotope labeled amino acids, such as ^{13}C or ^{15}N-labeled arginine or lysine. As a result, intensities of the "heavy" and "light" peptides analyzed by LC-MS/MS allow for comparison of their relative abundance in the sample (Chen et al., 2015). As an alternative to SILAC, several tagging systems for chemical labeling of peptides are widely used, such as iTRAQ (*isobaric tags for relative and absolute quantitation*)(Ross et al., 2004) or TMT (*isobaric tandem mass tags*)(Thompson et al., 2003). The known mass difference between labeled and unlabeled peptides is used to distinguish the individual studied conditions when analyzing the LC-MS/MS data. In addition to SILAC and isobaric tags, label free quantification methods based on measuring ion intensity changes or spectrum counting provide an efficient and less expensive alternative to labeling methods (Cox et al., 2014; Neilson et al., 2011).

2.2.2. Direct LC-MS/MS methods

Direct LC-MS/MS methods focused on kinase signaling are generally based either on direct interaction of the studied kinase with its substrates or on phosphorylation with ATP analogs that allow for specific identification of the phosphorylated substrates.

The kinase-substrate interaction screens are based on the notion that the kinases have to be in the direct interaction with their substrates to phosphorylate them. However, several issues in specificity and effectiveness of this approach are raised. First of all, interaction of the kinase with its substrate is transient and, normally, when the substrate is phosphorylated the interaction is lost. Moreover, a number of false positives can be identified in case the kinase interacts with scaffold proteins or acts as an adaptor protein itself (Jurcik et al., 2020; Miller and Turk, 2018).

Recently, a new method for direct substrate identification was described using radiolabeled ATP in an *in vitro* kinase reaction coupled with quantitative mass spectrometry (HAKA-MS). The approach combines irreversible inhibition of all endogenous kinases by FSBA (5′ -[p-(fluorosulfonyl)benzoyl]adenosine) and the use of stable γ-$^{18}O_2$-labelled version of ATP which allows for specific detection of phosphorylated substrates (Müller et al., 2016).

Another direct LC-MS/MS approach used to identify kinase substrates is based on the use of analog-sensitive kinases and will be discussed in detail in the following chapter.

2.2.2.1. Analog-sensitive kinases

The concept of analog-sensitive (AS) kinases emerged as a chemical-genetic tool to specifically target engineered kinases with small molecular inhibitors and, therefore, study the precise role of individual kinases in cellular signaling (Bishop et al., 2000). The initial studies were performed on v-Src kinase and showed, that mutation of Ile338, a gatekeeper residue located in the ATP-binding pocket of the kinase, affected the ability of the small molecular inhibitor PP1 to inhibit the activity of Src. The substitution of Ile338 for a larger amino acid, such as phenylalanine or methionine, decreased the potency of PP1, and, conversely, when a smaller residue, glycine or alanine, was used to substitute Ile338, inhibition of Src by PP1 was increased. Importantly, mutation of this gatekeeper residue for a smaller amino acid resulted in the opening of the ATP-binding pocket and the mutated kinase could use synthetic ATP analogs with a bulky group added to the N^6 position as a cofactor in phosphorylation, while the WT kinase could not (Figure 3.). Similarly, bulky analogs of PP1 inhibitor exhibited increase in both potency and specificity when used with AS kinase, providing an important tool to study Src-mediated signaling (Bishop et al., 1999; Liu et al., 1998, 1999; Shah and Shokat, 2002). Interestingly, mutation of the gatekeeper residue was demonstrated to result in increased activity of several kinases which was reflected also in their increased transforming ability. A spontaneous gatekeeper mutation was shown to confer resistance of BCR-ABL fusion kinase to Imatinib (STI-571, Gleevec), an inhibitor used for the treatment of patients with chronic myeloid leukemia (CML), underlining the importance of this residue in phosphorylation catalysis and kinase targeting (Azam et al., 2008; Gorre et al., 2001). Moreover, by using AS variant of BCR-ABL and a specific NaPP1 small molecular inhibitor it was shown, that inhibition of BCR-ABL alone is not sufficient to eliminate all the cell populations with myeloproliferative disorder suggesting that the off-target effects of Imatinib are required for effective CML treatment (Wong et al., 2004).

Since the first studies, more than 20 AS kinases were engineered. Use of these kinases in different cellular and organismal contexts, ranging from yeasts (Alonso-Rodríguez et al., 2016; Cipak et al., 2012, 2014; Floor et al., 2016; Gregan et al., 2007), plants (Harashima et al., 2016), zebrafish (Cibrián Uhalte et al., 2012), to mice (Maas et al., 2014; Michowski et al., 2020) and human cells (Banko et al., 2011; Bartkowiak et al., 2015; Decker et al., 2019), highlights the

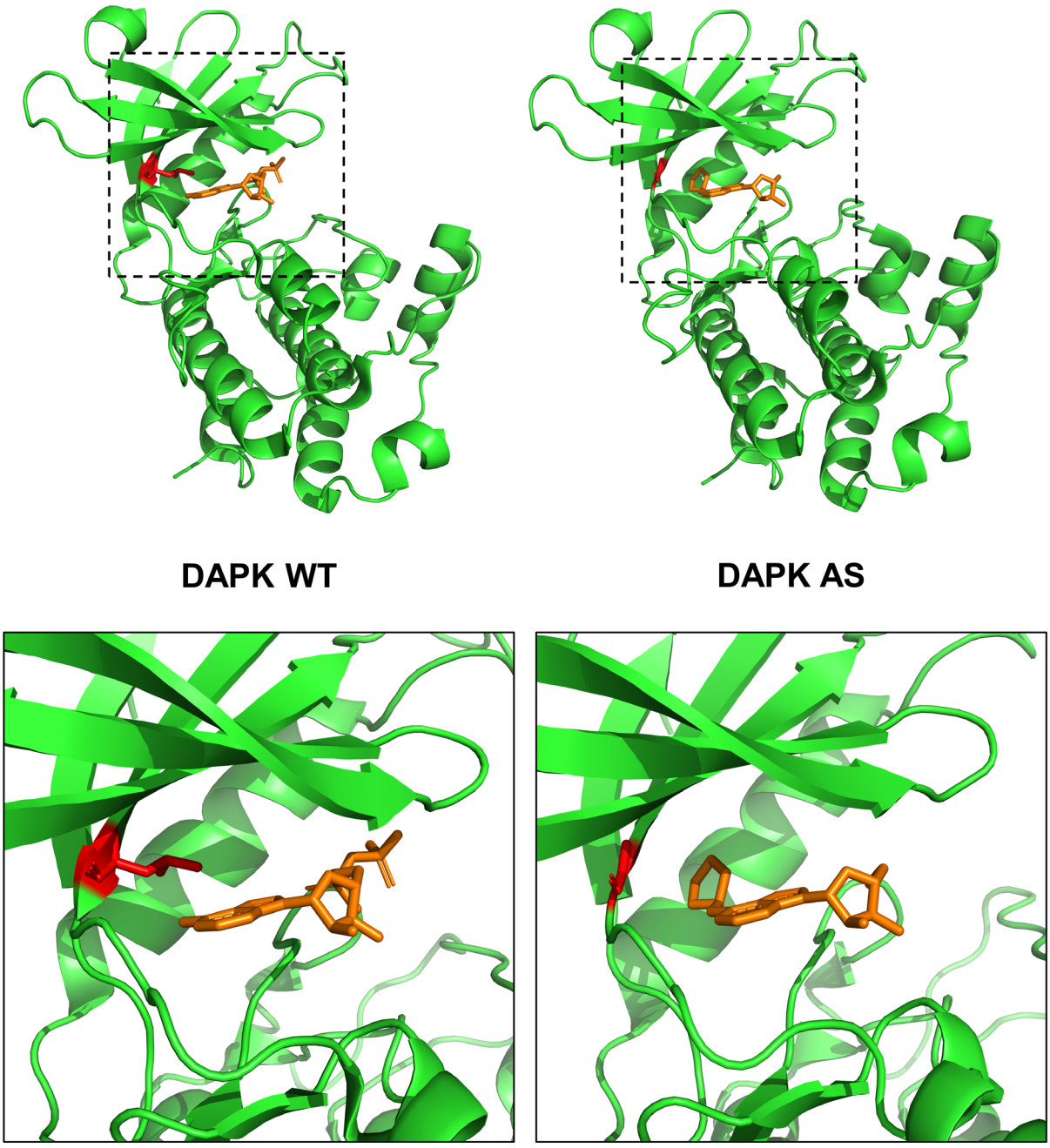

Figure 3. Structural comparison of WT and AS kinase domain of DAPK kinase. The upper panel shows the cartoon structures of WT (left) and AS (Leu93Gly, right) catalytic domain of DAPK (*death-associated protein kinase*) kinase with the gatekeeper residues highlighted in red (displayed in sticks). Dashed squares mark the approximate areas corresponding to ATP-binding sites of individual kinase domain enlarged in the lower panel. Catalytic domain of DAPK WT is complexed with ADP (*adenosine diphosphate*, orange) while the catalytic domain of DAPK AS is in complex with N^6-cyclopentyladenosine (orange). Substitution of the gatekeeper residue Leu93 for glycine leads to enlargement of the ATP binding region which allows the entry of N^6-substituted bulky analogs of ATP and their use in phosphorylation. PDB 3F5G (DAPK WT, resolution 1,85Å) and 3GU8 (DAPK AS, resolution 1,6Å). Visualized and rendered in PyMOL.

versatility of the AS kinase approach in the study of the kinase signaling. Moreover, endogenous AS alleles have been recently generated by CRISPR/Cas9-mediated knock-in and successfully used to study signaling of several cyclin-dependent kinases (Gressel et al., 2017; Michowski et al., 2020), providing an interesting tool to study kinase signaling in endogenous context.

A lot of different protocols have been used when performing phosphoproteomic screens using AS kinases (Allen et al., 2007; Carlson and White, 2012; Cipak et al., 2014; Gregan et al., 2007; Hertz et al., 2010) all of them sharing the principal idea which is the use of bulky, N^6-substituted analogs of ATPγS. Use of these analogs provides both specificity and selectivity to the screen – N^6 bulky group ensures that only the AS kinase will be able to use the analog for transfer of the thiophosphate, which will then allow for selective visualization or enrichment of the kinase substrates (Allen et al., 2007). Two ways of substrate enrichment are typically used in AS kinase screens. First, lysate containing thiophosphorylated substrates can be treated with *p-nitrobenzyl mesylate* (PNBM) alkylation reagent creating a thiophosphate ester, which is then immunoprecipitated using a specific antibody. Alternatively, after the protein denaturation and enzymatic digestion, the thiophosphorylated peptides can be enriched using iodoacetyl beads and released by oxidation in form of phosphopeptides for subsequent LC-MS/MS analysis (Figure 4.) (Allen et al., 2007; Hertz et al., 2010).

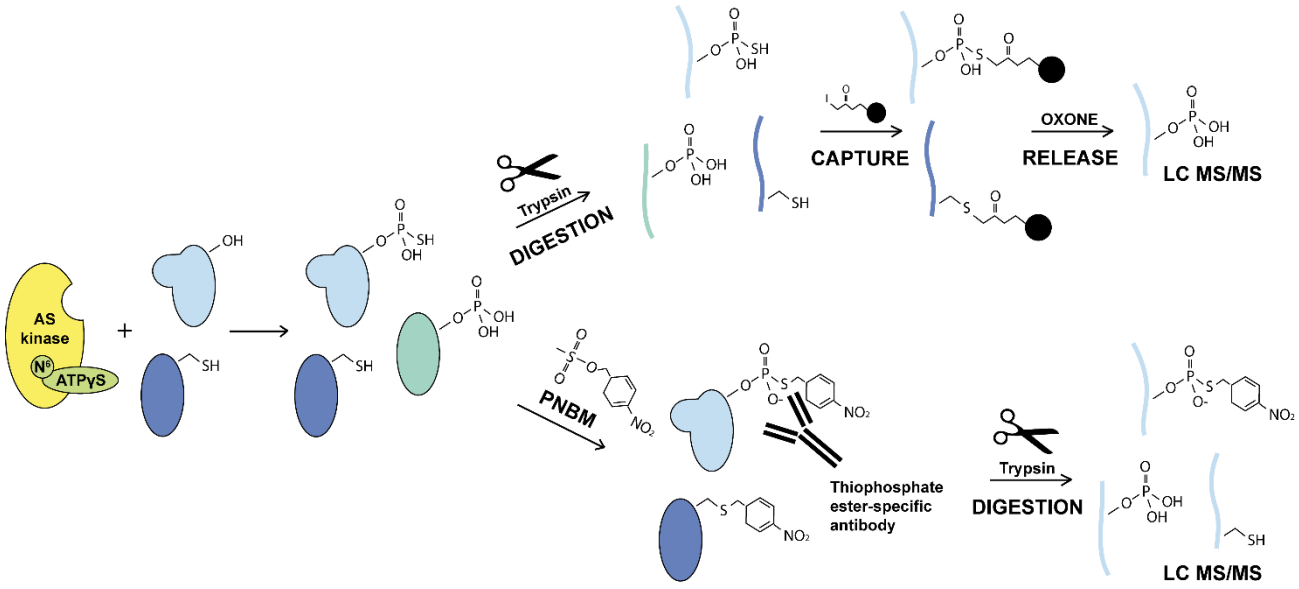

Figure 4. Overview of the AS kinase-based phosphoproteomic approaches. After thiophosphorylation of substrates by AS kinase two different ways of enrichment are usually applied. First, after the protein denaturation and enzymatic digestion the thiophosphorylated peptides can be enriched using iodoacetyl beads and released by oxidation in form of phosphopeptides for subsequent LC-MS/MS analysis. Alternatively, the lysate containing thiophosphorylated substrates can be treated with *p-nitrobenzyl mesylate* (PNBM) alkylation reagent creating a thiophosphate ester, which is then immunoprecipitated using a specific antibody with subsequent digestion and LC-MS/MS analysis.

2.3. Signaling of small Rho GTPases

Family of small Rho (*Ras homolog*) GTPases (18-21 kDa) belongs to the Ras superfamily and is represented by 20 monomeric G proteins. They are indispensable for spatial and temporal organization of cytoskeleton and, therefore, for regulation of cell morphology, formation of cellular protrusions, migration, cell cycle and other processes. Although 20 members have been described to date, three of the small Rho GTPases, RhoA, Rac1 and Cdc42, were studied most extensively and represent the key nodes in signaling leading to formation of important actin-based migratory structures, such as stress fibers, lamellipodia or filopodia, respectively (Nobes and Hall, 1995).

Structurally, small Rho GTPases are formed by a G domain core, insert helix and hypervariable *C*-terminal region. The G domain contains 5 conserved sequence motifs (G1-G5) which are responsible for mediating the interaction with guanine nucleotide. G1 motif, also known as the P-loop, together with G4 and G5 motifs play a role in coordination of nucleotide binding with Mg^{2+} ion which is indispensable for this process. G2 and G3 motifs, also known as switch I and switch II, respectively, sense whether the bound nucleotide is in a GDP or a GTP form and change the conformation accordingly. Between G4 and G5 motifs there is a short insert helix which promotes the activation of several effector proteins and participates in interaction with a number regulatory proteins, together with the *C*-terminal hypervariable region which is the main determinant of the interaction specificity (Figure 5.). At the *C*-terminus there is a CAAX-box which serves as an attachment site for lipid anchors (mostly farnesyl, geranylgeranyl and palmitoyl groups) that mediate binding of Rho GTPases to the membrane (Hodge and Ridley, 2016; Schaefer et al., 2014).

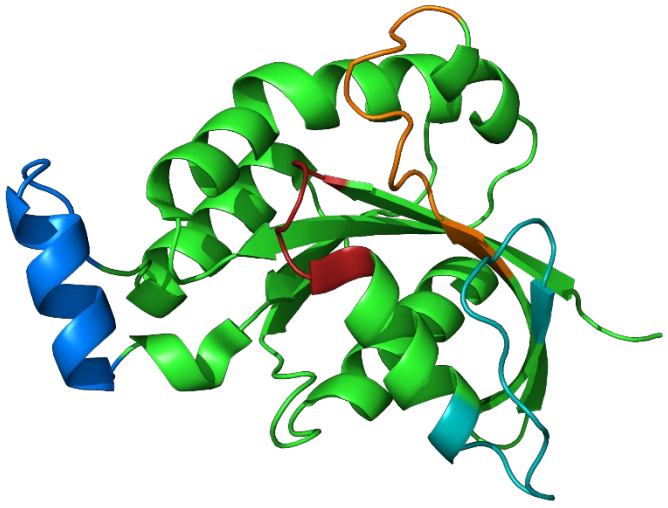

Figure 5. The ribbon structure of RhoA. The structure contains the first 180 amino acids of RhoA (out of 193 amino acids), *C*-terminal hypervariable region with CAAX-box is excluded. P-loop/G1 motif – brown, switch I region/G2 motif – cyan, switch II region/G3 motif – orange, insert helix – blue. PDB 5EZ6, resolution 1.80 Å. Visualized and rendered in PyMOL.

Rho GTPases play a fundamental role in the regulation of cytoskeletal organization and represent a key node in regulation of cell shape and motility. Especially, cell migration and invasion are of utmost importance in the field of cancer progression and formation of secondary tumor sites. Cell migration can be defined as a multistep process involving several steps, such as extension of lamellipodia at the leading edge of the cell followed by formation of focal contacts with the extracellular matrix (ECM), cell body contraction by actomyosin complexes and, finally, detachment of the tail part of the cell (Lauffenburger and Horwitz, 1996; Parri and Chiarugi, 2010). To exert their function in orchestration of these processes Rho GTPases act through several effector proteins (Figure 6.). Among the most studied effector proteins of RhoA belong the ROCK kinases (*Rho-associated protein kinase*), actin nucleating proteins from the formin family, such as mDia, or PKN (*protein kinase N*) kinases which will be described in detail in the following chapters (Kühn and Geyer, 2014; Lammers et al., 2008; Watanabe et al., 1997, 1999). The activation of ROCK1 or ROCK2 kinases by RhoA leads to inhibition of MLCP (*myosin light chain phosphatase*) activity via phosphorylation of its MYPT1 (*myosin phosphatase target subunit 1*) subunit and, therefore, to the increased levels of MLC (*myosin light chain*) phosphorylation resulting in enhanced actomyosin contractility. ROCK kinases can also activate LIMK (*LIM kinase*) which is involved in regulation of actin dynamics via phosphorylation and inactivation of actin-binding protein cofilin. (Amano et al., 1996, 2001; Bernard, 2007; Cardama et al., 2017; Feng et al., 1999; Kimura et al., 1996; Wei et al., 2016). In contrast with RhoA, Rac1 GTPase is implicated in the formation of lamellipodia at the leading edge of the migrating cells via activation of WAVE (*WASP family Verprolin-homologous protein*) protein and subsequent Arp2/3 (*actin related protein 2/3*) complex-mediated actin nucleation (Miki et al., 1998). Similarly as the GTPases from RhoA subfamily, Rac1 can regulate actin dynamics via LIMK-mediated cofilin inhibition. In the case of Rac1 signaling, however, LIMK is activated by PAK (*p21-activated kinase*) kinases (Edwards et al., 1999). Finally, Cdc42 acts mainly via WASP (*Wiskott-Aldrich syndrome protein*) protein resulting in Arp2/3-mediated formation of filopodia (Parri and Chiarugi, 2010). Moreover, the Rho GTPases also exert their actions through the activation of formin proteins from mDia subfamily which lead to increased actin polymerization (Kühn and Geyer, 2014).

2.3.1. Classification of small Rho GTPases and regulation of their activity

Based on the common features in their activation and regulation, Rho GTPases are classified in two main groups, *classical* and *atypical*, which can be further divided into eight subgroups (Table 1.). The proteins belonging to the group of classical Rho GTPases containing Rho, RhoF, Rac and Cdc42 subfamilies, act as molecular switches transitioning between the inactive (GDP) and active (GTP) state. These transitions are facilitated by two classes of proteins – guanine

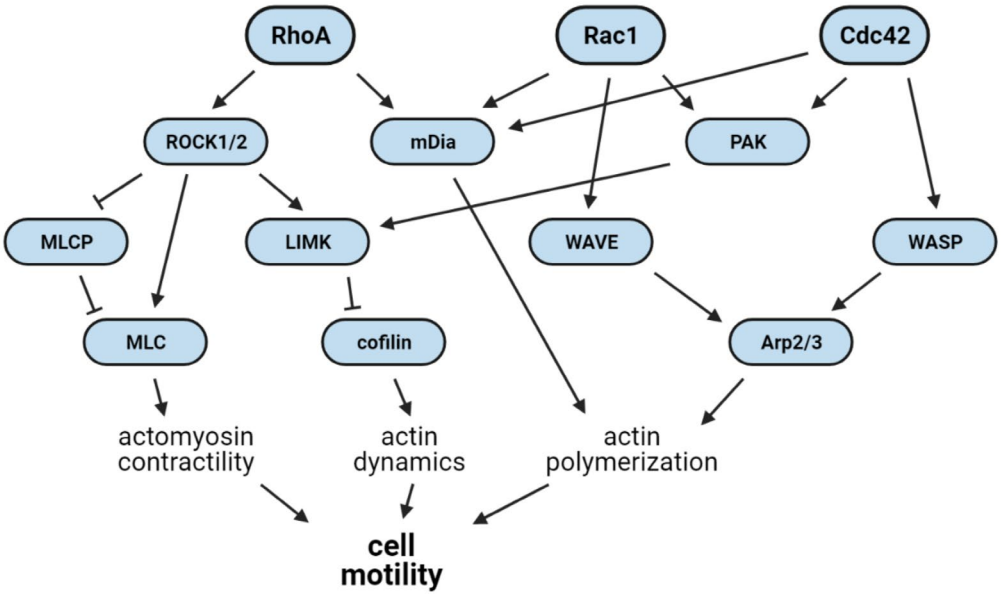

Figure 6. Rho GTPases and their main effector proteins in regulation of cell motility.

nucleotide exchange factors (GEFs) and GTPase-activating proteins (GAPs)(Figure 7.). GEFs mediate the exchange of GDP for GTP and, therefore, activate the Rho GTPases. On the other hand, GAP proteins stimulate the intrinsic GTPase activity of the Rho GTPases which results in their inactivation. Alternatively, Rho GTPases can be sequestered by guanine nucleotide dissociation inhibitors (GDIs) that inhibit their activation by GEF proteins. Rho GTPases that are not regulated by GEF and GAP proteins are classified as atypical and include four remaining subfamilies – RhoH, RhoU/RhoV, RhoBTB and Rnd. RhoU and RhoV, also known as fast-cycling Rho GTPases, are characterized by significantly increased ability of intrinsic GTP hydrolysis. In contrast, RhoH and Rnd GTPases are defective in their GTPase activity and act as constitutively active (Aspenström, 2020; Dahmene et al., 2020; Hodge and Ridley, 2016).

Classical Rho GTPases	**Rho subfamily**	**Rac subfamily**	**Cdc42 subfamily**	**RhoF subfamily**
	RhoA RhoB RhoC	Rac1 Rac2 Rac3 RhoG	Cdc42 RhoJ RhoQ	RhoD RhoF
Atypical Rho GTPases	**RhoBTB subfamily**	**RhoH subfamily**	**RhoU/RhoV subfamily**	**Rnd subfamily**
	RhoBTB1 RhoBTB2	RhoH	RhoU RhoV	Rnd1 Rnd2 Rnd3

Table 1. Classification of mammalian Rho GTPases. Rho GTPases can be classified into two main groups, *classical* and *atypical*, each of them containing four subfamilies.

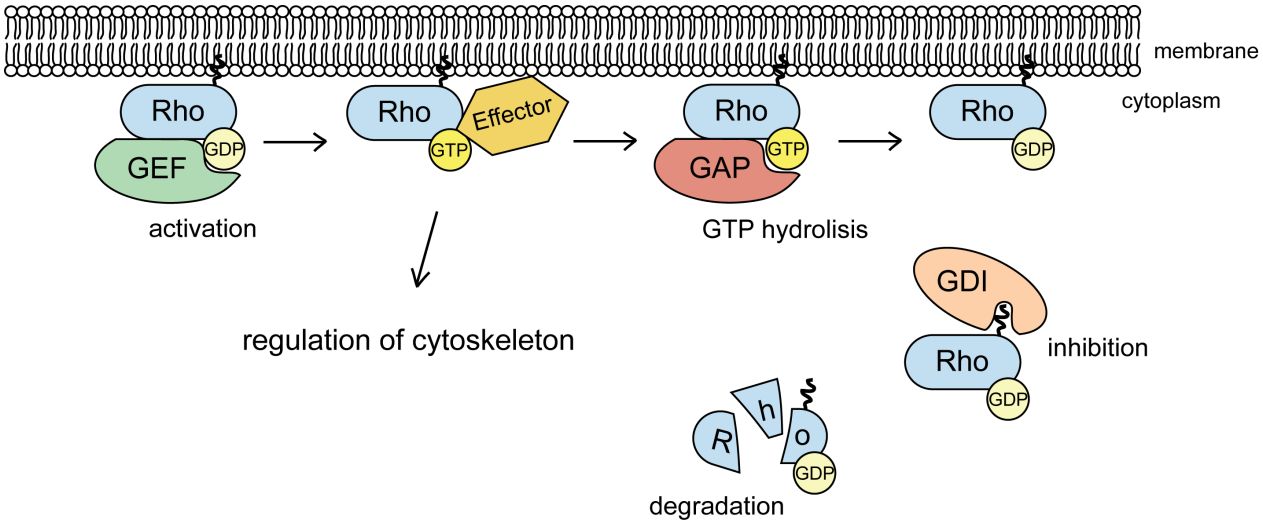

Figure 7. Regulation of activity of the classical Rho GTPases. Classical Rho GTPases are activated by GEF proteins that mediate the exchange of GDP for GTP. In the active state, Rho GTPases signal through their effector proteins to regulate the cytoskeleton organization and dynamics. GAP proteins stimulate the intrinsic activity of Rho GTPases resulting in hydrolysis of GTP and, therefore, their inactivation. To prevent their downstream signaling, Rho GTPases can be further sequestered to cytosol by GDI proteins, representing another level of negative regulation. Without the protective function of GDI, cytosolic Rho GTPases are rapidly degraded by ubiquitin-proteasome system.

2.3.2. Rho GAP proteins

Rho GAPs represent a very diverse family of proteins negatively regulating the activity of small Rho GTPases. Currently, more than 70 Rho GAPs have been described across different species (Tcherkezian and Lamarche-Vane, 2007). In human, there are 66 Rho GAPs encoded in the genome, 57 of which possess a catalytic GAP domain able to activate the GTPase activity of the small Rho GTPases (Amin et al., 2016). Structurally, GAP domain of the Rho GAP proteins consists of 9 α-helical segments. The core of the GAP domain is formed by a four-helix bundle which mediates the interaction with switch I, switch II and P-loop region of Rho GTPases. There is a conserved arginine residue in the central part of the GAP domain core region, also known as the arginine finger, which is essential for the stimulation of the activity of small Rho GTPases (Amin et al., 2016; Gamblin and Smerdon, 1998; Rittinger et al., 1997; Scheffzek et al., 1998).

Notably, the vast majority of Rho GAPs exhibit high domain modularity and apart from GAP domain they encode many others, such as SH2, SH3 (*Src-homology 3*), WW, PH (*pleckstrin homology*), BAR (*Bin/ amphiphysin/Rvs*), and others. It is the presence of these domains that is believed to provide the specificity of Rho GAP proteins towards individual Rho GTPases and to regulate their activity in both spatial and temporal manner by ensuring the proper localization and activation of Rho GAPs (Amin et al., 2016).

A short introduction to the function, regulation and signaling of two Rho GAP proteins, ARHGAP18 and ARHGAP42, will be discussed in the following chapters.

2.3.2.1. ARHGAP18

ARHGAP18 is a member of a Rho GAP protein family also known by an alternative name, SENEX, which is connected to observed induction of premature senescence of endothelial cells overexpressing this protein (Coleman et al., 2010). Interestingly, cell type-dependent specificity of ARHGAP18 towards individual Rho GTPases has been described in literature. In cancer cells, it exhibits specificity towards RhoA (Maeda et al., 2011) whereas in endothelial cells it was shown to act preferentially on RhoC (Chang et al., 2014). However, GAP activity towards RhoA has recently been observed also in endothelial cells (Li et al., 2020). One of the possible explanations for the cell-type dependent ARHGAP18 specificity could be the absence of proper docking domains that would ensure a specific subcellular localization. Indeed, it is notable that the GAP domain is the only well-defined classical domain in ARHGAP18 protein sequence and the rest of the tertiary structure remains unresolved.

ARHGAP18 was shown to regulate the organization of actin cytoskeleton downstream of IP3R3 (*inositol 1,4,5-trisphosphate receptor 3*) via the RhoA/mDia1/FAK (*focal adhesion kinase*) signaling pathway (Vautrin-Glabik et al., 2018) and to associate with microtubules in a GAP-dependent manner (Lovelace et al., 2017). Moreover, it regulates the cell shape and tissue tension homeostasis in development downstream of YAP (*Yes associated protein*) (Porazinski et al., 2015) and localizes to the leading edge during cell spreading and migration (Maeda et al., 2011). As mentioned previously, overexpression of ARHGAP18 in endothelial cells leads to premature senescence (Coleman et al., 2010). Moreover, ARHGAP18 acts as a negative regulator of angiogenesis and contributes to vascular stabilization (Chang et al., 2014), as well as to athero-protective alignment of endothelial cells in response to laminar shear flow (Coleman et al., 2020; Lay et al., 2019).

The role of ARHGAP18 in cancer development and signaling is still very contradictory, as both overexpression (Li et al., 2018) and downregulation (Aguilar-Rojas et al., 2018; Humphries et al., 2017) of ARHGAP18 were shown to result in inhibition of cancer cell migration, invasion and tumor growth. Moreover, high expression levels of ARHGAP18 were associated with both better outcome (Aleskandarany et al., 2017), but also with worse metastasis-free and overall survival (Humphries et al., 2017) of breast cancer patients, suggesting a highly context-dependent behavior of ARHGAP18 in cancer cells, similarly as in case of specificity towards individual Rho GTPases.

2.3.2.2. ARHGAP42

ARHGAP42, also known as GRAF3, is a Rho GAP which belongs to the family of GRAF (*GTPase regulator associated with FAK*) proteins. There are three other members in this family: GRAF1 (ARHGAP26), GRAF2 (ARHGAP10, PSGAP (*PH and SH3 domain containing RhoGAP*)) and OPHN1 (*oligophrenin-1*). All the members of the GRAF family share similar domain organization. At the *N*-terminus of the protein, there is a BAR domain followed by PH domain, GAP domain and, with the exception of OPHN1, SH3 domain (Figure 8.) (Aspenstrom, 2018). The role of the BAR domain in shaping the membrane and balancing the membrane tension has been described in multiple BAR domain-containing proteins. It is formed by three α-helices that dimerize into crescent-shaped structures (Aspenstrom, 2018; Peter et al., 2004; Salzer et al., 2017). The importance of BAR domain in GRAF proteins was demonstrated in several studies showing that BAR domain of GRAF1 is essential for mediating clathrin-independent endocytosis by formation of tubular membrane structures. Moreover, depletion of GRAF1 affected the membrane tension resulting in increased cell blebbing (Eberth et al., 2009; Holst et al., 2017; Lundmark et al., 2008). On the other hand, the *C*-terminal SH3 domain of GRAF1 and GRAF2 proteins was shown to mediate interaction with polyproline regions of several interacting proteins, such as FAK, Pyk2 or PKN3 (Ren et al., 2001; Shibata et al., 2001).

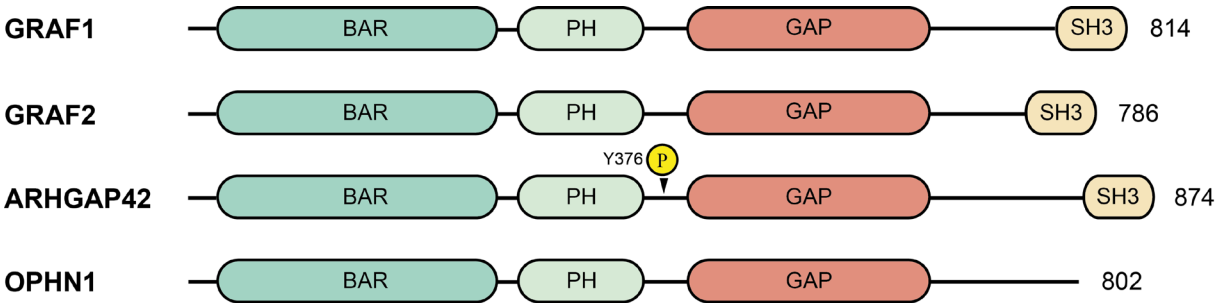

Figure 8. Domain organization of individual GRAF family proteins. For ARHGAP42 the major site of Src-mediated phosphorylation, Tyr376 (Y376), is depicted.

Expression of ARHGAP42 is restricted to smooth muscle cells (SMC) where it controls the levels of blood pressure as it was shown in a gene trap mouse model. Downregulation of ARHGAP42 leads to increased blood pressure in a dose-dependent manner via activation of RhoA signaling (Bai et al., 2013). Interestingly, further studies suggested ARHGAP42 could act as a rheostat of RhoA activation in SMC as a result of transcriptionally mediated negative feedback loop downstream of RhoA signaling (Bai et al., 2018). Recently, in a genome-wide association study it was confirmed that patients with haploinsufficiency in ARHGAP42 suffer with hypertension (Fjorder et al., 2019). Moreover, a common ARHGAP42 polymorphism

(rs604723) has been described to influence the expression of ARHGAP42 in SMC via binding of serum response factor to intronic regulatory element (Bai et al., 2017).

In the field of cancer, ARHGAP42 remains largely understudied. High expression of ARHGAP42 was observed in nasopharyngeal cancer (NPC) tissues, with even higher expression in metastatic NPC which negatively correlated with overall survival of patients with NPC (Hu et al., 2018). Hu with colleagues also showed overexpression of ARHGAP42 promoted proliferation, migration and invasion of NPC cells (Hu et al., 2018). Moreover, YAP-dependent upregulation of ARHGAP42 upon knockdown of SASH1 (*SAM and SH3 domain containing 1*) has been recently shown to regulate cell invasion of triple-negative breast cancer cells (Jiang et al., 2020).

2.4. PKN kinases

The family of PKN kinases, also known as PRK (*protein kinase C-related kinases*) includes three members – PKN1/PRK1/PKNα, PKN2/PRK2/PKNγ and PKN3/PKNβ. They are Ser/Thr kinases of AGC type and belong to the superfamily of PKC kinases. As one of the main effectors of signaling mediated by Rho GTPases, PKN kinases are involved in cytoskeletal rearrangement and contribute to the regulation of processes such as cell motility or cell cycle and to development of several diseases. In this chapter, structure and function of PKN kinases will be described with the main focus on PKN3.

2.4.1.1. Structure of PKN kinases

HR1 domains

At the *N*-terminal part of PKN kinases there are three highly conserved homologous repetitions called HR1 domains (HR1a, HR1b, HR1c; *protein kinase C-related kinase homology region 1*)(Figure 9.), also known as ACC (*antiparallel coiled-coil*) domains or CZ (*charged aminoacid and Leucince zipper-like sequence*) regions, which are important in mediating the interaction with Rho GTPases (Maesaki et al., 1999a; Mukai and Ono, 1994). Extensive work has been done to define the structure and characterize the interaction of HR1 domains with Rho GTPases (Flynn et al., 1998; Hutchinson et al., 2011, 2013; R Maesaki et al., 1999; Ryoko Maesaki et al., 1999; Modha et al., 2008; Owen et al., 2003; Shibata et al., 1996; Zong et al., 1999). The first structural studies of HR1 domains in PKN1 showed they are formed by a coiled coil of two α-helices. Although resolving the structure of HR1a domain with

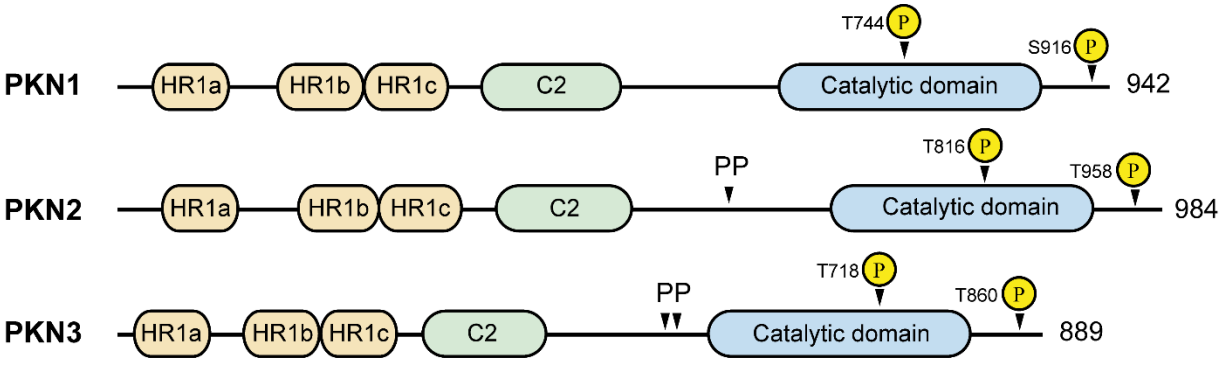

Figure 9. Domain organization of individual PKN kinases. Individual domains of PKN kinases and the phosphorylation sites important for activation of PKN kinases are shown. In PKN2 and PKN3 the corresponding position polyproline motifs (PP) that mediate the interaction with SH3 domain-containing proteins is depicted.

RhoA revealed two possible ways of interaction, referred to as contact I and contact II and delineated the differences of effector recognition between RhoA, Cdc42 and Rac (Maesaki et al., 1999a), mutational analysis of respective contact sites performed on the RhoA-HR1a interaction model revealed that only residues of contact II are involved in RhoA binding to HR1a (Hutchinson et al., 2011). While both HR1a and HR1b domains of PKN1 have been shown to bind Rho GTPases, HR1c is unable to do so and its function in PKN kinases remains unclear (Flynn et al., 1998). Further biophysical studies of HR1a and HR1b domains have shown there are slight differences in the structure of HR1 domains between the PKN isoforms, such as in helical content and thermal stability (Hutchinson et al., 2011, 2013). These differences most likely influence the affinity of Rho GTPases to HR1 domains of individual PKN kinases. Interestingly, while only a little difference in binding affinity of full length RhoB or RhoB lacking the *C*-terminal polybasic region to PKN1 and PKN2 was observed, PKN3 showed significantly higher affinity to full length RhoB, similarly, as it was described for interaction of PKN1 with Rac1, stressing out the differences in individual PKN-Rho GTPase interactions (Hutchinson et al., 2013; Modha et al., 2008). Although all PKN isoforms have been shown to bind RhoB with highest affinity *in vitro*, association studies in living cells showed PKN3 interacts preferentially with RhoC (Hutchinson et al., 2013; Unsal-Kacmaz et al., 2012).

C2 domain

In the central part of PKN kinases, there is a region homologous to the C2 domain of PKC, where it has been first described (Figure 9.)(Coussens et al., 1986; Knopf et al., 1986; Nishizuka, 1988). C2 domain is present in more than a hundred of proteins, such as PKC, PI3K (*phosphatidyl-inositol 3 kinase*) (Hiles et al., 1992), PLC (*phospholipase C*) (Rhee et al., 1989), synaptotagmin (Perin et al., 1990) or rabphilin (Shirataki et al., 1993), and it is responsible for lipid/membrane binding in either a Ca^{2+}-dependent or independent manner. Several structural studies showed the approximately 130-amino acid long C2 domain is organized into a β-sandwich of two four-stranded antiparallel β-sheets. Furthermore, there are two main different topologies C2 domains can adopt, topology I and II, which differ in connectivity of the individual β-strands and influence the orientation of the domain in respect to the neighboring regions (Figure 10.) (reviewed in Kretsinger et al., 2013; Nalefski and Falke, 1996; Rizo and Sudhof, 1998). The C2 domains of all three PKN kinases are of topology II and are unable to bind Ca^{2+}. However, they are responsible for increased catalytic activity of PKN kinases upon binding of phospholipids, except for PKN3, which is not stimulated by any lipids. In both PKN1 and PKN2 a huge increase in activity was observed when assayed in the presence of several lipids, such as PIP2 (*phosphatidylinositol (4,5)-bisphosphate*), PIP3 (*phosphatidylinositol (3,4,5)-trisphosphate*) or arachidonic acid (Falk et al., 2014; Oishi et al., 1999).

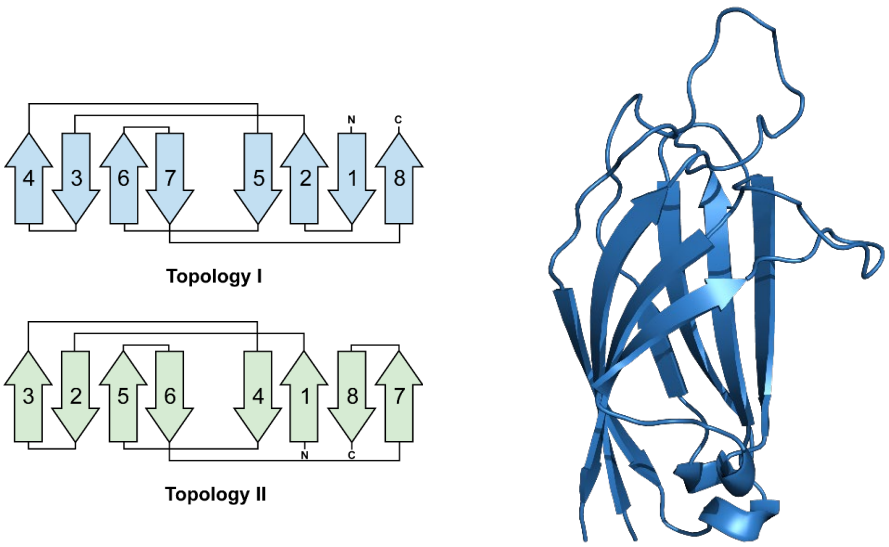

Figure 10. Structure of the C2 domain. Left panel – a schematic drawing of individual C2 domain topologies which differ in the connectivity of individual β-strands. Right panel – structure of PLCδ1 (*phospholipase C delta 1*) C2 domain (topology II). PDB 1DJI, resolution 2.50 Å. Visualized and rendered in PyMOL

Region linking the C2 domain and the catalytic domain

A short region following the C2 domain of PKN kinases was described to negatively regulate the interaction of PKN kinases with PDK1 (*3-phosphoinositide-dependent protein kinase-1*). This inhibition is released upon binding of Rho GTPases to the HR1 domain highlighting the role of Rho-GTP/PKN/PDK1 triple-complex formation in full activation of PKN kinases (Bauer et al., 2012; Flynn et al., 2000; Unsal-Kacmaz et al., 2012). There is also a short polyproline region between the C2 domain and the catalytic domain of PKN2 and PKN3 containing one or two polyproline motifs, respectively (Figure 9.)(Oishi et al., 1999), which mediate interaction with SH3 domain of several proteins, such as Graf1 and Graf2 in case of PKN3 (Shibata et al., 2001) or Nck in case of PKN2 (Quilliam et al., 1996). Recently, in a screen for new interaction partners of SH3 domain of adaptor protein p130Cas (*Crk-associated substrate*) we have predicted and confirmed a direct interaction between the SH3 domain of p130Cas and polyproline motif of PKN3. The interaction of the two proteins was abrogated either upon substitution of Tyr12 to phosphomimicking aspartate in the p130Cas SH3 domain or mutation in the polyproline motif of PKN3 (PPPKPPRL$_{507}$ to PAPSAPRL$_{507}$) (Gemperle et al., 2017, 2019).

Catalytic domain

The *C*-terminally located catalytic domain of PKN3 kinase exhibits a high sequential identity of 66 % and 62 % with those of PKN1 and PKN2, respectively (Oishi et al., 1999). The catalytic domains of PKN kinases adopt a structure of the classical kinase fold composed of

a small amino-terminal lobe (*N*-lobe) and a larger carboxy-terminal lobe (*C*-lobe). Between the two lobes a catalytic groove is formed were the ATP molecule is bound during phosphorylation catalysis. In the ATP-binding site-adjacent region of the *C*-lobe, there is a so-called activation loop which upon phosphorylation induces conformational changes mainly in the αC helix connecting the activation loop with the *N*-lobe. In the activation loop, there is also a highly conserved DFG (Asp-Phe-Gly) motif which ensures proper positioning of ATP during phosphorylation. The conformational changes induced by phosphorylation of the activation loop (Thr744 in PKN1, Thr816 in PKN2 and Thr718 in PKN3) are important for the formation of a crucial network of hydrogen bonds between ATP and the residues of the catalytic cleft that is essential for the proper activity of the kinase. In most of the AGC kinases, phosphorylation of both the activation loop and a hydrophobic motif which is located in the *C*-terminal tail of the kinase domain is necessary for the activation of the kinase. In PKN kinases, however, phosphorylation of the hydrophobic motif is not necessary since it contains phosphomimicking aspartate or glutamate residue instead of serine or threonine. This motif binds to the PIF pocket of PDK1 kinase which, in turn, phosphorylates the activation loop and activates the kinase (Arencibia et al., 2013; Flynn et al., 2000; Mora et al., 2004; Pearce et al., 2010). There is also another motif present in the *C*-terminal tail of the kinase domain of several AGC kinases called the turn motif which promotes their stability and activity. In PKN kinases it corresponds to Ser916 in PKN1, Thr958 in PKN2 and Thr860 in PKN3 (Falk et al., 2014; Pearce et al., 2010).

The specificity of PKN1 and PKN3 towards their substrates was assayed in several studies using phosphorylation of peptide arrays. Similarly to other basophilic AGC kinases, such as PKCs, PKN kinases exhibit strong preference for arginine residue in the position -3 and for hydrophobic amino acids in the position +1 (Figure 11.). Although PKN1 and PKN3 partially shared recognition of the target peptide motifs, they still retained some level of specificity (Browne et al., 2019; Collazos et al., 2011; Miller and Turk, 2018). A specific linear phosphorylation motif surrounding the phosphoacceptor is, however, not the only key determinant that drives the substrate phosphorylation. First, docking interactions between the kinase and the substrate proteins mediated by short linear motifs or large binding interfaces can facilitate substrate phosphorylation of non-consensus linear sequences. Similarly, phosphorylation can also occur based on a structural context where the consensus residues located far from the phosphoacceptor site in the linear sequence are brought together in the secondary structure of the substrate (Duarte et al., 2014; Miller and Turk, 2018).

2.4.2. Expression, activation and function of PKN3

While PKN1 and PKN2 are abundantly expressed in most of the adult human tissues (Hashimoto et al., 1998; Mukai and Ono, 1994), expression of PKN3 is restricted mainly to

osteoclasts, endothelial cells and numerous cancer cell types (Aleku et al., 2008; Leenders et al., 2004; Oishi et al., 1999; Uehara et al., 2017; Unsal-Kacmaz et al., 2012).

In osteoclasts, Uehara and colleagues have recently discovered the role of PKN3 in regulation of their bone resorbing activity, where PKN3 is activated downstream of non-canonical Wnt signaling as a RhoA effector kinase and contributes to maturation of podosomes and sealing zone by complex formation with Src, Pyk2 and p130Cas (Gemperle et al., 2019; Uehara et al., 2017; Uehara et al., 2019). In endothelial cells, PKN3 expression correlates with their migratory phenotype and its downregulation impairs the formation of characteristic tubular structures of endothelial cells in 3D *in vitro* culture conditions (Aleku et al., 2008).

In cancer cells, PKN3 was shown to act downstream of activated PI3K kinase promoting the malignant growth of PC-3 cells (prostate adenocarcinoma). Similarly, overexpression of PKN3 in breast cancer cells leads to pro-invasive growth of these cells *in vitro*. Conversely, inhibition of PKN3 expression in cancer cells impairs both the primary tumor growth and the formation of metastases (Leenders et al., 2004; Unsal-Kacmaz et al., 2012). Recently we have characterized the interaction of PKN3 with p130Cas and showed it promotes pro-malignant growth of cancer cells, which could partially explain PKN3-mediated phenotype (Gemperle et al., 2019).

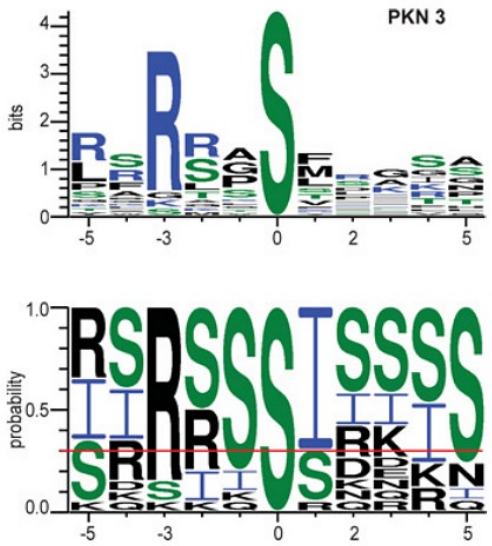

Figure 11. Consensus phosphorylation motif of PKN3. Position of individual amino acids is show in respect to phosphorylated Ser/Thr in position 0. The upper panel represents the preference for specific amino acids surrounding the phosphorylation site. The height of the letters are proportional to the frequency in the top 20 peptides phosphorylated in the peptide array. The lower panel represents grouped amino acid probability. R group includes hydrophilic amino acids (Arg, Lys, Asp, Glu, Asn, Gln), S group represents neutral amino acids (Ser, Gly, His, Thr, Ala, Pro), I group includes hydrophobic amino acids (Ile, Met, Leu, Val, Phe, Trp, Tyr). 70 % probability is depicted by red line. Figure from Collazos et al., 2011.

2.4.3. PKN3 as a therapeutic target

Since PKN kinases were shown to promote tumor growth and development they became a potential target in anticancer therapy. In fact, inhibition of all three PKN kinases was proposed to be the best option possible to overcome the redundancy in signaling of individual PKN kinases in targeting the invasive behavior of cancer cells (Lachmann et al., 2011).

To specifically target PKN3 in primary endothelial cells, Atu027, a liposomal siRNA was developed by Aleku and colleagues and has recently completed phase I/II clinical trials (Aleku et al., 2008; Schultheis et al., 2014, 2020; NCT00938574, NCT01808638). Systemic administration of Atu027 leads to downregulation of PKN3 in endothelial cells and inhibits formation of both micro- and macrometastases in xenogeneic (MDA-MB-231, MDA-MB-435) breast cancer and syngeneic (LCC, B16V) lung cancer metastasis mouse models, probably by inhibiting the maturation of glycosylation of several adhesion molecules, such as ICAM1 or VCAM1, needed for proper cancer cell migration (Aleku et al., 2008; Mukai et al., 2016). A combination of Atu027 and gemcitabine for treatment of patients with advanced pancreatic adenocarcinoma showed a significantly improved outcome, highlighting the importance of PKN3 as a therapeutic target (Schultheis et al., 2020; NCT01808638).

Generally, small molecular inhibitors are used to target kinases in cancer therapy. There are currently more than 35 FDA approved Ser/Thr and Tyr kinase inhibitors used to treat both solid and liquid malignancies (Bhullar et al., 2018). While there are no inhibitors selectively targeting PKN3, several commercially available kinase inhibitors showed surprising specificity and selectivity towards PKN kinases. Inhibitors of Src (PP1), p38 MAPK (SB-202190) or ROCK (Y27632) kinases displayed strong inhibitory effect towards PKN3 with K*i* (inhibitory constant that defines the concentration of inhibitor necessary to reduce the kinase activity to 50 %) in nanomolar values (Falk et al., 2014). Interestingly, JZ128, a new covalent inhibitor of PKN3 binding to Cys840 was identified by Browne and colleagues, providing an important tool for future study of PKN3 signaling (Browne et al., 2019).

3. Publications

Dibus, M., Brábek, J., & Rösel, D. (2020). A Screen for PKN3 Substrates Reveals an Activating Phosphorylation of ARHGAP18. International journal of molecular sciences, 21(20), E7769.

Luo, W., Janoštiak, R., Tolde, O., Ryzhova, L. M., Koudelková, L., Dibus, M., Brábek, J., Hanks, S. K., & Rosel, D. (2017). ARHGAP42 is activated by Src-mediated tyrosine phosphorylation to promote cell motility. Journal of cell science, 130(14), 2382–2393.

International Journal of
Molecular Sciences

MDPI

Article

A Screen for PKN3 Substrates Reveals an Activating Phosphorylation of ARHGAP18

Michal Dibus [1,2], Jan Brábek [1,2] and Daniel Rösel [1,2,*]

[1] Department of Cell Biology, Charles University, Viničná 7, 12800 Prague, Czech Republic; michal.dibus@natur.cuni.cz (M.D.); brabek@natur.cuni.cz (J.B.)
[2] Biotechnology and Biomedicine Centre of the Academy of Sciences and Charles University (BIOCEV), Průmyslová 595, 25242 Vestec u Prahy, Czech Republic
* Correspondence: rosel@natur.cuni.cz

Received: 30 September 2020; Accepted: 17 October 2020; Published: 20 October 2020

Abstract: Protein kinase N3 (PKN3) is a serine/threonine kinase implicated in tumor progression of multiple cancer types, however, its substrates and effector proteins still remain largely understudied. In the present work we aimed to identify novel PKN3 substrates in a phosphoproteomic screen using analog sensitive PKN3. Among the identified putative substrates we selected ARHGAP18, a protein from RhoGAP family, for validation of the screen and further study. We confirmed that PKN3 can phosphorylate ARHGAP18 in vitro and we also characterized the interaction of the two proteins, which is mediated via the *N*-terminal part of ARHGAP18. We present strong evidence that PKN3-ARHGAP18 interaction is increased upon ARHGAP18 phosphorylation and that the phosphorylation of ARHGAP18 by PKN3 enhances its GAP domain activity and contributes to negative regulation of active RhoA. Taken together, we identified new set of potential PKN3 substrates and revealed a new negative feedback regulatory mechanism of Rho signaling mediated by PKN3-induced ARHGAP18 activation.

Keywords: PKN3; phosphorylation; phosphoproteomic screen; ARHGAP18; Rho-GTP

1. Introduction

PKN3 (protein kinase N3) is a serine/threonine kinase belonging to the PKN family of kinases that act downstream of small Rho GTPases. While the expression of PKN1 and PKN2 is ubiquitous in most of the adult tissues [1–3], the expression of PKN3 is restricted mainly to endothelial cells [4], osteoclasts [5,6] and several cancer cell types [7–9]. In endothelial cells, downregulation of PKN3 was shown to block cell migration and formation of tubular structures in both 2D and 3D as a result of impaired actin reorganization [4,10]. Selective targeting of PKN3 expression in endothelial cells by systemic administration of small liposomal siRNA, Atu027, impaired the formation of micro- and macro-metastases in lungs in both experimental and spontaneous metastasis mouse models [11]. In cancer cells, PKN3 was shown to act downstream of activated PI3K (phosphatidylinositol 3-kinase) promoting the malignant progression of prostate cancer [8]. Moreover, downregulation of PKN3 expression led to impaired primary tumor growth and inhibition of metastasis in breast and prostate cancer [9]. Recently, we have identified interaction between PKN3 and adaptor protein p130Cas (Crk-associated substrate; BCAR1 in human) [12] which promotes the pro-malignant growth of cancer cells and could partly explain PKN3-mediated phenotype [13]. The effect of PKN3 expression on regulation of cancer development was further highlighted in PKN3 knock-out mice that showed slower rates of leukemia development induced by the loss of PTEN (phosphatase and tensin homolog) [14] and a decrease in the number of secondary tumor sites [15].

Since PKN3 downstream signaling still remains largely understudied, we decided to perform a phosphoproteomic screen to identify new PKN3 substrates using a chemical genetic approach based on the mutation in gatekeeper residue of the kinase [16,17]. Among the newly identified putative substrates of PKN3, we selected ARHGAP18 (Rho GTPase Activating Protein 18) for validation of the screen and further study.

ARHGAP18—also known as SENEX—is a member of a RhoGAP protein family which plays a role in regulation of activity of small Rho GTPases. Interestingly, ARHGAP18 exhibits different specificity towards individual Rho GTPases. In endothelial cells, ARHGAP18 was shown to act preferentially on RhoC [18], whereas in cancer cells it shows specificity mainly for RhoA [19]. However, recent findings suggest RhoA activity could also be regulated by ARHGAP18 in endothelial cells [20]. ARHGAP18 was found to regulate cell polarization, cell shape and migration of cancer cells [19]. Moreover, it was shown to act downstream of YAP (Yes-associated protein) in regulation of cell shape and tissue tension homeostasis in development [21] and to regulate actin cytoskeleton organization downstream of IP3R3 (inositol 1,4,5-trisphosphate receptor 3) via the RhoA/mDia1/FAK signaling pathway [22]. It associates with microtubules in a GAP domain-dependent manner [23] and localizes to the leading edge during cell spreading and migration [19]. However, the effect of ARHGAP18 expression in cancer cells is still contradictory in individual studies, since inhibition of cancer cell migration, invasion and tumor growth was observed after both overexpression [24] and downregulation [25,26] of ARHGAP18. Moreover, high levels of ARHGAP18 expression were associated with better outcome [27], as well as with worse metastasis-free and overall survival [25]. In endothelial cells, expression of ARHGAP18 contributes to vascular stabilization and acts as a negative regulator of angiogenesis [18]. Overexpression of ARHGAP18 leads to premature senescence of endothelial cells [28]. Recently, it was shown to facilitate athero-protective endothelial cell alignment in response to laminar shear flow [29,30].

In our study, we found that PKN3 interacts with ARHGAP18 and we present strong evidence that PKN3 phosphorylation of ARHGAP18 leads to the activation of its GAP domain, resulting in a decrease of RhoA activity.

2. Results

2.1. Phosphoproteomic Screen for Novel PKN3 Substrates

In order to identify new PKN3 substrates we decided to use an analog-sensitive mutant of PKN3 (PKN3 AS). This approach is based on mutation of the gatekeeper residue allowing the kinase to use synthetic ATP analogs with a bulky group in the N6 position, thus providing specificity to the screen [16]. Therefore, we designed and created PKN3 AS by substitution of Thr639 for glycine. Given the high structural similarity of PKN3 with PKC kinases we chose N6-Benzyl ATPγS (N6-Bn ATPγS) (Figure 1a) for our studies since two of the PKC kinases with a mutation in gatekeeper residue have already been shown to effectively use it [16,31]. To test whether PKN3 AS is able to use N6-Bn ATPγS, we performed a kinase reaction with GST-fused peptide derived from GSK3 in the presence of either ATPγS or N6-Bn ATPγS. Thiophosphorylated substrates were then treated with alkylation agent PNBM (*p*-nitrobenzyl mesylate) and immunoblotted with an antibody recognizing thiophosphate-ester (clone 51-8). As expected, both PKN3 WT and PKN3 AS were able to use ATPγS but N6-Bn ATPγS could only be used by PKN3 AS (Figure 1b). The phosphoproteomic screen was performed in the lysate of MDA-MB-231 breast cancer cells expressing either PKN3 AS or PKN3 KD (kinase dead) as a control. After the reaction, the samples were denatured, digested and the thiol containing peptides were captured using iodoacetyl beads. The phosphopeptides released after the oxidation with Oxone were analyzed by LC MS/MS (liquid chromatography with tandem mass spectrometry) (Figure 1c). The list of the 20 highest-scoring targets with putative PKN3 phosphorylation site is shown in Table 1 (complete list is presented in Supplementary Table S1). We subjected the list of identified putative substrate proteins to GO (gene ontology) enrichment analysis using ShinyGO [32], however, no significant enrichment was found on the FDR (false discovery rate) level of 0.05.

Since PKN3 is a kinase acting downstream of active Rho GTPases and was shown previously to interact with two RhoGAP proteins and phosphorylate them (GRAF1, GRAF2) [33], we decided to choose ARHGAP18 for validation of the screen and further study.

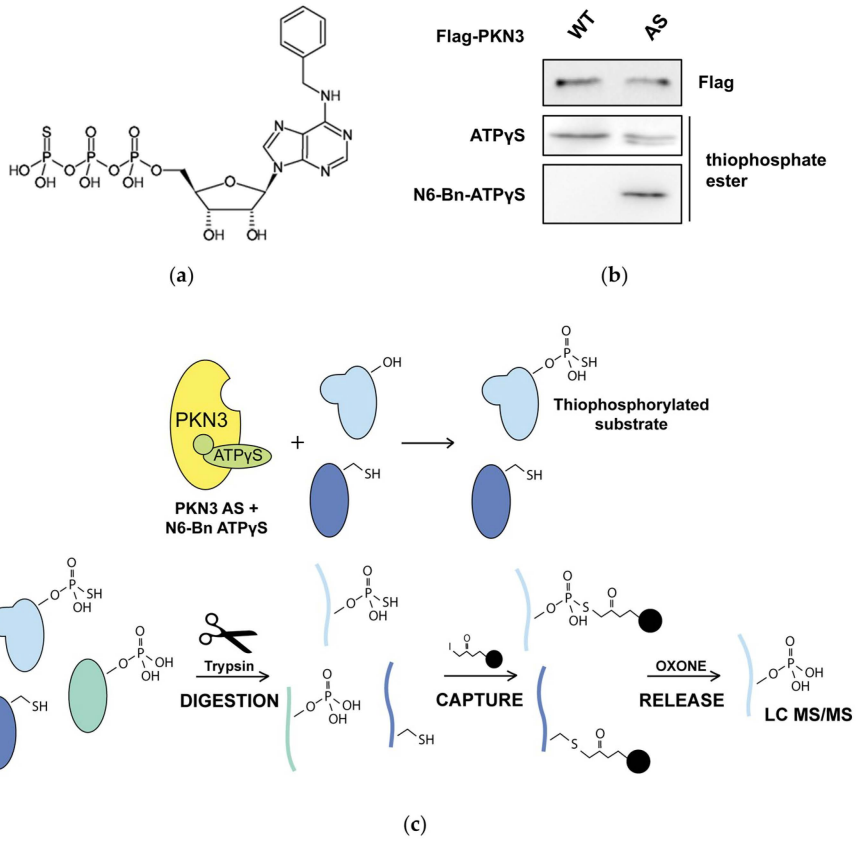

Figure 1. (**a**) Structural formula of N6-Benzyl ATPγS (N6-Bn ATPγS). (**b**) GST-fused peptide derived from GSK3 was used as a substrate in a kinase reaction with either Flag-PKN3 (Protein Kinase N3) WT or AS (analog sensitive). ATPγS or N6-Bn ATPγS were used as cofactors for phosphorylation. Thiophosphorylated substrates were alkylated with PNBM (*p*-nitrobenzyl mesylate) and immunoblotted with anti-thiophosphate ester antibody. (**c**) An outline of the phosphoproteomic screen: PKN3 AS thiophosphorylates its substrates using N6-Bn ATPγS in a lysate of MDA-MB-231 cells. Proteins are denatured and digested by trypsin. Thiol-containing peptides are captured by iodoacetyl beads and after oxidation only phosphopeptides are released and analyzed by LC MS/MS (liquid chromatography with tandem mass spectrometry).

Table 1. The list of 20 putative PKN3 substrates with the highest identification score. Surrounding sequence of +/−8 amino acids around the identified phosphosite is shown. PLP—phosphosite localization probability.

Gene	Site	Surrounding Sequence	PLP	Score
ARHGAP18	T158	KRVETVSQTLRKKNKQY	1.00	111.46
	S156	VQKRVETVSQTLRKKNK	1.00	111.46
BRD4	S601	SKPPPTYESEEEDKCKP	1.00	101.9
CCDC144A	S805	EMARKKMNSEISHRHQK	0.99	82.029
CEACAM16	T402	NLTDTGRYTLKTVTVQG	1.00	100.25
	T398	VQKLNLTDTGRYTLKTV	1.00	100.25
DCAF12L1	S8	_MAQQQTGSRKRKAPAV	1.00	83.801
DSCAM	S1408	LPGDNGGSSIRGYILQY	0.98	87.498
IGSF22	S318	LSVGDKRMSAELTVLDE	0.99	84.817
KIF27	S754	TGNDAKSVSKQYSLKVT	1.00	120.77
	T746	DLIKELIKTGNDAKSVS	0.99	120.77
NFE2L2	T137	KLHHNYKITIYSM____	1.00	99.139
ODF1	S10	AALSCLLDSVRRDIKKV	1.00	103.7
OR4K15	T158	ICKPLHYMTVMSRRVCV	0.99	79.906
POLE1	S891	VKKPKVTISYPGAMLNI	1.00	82.483
	T889	TNVKKPKVTISYPGAML	1.00	82.483
PRDM16	S1218	DVLNSTLDSEALKHTLC	0.99	96.371
RETSAT	S322	VLTKATVQSVLLDSAGK	0.98	99.53
SACS	S1222	GIFTKPSLSAVLKHFKI	1.00	86.512
SPATA31D1	T1339	VLGSKSSPTLKTQPPPE	0.87	86.189
USP42	T786	PRDPGTPATKEGAWEAM	1.00	93.096
UTP20	S926	HLQVFSKFSNPRALYLE	1.00	101.65
VPS33B	S476	AGKITDAFSSLAKRSNF	0.78	83.206
	S477	GKITDAFSSLAKRSNFR	0.78	83.206
VWA3B	T99	EDGRVYNLTAKSELIYQ	1.00	84.244

2.2. *ARHGAP18 is Phosphorylated by PKN3*

In the phosphoproteomic screen we identified two phosphorylated residues in the sequence of ARHGAP18 – Ser156 and Thr158. Interestingly, we noticed that although phosphorylation of Thr154 did not appear in our phosphoproteomic results, the region surrounding this residue strongly resembles the PKN3 phosphorylation consensus motif [34], mainly due to the presence of a preferred arginine residue in the position -3, suggesting it could be also phosphorylated by PKN3. To validate our results and hypothesis, we fused the first 200 amino acids of ARHGAP18 to GST (GST-N200), substituted Thr154, Ser156 and Thr158 for unphosphorylatable alanine (GST-N200 TST-AAA) and subjected to in vitro kinase reaction. Since there are no phospho-specific antibodies available for ARHGAP18 we used ATPγS as a cofactor for phosphorylation with subsequent alkylation to detect PKN3-mediated phosphorylation as described above. As shown in Figure 2a, GST-N200 was readily phosphorylated by PKN3, however, the substitution of the candidate sites for alanine led to a significant reduction of phosphorylation (Figure 2a,b). In order to support our results, we further performed an in vitro kinase reaction also with the full-length GFP-fused variants of ARHGAP18 (WT and TST-AAA). As expected, PKN3 was able to phosphorylate also the full-length ARHGAP18 (upper band) and, importantly, phosphorylation of GFP-ARHGAP18 TST-AAA was reduced to a comparable extent as in GST-N200 (Figure 2c,d). These results support our data from phosphoproteomic screen and suggest that ARHGAP18 can be phosphorylated by PKN3 on Thr154, Ser156 and Thr158.

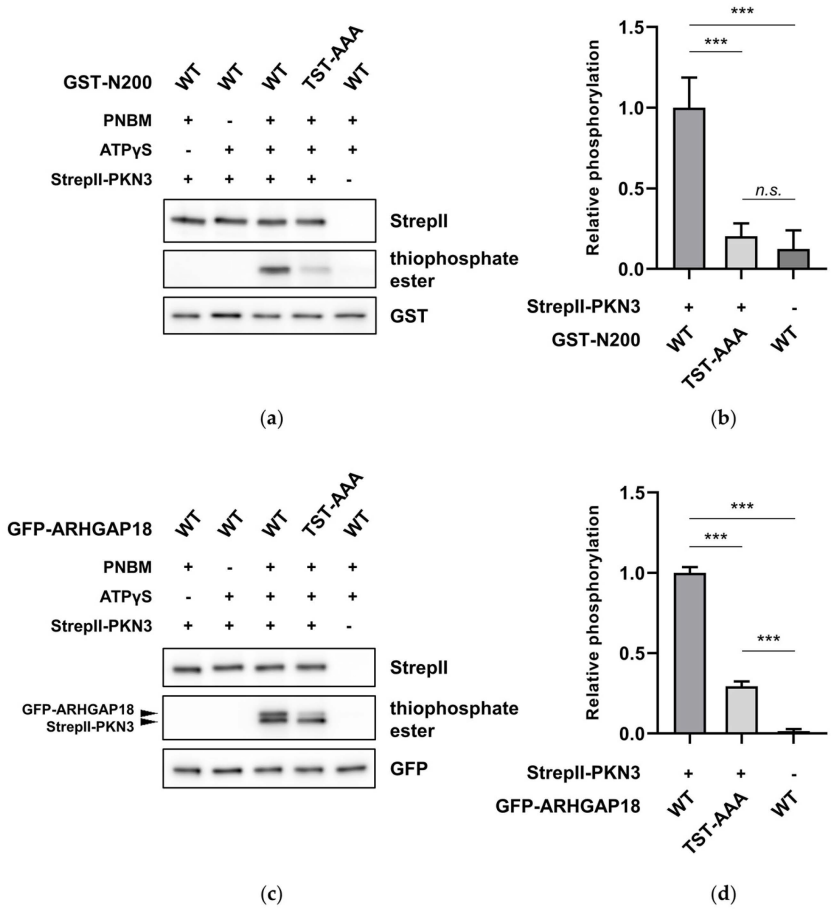

Figure 2. PKN3 phosphorylates ARHGAP18 (Rho GTPase Activating Protein 18) on Thr154, Ser156 and Thr158. An in vitro kinase reaction of WT and unphosphorylatable TST-AAA (Thr154, Ser156 and Thr158 to alanine) variants of (**a**) GST-fused fragment of ARHGAP18 comprising the first 200 amino acids or (**c**) the full-length GFP-ARHGAP18 (upper band; lower band corresponds to StrepII-PKN3 autophosphorylation) in the presence of StrepII-PKN3 and ATPγS. Thiophosphorylated substrates were treated with PNBM and immunoblotted using anti-thiophosphate ester antibody. Reactions with ATPγS or PNBM only were used as specificity controls. Quantification of relative phosphorylation from three independent experiments is shown for both (**b**) GST-N200 and (**d**) full-length GFP-ARHGAP18 variants. Statistical analysis was performed using ANOVA with Tukey's multiple comparison test: *** $p \leq 0.001$, n.s.—not significant.

2.3. PKN3 Interacts with ARHGAP18 via its N-Terminal Region

PKN3 was shown to directly interact with two other Rho-GAP proteins from the Graf family via their SH3 domain [33]. Therefore, we next analyzed whether PKN3 and ARHGAP18 can also interact with each other. Since there is no SH3 domain in ARHGAP18 we decided to narrow down the potential interaction interface producing mutants of GFP-ARHGAP18 deleting either the first 200 amino acids (ΔN200), the region between amino acids 201 and GAP domain (Δ201-323), GAP domain (ΔGAP) or the *C*-terminal region following the GAP domain (ΔC525) (Figure 3a). Co-immunoprecipitation of individual deletion mutants with Flag-PKN3 indicated there is indeed an interaction between ARHGAP18 and PKN3. Surprisingly, GFP-ARHGAP18 Δ201-323, ΔGAP and ΔC525 exhibited very strong interaction with PKN3 when compared to full-length GFP-ARHGAP18 and ΔN200 (Figure 3b). This suggested that the interaction is mediated via the *N*-terminal part of ARHGAP18 and is inhibited by the following regions. To test this, we created a construct comprising only the first 200 amino acids fused to GFP (N200) and subjected to co-immunoprecipitation with Flag-PKN3. We observed a significant increase in binding of the GFP-ARHGAP18 N200 with PKN3 when compared to full-length GFP-ARHGAP18

(Figure 3c). To further specify the region of interaction we created deletion mutants of GFP-ARHGAP18 N200 sequentially lacking 50 amino acids: 1–50 (N200 Δ1–50), 51–100 (N200 Δ51–100), 101–150 (N200 Δ101–150) or 151–200 (N200 Δ151–200). Deletion of the first 50 amino acids (GFP-ARHGAP18 N200 Δ50) led to strong decrease of the binding to PKN3 suggesting that the binding sequence resides within this region (Figure 3d). To further confirm our results, we performed a pull-down of GFP-PKN3 with GST-bound fragment of ARHGAP18 containing only the first 50 amino acids (N50). As anticipated, we were able to pull-down GFP-PKN3 with GST-ARHGAP18 N50 but not with GST alone (Figure 3e). To finally pinpoint the binding sequence, we created deletion mutants of GFP-ARHGAP18 N200 lacking the amino acids 1–12, 13–25, 26–37 or 38–50 and subjected to co-immunoprecipitation. We found that both GFP-ARHGAP18 N200 Δ1–12 and Δ13–25 almost completely lost the ability to interact with PKN3 (Figure 3f). Taken together, these results suggest PKN3 is able to interact with ARHGAP18 and the first 25 amino acids of ARHGAP18 are necessary for the interaction.

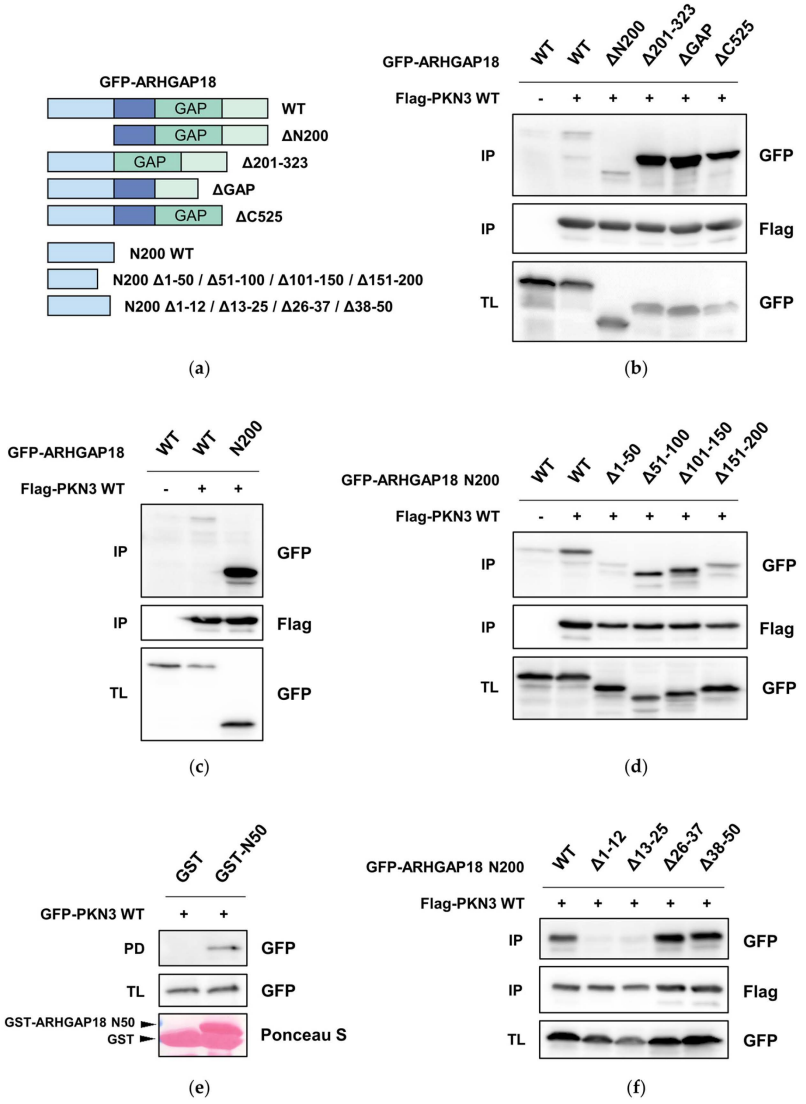

Figure 3. ARHGAP18 interacts with PKN3 (**a**) Schematic representation of ARHGAP18 mutants used throughout the study. (**b**–**d**,**f**) Co-immunoprecipitation experiments of indicated GFP-ARHGAP18 variants with Flag-PKN3. (**e**) Pull-down of GFP-PKN3 using either GST only or GST-fused fragment encompassing the first 50 amino acids of ARHGAP18 (GST-ARHGAP18 N50). All the samples were subjected to SDS-PAGE and immunoblotted with respective antibodies. GST-fused proteins were stained using Ponceau S staining. IP—immunoprecipitation; PD—pull-down; TL—total lysate.

2.4. Phosphorylation of ARHGAP18 Isoform1 but not Isoform2, Promotes Interaction with PKN3

Two isoforms of ARHGAP18 have been described with the only difference between the two being, that isoform 2 (Iso2) is missing the first 45 amino acids [18,19]. Since we showed that the interaction of ARHGAP18 with PKN3 is predominantly mediated via the first 25 amino acids of ARHGAP18, we hypothesized there could be a difference in interaction of individual ARHGAP18 isoforms with PKN3. Therefore, we created GFP-ARHGAP18 Iso2 WT by deleting the first 45 amino acids and showed that, indeed, ARHGAP18 Iso2 almost completely lost the ability to interact with PKN3 (Figure 4a). Interestingly, despite the differences in the ability of individual ARHGAP18 isoforms to interact with PKN3, both isoforms can be phosphorylated by PKN3 to a similar extent (Figure 4b). To test whether ARHGAP18 phosphorylation could affect its interaction with PKN3, we created a phosphomimicking mutant of ARHGAP18 by substitution of Thr154, Ser156 and Thr158 for aspartate (TST-DDD). In a co-immunoprecipitation of either phosphomimicking (TST-DDD) or unphosphorylatable (TST-AAA) variant of ARHGAP18 with Flag-PKN3 we observed more than three-fold increase in the interaction of ARHGAP18 TST-DDD with PKN3 when compared to WT (Figure 4c,d). Finally, we showed that interaction with PKN3 was promoted only in case of TST-DDD but not Iso2 TST-DDD ARHGAP18 (Figure 4e,f). These results suggest PKN3 is able to phosphorylate both ARHGAP18 isoforms but only Iso1 exhibits increased interaction with PKN3 after phosphorylation.

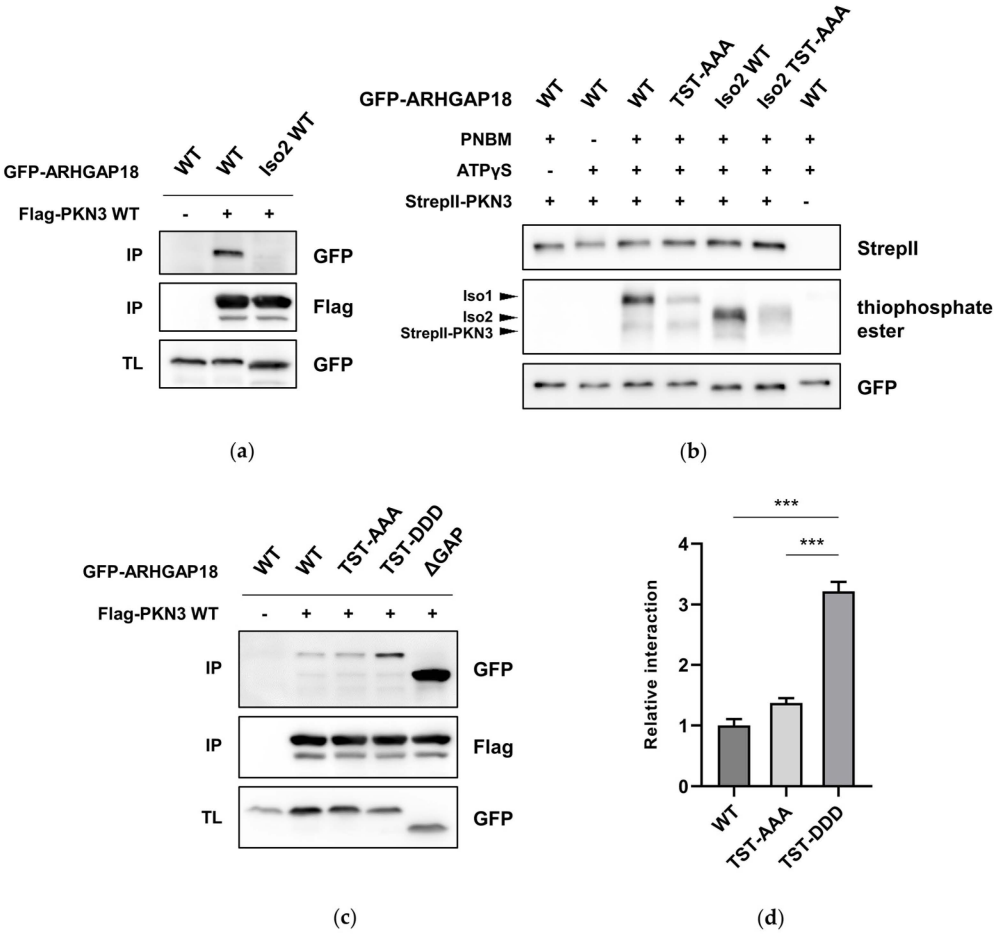

Figure 4. *Cont.*

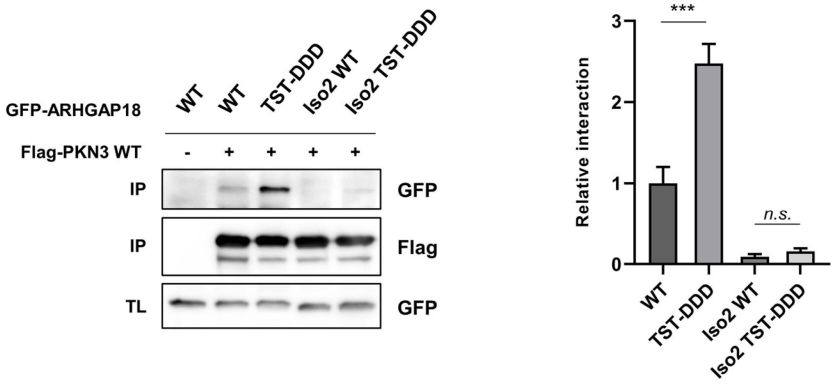

(**e**) (**f**)

Figure 4. Differential effects of ARHGAP18 isoforms. (**a**) GFP-ARHGAP18 WT and Iso2 (isoform 2) WT were immunoprecipitated with Flag-PKN3 using Anti-Flag Affinity Gel. Samples were subjected to SDS-PAGE and immunoblotted with the respective antibodies. (**b**) An in vitro kinase reaction of WT and unphosphorylatable (TST-AAA) variants of both GFP-ARHGAP18 isoforms in the presence of StrepII-PKN3 and ATPγS. Thiophosphorylated substrates were treated with PNBM and immunoblotted using anti-thiophosphate ester antibody. Reactions with ATPγS or PNBM only were used as specificity controls. (**c**,**e**) Individual variants of GFP-ARHGAP18 were immunoprecipitated with Flag-PKN3. Samples were subjected to SDS-PAGE and immunoblotted using respective antibodies. (**d**,**f**) Quantification of three independent immunoprecipitation experiments is shown. Statistical analysis was performed using ANOVA with (**d**) Dunnett's or (**f**) Tukey's multiple comparison test: *** $p \leq 0.001$; n.s.—not significant. IP—immunoprecipitation; TL—total lysate.

2.5. Phosphorylation of ARHGAP18 Leads to Activation of Its GAP Domain

To assess whether the phosphorylation of ARHGAP18 could have some effect on its function we first focused on the levels of active RhoA. U2OS cells expressing individual variants of GFP-ARHGAP18 were subjected to RhoA-GTP pull-down assay using immobilized GST-Rhotekin. Interestingly, a significant decrease in the levels of active RhoA was observed in cells expressing GFP-ARHGAP18 TST-DDD when compared to WT suggesting that phosphorylation of ARHGAP18 leads to activation of its GAP domain (Figure 5a,b). To support our results, we analyzed the effect of ARHGAP18 phosphorylation on the activation of its GAP domain by a pull-down assay using constitutively active RhoA (RhoA CA). We observed that the phosphomimicking variant of both ARHGAP18 isoforms displayed a substantial increase in interaction with RhoA CA when compaired to the corresponding WT (Figure 5c,d). Taken together, these data suggest phosphorylation of ARHGAP18 by PKN3 leads to activation of ARHGAP18 GAP domain resulting in decrease of the levels of active RhoA.

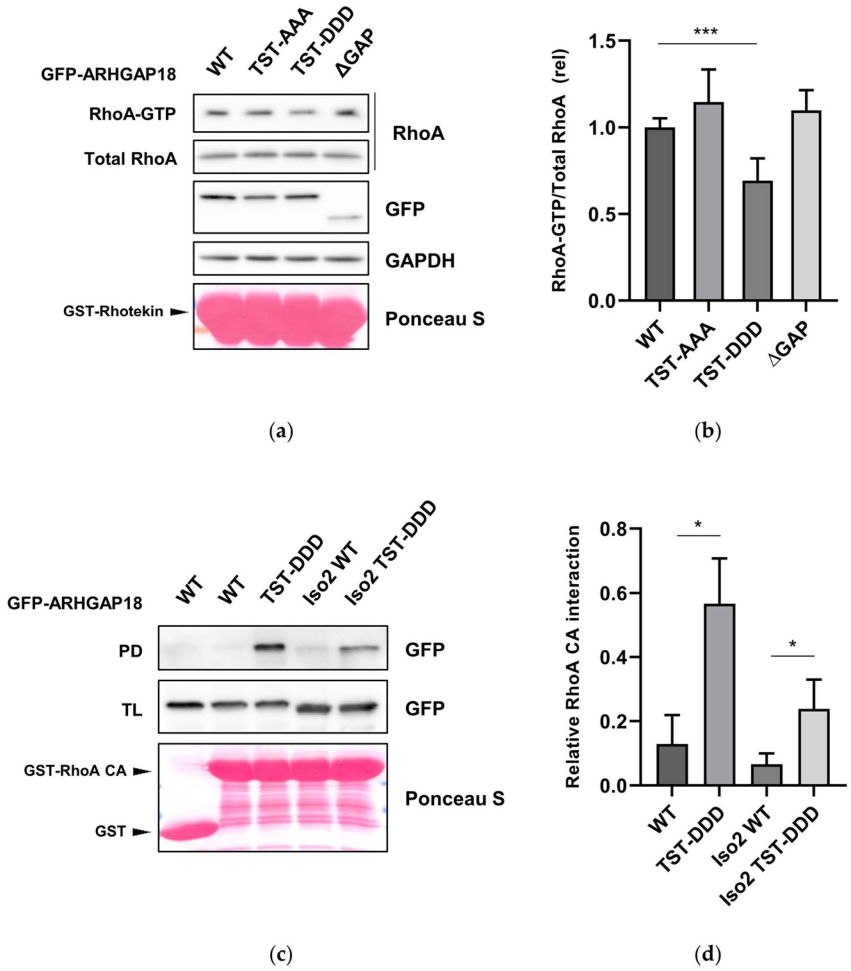

Figure 5. Phosphorylation of ARHGAP18 by PKN3 leads to activation of its GAP domain (**a**) U2OS cells expressing indicated variants of GFP-ARHGAP18 were subjected to pull-down of active RhoA using GST-fused Rhotekin. (**b**) Quantification of three independent RhoA-GTP pull-down experiments was performed. (**c**) Pull-down of individual GFP-ARHGAP18 variants using GSH-agarose-bound constitutively active RhoA (RhoA CA). (**d**) Quantification of three independent pull-down experiments using GST-RhoA CA is shown. All the samples were subjected to SDS-PAGE and immunoblotted with respective antibodies. GST-Rhotekin and GST-RhoA CA were stained by Ponceau S. Statistical analysis was performed using ANOVA with (**b**) Dunnett's multiple comparison test: * $p \leq 0.05$ and *** $p \leq 0.001$. PD—pull-down; TL—total lysate.

3. Discussion

Although PKN3 is an important effector kinase of small Rho GTPases and a key player in regulation of processes such as cytoskeleton organization [4], proliferation and promotion of malignant growth of various cancer types [8,9,13], its downstream signaling remains largely understudied. In order to identify novel PKN3 substrates we performed a phosphoproteomic screen using analog sensitive PKN3. We identified 418 putative PKN3 phosphorylation sites in 281 proteins. Surprisingly, however, we found no significant functional enrichment in GO terms among the newly identified substrates. Recently, another screen for PKN3 substrates was performed using JZ128, a new selective covalent inhibitor of PKN3 in a novel chemoproteomic approach—CITe-Id (Covalent Inhibitor Target-site Identification) [35]. When we compared the two datasets, three proteins were identified in both of the screens – ARFGEF2, FAM21A and LRRC16A (Figure 6a). Both FAM21A, a component of the WASH complex and LRRC16A, also known as CARMIL, were shown to play a role in regulation of actin remodeling [36–38], highlighting the possible signaling crosstalk with PKN3. It is also surprising that

proteins previously reported to be phosphorylated by PKN3, such as GRAF1, GRAF2 or BCAR1 [13,33] were not identified as PKN3 substrates in any of the screens.

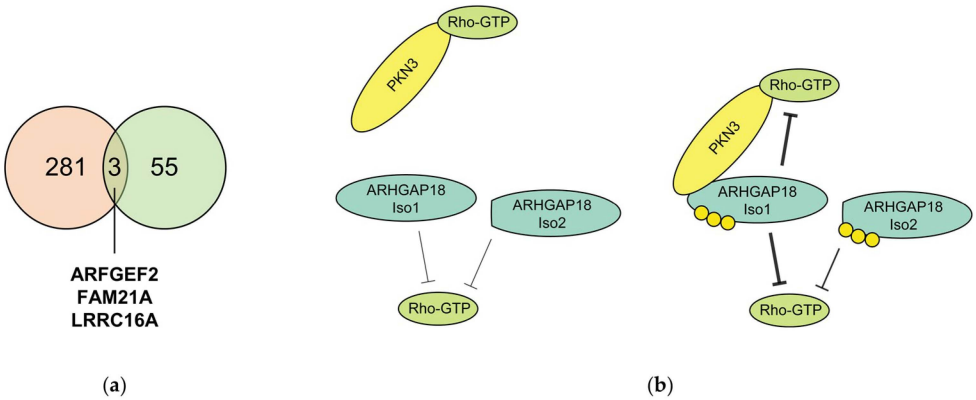

Figure 6. (**a**) Venn diagram representing the overlap between the proteins identified as putative PKN3 substrates in this study (orange) and the phosphoproteomic data presented in Browne et al., 2019 (green) [35]. Three genes were identified in both datasets: ARFGEF2, FAM21A and LRRC16A. (**b**) A model proposing PKN3-mediated regulation of ARHGAP18 activity. ARHGAP18 in its unphosphorylated form exhibits low GAP activity and its *N*-terminus is potentially sterically blocked and therefore inaccessible for interactions. ARHGAP18 phosphorylation (yellow circles) by PKN3 induces structural change leading to activation of GAP domain and in case of ARHGAP18 Iso1 also to great strengthening of ARGAP18 and PKN3 interaction mediated by the release of its *N*-terminus which becomes accessible for interaction with PKN3.

Among the identified putative substrates of PKN3 we selected ARHGAP18 for further study and validation. In an in vitro kinase reaction using either truncated or full-length protein we confirmed that PKN3 is able to phosphorylate ARHGAP18 on Thr154, Ser156 and Thr158. Although there are 80 serine and threonine residues present in the 663 amino acids-long sequence of ARHGAP18, mutation in these three candidate sites alone was sufficient to substantially impair the phosphorylation of ARHGAP18 by PKN3, suggesting the candidate sites are phosphorylated in a highly specific-manner. However, since the decrease in phosphorylation was not complete, we expect there are another residues in the sequence of ARHGAP18 phosphorylated by PKN3. We next found that PKN3 is able to interact with ARHGAP18 and we mapped the interaction interface to the first 25 amino acids in the sequence of ARHGAP18. Importantly, this region is missing in ARHGAP18 Iso2 which is translated from an alternative downstream start codon [18,19]. Interestingly, although we observed differences in interaction of PKN3 with individual isoforms of ARHGAP18, both isoforms were phosphorylated to a similar extent. It is notable, that phosphorylation of several RhoGAP proteins was reported to have different effects on their function [39–41]. Recently, we have described an activating phosphorylation of ARHGAP42 Tyr376 by Src kinase [42]. Similarly, we found that phosphorylation of ARHGAP18 by PKN3 on Thr154, Ser156 and Thr158 leads to activation of its GAP domain, thus decreasing the levels of active RhoA.

Notably, PKN3 and ARHGAP18 share a lot of similar traits in the signaling of endothelial cells. After downregulation of either ARHGAP18 or PKN3 in endothelial cells, the cells lose the capacity of characteristic tube formation in both 2D and 3D environment [4,10,28] and exhibit disrupted cell junctions [10,18]. Recently, the role of ARHGAP18 has been extensively studied in the context of atherosclerosis, a chronic inflammatory disease of the arteries [43]. ARHGAP18 was shown to act as an anti-inflammatory and athero-protective gene that facilitates flow-responsive endothelial cell alignment via ARHGAP18/YAP axis [29,30]. Interestingly, PKN3 was identified in a module of genes associated to transendothelial migration of leukocytes leading to coronary artery disease [44]. Moreover, depletion of PKN3 was shown to attenuate pro-inflammatory activation of endothelial cells caused

by defects in glycosylation of ICAM-1 adhesion molecules, suggesting its potential involvement in the promotion of atherosclerosis [10,15]. Finally, PKN3 has been recently demonstrated to play a role in bone resorption downstream of non-canonical Wnt5a/ Ror2 signaling cascade [5,6] that regulates the secretion of pro-inflammatory cytokines necessary for atherosclerosis development [45]. All these findings highlight potential crosstalk of ARHGAP18 and PKN3 and should be considered in the future research.

Based on our results we propose a model, where ARHGAP18 in its unphosphorylated form exhibits low GAP activity and its *N*-terminus is potentially sterically blocked and, therefore, inaccessible for interactions. ARHGAP18 phosphorylation induces structural change leading to activation of GAP domain and in case of ARHGAP18 Iso1 also to a great strengthening of ARHGAP18 and PKN3 interaction mediated by the release of its *N*-terminus, which becomes accessible for interaction with PKN3. Our data also suggest that phosphorylation of both ARHGAP18 isoforms could facilitate a negative feedback loop in regulation of signaling mediated by Rho GTPases. In case of ARHGAP18 Iso1 this feedback mechanism is further strengthened by formation of a ternary complex between ARHGAP18, PKN3 and Rho GTPases (Figure 6b).

Taken together, based on the results of our phosphoproteomic screen we identified ARHGAP18 as a new PKN3 substrate and interaction partner. We showed that phosphorylation of ARHGAP18 by PKN3 leads to activation of its GAP domain and contributes to regulation of active RhoA levels, implying the possible crosstalk of PKN3 and ARHGAP18 signaling in cancer and other diseases. We also believe the results of our screen will serve as a basis for better understanding of PKN3 signaling and its future study.

4. Materials and Methods

4.1. Cell Lines and Cell Cultivation

All the cell lines were cultured in DMEM (Sigma, Piscataway, NJ, USA) supplemented with 10% FBS (Sigma, Piscataway, NJ, USA) and 10 µg/mL ciprofloxacin (Sigma, Piscataway, NJ, USA) in humidified incubator with 5% CO_2. U2OS cells were purchased from ATCC (#HTB-96), MDA-MB-231 cells were obtained from Dr. Zadinová as described previously [13]. Unless otherwise stated, all the experiments were performed using MDA-MB-231 cells.

4.2. Plasmid Construction

Human Flag-PKN3 WT and KD (kinase dead) in pcDNA3, as well as StrepII-PKN3 in pcDNA3 were used previously [13]. Analog-sensitive (AS, T639G) PKN3 was designed based on a prediction of gatekeeper residue as described in Hertz et al. [17] and created using Q5® Site-Directed Mutagenesis Kit (New England Biolabs, Ipswich, MA, USA) following the manufacturer's instructions with the corresponding primers (T639G F/ R) listed in Supplementary Table S2.

cDNA encoding human ARHGAP18 isoform 1 was newly synthesized using GeneArt Gene Synthesis (Thermo Scientific, Waltham, MA, USA) (sequence shown in Supplementary Table S3). Silent mutations were introduced in the design of ARHGAP18 cDNA in order to disrupt *XhoI*, *SacI*, *BamHI* and *NcoI* restriction sites. Synthesized sequence was cloned into pEGFP c1 vector using *BglII* and *EcoRI* sites. ARHGAP18 N200 constructs were created by PCR amplification with respective primers (ARHGAP18 N200 F/R), digested with *EcoRI/BamHI* and cloned into pEGFP c1 via *EcoRI/BglII* sites and into pGEX 2T bacterial expression vector via *EcoRI/BamHI* sites. All the mutants of ARHGAP18 WT or N200 (Iso2 WT, ΔN200, Δ201-323, ΔGAP, ΔC525, TST-AAA, TST-DDD, Iso2 TST-DDD and Iso2 TST-AAA) in either pEGFP c1 or pGEX 2T were created by whole plasmid synthesis approach (WHOPS) with Pfu-X7 polymerase and subsequent *DpnI* treatment with the respective primers listed in the Supplementary Table S2. The deletion variants of ARHGAP18 N200 (Δ1–50, Δ51–100, Δ101–150, Δ151–200, Δ1–12, Δ13–25, Δ26–37, Δ38–50) were created using WHOPS using the primers listed in the Supplementary Table S2 and ARHGAP18 N200 WT pEGFP c1 as a template. GST-RHG18 N50

construct was created by PCR amplification with ARHGAP18 N200 F and ARHGAP18 N50 R primers and cloned into pGEX 2T bacterial expression vector via *EcoRI*/*BamHI* sites. All the created constructs were verified by sequencing.

4.3. Protein Expression and Purification

GST alone and GST-fused proteins (GST-GSK3 peptide, GST-ARHGAP18 N200 WT/TST-AAA, GST-Rhotekin, GST-RhoA CA (G14V)), were purified using BL21 (DE3) *E. coli* strain. Briefly, cells were grown in 1.5 × LB medium (Duchefa Biochemie, Haarlem, The Netherlands) and cultured to 0.8 OD_{595}. IPTG was added to the final concentration of 0.4 mM and incubated overnight at room temperature. Proteins were purified from cleared lysates using Pierce® Glutathione Agarose (Thermo Scientific, Waltham, MA, USA).

4.4. Screen for PKN3 Substrates, Sample Preparation and Data Analysis

The screen was performed following the protocol published by Hertz and colleagues [17]. Briefly, lysates of MDA-MB-231 cells transfected with either PKN3 AS or PKN3 KD were prepared using 1% Triton X-100 (Sigma, Piscataway, NJ, USA) in TBS (50 mM Tris-HCl, pH 7.1 (20 °C), 150 mM NaCl), sonicated and cleared by centrifugation. For each sample, 3 mg of total protein was used and kinase reactions were incubated for 40 min at room temperature in the presence of 200 µM ATP (Sigma, Piscataway, NJ, USA), 3 mM GTP (Sigma, Piscataway, NJ, USA) and 200 µM N^6-benzyl-ATPγS (Jena Bioscience, Jena, Germany). Afterwards, denaturation buffer (8 M Urea (Sigma, Piscataway, NJ, USA), 10 mM TCEP (Sigma, Piscataway, NJ, USA), 100 mM NH_4HCO_3 (Sigma, Piscataway, NJ, USA), 2 mM EDTA (Sigma, Piscataway, NJ, USA)) was added to the samples to 6 M final concentration of Urea, incubated for 1 h at 55 °C and cooled to RT for 10 min. Samples were diluted using 50 mM NH_4HCO_3 to a 2 M final concentration of Urea and 1 M TCEP was added to final concentration of 10 mM. 50 µg of Trypsin (Thermo Scientific, Waltham, MA, USA) was added to each sample and incubated overnight in 37 °C with gentle agitation. Samples were then acidified to the final concentration of 0.1% TFA (Sigma, Piscataway, NJ, USA) and peptides were extracted using Oasis® PRiME HLB columns (Waters, Milford, MA, USA). Peptides washed with 0.1% TFA in water were eluted with 1 mL of 0.1% TFA in 50% Acetonitrile in water and concentrated to 50 µL using speed vacuum. For capture of thiophosphorylated peptides, 100 µL of UltraLink® Iodoacetyl beads (Thermo Scientific, Waltham, MA, USA) per sample was washed with 200 mM HEPES pH 7.0 and blocked for 10 min in dark with 5 µL of 5 mg/mL BSA (Sigma, Piscataway, NJ, USA) in 50% Acetonitrile 50% 20 mM Hepes pH 7.0. Samples adjusted to a final concentration of 20 mM HEPES pH 7.0 and 50% Acetonitrile were added to the beads and incubated in dark place overnight at RT. After incubation, the beads were washed in the following order with 1 mL of water, 5 M NaCl, 50% Acetonitrile, 5% Formic Acid and incubated in 10 mM DTT for 10 min. Finally, samples were eluted for 10 min in 1 mg/mL OXONE (Sigma, Piscataway, NJ, USA) pH 3.5, desalted with ZipTip and analyzed by Thermo Orbitrap Fusion coupled with Thermo Ultimate 3000 HPLC. Raw data were analyzed using MaxQuant software with MaxLFQ algorithm and the MS/MS spectra were searched against Uniprot-SwissProt human database both in forward and reverse using Andromeda search engine. Search parameters were set to standard trypsin digestion with two missed cleavages, variable *N*-terminal carbamylation, variable methionine oxidation and variable serine/threonine phosphorylation with the maximum number of modifications per peptide set to 5. The identified peptides were filtered based on 1% FDR. For selection of putative PKN3 phosphorylation sites, all the phosphosites identified in the control samples were eliminated from the analysis, together with phosphopeptides with localization probability below the cutoff value 0.75.

4.5. Immunoprecipitation and Immunoblotting

MDA-MB-231 cells were transfected using PEI (Polysciences, Inc.,Warrington, PA, USA). After 48 h, the cells were washed with ice-cold PBS, lysed using 1% Triton X-100 in TBS (50 mM Tris-HCl, pH 7.1 (20 °C), 150 mM NaCl) and the lysates were cleared by centrifugation. Subsequently, 20 µL

of Anti-Flag Affinity Gel (Bimake, Houston, TX, USA) was added to each lysate and rotated for 3 h in 4 °C. After the incubation, the beads were washed twice with ice-cold lysis buffer, once with TBS and resuspended in SDS-PAGE sample buffer. After the separation of the samples using gradient SDS polyacrylamide gels (6–15%), proteins were transferred to Amersham Protran 0.45 µm nitrocellulose membrane (GE Healthcare, Chicago, IL, USA) using Transblot Turbo (Bio-Rad Laboratories, Hercules, California, CA, USA) in a buffer containing 300 mM Tris, 300 mM Glycine, 0.025% SDS and 20% EtOH. After the transfer, the membranes were stained in Ponceau S (Sigma, Piscataway, NJ, USA) for total protein, washed in TBS and blocked with 4% BSA (Sigma, Piscataway, NJ, USA) in TBS for 30 min in RT. The membranes were incubated with respective antibodies diluted in 1% BSA (Sigma, Piscataway, NJ, USA) in TBST overnight in 4 °C. The antibody against thiophosphate ester (clone 51-8, Abcam, Cambridge, UK) was diluted 1:5000 in 5% milk in TBST. Secondary antibodies were diluted in 2% milk in TBST. The membranes were developed with either WesternBright ECL (Advansta, San Jose, CA, USA) or SuperSignal™ West Femto Maximum Sensitivity Substrate (Thermo Scientific, Waltham, MA, USA) using Amersham Imager 600 (GE Healthcare, Chicago, IL, USA).

4.6. Antibodies

StrepII Tag antibody (clone 517, #NBP2-43735) was purchased from Novus Biologicals. Anti-thiophosphate ester antibody (clone 51-8, #ab133473) and GFP antibody used for immunoblotting (#ab290) were purchased from Abcam (Cambridge, UK). RhoA antibody (clone 67B9, #2117) was purchased from Cell Signaling Technology. GFP antibody used for immunoprecipitation (clone 3E6, #A-11120) was purchased from Invitrogen. Flag tag monoclonal antibody (clone M2, #F1804) and GST antibody (#G7781) were purchased from Sigma.

4.7. Kinase Assays

Kinase assays were performed as described previously [13]. Briefly, StrepII-PKN3-transfected MDA-MB-231 cells were lysed using 1% Triton X-100 in TBS (50 mM Tris-HCl, pH 7.1 (20 °C), 150 mM NaCl) supplemented with 10 mM Glycerol-2-Phosphate (Sigma, Piscataway, NJ, USA) and inhibitors of proteases and phosphatases (1:100 each, Bimake, Houston, TX, USA). The kinase was precipitated from the cleared lysate for 3 h in 4 °C using Strep-Tactin® Superflow® resin (IBA Lifesciences, Göttingen, Germany) and eluted with 1.25× Buffer E (Strep-Tactin Elution Buffer, IBA Lifesciences, Göttingen, Germany).

As a positive control for testing of PKN3 AS, a peptide derived from GSK3 was used [9]. GST-fused *N*-terminal fragments of ARHGAP18 (N200 WT, N200 TST-AAA) were produced and purified as described above (see Protein expression and purification). For the kinase assays of full-length ARHGAP18 proteins, individual GFP-ARHGAP18 variants (WT, TST-AAA, Iso2 WT, Iso2 TST-AAA) were immunoprecipitated from transiently transfected U2OS cells. Lysates were prepared with the lysis buffer containing 1% Triton X-100 in TBS as described above and proteins were precipitated using anti-GFP 3E6 antibody (Invitrogen) and Protein A Sepharose 4 Fast Flow (GE Healthcare, Chicago, IL, USA). Immobilized proteins were eluted using 0.1 M Glycine pH 3.5 for 10 min in RT, corresponding volume of 1 M Tris pH 9.2 was added to adjust the pH to 7.5 and eluted proteins were used as a substrate in kinase reaction.

All the kinase reactions were carried out in the kinase buffer containing 30 mM Tris pH 7.5, 4 mM $MgCl_2$ (Sigma, Piscataway, NJ, USA), 10 mM Glycerol-2-Phosphate (Sigma, Piscataway, NJ, USA) and 5 mM DTT (Sigma, Piscataway, NJ, USA). N^6-benzyl-ATPγS or ATPγS were used as indicated in the final concentration of 1 mM. Reactions were incubated for 45 min in 35 °C and stopped by adding 0.5 mM EDTA pH 8.0 to the final concentration of 20 mM. Thiophosphorylated proteins were then alkylated with 50 mM PNBM (*p*-Nitrobensyl mesylate) (Abcam, Cambridge, UK) at RT for 2 h, subjected to SDS-PAGE and immunoblotted using anti-thiophosphate ester antibody (clone 51-8, Abcam, Cambridge, UK).

4.8. RhoA-GTP Pull-Down Assay

For the analysis of active RhoA, U2OS cells were transfected with individual variants of GFP-ARHGAP18 (WT, TST-AAA, TST-DDD, ΔGAP) or GFP alone, starved for 3 h and then lysed in 1% Triton X-100 in TBS (50 mM Tris-HCl, pH 7.1 (20 °C), 150 mM NaCl) with inhibitors of proteases and phosphatases (1:100, Bimake, Houston, TX, USA) after 5 min stimulation by DMEM with 10% FBS. The lysates were centrifuged (13,000× *g*, 13 min) and the supernatants were equalized for total protein (DC™ Protein Assay, Bio-Rad, Hercules, California, CA, USA). Agarose-bound GST-Rhotekin (20 µg) was added to each lysate and rotated for 45 min in 4 °C. Afterwards, the beads were washed twice with ice-cold lysis buffer, once with TBS and resuspended in SDS-PAGE sample buffer. The samples were subjected to SDS-PAGE and immunoblotted with respective antibodies as described above.

4.9. RhoA Pull-Down Assay

The RhoA pull-down assay was performed using purified constitutively active form of RhoA (RhoA-CA, G14V) as described in García-Mata et al. [46]. Cells transfected with individual variants of GFP-ARHGAP18 were washed twice with ice-cold HBS (20 mM HEPES pH 7.5, 150 mM NaCl) and lysed in HBS containing 1% Triton X-100, 5 mM $MgCl_2$ (Sigma, Piscataway, NJ, USA) and 1mM DTT supplied with inhibitors of proteases (1:100, Bimake, Houston, TX, USA) and phosphatases (1:100, Bimake, Houston, TX, USA). The lysates were equalized for the total amount of GFP signal. Agarose-bound RhoA-CA (15 µg) was added to each lysate and rotated for 1 h at 4 °C. The beads were washed three times with lysis buffer and resuspended in SDS-PAGE sample buffer. The samples were subjected to SDS-PAGE and analyzed by immunoblotting as described above.

Supplementary Materials: Supplementary materials can be found at http://www.mdpi.com/1422-0067/21/20/7769/s1. Table S1: A complete list of putative PKN3 substrates identified in the phosphoproteomic screen; Table S2: The list of primers used in the study; Table S3: The sequence of synthesized ARHGAP18.

Author Contributions: Conceptualization, M.D.; methodology, M.D.; validation, M.D.; investigation, M.D.; writing—original draft preparation, M.D.; writing—review and editing, M.D., D.R. and J.B.; visualization, M.D.; supervision, D.R. and J.B.; funding acquisition, M.D., D.R. and J.B. All authors have read and agreed to the published version of the manuscript.

Funding: This research was supported by "Center for Tumor Ecology-Research of the Cancer Microenvironment Supporting Cancer Growth and Spread" (reg. No. CZ.02.1.01/0.0/0.0/16_019/0000785), Operational Program Research, Development and Education and by Charles University Grant Agency (GAUK n°740120). The work was also funded in part by Czech Science Foundation grant 19-08410S. A part of the study was performed with the equipment for metabolomics and cell analyses (Grant no. CZ.1.05/2.1.00/19.0400) supported by the Research and Development for Innovations Operational Program, co-financed by the European regional development fund and the state budget of the Czech Republic.

Acknowledgments: We thank Marie Charvátová for outstanding technical assistance. We thank to Karel Harant and Pavel Talacko from the Laboratory of Mass Spectrometry, BIOCEV. We thank to Magdalena Raška and Nikol Dibusová for proofreading.

Conflicts of Interest: The authors declare no conflict of interest.

Abbreviations

PKN3	Protein Kinase N3
ARHGAP18	Rho GTPase Activating Protein 18
N6-Bn ATPγS	N6-Benzyl ATPγS
PNBM	*p*-nitrobenzyl mesylate

References

1. Hashimoto, T.; Mukai, H.; Kawamata, T. Localization of PKN mRNA in the rat brain. *Mol. Brain Res.* **1998**. [CrossRef]
2. Mukai, H.; Ono, Y. A novel protein kinase with leucine zipper-like sequences: Its catalytic domain is highly homologous to that of protein kinase C. *Biochem. Biophys. Res. Commun.* **1994**. [CrossRef] [PubMed]

3. Quilliam, L.A.; Lambert, Q.T.; Mickelson-Young, L.A.; Westwick, J.K.; Sparks, A.B.; Kay, B.K.; Jenkins, N.A.; Gilbert, D.J.; Copeland, N.G.; Der, C.J. Isolation of a NCK-associated kinase, PRK2, an SH3-binding protein and potential effector of Rho protein signaling. *J. Biol. Chem.* **1996**, *271*, 28772–28776. [CrossRef] [PubMed]
4. Aleku, M.; Schulz, P.; Keil, O.; Santel, A.; Schaeper, U.; Dieckhoff, B.; Janke, O.; Endruschat, J.; Durieux, B.; Röder, N.; et al. Atu027, a liposomal small interfering RNA formulation targeting protein kinase N3, inhibits cancer progression. *Cancer Res.* **2008**, *68*, 9788–9798. [CrossRef] [PubMed]
5. Uehara, S.; Udagawa, N.; Mukai, H.; Ishihara, A.; Maeda, K.; Yamashita, T.; Murakami, K.; Nishita, M.; Nakamura, T.; Kato, S.; et al. Protein kinase N3 promotes bone resorption by osteoclasts in response to Wnt5a-Ror2 signaling. *Sci. Signal.* **2017**, *10*, 1–12. [CrossRef]
6. Uehara, S.; Udagawa, N.; Kobayashi, Y. Regulation of osteoclast function via Rho-Pkn3-c-Src pathways. *J. Oral Biosci.* **2019**, *61*, 135–140. [CrossRef]
7. Oishi, K.; Mukai, H.; Shibata, H.; Takahashi, M.; Ona, Y. Identification and characterization of PKNβ, a novel isoform of protein kinase PKN: Expression and arachidonic acid dependency are different from those of PKNα. *Biochem. Biophys. Res.* **1999**, *814*, 808–814. [CrossRef]
8. Leenders, F.; Möpert, K.; Schmiedeknecht, A.; Santel, A.; Czauderna, F.; Aleku, M.; Penschuck, S.; Dames, S.; Sternberger, M.; Röhl, T.; et al. PKN3 is required for malignant prostate cell growth downstream of activated PI 3-kinase. *EMBO J.* **2004**, *23*, 3303–3313. [CrossRef]
9. Unsal-Kacmaz, K.; Ragunathan, S.; Rosfjord, E.; Dann, S.; Upeslacis, E.; Grillo, M.; Hernandez, R.; Mack, F.; Klippel, A. The interaction of PKN3 with RhoC promotes malignant growth. *Mol. Oncol.* **2012**, *6*, 284–298. [CrossRef]
10. Möpert, K.; Löffler, K.; Röder, N.; Kaufmann, J.; Santel, A. Depletion of protein kinase N3 (PKN3) impairs actin and adherens junctions dynamics and attenuates endothelial cell activation. *Eur. J. Cell Biol.* **2012**, *91*, 694–705. [CrossRef]
11. Santel, A.; Aleku, M.; Roder, N.; Mopert, K.; Durieux, B.; Janke, O.; Keil, O.; Endruschat, J.; Dames, S.; Lange, C.; et al. Atu027 Prevents Pulmonary Metastasis in Experimental and Spontaneous Mouse Metastasis Models. *Clin. Cancer Res.* **2010**, *16*, 5469–5480. [CrossRef] [PubMed]
12. Gemperle, J.; Hexnerová, R.; Lepšík, M.; Tesina, P.; Dibus, M.; Novotný, M.; Brábek, J.; Veverka, V.; Rosel, D. Structural characterization of CAS SH3 domain selectivity and regulation reveals new CAS interaction partners. *Sci. Rep.* **2017**, *7*, 8057. [CrossRef] [PubMed]
13. Gemperle, J.; Dibus, M.; Koudelková, L.; Rosel, D.; Brábek, J. The interaction of p130Cas with PKN3 promotes malignant growth. *Mol. Oncol.* **2019**, *13*, 264–289. [CrossRef] [PubMed]
14. Kraus, M.; Dolinski, B.; Rosahl, T.W.; Magee, J.A. Protein kinase N3 deficiency impedes PI3-kinase pathway-driven leukemogenesis without affecting normal hematopoiesis. *Leukemia* **2014**, *29*, 255–258. [CrossRef] [PubMed]
15. Mukai, H.; Muramatsu, A.; Mashud, R.; Kubouchi, K.; Tsujimoto, S.; Hongu, T.; Kanaho, Y.; Tsubaki, M.; Nishida, S.; Shioi, G.; et al. PKN3 is the major regulator of angiogenesis and tumor metastasis in mice. *Sci. Rep.* **2016**, *6*, 18979. [CrossRef]
16. Allen, J.J.; Li, M.; Brinkworth, C.S.; Paulson, J.L.; Wang, D.; Hübner, A.; Chou, W.-H.; Davis, R.J.; Burlingame, A.L.; Messing, R.O.; et al. A semisynthetic epitope for kinase substrates. *Nat. Methods* **2007**, *4*, 511–516. [CrossRef]
17. Hertz, N.T.; Wang, B.T.; Allen, J.J.; Zhang, C.; Dar, A.C.; Burlingame, A.L.; Shokat, K.M. Chemical Genetic Approach for Kinase-Substrate Mapping by Covalent Capture of Thiophosphopeptides and Analysis by Mass Spectrometry. *Curr. Protoc. Chem. Biol.* **2010**, *2*, 15–36. [CrossRef]
18. Chang, G.H.; Lay, A.J.; Ting, K.K.; Zhao, Y.; Coleman, P.R.; Powter, E.E.; Formaz-Preston, A.; Jolly, C.J.; Bower, N.I.; Hogan, B.M.; et al. Arhgap18: An endogenous inhibitor of angiogenesis, limiting tip formation and stabilizing junctions. *Small GTPases* **2014**, *5*. [CrossRef]
19. Maeda, M.; Hasegawa, H.; Hyodo, T.; Ito, S.; Asano, E.; Yuang, H.; Funasaka, K.; Shimokata, K.; Hasegawa, Y.; Hamaguchi, M.; et al. ARHGAP18, a GTPase-activating protein for RhoA, controls cell shape, spreading and motility. *Mol. Biol. Cell* **2011**, *22*, 3840–3852. [CrossRef]
20. Li, X.; Tao, Y.; Wang, X.; Wang, T.; Liu, J. Advanced glycosylation end products (AGEs) controls proliferation, invasion and permeability through orchestrating ARHGAP18/RhoA pathway in human umbilical vein endothelial cells. *Glycoconj. J.* **2020**, *37*, 209–219. [CrossRef]

21. Porazinski, S.; Wang, H.; Asaoka, Y.; Behrndt, M.; Miyamoto, T.; Morita, H.; Hata, S.; Sasaki, T.; Krens, S.F.G.; Osada, Y.; et al. YAP is essential for tissue tension to ensure vertebrate 3D body shape. *Nature* **2015**, *521*, 217–221. [CrossRef] [PubMed]
22. Vautrin-Glabik, A.; Botia, B.; Kischel, P.; Ouadid-Ahidouch, H.; Rodat-Despoix, L. IP3R3 silencing induced actin cytoskeletal reorganization through ARHGAP18/RhoA/mDia1/FAK pathway in breast cancer cell lines. *Biochim. Biophys. Acta - Mol. Cell Res.* **2018**, *1865*, 945–958. [CrossRef] [PubMed]
23. Lovelace, M.D.; Powter, E.E.; Coleman, P.R.; Zhao, Y.; Parker, A.; Chang, G.H.; Lay, A.J.; Hunter, J.; McGrath, A.P.; Jormakka, M.; et al. The RhoGAP protein ARHGAP18/SENEX localizes to microtubules and regulates their stability in endothelial cells. *Mol. Biol. Cell* **2017**, *28*, 1066–1078. [CrossRef] [PubMed]
24. Li, Y.; Ji, S.; Fu, L.; Jiang, T.; Wu, D.; Meng, F. Over-expression of ARHGAP18 suppressed cell proliferation, migration, invasion and tumor growth in gastric cancer by restraining over-activation of MAPK signaling pathways. *Onco. Targets. Ther.* **2018**, *11*, 279–290. [CrossRef] [PubMed]
25. Humphries, B.; Wang, Z.; Li, Y.; Jhan, J.R.; Jiang, Y.; Yang, C. ARHGAP18 downregulation by miR-200b suppresses metastasis of triple-negative breast cancer by enhancing activation of RhoA. *Cancer Res.* **2017**, *77*, 4051–4064. [CrossRef] [PubMed]
26. Aguilar-Rojas, A.; Maya-Núñez, G.; Huerta-Reyes, M.; Pérez-Solis, M.A.; Silva-García, R.; Guillén, N.; Olivo-Marin, J.C. Activation of human gonadotropin-releasing hormone receptor promotes down regulation of ARHGAP18 and regulates the cell invasion of MDA-MB-231 cells. *Mol. Cell. Endocrinol.* **2018**, *460*, 94–103. [CrossRef] [PubMed]
27. Aleskandarany, M.A.; Sonbul, S.; Surridge, R.; Mukherjee, A.; Caldas, C.; Diez-Rodriguez, M.; Ashankyty, I.; Albrahim, K.I.; Elmouna, A.M.; Aneja, R.; et al. Rho-GTPase activating-protein 18: A biomarker associated with good prognosis in invasive breast cancer. *Br. J. Cancer* **2017**, *117*, 1176–1184. [CrossRef]
28. Coleman, P.R.; Hahn, C.N.; Grimshaw, M.; Lu, Y.; Li, X.; Brautigan, P.J.; Beck, K.; Stocker, R.; Vadas, M.A.; Gamble, J.R. Stress-induced premature senescence mediated by a novel gene, SENEX, results in an anti-inflammatory phenotype in endothelial cells. *Blood* **2010**, *116*, 4016–4024. [CrossRef]
29. Lay, A.J.; Coleman, P.R.; Formaz-Preston, A.; Ka Ting, K.; Roediger, B.; Weninger, W.; Schwartz, M.A.; Vadas, M.A.; Gamble, J.R. ARHGAP18: A flow-responsive gene that regulates endothelial cell alignment and protects against atherosclerosis. *J. Am. Heart Assoc.* **2019**, *8*. [CrossRef]
30. Coleman, P.R.; Lay, A.J.; Ting, K.K.; Zhao, Y.; Li, J.; Jarrah, S.; Vadas, M.A.; Gamble, J.R. YAP and the RhoC regulator ARHGAP18, are required to mediate flow-dependent endothelial cell alignment. *Cell Commun. Signal.* **2020**, *18*. [CrossRef]
31. Cibrián Uhalte, E.; Kirchner, M.; Hellwig, N.; Allen, J.J.; Donat, S.; Shokat, K.M.; Selbach, M.; Abdelilah-Seyfried, S. In Vivo Conditions to Identify Prkci Phosphorylation Targets Using the Analog-Sensitive Kinase Method in Zebrafish. *PLoS ONE* **2012**, *7*, e40000. [CrossRef] [PubMed]
32. Ge, S.X.; Jung, D.; Jung, D.; Yao, R. ShinyGO: A graphical gene-set enrichment tool for animals and plants. *Bioinformatics* **2020**, *36*, 2628–2629. [CrossRef] [PubMed]
33. Shibata, H.; Oishi, K.; Yamagiwa, A.; Matsumoto, M.; Mukai, H.; Ono, Y. PKNbeta interacts with the SH3 Domains of Graf and a Novel Graf Related Protein, Graf 2, Which Are GTPase Activating Proteins for Rho. *J. Biochem.* **2001**, *31*, 23–31. [CrossRef] [PubMed]
34. Collazos, A.; Michael, N.; Whelan, R.D.H.; Kelly, G.; Mellor, H.; Pang, L.C.H.; Totty, N.; Parker, P.J. Site recognition and substrate screens for PKN family proteins. *Biochem. J.* **2011**, *438*, 535–543. [CrossRef]
35. Browne, C.M.; Jiang, B.; Ficarro, S.B.; Doctor, Z.M.; Johnson, J.L.; Card, J.D.; Sivakumaren, S.C.; Alexander, W.M.; Yaron, T.M.; Murphy, C.J.; et al. A Chemoproteomic Strategy for Direct and Proteome-Wide Covalent Inhibitor Target-Site Identification. *J. Am. Chem. Soc.* **2019**, *141*, 191–203. [CrossRef]
36. Linardopoulou, E.V.; Parghi, S.S.; Friedman, C.; Osborn, G.E.; Parkhurst, S.M.; Trask, B.J. Human Subtelomeric WASH Genes Encode a New Subclass of the WASP Family. *PLoS Genet.* **2007**, *3*, e237. [CrossRef]
37. Yang, C.; Pring, M.; Wear, M.A.; Huang, M.; Cooper, J.A.; Svitkina, T.M.; Zigmond, S.H. Mammalian CARMIL inhibits actin filament capping by capping protein. *Dev. Cell* **2005**, *9*, 209–221. [CrossRef]
38. Liang, Y.; Niederstrasser, H.; Edwards, M.; Jackson, C.E.; Cooper, J.A. Distinct roles for CARMIL isoforms in cell migration. *Mol. Biol. Cell* **2009**, *20*, 5290–5305. [CrossRef]
39. Mori, K.; Amano, M.; Takefuji, M.; Kato, K.; Morita, Y.; Nishioka, T.; Matsuura, Y.; Murohara, T.; Kaibuchi, K. Rho-kinase contributes to sustained RhoA activation through phosphorylation of p190A RhoGAP. *J. Biol. Chem.* **2009**, *284*, 5067–5076. [CrossRef]

40. Jiang, W.; Betson, M.; Mulloy, R.; Foster, R.; Lévay, M.; Ligeti, E.; Settleman, J. P190A RhoGAP is a glycogen synthase kinase-3-β substrate required for polarized cell migration. *J. Biol. Chem.* **2008**, *283*, 20978–20988. [CrossRef]
41. Minoshima, Y.; Kawashima, T.; Hirose, K.; Tonozuka, Y.; Kawajiri, A.; Bao, Y.C.; Deng, X.; Tatsuka, M.; Narumiya, S.; May, W.S.; et al. Phosphorylation by Aurora B converts MgcRacGAP to a RhoGAP during cytokinesis. *Dev. Cell* **2003**, *4*, 549–560. [CrossRef]
42. Luo, W.; Janoštiak, R.; Tolde, O.; Ryzhova, L.M.; Koudelková, L.; Dibus, M.; Brábek, J.; Hanks, S.K.; Rosel, D. ARHGAP42 is activated by Src-mediated tyrosine phosphorylation to promote cell motility. *J. Cell Sci.* **2017**, *130*, 2382–2393. [CrossRef] [PubMed]
43. Lusis, A.J. Atherosclerosis. *Nature* **2000**, *407*, 233–241. [CrossRef]
44. Hägg, S.; Skogsberg, J.; Lundström, J.; Noori, P.; Nilsson, R.; Zhong, H.; Maleki, S.; Shang, M.M.; Brinne, B.R.; Bradshaw, M.; et al. Multi-organ expression profiling uncovers a gene module in coronary artery disease involving transendothelial migration of leukocytes and LIM domain binding 2: The Stockholm Atherosclerosis Gene Expression (STAGE) study. *PLoS Genet.* **2009**, *5*, e1000754. [CrossRef]
45. Zhang, C.J.; Zhu, N.; Liu, Z.; Shi, Z.; Long, J.; Zu, X.Y.; Tang, Z.W.; Hu, Z.Y.; Liao, D.F.; Qin, L. Wnt5a/Ror2 pathway contributes to the regulation of cholesterol homeostasis and inflammatory response in atherosclerosis. *Biochim. Biophys. Acta - Mol. Cell Biol. Lipids* **2020**, *1865*, 158547. [CrossRef]
46. García-Mata, R.; Wennerberg, K.; Arthur, W.T.; Noren, N.K.; Ellerbroek, S.M.; Burridge, K. Analysis of activated GAPs and GEFs in cell lysates. *Methods Enzymol.* **2006**, *406*, 425–437. [CrossRef]

Supplementary Table 1

Supplementary Table 1 contains a curated list of putative PKN3 substrates and phosphorylation sites. All the phosphosites with missing values or those identified in control samples were filtered. The cutoff score for phosphosite localization was set to 0.75.

Gene	Protein names	UniProt identifier	Site	Position	Phosphosite localization probability	Sequence surrounding the phosphosite	Score
ADM2	Adrenomedullin-2	Q7Z4H4	S	24	0.990	LGCISLLCLQLPGSLSRSLGGDPRPVKPREP	49.094
ADRBK2	Alternative protein ADRBK2	L8EAE0	T	42	0.953	CHHSCKVLMPLIGPFTDVTISGPMFKKKGLA	44.391
ADRBK2	Alternative protein ADRBK2	L8EAE0	T	45	0.795	SCKVLMPLIGPFTDVTISGPMFKKKGLAGHD	44.391
AK3	GTP:AMP phosphotransferase AK3, mitochondrial	Q7Z531	S	13	0.980	___MGAPGSGKGTVSSRISTHFELKHLSSGD	46.88
AK7	Adenylate kinase 7	Q96M32	T	154	0.965	EVSHFEKRKLFILLSTVMTWARSKALDPEDS	45.28
AK7	Adenylate kinase 7	Q96M32	S	153	0.931	EEVSHFEKRKLFILLSTVMTWARSKALDPED	45.28
ALPK2	Alpha-protein kinase 2	Q86TB3	S	27	0.998	LCFLSTLLSQKVPEKSDAVLRCIISGQPKPE	49.049
ANGPTL5	Angiopoietin-related protein 5	Q86XS5	S	320	1.000	VDNDGCRPACLVNGQSVKSCSHLHNKTGWWF	66.595
ANK3	Ankyrin-3	Q12955	T	1015	1.000	SRHHGMRIIIPPRKCTAPTRITCRLVKRHKL	75.387
ANK3	Ankyrin-3	Q12955	T	1018	1.000	HGMRIIIPPRKCTAPTRITCRLVKRHKLANP	75.387
ANKRD26	Ankyrin repeat domain-containing protein 26	Q9UPS8	S	1435	0.944	LHLDTKNQILQEELLSMKTVQKKCEKLQKNK	74.966
ANKRD50	Ankyrin repeat domain-containing protein 50	Q9ULJ7	T	591	0.996	AHGHTPLTLAARQGHTKVVNCLIGCGANINH	40.937
ANKRD50	Ankyrin repeat domain-containing protein 50	Q9ULJ7	T	583	0.995	GADLEIEDAHGHTPLTLAARQGHTKVVNCLI	40.937
ANLN	Actin-binding protein anillin	Q9NQW6	T	916	0.994	KSKAITPKRLLTSITTKSNIHSSVMASPGGL	74.415
ANLN	Actin-binding protein anillin	Q9NQW6	T	912	0.858	KKTSKSKAITPKRLLTSITTKSNIHSSVMAS	74.415
ANLN	Actin-binding protein anillin	Q9NQW6	T	915	0.774	SKSKAITPKRLLTSITTKSNIHSSVMASPGG	74.415
APBA1	Amyloid beta A4 precursor protein-binding family A member 1	Q02410	S	491	1.000	TPSKNVRMMQAQEAVSRIKAPEGESQPMTEV	69.716
AQR	Intron-binding protein aquarius	O60306	S	1225	1.000	LFMYMCLLGYPADKISILTTYNGQKHLIRDI	41.56
AQR	Intron-binding protein aquarius	O60306	T	1228	1.000	YMCLLGYPADKISILTTYNGQKHLIRDIINR	41.56
AQR	Intron-binding protein aquarius	O60306	T	1229	1.000	MCLLGYPADKISILTTYNGQKHLIRDIINRR	41.56
ARFGEF2	Brefeldin A-inhibited guanine nucleotide-exchange protein 2	Q9Y6D5	S	87	1.000	FELACQSKSPRVVSTSLDCLQKLIAYGHITG	54.486
ARFGEF2	Brefeldin A-inhibited guanine nucleotide-exchange protein 2	Q9Y6D5	S	85	0.997	LPFELACQSKSPRVVSTSLDCLQKLIAYGHI	54.486
ARFGEF2	Brefeldin A-inhibited guanine nucleotide-exchange protein 2	Q9Y6D5	T	86	0.997	PFELACQSKSPRVVSTSLDCLQKLIAYGHIT	54.486
ARHGAP18	Rho GTPase-activating protein 18	Q8N392	T	158	1.000	TQAAAVQKRVETVSQTLRKKNKQYQIPDVRD	111.46
ARHGAP18	Rho GTPase-activating protein 18	Q8N392	S	156	0.996	TRTQAAAVQKRVETVSQTLRKKNKQYQIPDV	111.46
ATAD5	ATPase family AAA domain-containing protein 5	Q96QE3	T	69	0.992	FAPPKPSNILDYFRKTSPTNEKTQLGKECKI	54.539
ATAD5	ATPase family AAA domain-containing protein 5	Q96QE3	S	70	0.973	APPKPSNILDYFRKTSPTNEKTQLGKECKIK	54.539
ATAD5	ATPase family AAA domain-containing protein 5	Q96QE3	T	175	0.937	RYKKQVEVLAENIQDTKSQPNTMTSLQNSKK	43.956
ATP7B	Cu++ transporting ATPase beta polypeptide	A6N865	T	56	0.973	GTAEASSENPLGVAVTKYCKE_____	44.1
ATR	Serine/threonine-protein kinase ATR	Q13535	S	176	1.000	RRNVMGHAVEWPVVMSRFLSQLDEHMGYLQS	49.066
ATXN7L3	Ataxin-7-like protein 3	Q14CW9	S	157	1.000	NDWSYGSEKKAKKRKSDKNPNSPRRSKSLKH	49.632

BCL2L10	Bcl-2-like protein 10	H0YMD5	T	205	0.999	LSLLQDPLSTGFLEKTAGPGFSVMLVNNSLH	48.182
BICC1	Protein bicaudal C homolog 1	Q9H694	S	124	0.986	SGKKEDVKEAKEMIMSVLDTKSNRVTLKMDV	41.257
BLOC1S4	Biogenesis of lysosome-related organelles complex 1 subunit 4	Q9NUP1	T	176	1.000	AELGTFPRAFKKLLHTMNVPSLFSKSAPSRP	47.844
BLOC1S4	Biogenesis of lysosome-related organelles complex 1 subunit 4	Q9NUP1	S	184	0.855	AFKKLLHTMNVPSLFSKSAPSRPQQAGYEAP	47.844
BOD1	Biorientation of chromosomes in cell division protein 1	Q96IK1	S	134	0.996	VVQSGMLEAGVDRIISQVVDPKLNHIFRP__	46.099
BOD1	Biorientation of chromosomes in cell division protein 1	Q96IK1	S	118	0.820	___MNKNQLRNGLRQSVVQSGMLEAGVDRII	46.099
BRD4	Bromodomain-containing protein 4	O60885	S	601	1.000	KEPAPMKSKPPPTYESEEEDKCKPMSYEEKR	101.9
BRF1	Transcription factor IIIB 90 kDa subunit	Q92994	S	535	0.989	TAREAIEKMLEQKKISSKINYSVLRGLSSAG	75.109
C10orf12	Uncharacterized protein C10orf12	Q8N655	T	1168	1.000	SAGKSCPPSRKEKENTNKRPSQSIASETLTK	53.554
C19orf44	Uncharacterized protein C19orf44	Q9H6X5	S	599	0.999	SPAVLALHDVLKQQLSLTQQFIQASRHLHAS	45.957
C19orf44	Uncharacterized protein C19orf44	Q9H6X5	T	601	0.998	AVLALHDVLKQQLSLTQQFIQASRHLHASLL	45.957
C21orf105	C21orf105 protein	Q9BSD2	S	147	0.801	IHRTRVKLTPKAASSSKTLTAKCLSGPISPT	68.44
C21orf105	C21orf105 protein	Q9BSD2	S	146	0.769	WIHRTRVKLTPKAASSSKTLTAKCLSGPISP	68.44
C5orf42	Uncharacterized protein C5orf42	Q9H799	T	2936	0.992	QEHDPFCPRSNPLYMTSREIRLRQKMKHEKD	42.718
C5orf42	Uncharacterized protein C5orf42	Q9H799	S	2937	0.989	EHDPFCPRSNPLYMTSREIRLRQKMKHEKDR	42.718
C5orf60	Putative uncharacterized protein C5orf60	A6NFR6	S	173	0.998	TSFHVSPRAPLAPLASMPSSVPKTSVESLGS	48.44
CARD18	Caspase recruitment domain-containing protein 18	G5EA35	T	10	1.000	______MNKVRDENDTVMDKARVLIDLVTGK	51.03
CASP3	Caspase-3	P42574	T	4	0.974	_____MENTENSVDSKSIKNLEPK	60.478
CCDC144A	Coiled-coil domain-containing protein 144A	A2RUR9	S	805	0.992	TSKQKELEMARKKMNSEISHRHQKEKDLFHE	82.029
CCDC152	Alternative protein CCDC152	L0R835	S	44	1.000	FTKVFIFESLEQIYKSLFNKLIEIGIMREK_	62.408
CCDC169	Coiled-coil domain-containing protein 169	A6NNP5	S	107	1.000	_____MPVESLNTLLKQLEEEKKTL	45.908
CCDC169	Coiled-coil domain-containing protein 169	A6NNP5	T	110	1.000	_____MPVESLNTLLKQLEEEKKTLESQ	45.908
CCDC33	Coiled-coil domain-containing protein 33	Q8N5R6	S	651	1.000	NNYRRAMQKMAEDILSLRRQASILEGENRIL	63.624
CCT5	T-complex protein 1 subunit epsilon	P48643	T	521	0.999	VIETLIGKKQQISLATQMVRMILKIDDIRKP	60.401
CD226	CD226 antigen	Q15762	T	149	0.996	VPSNSHIVSEPGKNVTLTCQPQMTWPVQAVR	43.841
CDH8	Alternative protein CDH8	L8E7B0	T	34	1.000	KMENPAKSFKLLAPWTKMIPKTDIISYTVSF	75.738
CDK13	Cyclin-dependent kinase 13	Q14004	S	927	1.000	PIFQANQELAQLELISRICGSPCPAVWPDVI	62.104
CEACAM16	Carcinoembryonic antigen-related cell adhesion molecule 16	Q2WEN9	T	402	1.000	SLLVQKLNLTDTGRYTLKTVTVQGKTETLEV	100.25
CEACAM16	Carcinoembryonic antigen-related cell adhesion molecule 16	Q2WEN9	T	398	1.000	FPNCSLLVQKLNLTDTGRYTLKTVTVQGKTE	100.25
CEACAM20	Carcinoembryonic antigen-related cell adhesion molecule 20	Q6UY09	T	482	0.852	YFLCIRNARRPSRKTTEDPSHETSQPIPKEE	42.185
CEACAM20	Carcinoembryonic antigen-related cell adhesion molecule 20	Q6UY09	T	481	0.852	GYFLCIRNARRPSRKTTEDPSHETSQPIPKE	42.185
CENPE	Centromere-associated protein E	Q02224	T	302	1.000	KLTRILQNSLGGNAKTRIICTITPVSFDETL	50.874
CENPE	Centromere-associated protein E	Q02224	T	289	0.984	DGQVGGFINYRDSKLTRILQNSLGGNAKTRI	50.874
CERS3	Ceramide synthase 3	Q8IU89	T	81	0.977	KSFGIKETVRKVTPNTVLENFFKHSTRQPLQ	58.04
CERS3	Ceramide synthase 3	Q8IU89	S	90	0.850	RKVTPNTVLENFFKHSTRQPLQTDIYGLAKK	58.04
CFAP45	Cilia- and flagella-associated protein 45	Q9UL16	T	344	1.000	LLAQEKLADQMVMEFTKKKMAREAEFEAEQE	63.091
CHURC1	Protein Churchill	Q8WUH1	T	83	1.000	ITNKSLKEEDGEEIVTYDHLCKNCHHVIARH	54.953
CIDEB	Cell death activator CIDE-B	Q9UHD4	T	135	1.000	LGRERPKHSKDIARFTFDVYKQNPRDLFGSL	42.336
CKAP2L	Cytoskeleton-associated protein 2-like	Q8IYA6	S	120	0.999	SECVSSNPYSKPSSKSFQQCEAGSSTTGELS	58.361
CLASRP	CLK4-associating serine/arginine-rich protein	A0A0A0MQS2	T	166	0.990	DEKKKLAEKKASIGYTYEDSTVAEVEKAAEK	63.037
CMIP	C-Maf-inducing protein	Q8IY22	T	70	0.976	LQEGDIQVCVIRHPRTFLSKILTSKFLRRWE	70.816
CNTN3	Contactin-3	Q9P232	T	500	1.000	FGKANGTTHLVVTEPTRITLAPSNMDVSVGE	69.721
COX7B2	Cytochrome c oxidase subunit 7B2, mitochondrial	Q8TF08	S	11	0.997	_____MMFPLARNALSSLKIQSILQSMARHS	44.5
COX7B2	Cytochrome c oxidase subunit 7B2, mitochondrial	Q8TF08	S	12	0.997	____MMFPLARNALSSLKIQSILQSMARHSH	44.5
CRISPLD2	Cysteine-rich secretory protein LCCL domain-containing 2	Q9H0B8	S	279	0.957	WLQPRVMRPTKPKKTSAVNYMTQVVRCDTKM	79.461
CROCC	Rootletin	Q5TZA2	T	725	0.969	LTKAEAGRVELELSMTKLRAEEASLQDSLSK	40.094
CRYBG3	Very large A-kinase anchor protein	Q68DQ2	S	844	1.000	HSGRGKTISLSKVSLSKVEPRNISQDKMSSF	68.277

CRYBG3	Very large A-kinase anchor protein	Q68DQ2	S	839	0.998	VLVESHSGRGKTISLSKVSLSKVEPRNISQD	68.277
CRYBG3	Very large A-kinase anchor protein	Q68DQ2	S	842	0.907	ESHSGRGKTISLSKVSLSKVEPRNISQDKMS	68.277
CXorf66	Uncharacterized protein CXorf66	Q5JRM2	S	174	0.950	SYPKRSSKSSCSKKLSKSSHLEKAHKKGSLE	45.368
CYTB	Cytochrome b	Q85KT0	S	8	0.959	________MTPMRKISPLMKLINHSFIDLPT	49.448
DCAF12L1	DDB1- and CUL4-associated factor 12-like protein 1	Q5VU92	S	8	1.000	________MAQQQTGSRKRKAPAVEAGAGSS	83.801
DENND4B	DENN domain-containing protein 4B	O75064	T	1480	1.000	SMGKEELRHRRAQMPTPKAIDCRKCFGAPPE	59.931
DGKZ	Diacylglycerol kinase zeta	Q13574	T	215	0.973	GGRRASGTTAGTMLPTRVRPLSRRRQVALRR	45.363
DGKZ	Diacylglycerol kinase zeta	Q13574	S	205	0.858	RRPSGQHPGPGGRRASGTTAGTMLPTRVRPL	45.363
DHX33	Putative ATP-dependent RNA helicase DHX33	Q9H6R0	S	441	1.000	FDKMTVPEIQRCNLASVMLQLLAMKVPNVLT	65.627
DIABLO	Diablo homolog, mitochondrial	Q9NR28	S	63	0.997	______MKSDFYFQKSEPHSLSSEALMRRAV	58.674
DKFZp566F0947	Uncharacterized protein DKFZp566F0947	Q9NT59	S	73	1.000	RGTEARNTPALAFQASRGWIIRAFRRRGREE	78.326
DKFZp566F0947	Uncharacterized protein DKFZp566F0947	Q9NT59	T	65	0.999	ASNNHPHRRGTEARNTPALAFQASRGWIIRA	78.326
DKFZp781F05101	Uncharacterized protein DKFZp781F05101	Q5H9R5	T	340	0.994	AWEARPPRESSDVPPTKRNNWIFIDEEQAFG	40.067
DKFZp781F05101	Uncharacterized protein DKFZp781F05101	Q5H9R5	S	335	0.840	EKPDKAWEARPPRESSDVPPTKRNNWIFIDE	40.067
DLD	Dihydrolipoyl dehydrogenase, mitochondrial	P09622	T	163	1.000	VHVNGYGKITGKNQVTATKADGGTQVIDTKN	66.962
DLD	Dihydrolipoyl dehydrogenase, mitochondrial	P09622	T	165	1.000	VNGYGKITGKNQVTATKADGGTQVIDTKNIL	66.962
DNHD1	Dynein heavy chain domain-containing protein 1	Q96M86	T	3800	1.000	LDTCKAVEAAEERLLTMLLFQNPKRQKPAKF	45.081
DSCAM	Down syndrome cell adhesion molecule	O60469	S	1408	0.983	SSITLSWLPGDNGGSSIRGYILQYSEDNSEQ	87.498
DSCAM	Down syndrome cell adhesion molecule	O60469	S	1633	1.000	RRRREQRLKRLRDAKSLAEMLMSKNTRTSDT	64.73
DSCAM	Down syndrome cell adhesion molecule	O60469	S	1640	0.800	LKRLRDAKSLAEMLMSKNTRTSDTLSKQQQT	64.73
DUSP26	Dual specificity protein phosphatase 26	Q9BV47	S	24	0.991	ASMTFMARFSRSSSRSPVRTRGTLEEMPTVQ	44.203
DYNC2H1	Cytoplasmic dynein 2 heavy chain 1	Q8NCM8	S	1818	1.000	KLPDNLKQLFRPVAMSHPDNELIAEVILYSE	42.64
ECT2L	Epithelial cell-transforming sequence 2 oncogene-like	Q008S8	S	765	1.000	TIEKMKQNITMKDHLSDIQRIIWGCPTLSEV	76.357
EHMT1	Histone-lysine N-methyltransferase EHMT1	Q9H9B1	S	318	0.855	KTKVLKQRTVIEMFKSITHSTVGSKGEKDLG	45.335
EIF2B2	Translation initiation factor eIF-2B subunit beta	H0YK01	T	24	0.997	AIFAVMSRVNKVIIGTKTILANGALRAVTGT	49.66
ESR1	Estrogen receptor alpha splice variant	B5TZ79	S	83	1.000	RRGGRMLKHKLLLILSHIRHMSNKGMEHLYS	48.091
ESR1	Estrogen receptor alpha splice variant	B5TZ79	S	89	1.000	LKHKLLLILSHIRHMSNKGMEHLYSMKCKNV	48.091
F8	Coagulation factor VIII	P00451	T	1280	0.923	PVLQDFRSLNDSTNRTKKHTAHFSKKGEEEN	53.124
F8	Coagulation factor VIII	P00451	T	2260	0.979	PKEWLQVDFQKTMKVTGVTTQGVKSLLTSMY	52.52
F8	Coagulation factor VIII	P00451	T	2263	0.862	WLQVDFQKTMKVTGVTTQGVKSLLTSMYVKE	52.52
FAM175A	BRCA1-A complex subunit Abraxas 1	E9PHB9	S	12	0.997	____MMLKLFIQLMESHSVAQTGVKWHDLGS	42.123
FAM175A	BRCA1-A complex subunit Abraxas 1	E9PHB9	S	14	0.981	__MMLKLFIQLMESHSVAQTGVKWHDLGSLQ	42.123
FAM186B	Protein FAM186B	Q8IYM0	T	697	0.847	LRLPHYLRSKALELTTTTMELGALRLQYLCH	56.569
FAM186B	Protein FAM186B	Q8IYM0	T	698	0.825	RLPHYLRSKALELTTTTMELGALRLQYLCHK	56.569
FAM186B	Protein FAM186B	Q8IYM0	S	374	0.998	QEPMKEEQLFSPLPPSPMAMIRDSGAIAAGH	49.34
FAM200A	Protein FAM200A	Q8TCP9	S	494	0.996	QLSSSFTLKNYYKILSLSAFWIKIKDDFPLL	51.643
FAM21A	WASH complex subunit FAM21A	Q641Q2	S	940	0.962	SKEKGIWKPETPQDSSGLAPFKTKEPSTRIG	69.672
FAM21A	WASH complex subunit FAM21A	Q641Q3	T	935	0.962	ESIQGSKEKGIWKPETPQDSSGLAPFKTKEP	69.672
FANCI	Fanconi anemia group I protein	Q9NVI1	S	1284	0.888	KKSKVNLMQHMKLSTSRDFKIKGNILDMVLR	54.393
FASTKD3	FAST kinase domain-containing protein 3	Q14CZ7	S	284	0.777	KVDEHQTFLNKINNFSLSIVSNLSPKLISQM	45.992
FAT3	Protocadherin Fat 3	Q8TDW7	T	448	1.000	RPLNTVKKEVYKLEVTNKEGDLKAQVTISIE	58.37
FBXO40	F-box only protein 40	Q9UH90	S	643	0.836	HGGTSWRVHREIWQFSSLFSKIKSWEFNEVT	43.523
FCER2	Low affinity immunoglobulin epsilon Fc receptor	P06734	S	321	1.000	PDPDGRLPTPSAPLHS_____	42.869
FCER2	Low affinity immunoglobulin epsilon Fc receptor	P06734	S	316	0.999	GPDSRPDPDGRLPTPSAPLHS_____	42.869
FLJ00275	FLJ00275 protein	Q8NF80	S	5	0.997	_____GMGMSWDPASDSILGTLPKP	65.563
FLJ00304	FLJ00304 protein	Q6ZNK3	S	50	0.873	HYVQHSAKNTASSSCSLVSPAGLSLLAFPLP	44.916
FLJ00304	FLJ00304 protein	Q6ZNK3	S	53	0.810	QHSAKNTASSSCSLVSPAGLSLLAFPLPPLK	44.916

FLT-1	Receptor protein-tyrosine kinase	S5TRK2	T	12	1.000	____GATASEYKALMTELKILTHIGHHLNVV	50.088
FNDC1	Fibronectin type III domain-containing protein 1	Q4ZHG4	S	741	0.794	SSRLLPTQPHLSSPLSKGGKDGEDAPATNSN	78.513
FRMPD3	FERM and PDZ domain-containing protein 3	Q5JV73	T	126	0.938	RLIELIRSAKEFIVLTVLHTHQSPKSAFISA	47.808
FSIP2	Fibrous sheath-interacting protein 2	Q5CZC0	T	5911	0.998	MMRKPSSDKIPSIDKTLVNKVVHSSVCNILN	41.412
FSIP2	Fibrous sheath-interacting protein 2	Q5CZC0	S	5907	0.952	PMHKMMRKPSSDKIPSIDKTLVNKVVHSSVC	41.412
GALIG	Cytogaligin	Q9H2J6	T	11	0.997	_____MMRYLGLETQTLKDGLAHGGTSLLGQ	58.815
GATAD2B	Transcriptional repressor p66-beta	Q8WXI9	S	138	0.890	PDIIVLSDNEASSPRSSSRMEERLKAANLEM	43.297
GDF5	Growth/differentiation factor 5	P43026	S	142	0.882	QLPGGKAPPKAGSVPSSFLLKKAREPGPPRE	41.109
GDF5	Growth/differentiation factor 5	P43026	S	143	0.882	LPGGKAPPKAGSVPSSFLLKKAREPGPPREP	41.109
GOLGA8A	Golgin subfamily A member 8A	A7E2F4	T	167	1.000	EGQIQRLNIEKKKLNTDLYHMKHSLRYFEEE	53.034
GPAT2	Glycerol-3-phosphate acyltransferase 2, mitochondrial	Q6NUI2	T	463	0.838	CHVLSASVGSSAVMSTAIMATLLLFKHQKLL	40.104
GPAT2	Glycerol-3-phosphate acyltransferase 2, mitochondrial	Q6NUI2	S	462	0.820	SCHVLSASVGSSAVMSTAIMATLLLFKHQKL	40.104
GPC2	Glypican-2;Secreted glypican-2	Q8N158	T	162	0.981	RLRDFYGESGEGLDDTLADFWAQLLERVFPL	42.705
GPR31	12-(S)-hydroxy-5,8,10,14-eicosatetraenoic acid receptor	O00270	S	97	1.000	LGRVGCWALHFLLDLSRSVGMAFLAAVALDR	45.618
GRM3	Metabotropic glutamate receptor 3	Q14832	T	52	1.000	GDLVLGGLFPINEKGTGTEECGRINEDRGIQ	58.592
GRM3	Metabotropic glutamate receptor 3	Q14832	T	54	1.000	LVLGGLFPINEKGTGTEECGRINEDRGIQRL	58.592
HAAO	3-hydroxyanthranilate 3,4-dioxygenase	P46952	S	17	1.000	ERRLGVRAWVKENRGSFQPPVCNKLMHQEQL	76.478
hCG_2040263	HCG2040263, isoform CRA_b	B4DSL7	S	6	0.891	__________MSSKRSHYDSALKRKVIVYAE	68.033
HES2	Transcription factor HES-2	K7EJQ0	S	73	0.939	DVLEMTVRFLQELPASSWPTAAPRE______	66.663
HKDC1	Hexokinase HKDC1	Q2TB90	T	888	0.995	ILQETVKELAPRCDVTFMLSEDGSGKGAALI	40.369
HKDC1	Hexokinase HKDC1	Q2TB90	S	892	0.817	TVKELAPRCDVTFMLSEDGSGKGAALITAVA	40.369
HLA-C	MHC class I antigen	F6IQM2	T	20	0.787	APRTLILLLSGALALTETWASSHSMRYFDTA	43.494
HLA-DRB1	HLA-DRB1 protein	Q8NEI3	S	24	0.784	GSCMAVLTVTLMVLSSPLVLAGDTRPRFLEY	41.432
HLA-DRB1	HLA-DRB1 protein	Q8NEI3	S	23	0.774	GGSCMAVLTVTLMVLSSPLVLAGDTRPRFLE	41.432
HRC	Alternative protein HRC	L8E9Z3	T	172	0.965	RMSQMDTIIMAPATGTKAMKKMTMMMMMMM	55.975
HRC	Alternative protein HRC	L8E9Z3	T	170	0.930	RMRMSQMDTIIMAPATGTKAMKKMTMMMMM	55.975
HSPG2	Basement membrane-specific heparan sulfate proteoglycan core protein	P98160	S	97	0.989	VYFRALVNFTRSIEYSPQLEDAGSREFREVS	65.038
IARS2	Isoleucine--tRNA ligase, mitochondrial	Q9NSE4	T	63	0.911	ASNHQPNSNSGRYRDTVLLPQTSFPMKLLGR	49.418
IDE	Insulin-degrading enzyme	P14735	T	869	1.000	KPPHYLESRVEAFLITMEKSIEDMTEEAFQK	43.246
IGSF22	Immunoglobulin superfamily member 22	Q8N9C0	S	318	0.989	NDAGIYSLSVGDKRMSAELTVLDEPLKFLGE	84.817
IKZF2	Zinc finger protein Helios	Q9UKS7	S	66	1.000	KLEMQSDEECDRKPLSREDEIRGHDEGSSLE	72.879
IL31RA	Interleukin-31 receptor subunit alpha	Q8NI17	S	411	1.000	ISVYPMLHDKVGEPYSIQAYAKEGVPSEGPE	43.494
ING5	Inhibitor of growth protein 5	Q8WYH8	S	57	1.000	IDILAAEYISTVKTLSPDQRVERLQKIQNAY	44.98
ING5	Inhibitor of growth protein 5	Q8WYH8	T	55	1.000	AEIDILAAEYISTVKTLSPDQRVERLQKIQN	44.98
IQGAP3	Ras GTPase-activating-like protein IQGAP3	Q86VI3	T	1496	0.822	KAELVKLQATLQGLSTKTTFYEEQGDYYSQY	64.476
IRX2	Iroquois-class homeodomain protein IRX-2	Q9BZI1	S	314	1.000	PPEAAPRGGRKTPQGSRTSPGAPPPASKPKL	76.24
IRX2	Iroquois-class homeodomain protein IRX-2	Q9BZI1	T	310	1.000	LLSPPPEAAPRGGRKTPQGSRTSPGAPPPAS	76.24
JARID2	Protein Jumonji	Q92833	S	399	1.000	AKTRKQVLSLGGASKSTGPAVNGLKVSGRLN	44.382
JARID2	Protein Jumonji	Q92833	S	410	1.000	GASKSTGPAVNGLKVSGRLNPKSCTKEVGGR	44.382
JARID2	Protein Jumonji	Q92833	T	400	1.000	KTRKQVLSLGGASKSTGPAVNGLKVSGRLNP	44.382
JPH1	Junctophilin-1	Q9HDC5	T	520	1.000	QVTAIVNKPLMSKAPTKEAGAVVPQSKYSGR	50.358
JPH1	Junctophilin-1	Q9HDC5	S	516	0.999	VADEQVTAIVNKPLMSKAPTKEAGAVVPQSK	50.358
KAL1	Anosmin-1	P23352	S	338	0.931	IPVHHYKVFWSWMVSSKSLVPTKKKRRKTTD	43.592
KAL1	Anosmin-1	P23352	S	337	0.926	DIPVHHYKVFWSWMVSSKSLVPTKKKRRKTT	43.592
KIAA1551	Uncharacterized protein KIAA1551	Q9HCM1	S	1331	1.000	QASQETRQKKHVTQNSRPLKTKTAFLPNKDV	45.997
KIAA1551	Uncharacterized protein KIAA1551	Q9HCM1	T	1328	1.000	SYEQASQETRQKKHVTQNSRPLKTKTAFLPN	45.997
KIAA1551	Uncharacterized protein KIAA1551	Q9HCM1	T	1336	1.000	TRQKKHVTQNSRPLKTKTAFLPNKDVYKKHS	45.997

KIF20B	Kinesin-like protein KIF20B	Q96Q89	S	351	1.000	HQSVAFTKLNNASSRSHSIFTVKILQIEDSE	60.961
KIF20B	Kinesin-like protein KIF20B	Q96Q89	S	353	1.000	SVAFTKLNNASSRSHSIFTVKILQIEDSEMS	60.961
KIF20B	Kinesin-like protein KIF20B	Q96Q89	T	356	1.000	FTKLNNASSRSHSIFTVKILQIEDSEMSRVI	60.961
KIF20B	Kinesin-like protein KIF20B	Q96Q89	T	818	0.996	EPPAKKGSIHVSSAITEDQKKSEEVRPNIAE	52.731
KIF20B	Kinesin-like protein KIF20B	Q96Q89	S	815	0.819	QQDEPPAKKGSIHVSSAITEDQKKSEEVRPN	52.731
KIF27	Kinesin-like protein KIF27	Q86VH2	S	754	0.997	LIKELIKTGNDAKSVSKQYSLKVTKLEHDAE	120.77
KIF27	Kinesin-like protein KIF27	Q86VH2	T	746	0.987	INIKMKEDLIKELIKTGNDAKSVSKQYSLKV	120.77
KIR2DL4	Killer cell immunoglobulin-like receptor 2DL4	Q99706	S	317	1.000	QLDHCIFTQRKITGPSQRSKRPSTDTSVCIE	61.679
KIR2DL4	Killer cell immunoglobulin-like receptor 2DL4	Q99706	T	314	0.999	TYAQLDHCIFTQRKITGPSQRSKRPSTDTSV	61.679
KLHL11	Kelch-like protein 11	Q9NVR0	T	449	0.994	EHVCSLMTRKHSFGLTEVKGKLYSIGGHGNF	79.474
LAMA1	Laminin subunit alpha-1	P25391	T	2467	0.965	KSFVGCIKNLEISRSTFDLLRNSYGVRKGCL	79.466
LGI2	Leucine-rich repeat LGI family member 2	Q8N0V4	S	154	1.000	SLANNHIKALPRDVFSDLDSLIELDLRGNKF	61.186
LGI2	Leucine-rich repeat LGI family member 2	Q8N0V4	S	158	1.000	NHIKALPRDVFSDLDSLIELDLRGNKFECDC	61.186
LMOD2	Leiomodin-2	B4DRR2	S	11	0.907	_____MSTFGYRRGLSKYESIDEDELLASLS	44.246
LOC401408	LOC401408	A4D1S1	T	10	1.000	______MEILLFLKLTTPSALKAHLGVSTKT	76.035
LOC401408	LOC401408	A4D1S1	T	11	0.822	_____MEILLFLKLTTPSALKAHLGVSTKTS	76.035
LPPR2	Alternative protein LPPR2	L0R5B8	T	9	0.994	_______MTVPTPSPTQGLRLPAECLLLLST	44.98
LPPR2	Alternative protein LPPR2	L0R5B8	S	7	0.960	_________MTVPTPSPTQGLRLPAECLLLL	44.98
LPPR2	Alternative protein LPPR2	L0R5B8	T	5	0.867	_________MTVPTPSPTQGLRLPAECLL	44.98
LRIG1	Leucine-rich repeats and immunoglobulin-like domains protein 1	Q96JA1	S	473	0.913	RMLQAFVTATCAHPESLKGQSIFSVPPESFV	79.23
LRRC16A	Leucine-rich repeat-containing protein 16A	Q5VZK9	T	902	0.996	EEKPVKRSIITVEELTEIERLEDLDTCMMTP	46.955
LRRC16A	Leucine-rich repeat-containing protein 16A	Q5VZK9	T	897	0.969	EIELAEEKPVKRSIITVEELTEIERLEDLDT	46.955
LRRC53	Leucine-rich repeat-containing protein 53	A6NM62	T	1189	0.859	NIQPDKDSAHKEGAMTVETHEALSFLPGLKD	43.799
LRRC56	Leucine-rich repeat-containing protein 56	Q8IYG6	S	287	0.984	PIRRLDPELSLPETQSRASRPWPFSLLVRGG	65.5
LRRK2	Leucine-rich repeat serine/threonine-protein kinase 2	Q5S007	T	838	0.932	PDKTSNLRKQTNIASTLARMVIRYQMKSAVE	40.725
LSM8	U6 snRNA-associated Sm-like protein LSm8	O95777	S	18	0.992	SALENYINRTVAVITSDGRMIVGTLKGFDQT	53.565
LSM8	U6 snRNA-associated Sm-like protein LSm8	O95777	T	17	0.965	TSALENYINRTVAVITSDGRMIVGTLKGFDQ	53.565
LTA4H	Leukotriene A(4) hydrolase;Leukotriene A-4 hydrolase	P09960	S	595	0.984	KSHDQAVRTYQEHKASMHPVTAMLVGKDLKV	57.836
LYST	Lysosomal-trafficking regulator	Q99698	T	3096	1.000	QLRDNAVEIFLTNGRTLLLAFDNTKVRDDVY	56.225
MACF1	Microtubule-actin cross-linking factor 1, isoforms 1/2/3/5	Q9UPN3	T	7077	0.819	TRQEFIDGILASKFPTTKLEMTAVADIFDRD	71.08
MAGI3	Membrane-associated guanylate kinase, WW and PDZ domain-containing protein 3	Q5TCQ9	T	1496	0.909	LITPGPWKVPSGNKVTGTIGMAEKRQ_____	68.787
MARS2	Methionine--tRNA ligase, mitochondrial	Q96GW9	S	16	1.000	MLRTSVLRLLGRTGASRLSLLEDFGPRYYSS	46.606
MARS2	Methionine--tRNA ligase, mitochondrial	Q96GW9	T	13	0.998	___MLRTSVLRLLGRTGASRLSLLEDFGPRY	46.606
MDN1	Midasin	Q9NU22	S	4247	0.972	LMKMLVRQRRSLTTLSEQWIILRNLLSCVQE	79.346
MED26	Mediator of RNA polymerase II transcription subunit 26	O95402	T	51	0.998	SSLEKYPITKEALEETRLGKLINDVRKKTKN	44.132
MINA	Bifunctional lysine-specific demethylase and histidyl-hydroxylase MINA	Q8IUF8	T	322	0.846	RLSGFLRTLADRLEGTKELLSSDMKKDFIMH	73.499
MLH3	DNA mismatch repair protein Mlh3	Q9UHC1	T	652	0.942	RAQETFGNRTRHSVETPDIKDLASTLSKESG	47.942
MLH3	DNA mismatch repair protein Mlh3	Q9UHC1	T	646	0.778	VRPGPTRAQETFGNRTRHSVETPDIKDLAST	47.942
MLIP	Muscular LMNA-interacting protein	E9PCK9	T	318	0.978	SLKSNSASYIPVRIVTHSLSPSPKPFTSSFH	51.346
MPND	MPN domain-containing protein	Q8N594	S	445	0.770	EPWSQEHTYLDKLKISLASRTPKDQSLCHVL	54.776
MPND	MPN domain-containing protein	Q8N594	S	448	0.770	SQEHTYLDKLKISLASRTPKDQSLCHVLEQV	54.776
MROH2A	Maestro heat-like repeat-containing protein family member 2A	A6NES4	T	1189	0.892	AEVWLAVSENVPFARTMLHSLMGRLQSRLSP	72.848
MRPL2	60S ribosomal protein L8	A0A024RD44	S	10	1.000	______MQAGDTILNSNHIGRMAVAAREGDA	77.185
MTUS1	Microtubule-associated tumor suppressor 1	Q9ULD2	S	1249	0.991	LHNGDLCSPKRSPTSSAIPLQSPRNSGSFPS	66.56
MTUS1	Microtubule-associated tumor suppressor 1	Q9ULD2	T	1247	0.797	WKLHNGDLCSPKRSPTSSAIPLQSPRNSGSF	66.56
MUC6	Mucin-6	Q6W4X9	S	458	1.000	GVSHSETSLVAVVYLSRQDKIVISQDEVVTN	62.165
MUC6	Mucin-6	Q6W4X9	T	449	0.895	ALMAVYDKSGVSHSETSLVAVVYLSRQDKIV	62.165

MYO7A	Unconventional myosin-VIIa	Q13402	S	659	0.993	PMLFDRHLCVRQLRYSGMMETIRIRRAGYPI	40.589
NADSYN1	Glutamine-dependent NAD(+) synthetase	H0YCQ6	T	247	1.000	DVQTRKNGLLLPQMETNPKCTNTTKSNF___	55.899
NCKIPSD	NCK-interacting protein with SH3 domain	Q9NZQ3	S	105	0.994	RGVLQKLIHHRKETLSRRGPSASSVAVMTSS	64.297
NEXN	Nexilin	Q0ZGT2	T	606	0.997	TSVVDSEPVRFTVKVTGEPKPEITWWFEGEI	42.396
NFE2L2	Nuclear factor erythroid 2-related factor 2	C9JFL6	T	137	1.000	KITWLIEKLHHNYKITIYSM__________	99.139
NIT2	Omega-amidase NIT2	Q9NQR4	S	14	1.000	__MTSFRLALIQLQISSIKSDNVTRACSFIR	49.536
NIT2	Omega-amidase NIT2	Q9NQR4	S	15	1.000	_MTSFRLALIQLQISSIKSDNVTRACSFIRE	49.536
NLRC3	NLR family CARD domain-containing protein 3	Q7RTR2	T	143	0.785	FLPLSRVSVPPRVSITIGVAGMGKTTLVRHF	45.873
NLRP9	NACHT, LRR and PYD domains-containing protein 9	Q7RTR0	T	474	1.000	LKRPKDDPNPAIGSITQLVRASVVQPQTLLT	54.7
NPAS2	Neuronal PAS domain-containing protein 2	Q99743	S	622	1.000	STQGPKPMRSSQLMQSSGRSGSSLVSPFSSA	52.579
NPAS2	Neuronal PAS domain-containing protein 2	Q99743	S	623	1.000	TQGPKPMRSSQLMQSSGRSGSSLVSPFSSAT	52.579
NPAS2	Neuronal PAS domain-containing protein 2	Q99743	T	608	0.999	QVTSQHLLRESSVISTQGPKPMRSSQLMQSS	47.189
NR3C1	Glucocorticoid receptor	P04150	S	673	1.000	VSYEEYLCMKTLLLLSSVPKDGLKSQELFDE	46.39
NR3C1	Glucocorticoid receptor	P04150	S	674	1.000	SYEEYLCMKTLLLLSSVPKDGLKSQELFDEI	46.39
NR3C1	Glucocorticoid receptor	P04150	T	668	1.000	LHRLQVSYEEYLCMKTLLLLSSVPKDGLKSQ	46.39
NSFL1C	NSFL1 cofactor p47	Q9UNZ2	S	177	0.990	EEESAYVAGEKRQHSSQDVHVVLKLWKSGFS	51.252
NT5DC3	5'-nucleotidase domain-containing protein 3	Q86UY8	S	304	0.778	ADHGKKMFLITNSPSSFVDKGMSYIVGKDWR	67.207
NUCKS1	Nuclear ubiquitous casein and cyclin-dependent kinase substrate 1	Q9H1E3	S	204	0.999	VGRPTASKASKEKTPSPKEEDEEPESPPEKK	54.765
NUMA1	Nuclear mitotic apparatus protein 1	Q14980	S	934	0.875	LETLVRKAGEQQETASRELVKEPARAGDRQP	53.211
NUMA1	Nuclear mitotic apparatus protein 1	H0YFY6	T	576	1.000	EEGTPLSITRHKALMTIIPDLSPNNPLSKLP	49.223
NUMA1	Nuclear mitotic apparatus protein 1	H0YFY6	S	582	0.995	SITRHKALMTIIPDLSPNNPLSKLPRTQPDG	49.223
NUMA1	Nuclear mitotic apparatus protein 1	Q14980	T	2106	0.998	ATTTASAATAAAIGATPRAKGKAKH_______	47.752
ODF1	Outer dense fiber protein 1	Q14990	S	10	0.999	_______MAALSCLLDSVRRDIKKVDRELRQL	103.7
ODF1	Outer dense fiber protein 1	Q14990	S	10	0.999	_______MAALSCLLDSVRRDIKKVDRELRQL	101.65
OR10A3	Olfactory receptor 10A3	P58181	T	231	0.767	LSYIRVLFAILKMPSTTGRQKAFSTCASHLT	48.467
OR2T12	Olfactory receptor 2T12	Q8NG77	T	85	1.000	MLVSTTVPKMAADYLTGNKAISRAGCGVQIF	66.663
OR4K15	Olfactory receptor 4K15	Q8NH41	T	158	0.992	AYDRYVAICKPLHYMTVMSRRVCVVLVLISW	79.906
ORAOV1	Protein LTO1 homolog	B4DFA5	S	119	1.000	EDLDKIRGKFKQTGLSPSAVMVRPPSYVELP	44.598
ORAOV1	Protein LTO1 homolog	B4DFA5	S	121	1.000	LDKIRGKFKQTGLSPSAVMVRPPSYVELPVT	44.598
ORAOV1	Protein LTO1 homolog	B4DFA5	T	116	1.000	KLHEDLDKIRGKFKQTGLSPSAVMVRPPSYV	44.598
OTUD3	OTU domain-containing protein 3	Q5T2D3	T	165	1.000	VVIHQLNAPLWQIRGTEKSSVRELHIAYRYG	45.696
OXTR	Oxytocin receptor isoform A	X5DRH4	T	35	1.000	RRGPRATAPPDPRGATRPWRAWRWRCCVSSC	64.776
PANK1	Pantothenate kinase 1	Q8TE04	S	528	1.000	DLARATLVTITNNIGSIARMCALNENIDRVV	44.543
PANK1	Pantothenate kinase 1	Q8TE04	T	523	1.000	SISKEDLARATLVTITNNIGSIARMCALNEN	44.543
PANK1	Pantothenate kinase 1	Q8TE04	T	521	0.999	RDSISKEDLARATLVTITNNIGSIARMCALN	44.543
PARP1	Poly [ADP-ribose] polymerase 1	P09874	T	432	0.965	GKLTGTANKASLCISTKKEVEKMNKKMEEVK	72.531
PARP1	Poly [ADP-ribose] polymerase 1	P09874	S	427	0.939	IEKLGGKLTGTANKASLCISTKKEVEKMNKK	72.531
PARP8	Protein mono-ADP-ribosyltransferase PARP8	D6R9T2	T	42	0.913	CLFADFRYSDSTFTFTYVGGPRR_________	46.844
PCBP4	Poly(rC)-binding protein 4	P57723	T	103	1.000	CAAPANGGNVSRPPVTLRLVIPASQCGSLIG	43.955
PDE4C	cAMP-specific 3',5'-cyclic phosphodiesterase 4C	Q08493	T	265	1.000	ETSRSGNQVSEYISRTFLDQQTEVELPKVTA	41.48
PDE4C	cAMP-specific 3',5'-cyclic phosphodiesterase 4C	Q08493	T	271	1.000	NQVSEYISRTFLDQQTEVELPKVTAEEAPQP	41.48
PER1	Period circadian protein homolog 1	O15534	T	779	0.999	VAPDPAPDAYRPVGLTKAVLSLHTQKEEQAF	48.623
PFKM	ATP-dependent 6-phosphofructokinase, muscle type	P08237	T	761	0.870	RPILKILAKYEIDLDTSDHAHLEHITRKRSG	51.819
PFKP	ATP-dependent 6-phosphofructokinase, platelet type	Q01813	S	142	1.000	GDGSLTGANLFRKEWSGLLEELARN_______	57.567
PGK2	Phosphoglycerate kinase 2	P07205	T	8	0.864	_________MSLSKKLTLDKLDVRGKRVIMRV	53.493
PHKA1	Phosphorylase b kinase regulatory subunit alpha, skeletal muscle isoform	P46020	T	303	1.000	QGRYGCCRFLRDGYKTPKEDPNRLYYEPAEL	42.031
PKMYT1	Membrane-associated tyrosine- and threonine-specific cdc2-inhibitory kinase	B4DZM6	T	544	0.999	SAFVWSLTCSSHHGRTFEARTKVDPLFKICG	40.268

PLAA	Phospholipase A-2-activating protein	Q9Y263	T	530	1.000	DPFTGNSAYRSAASKTMNIYFPKKEAVTFDQ	49.423
PLD2	Phospholipase D2	O14939	S	512	1.000	PDLSHNQFFWLGKDYSNLITKDWVQLDRPFE	66.285
PLD2	Phospholipase D2	O14939	T	516	1.000	HNQFFWLGKDYSNLITKDWVQLDRPFEDFID	66.285
POLE1	DNA polymerase epsilon catalytic subunit A	Q07864	S	891	1.000	FVFKTTNVKKPKVTISYPGAMLNIMVKEGFT	82.483
POLE1	DNA polymerase epsilon catalytic subunit A	Q07864	T	889	1.000	ENFVFKTTNVKKPKVTISYPGAMLNIMVKEG	82.483
POLR2D	DNA-directed RNA polymerase II subunit RPB4	O15514	T	79	0.962	TLNYTARFSRFKNRETIASVRSLLLQKKLHK	44.252
POLR2D	DNA-directed RNA polymerase II subunit RPB4	O15514	S	82	0.929	YTARFSRFKNRETIASVRSLLLQKKLHKFEL	44.252
PRDM16	PR domain zinc finger protein 16	Q9HAZ2	S	1218	0.994	EEAFEVKDVLNSTLDSEALKHTLCRQAKNQA	96.371
PRKCSH	Glucosidase 2 subunit beta	P14314	T	178	1.000	QAGKKSLEDQVEMLRTVKEEAEKPEREAKEQ	43.761
PSG8	Pregnancy-specific beta-1-glycoprotein 8	E7ENH0	T	141	0.989	MGGDENRGVTGHFTFTLYPKLPKPYITINNL	45.28
PTGER3	Prostaglandin E2 receptor EP3 subtype	P43115	S	167	1.000	AVERALAIRAPHWYASHMKTRATRAVLLGVW	53.013
PTGER3	Prostaglandin E2 receptor EP3 subtype	P43115	T	171	0.999	ALAIRAPHWYASHMKTRATRAVLLGVWLAVL	53.013
PTPN18	Tyrosine-protein phosphatase non-receptor type 18	Q99952	T	374	0.863	KRGAPAGAGSGTQTGTGTGTGARSAEEAPLY	48.376
PTPN7	Protein-tyrosine-phosphatase	A0A024R9A7	S	4	1.000	___________MGASFWPIRQAREQQRRAL	50.843
PTPRB	Receptor-type tyrosine-protein phosphatase beta	P23467	S	192	0.851	SKYNIAITAVSGGKRSFSVYTNGSTVPSPVK	47.545
PTPRS	Protein-tyrosine-phosphatase	Q59FX6	S	631	1.000	GAFTPVVRQRTLQSISPKNFKVKMIMKTSVL	47.559
PTPRS	Protein-tyrosine-phosphatase	Q59FX6	S	629	0.999	GLGAFTPVVRQRTLQSISPKNFKVKMIMKTS	47.559
PXYLP1	2-phosphoxylose phosphatase 1	B7Z3R9	T	5	0.998	___________MDVLTALLLVHLIPVSTPKN	45.363
PYCR2	Pyrroline-5-carboxylate reductase	A0A024R3Q9	T	17	0.999	NLPTVSALRKMGVNLTRSNKETVKHSDVLFL	40.066
QSOX1	Sulfhydryl oxidase 1	O00391	T	276	0.998	AYLQRLSGLTREAAQTTVAPTTANKIAPTVW	65.5
RAB11FIP4	Rab11 family-interacting protein 4	J3QLM3	T	3	1.000	_____MRTPPALGSQVSGGPGAG	47.189
RAB11FIP4	Rab11 family-interacting protein 4	J3QLM3	S	9	0.838	_____MRTPPALGSQVSGGPGAGARRAPA	47.189
RAB7A	Ras-related protein Rab-7a	P51149	T	47	1.000	KFSNQYKATIGADFLTKEVMVDDRLVTMQET	61.679
RALGAPA1	Ral GTPase-activating protein subunit alpha-1	Q6GYQ0	T	320	1.000	VIRWLVSFWLEPKPHTGPHIPGMEGEVLPKN	69.721
RASGRF1	Ras-specific guanine nucleotide-releasing factor 1	Q13972	S	506	1.000	QCFLFSKHLIICTRGSGGKLHLTKNGVISLI	48.131
RASGRF1	Ras-specific guanine nucleotide-releasing factor 1	Q13972	T	503	1.000	GERQCFLFSKHLIICTRGSGGKLHLTKNGVI	48.131
RASGRF1	Ras-specific guanine nucleotide-releasing factor 1	Q13972	T	513	1.000	HLIICTRGSGGKLHLTKNGVISLIDCTLLEE	48.131
RBM3	RNA binding motif (RNP1, RRM) protein 3	Q9H5V0	S	57	0.850	LSLWMVVRSVWIMQASLLGEPEEVALGPMGV	40.764
RETSAT	All-trans-retinol 13,14-reductase	Q6NUM9	S	322	0.984	IQRAGGAVLTKATVQSVLLDSAGKACGVSVK	99.53
RGS6	Regulator of G-protein-signaling 6	B7Z7N5	S	390	1.000	SNAYQDLLLAKKKPESEQGRRTSLEKFTRSV	51.771
RGS6	Regulator of G-protein-signaling 6	B7Z7N5	S	397	1.000	LLAKKKPESEQGRRTSLEKFTRSVGKSLAGK	51.771
RGS6	Regulator of G-protein-signaling 6	B7Z7N5	T	396	1.000	LLLAKKKPESEQGRRTSLEKFTRSVGKSLAG	51.771
RLTPR	Leucine-rich repeat-containing protein 16C	Q6F5E8	S	830	0.785	TLDTARSLCPQMLQGSSWREQLEGVLAGSRG	63.184
RND1	Rho-related GTP-binding protein Rho6	Q92730	S	192	1.000	HSIFRTASMLCLNKPSPLPQKSPVRSLSKRL	55.353
RNF10	RING finger protein 10	Q8N5U6	T	281	0.801	CYSSVHKKDLKSVVATESHQYVVGDTITMQL	44.105
RNF222	RING finger protein 222	A6NCQ9	T	68	0.999	GQVQRTLVCPICRYVTFLSKKSSRWPSMLDK	51.211
RPE65	Retinoid isomerohydrolase	Q16518	T	525	1.000	LSEVARAEVEINIPVTFHGLFKKS_______	44.601
RSPH3	Radial spoke head protein 3 homolog	Q86UC2	T	445	0.998	IEIGFLPWLMNEVEKTMEYSMVGRTVLDMLI	48.177
RSPH3	Radial spoke head protein 3 homolog	Q86UC2	S	449	0.972	FLPWLMNEVEKTMEYSMVGRTVLDMLIREVV	48.177
RXFP2	Relaxin receptor 2	Q8WXD0	T	370	1.000	LQSLDLERIEIPNINTRMFQPMKNLSHIYFK	45.707
RYR1	Ryanodine receptor 1	P21817	S	4186	1.000	EYFRPYLGRIEIMGASRRIERIYFEISETNR	53.995
RYR1	Ryanodine receptor 1	P21817	T	4748	0.990	YGRERIAELLGMDLATLEITAHNERKPNPPP	50.938
RYR1	Ryanodine receptor 1	P21817	T	2911	0.999	KGGGTHPLLVPYDTLTAKEKARDREKAQELL	47.204
RYR1	Ryanodine receptor 1	P21817	T	2909	0.991	EAKGGGTHPLLVPYDTLTAKEKARDREKAQE	47.204
SACS	Sacsin	Q9NZJ4	S	1222	0.999	VNLEKALGIFTKPSLSAVLKHFKIVVDWYSS	86.512
SCN10A	Sodium channel protein type 10 subunit alpha	Q9Y5Y9	T	1194	1.000	KPTVKALLEYTDRVFTFIFVFEMLLKWVAYG	47.774
SERPINA9	Serpin A9	Q86WD7	S	134	0.876	HSLTVPSKDLTLKMGSALFVKKELQLQANFL	53.569

SETX	Probable helicase senataxin	Q7Z333	S	1330	1.000	KTVGVVDTRKKTKLISPQNLSVRNNKKLLTS	79.471
SETX	Probable helicase senataxin	Q7Z333	S	1335	1.000	VDTRKKTKLISPQNLSVRNNKKLLTSQELQM	79.471
SGOL2	Shugoshin 2	C9JW92	T	77	0.884	AQALSREKENSRRITTEKMLLQKEVE_____	76.326
SHANK1	SH3 and multiple ankyrin repeat domains protein 1	Q9Y566	S	1928	0.992	PERTSSLQRQRLSDDSQSSLLSKPVSSLFQN	49.216
SHANK1	SH3 and multiple ankyrin repeat domains protein 1	Q9Y566	S	1930	0.970	RTSSLQRQRLSDDSQSSLLSKPVSSLFQNWP	49.216
SIT1	Signaling threshold-regulating transmembrane adapter 1	Q9Y3P8	T	113	1.000	TGRLSQDPEPDQQDPTLGGPARAAEEVMCYT	59.862
SLC20A2	Sodium-dependent phosphate transporter 2	Q08357	T	243	1.000	FFVWLFVCPWMRRKITGKLQKEGALSRVSDE	65.175
SLC26A10	Solute carrier family 26 member 10	Q8NG04	S	10	0.994	______MRLDLASLMSAPKSLGSAFKSWRLD	54.235
SMC6	Structural maintenance of chromosomes protein 6	Q96SB8	S	848	1.000	KRELDMKEKELEEKMSQARQICPERIEVEKS	69.672
SNED1	Sushi, nidogen and EGF-like domain-containing protein 1	Q8TER0	T	1399	0.981	DICFKESCESTSLKKTPNRKQSKSQTLEKS_	50.284
SNED1	Sushi, nidogen and EGF-like domain-containing protein 1	Q8TER0	T	1394	0.787	YRVHQDICFKESCESTSLKKTPNRKQSKSQT	50.284
SPAST	Spastin	Q9UBP0	T	183	1.000	GEQCERARRLQAKMMTNLVMAKDRLQLLEKM	51.771
SPATA31D1	Spermatogenesis-associated protein 31D1	Q6ZQQ2	T	1339	0.870	HNKTSGEVLGSKSSPTLKTQPPPENLFRKWM	86.189
SPECC1	Cytospin-B	Q5M775	S	810	0.769	VDAAGRWPGVCVSRTSPTPPESATTVKSLIK	65.157
SPINK5	Serine protease inhibitor Kazal-type 5	Q9NQ38	S	1042	0.960	LCHENLIRQTNTHIRSTGKCEESSTPGTTAA	40.352
SRRM2	Serine/arginine repetitive matrix protein 2	Q9UQ35	T	1003	0.998	SHSGSISPYPKVKAQTPPGPSLSGSKSPCPQ	48.188
SRRM2	Serine/arginine repetitive matrix protein 2	Q9UQ35	S	1008	0.930	ISPYPKVKAQTPPGPSLSGSKSPCPQ_____	48.188
SSFA2	Sperm-specific antigen 2	P28290	T	799	1.000	____MEHDGQSLVKSTIFISPSSVKKEEAPQ	60.019
STARD5	StAR-related lipid transfer protein 5	Q9NSY2	T	101	0.863	FEIIQSITDTLCVSRTSTPSAAMKLISPRDF	64.827
STK26	Serine/threonine-protein kinase 26	Q9P289	T	396	0.988	LEKSIAVAEAACPGITDKMVKKLIEKFQKCS	61.444
STK32A	Serine/threonine-protein kinase 32A	Q8WU08	S	193	0.780	TTMAGTKPYMAPEMFSSRKGAGYSFAVDWWS	47.016
STK35	Serine/threonine-protein kinase 35	Q8TDR2	T	345	0.791	RRPDPATNKSFMLQLTSAIAFLHKNHIVHRD	49.929
STRIP1	Striatin-interacting protein 1	Q5VSL9	S	213	0.960	ACSSAVRKPAISLADSTDLRVLLNIMYLIVE	57.148
STX16	Syntaxin-16	O14662	S	61	0.863	_________MALVSGISLDPEAAIGVTKRPPP	43.198
SUCLG1	Succinyl-CoA ligase [ADP/GDP-forming] subunit alpha, mitochondrial	P53597	T	94	1.000	GTKLVGGTTPGKGGQTHLGLPVFNTVKEAKE	43.297
SUCLG1	Succinyl-CoA ligase [ADP/GDP-forming] subunit alpha, mitochondrial	P53597	T	103	1.000	PGKGGQTHLGLPVFNTVKEAKEQTGATASVI	43.297
SYBU	Syntabulin	Q9NX95	T	277	1.000	PNPEQYLTPLQQKEVTVRHLKTKLKESERRL	69.598
SYBU	Syntabulin	Q9NX95	T	283	1.000	LTPLQQKEVTVRHLKTKLKESERRLHERESE	69.598
SYCP2	Synaptonemal complex protein 2	Q9BX26	S	478	0.884	NNSQLEKTTPSKRKMSEASMIVSGADRYTMR	48.004
TCEB3	Transcription elongation factor B polypeptide 3	Q14241	S	80	0.918	TVDILAETGVGKTVNSLRKHEHVGSFARDLV	44.336
TCF20	Transcription factor 20	Q9UGU0	T	1624	0.981	EPEIKLKYATQPLDKTDAKNKSFYPYIHVVN	62.924
TEAD2	Transcriptional enhancer factor TEF-4	Q15562	S	101	1.000	YIKLRTGKTRTRKQVSSHIQVLARRKAREIQ	47.603
TEAD2	Transcriptional enhancer factor TEF-4	Q15562	S	102	1.000	IKLRTGKTRTRKQVSSHIQVLARRKAREIQA	47.603
THNSL1	Threonine synthase-like 1	Q8IYQ7	T	657	1.000	HTAVAKVVADRVQDKTCPVIISSTAHYSKFA	47.971
TLR3	Toll-like receptor 3	O15455	T	4	0.996	____________MRQTLPCIYFWGGLLPFGM	40.254
TM7SF2	Delta(14)-sterol reductase	O76062	S	340	1.000	GLETISTATGRKLLVSGWWGMVRHPNYLGDL	48.794
TMEM200A	Transmembrane protein 200A	Q86VY9	T	4	1.000	____________MIATGGVITGLAALKRQDS	50.292
TMEM200A	Transmembrane protein 200A	Q86VY9	T	9	1.000	________MIATGGVITGLAALKRQDSARSQQ	50.292
TNFRSF21	Tumor necrosis factor receptor superfamily member 21	O75509	S	315	0.999	HQQGPHHRHILKLLPSMEATGGEKSSTPIKG	43.208
TNFRSF21	Tumor necrosis factor receptor superfamily member 21	O75509	T	319	0.957	PHHRHILKLLPSMEATGGEKSSTPIKGPKRG	43.208
TPR	Nucleoprotein TPR	P12270	S	722	1.000	LRSQNTKISTQLDFASKRYEMLQDNVEGYRR	47.288
TPR	Nucleoprotein TPR	P12270	T	716	0.813	QEQVTDLRSQNTKISTQLDFASKRYEMLQDN	47.288
TPR	Nucleoprotein TPR	P12270	S	715	0.757	LQEQVTDLRSQNTKISTQLDFASKRYEMLQD	47.288
TRAPPC11	Trafficking protein particle complex subunit 11	Q7Z392	S	127	1.000	EKQSECATRVEIVRQSLQGRNTKVAVVLIQK	72.705
TRAPPC11	Trafficking protein particle complex subunit 11	Q7Z392	T	133	1.000	ATRVEIVRQSLQGRNTKVAVVLIQKKTPLPP	72.705
TRPC1	Short transient receptor potential channel 1	P48995	T	157	1.000	IVKLMERIQNPEYSTTMDVAPVILAAHRNNY	41.475
TRPC1	Short transient receptor potential channel 1	P48995	T	156	1.000	TIVKLMERIQNPEYSTTMDVAPVILAAHRNN	41.475

TRPM8	Transient receptor potential cation channel subfamily M member 8	H7BZP4	T	103	1.000	VPSDVDGKPDLAQMETAWRRHLLPEPTPRAA	45.997
TSC2	Tuberin	P49815	T	913	1.000	IRCRLPFRKDFVPFITKGLRSNVLLSFDDTP	76.221
TTC6	Tetratricopeptide repeat protein 6	G3V2C3	S	5	1.000	_____MKAQSTASMPPARPAPRAFP	64.842
TTC6	Tetratricopeptide repeat protein 6	G3V2C3	S	8	1.000	_____MKAQSTASMPPARPAPRAFPAPQ	64.842
TTC6	Tetratricopeptide repeat protein 6	G3V2C3	T	6	1.000	_____MKAQSTASMPPARPAPRAFPA	64.842
TTN	Titin	Q8WZ42	T	25722	0.818	ILKLSNVGGTKSIPITVKVLDRPGPPEGPLK	73.76
TTN	Titin	Q8WZ42	S	216	0.995	AKKTKTIVSTAQISESRQTRIEKKIEAHFDA	54.524
U2SURP	Alternative protein U2SURP	L8E737	T	14	1.000	__MMILMECLWMQLKTQKRMSLYLKLPHQNG	51.059
UBA1	Ubiquitin-like modifier-activating enzyme 1	P22314	S	995	0.989	KTEHKLEITMLSQGVSMLYSFFMPAAKLKER	50.883
UBA1	Ubiquitin-like modifier-activating enzyme 1	P22314	S	991	0.961	LDYFKTEHKLEITMLSQGVSMLYSFFMPAAK	50.883
UGT1A1	Bilirubin UDP-glucuronosyltransferase	W6JIA6	S	42	0.889	AGKILLIPVNGSHWLSMLGAIQQLQQRGHEI	42.705
UNC45A	Protein unc-45 homolog A	Q9H3U1	T	233	0.999	TLVGICSEHQSRTVATLSILGTRRVVSILGV	71.379
URGCP	Up-regulator of cell proliferation	Q8TCY9	T	711	0.993	STVGVPGTGKSTLLNTMFGLRFATGKSCGPR	72.23
USP15	Ubiquitin carboxyl-terminal hydrolase 15	Q9Y4E8	S	14	0.999	__MAEGGAADLDTQRSDIATLLKTSLRKGDT	48.467
USP15	Ubiquitin carboxyl-terminal hydrolase 15	Q9Y4E8	T	18	0.999	EGGAADLDTQRSDIATLLKTSLRKGDTWYLV	48.467
USP42	Ubiquitin carboxyl-terminal hydrolase;Ubiquitin carboxyl-terminal hydrolase 42	Q9H9J4	T	786	1.000	STKKAPPPRDPGTPATKEGAWEAMAVAPEEP	93.096
UTP20	Small subunit processome component 20 homolog	O75691	S	926	1.000	AAKQLIAHLQVFSKFSNPRALYLESKLYELY	101.65
VPS26A	Vacuolar protein sorting-associated protein 26A	O75436	S	245	1.000	IAKYEIMDGAPVKGESIPIRLFLAGYDPTPT	47.75
VPS33B	Vacuolar protein sorting-associated protein 33B	Q9H267	S	476	0.781	KLVTDKAAGKITDAFSSLAKRSNFRAISKKL	83.206
VPS33B	Vacuolar protein sorting-associated protein 33B	Q9H267	S	477	0.781	LVTDKAAGKITDAFSSLAKRSNFRAISKKLN	83.206
VWA3B	von Willebrand factor A domain-containing protein 3B	Q502W6	T	99	1.000	FPQLYRAEDGRVYNLTAKSELIYQFVEHLTQ	84.244
WDFY4	WD repeat- and FYVE domain-containing protein 4	Q6ZS81	S	2311	0.836	RMRKRIKRLSPLEALSSGRHKESQDKNDHIS	43.594
WDR25	WD repeat-containing protein 25	H0YJW0	S	91	0.999	EGHKVLLSLSPRRMLSPSPKPPGSPGHGPWG	57.798
WDR25	WD repeat-containing protein 25	H0YJW0	S	93	0.992	HKVLLSLSPRRMLSPSPKPPGSPGHGPWGAW	57.798
WDR25	WD repeat-containing protein 25	H0YJW0	S	85	0.942	SRRRRYEGHKVLLSLSPRRMLSPSPKPPGSP	57.798
WDR6	WD repeat-containing protein 6	Q9NNW5	T	988	0.864	SLTLQAHSCGINSLHTLPTREGHHLVASGSE	43.799
WDR7	WD repeat-containing protein 7	Q9Y4E6	S	163	0.759	VLYSLVSKISPDWISSMSIIRS_____	51.927
XYLT2	Xylosyltransferase 2	Q9H1B5	S	845	0.989	PSPCPSLEPCRLTSWSSLSPDPKSELGPVKA	46.891
XYLT2	Xylosyltransferase 2	Q9H1B5	S	843	0.989	IGPSPCPSLEPCRLTSWSSLSPDPKSELGPV	46.891
ZBED9	SCAN domain-containing protein 3	Q6R2W3	S	592	0.999	DIEENLSVTPKVAEKSPPESRLRFLSCVVCE	44.318
ZBTB47	Zinc finger and BTB domain-containing protein 47	Q9UFB7	S	567	0.988	TCGKSFKRSMSLKVHSLQHSGEKPFRCENCN	61.524
ZC3H12B	Probable ribonuclease ZC3H12B	Q5HYM0	T	473	0.928	EASSVPSLVTALSVPTIPPPKSHAVGALNTR	48.854
ZMYND11	Zinc finger MYND domain-containing protein 11	Q15326	S	435	0.826	SSQEIPTMPQPIEKVSVSTQTKKLSASSPRM	44.616
ZMYND11	Zinc finger MYND domain-containing protein 11	Q15326	T	440	0.802	PTMPQPIEKVSVSTQTKKLSASSPRMLHRST	44.616
ZNF212	Zinc finger protein 212	F2Z3G9	S	43	1.000	PGAGLRGLDAAGVLVSRGCRWRG_____	63.918
ZNF224	Zinc finger protein 224	Q9NZL3	T	70	1.000	DTFHFLREEKIWMMKTAIQREGNS_____	61.161
ZNF385A	Zinc finger protein 385A	Q96PM9	S	347	0.887	LAVAAVMAAAAGSPLSLRPAPAAPLLQGPPI	42.663
ZNF440	ZNF440 protein	Q05DD3	S	132	1.000	TMERNPMNVKNAEKHSACLLPFIDMKRLTLE	58.132
ZNF510	Zinc finger protein 510	Q9Y2H8	S	445	1.000	KPFECSECGKTFSQKSHLSTHQRIHTAEKPY	48.284
ZNF510	Zinc finger protein 510	Q9Y2H8	S	448	1.000	ECSECGKTFSQKSHLSTHQRIHTAEKPYKCN	48.284
ZNF510	Zinc finger protein 510	Q9Y2H8	T	449	1.000	CSECGKTFSQKSHLSTHQRIHTAEKPYKCNE	48.284
ZNF512B	Zinc finger protein 512B	Q96KM6	T	225	1.000	IGISKPVSVGRPMPVTKAIPVTRPVPVTKPV	76.17
ZNF512B	Zinc finger protein 512B	Q96KM6	T	231	1.000	VSVGRPMPVTKAIPVTRPVPVTKPVTVSRPM	76.17
ZNF512B	Zinc finger protein 512B	Q96KM6	S	25	0.997	RRLPGSSKSGPGKDGSRKEVRLPMLHDPPKM	45.879
ZNF512B	Zinc finger protein 512B	Q96KM6	S	18	0.994	DPFCVGGRRLPGSSKSGPGKDGSRKEVRLPM	45.879
ZNF512B	Zinc finger protein 512B	Q96KM6	S	15	0.887	_MTDPFCVGGRRLPGSSKSGPGKDGSRKEVR	45.879
ZNF585B	Zinc finger protein 585B	F2Z3L4	S	151	1.000	GKSFTWKSQFKASQNSYRRKTI_____	66.568

ZNF585B	Zinc finger protein 585B	F2Z3L4	S	148	1.000	AEFGKSFTWKSQFKASQNSYRRKTI_____	66.568
ZNF608	Zinc finger protein 608	Q9ULD9	T	409	1.000	VTWRNKTYVGTLLDCTKHDWAPPRTQIQEHG	60.518
ZNF608	Zinc finger protein 608	Q9ULD9	T	400	0.870	TEEGVLVVNVTWRNKTYVGTLLDCTKHDWAP	60.518
ZNF644	Zinc finger protein 644	Q9H582	S	846	1.000	DFLHKMTVVVLQKLNSAEKKDSYETEDESSW	54.871
ZNF644	Zinc finger protein 644	Q9H582	T	837	1.000	GGEDLDSYPDFLHKMTVVVLQKLNSAEKKDS	54.871
ZNF732	Zinc finger protein 732	B4DXR9	T	494	1.000	CGKAFLCSRALNKHKTIHTGEKPYECEECGK	61.435
ZNF732	Zinc finger protein 732	B4DXR9	T	497	1.000	AFLCSRALNKHKTIHTGEKPYECEECGKAFG	61.435
ZNF845	Zinc finger protein 845	Q96IR2	T	923	1.000	IHTGEKPYKCNECGKTFRHNSVLVIHKTIHT	49.463
ZNF845	Zinc finger protein 845	Q96IR2	S	928	1.000	KPYKCNECGKTFRHNSVLVIHKTIHTGEKPY	49.463
ZNF845	Zinc finger protein 845	Q96IR2	T	935	0.999	CGKTFRHNSVLVIHKTIHTGEKPYKCNECGK	49.463
ZZEF1	Zinc finger ZZ-type and EF-hand domain-containing protein 1	O43149	S	1395	0.906	GIRIWMLEMKQKSLMSLGNEAEEKHSSEATE	45.022

Supplementary table 2. The list of primers used in the study.

Primer name	Sequence
PKN3 T639G F	TTTGTGGGTGAGTTTGTGCC
PKN3 T639G R	GCAGGCATGGCTGGAGGT
ARHGAP18 N200 F	TAGGATCCATGAGCTGGCTCTCCAGT
ARHGAP18 N200 R	TAGAATTCTCATTTGTTTTCATTTGTTCT
ARHGAP18 N50 R	TAGAATTCTCAGCTTTCCTGGTTCATAGT
ARHGAP18 Iso2 F	ACAAGTCCGGACTCAGATCTATGAACCAGGAAAGCACCACCA
ARHGAP18 Iso2 R	TGGTGGTGCTTTCCTGGTTCATAGATCTGAGTCCGGACTTGT
ARHGAP18 ΔN200 F	ATCTATGAGCTGGTACCAAGGAAGAGA
ARHGAP18 ΔN200 R	TCTCTTCCTTGGTACCAGCTCATAGAT
ARHGAP18 Δ201-323 F	CAAATGAAAACAAAGTTCCATTGACAGC
ARHGAP18 Δ201-323 R	GCTGTCAATGGAACTTTGTTTTCATTTG
ARHGAP18 ΔGAP F	CTGGTCTTTTTTGCCCCAAGTTTATTGT
ARHGAP18 ΔGAP R	ACAATAAACTTGGGGCAAAAAAGACCAG
ARHGAP18 ΔC525 F	AACTTCTGTGGACATAGAACTCGAGAATTC
ARHGAP18 ΔC525 R	GAATTCTCGAGTTCTATGTCCACAGAAGTT
ARHGAP18 N200 Δ1-50 F	CGGACTCAGATCCATGACCACCATCAAAGTTA
ARHGAP18 N200 Δ1-50 R	TAACTTTGATGGTGGTCATGGATCTGAGTCCG
ARHGAP18 N200 Δ51-100 F	TATGAACCAGGAAAGCGTCAAAGAGCCTGATG
ARHGAP18 N200 Δ51-100 R	CATCAGGCTCTTTGACGCTTTCCTGGTTCATA
ARHGAP18 N200 Δ101-150 F	TCAAGAGGTGGTTGTTCGAGTAGAGACGGTCT
ARHGAP18 N200 Δ101-150 R	AGACCGTCTCTACTCGAACAACCACCTCTTGA
ARHGAP18 N200 Δ151-200 F	AGCAGCAGTTCAGAAGTGAGAATTCTGCAGTC
ARHGAP18 N200 Δ151-200 R	GACTGCAGAATTCTCACTTCTGAACTGCTGCT
ARHGAP18 N200 Δ1-12 F	CGGACTCAGATCCATGACAGCCTACCACCCCA
ARHGAP18 N200 Δ1-12 R	TGGGGTGGTAGGCTGTCATGGATCTGAGTCCG
ARHGAP18 N200 Δ13-25 F	CCAGGGAGTGGTACTAAACAGCCATGCAAAG
ARHGAP18 N200 Δ13-25 R	CTTTGCATGGCTGTTTAGTACCACTCCCTGG
ARHGAP18 N200 Δ26-37 F	GGACCAGACCGTCGGGAGTCGCAGATATGGCC
ARHGAP18 N200 Δ26-37 R	GGCCATATCTGCGACTCCCGACGGTCTGGTCC
ARHGAP18 N200 Δ38-50 F	GGAGGAAGCCACGTCGACCACCATCAAAGTTA
ARHGAP18 N200 Δ38-50 R	TAACTTTGATGGTGGTCGACGTGGCTTCCTCC

Supplementary table 3. The sequence of synthesized ARHGAP18. Silent mutations were introduced in the design of ARHGAP18 cDNA in order to disrupt *XhoI*, *SacI*, *BamHI* and *NcoI* restriction sites.

ARHGAP18
TACAGATCTATGAGCTGGCTCTCCAGTTCCCAGGGAGTGGTACTAACAGCCTACCACCCCAGCGGCAAGGACC
AGACCGTCGGGAACAGCCATGCAAAGGCAGGGGAGGAAGCCACGTCGAGTCGCAGATATGGCCAGTACACTAT
GAACCAGGAAAGCACCACCATCAAAGTTATGGAGAAGCCTCCATTTGATCGATCAATTTCCCAGGATTCTTTG
GATGAACTATCTATGGAAGACTATTGGATAGAACTAGAAAACATCAAGAAATCTAGTGAAAACAGCCAAGAAG
ATCAAGAGGTGGTTGTTGTCAAAGAGCCTGATGAGGGAGAATTGGAAGAAGAGTGGCTTAAAGAGGCCGGTTT
ATCCAATCTCTTCGGAGAGTCTGCTGGAGATCCACAGGAAAGCATTGTGTTTTTATCAACATTGACGCGGACC
CAGGCAGCAGCAGTTCAGAAGCGAGTAGAGACGGTCTCCCAGACCTTGAGGAAAAAAAACAAACAGTACCAGA
TTCCTGACGTCAGAGACATATTTGCTCAACAGAGAGAATCAAAAGAAACAGCTCCAGGTGGCACTGAATCGCA
GTCACTTAGAACAAATGAAAACAAATACCAAGGAAGAGATGACGAGGCATCTAACCTTGTTGGTGAAGAGAAG
CTGATCCCACCTGAGGAGACGCCTGCCCCTGAAACAGACATCAACCTGGAGGTATCATTTGCCGAGCAAGCAC
TCAATCAGAAAGAGAGTTCCAAGGAGAAAATCCAGAAGAGCAAAGGCGATGATGCCACATTACCTAGTTTCAG
ATTGCCAAAAGACAAAACGGGTACCACAAGGATTGGTGACCTCGCACCCCAGGACATGAAGAAAGTTTGCCAT
TTAGCCCTAATTGAGCTGACTGCCCTCTATGATGTATTGGGTATTGAGCTGAAACAACAAAAAGCTGTGAAAA
TCAAAACAAAAGATTCTGGTCTTTTTTGCGTTCCATTGACAGCGCTATTAGAACAAGATCAGAGGAAAGTACC
AGGAATGCGAATACCCTTGATCTTTCAAAAACTGATTTCTCGAATTGAAGAGAGAGGTTTGGAAACAGAAGGC
CTCTTACGAATCCCTGGAGCTGCCATTAGAATCAAGAATCTTTGCCAAGAACTAGAAGCAAAGTTTTATGAAG
GGACTTTTAATTGGGAAAGTGTCAAACAGCATGATGCCGCCAGCCTGCTGAAGCTCTTCATTCGGGAGTTGCC
CCAGCCACTGCTCAGTGTGGAGTATCTCAAAGCCTTTCAGGCTGTCCAGAATCTTCCAACCAAGAAGCAGCAA
CTACAGGCTTTGAACCTTCTTGTCATCCTCCTACCTGATGCAAACAGGGACACACTGAAGGCCCTTCTTGAAT
TTCTCCAAAGAGTAATAGATAATAAAGAAAAAAATAAAATGACAGTCATGAATGTAGCAATGGTCATGGCCCC
GAATCTCTTTATGTGTCATGCATTGGGATTGAAGTCCAGTGAACAGCGAGAATTTGTAATGGCAGCTGGGACA
GCAAATACCATGCACTTATTGATTAAGTACCAAAAACTTCTGTGGACAATTCCCAAGTTTATTGTAAACCAAG
TGAGGAAGCAAAACACGGAAAATCATAAAAAGGATAAAAGAGCCATGAAGAAATTGCTGAAGAAAATGGCTTA
TGACCGAGAAAAATATGAAAAGCAAGATAAGAGTACAAATGATGCTGACGTTCCTCAGGGAGTGATTCGAGTG
CAAGCTCCCCATCTTTCGAAAGTTTCAATGGCAATACAGCTAACTGAAGAACTAAAAGCCAGTGATGTACTTG
CCAGGTTTCTCAGCCAAGAAAGTGGGGTTGCCCAGACTCTCAAGAAAGGAGAAGTTTTTTTGTATGAAATTGG
AGGAAATATTGGGGAACGCTGCCTTGATGATGACACTTACATGAAGGATTTATATCAGCTTAACCCAAATGCT
GAGTGGGTTATAAAGTCAAAGCCATTGTAGAACTCGAGAATTCTGA

© 2017. Published by The Company of Biologists Ltd | Journal of Cell Science (2017) 130, 2382-2393 doi:10.1242/jcs.197434

RESEARCH ARTICLE

ARHGAP42 is activated by Src-mediated tyrosine phosphorylation to promote cell motility

Weifeng Luo[3,‡], Radoslav Janoštiak[1,‡], Ondřej Tolde[1,2,‡], Larisa M. Ryzhova[3,*,‡], Lenka Koudelková[1,2], Michal Dibus[1,2], Jan Brábek[1,2], Steven K. Hanks[3] and Daniel Rosel[1,2,§]

ABSTRACT

The tyrosine kinase Src acts as a key regulator of cell motility by phosphorylating multiple protein substrates that control cytoskeletal and adhesion dynamics. In an earlier phosphotyrosine proteomics study, we identified a novel Rho-GTPase activating protein, now known as ARHGAP42, as a likely biologically relevant Src substrate. ARHGAP42 is a member of a family of RhoGAPs distinguished by tandem BAR-PH domains lying N-terminal to the GAP domain. Like other family members, ARHGAP42 acts preferentially as a GAP for RhoA. We show that Src principally phosphorylates ARHGAP42 on tyrosine 376 (Tyr-376) in the short linker between the BAR-PH and GAP domains. The expression of ARHGAP42 variants in mammalian cells was used to elucidate its regulation. We found that the BAR domain is inhibitory toward the GAP activity of ARHGAP42, such that BAR domain deletion resulted in decreased active GTP-bound RhoA and increased cell motility. With the BAR domain intact, ARHGAP42 GAP activity could be activated by phosphorylation of Tyr-376 to promote motile cell behavior. Thus, phosphorylation of ARHGAP42 Tyr-376 is revealed as a novel regulatory event by which Src can affect actin dynamics through RhoA inhibition.

KEY WORDS: Src, Motility, RhoA, GAP, GRAF, Focal adhesion, Tyrosine phosphorylation

INTRODUCTION

Src is a nonreceptor protein tyrosine kinase that becomes activated following the engagement of many different classes of cellular receptors, including receptor protein tyrosine kinases, integrins and other adhesion receptors, and cytokine and G protein-coupled receptors, and thereby participates in signaling pathways that control cell cycle progression, apoptosis, cell adhesion and migration (reviewed in Frame, 2004). Deregulation of Src activity by overexpression or mutation can result in oncogenic cell transformation and invasive properties. Elevated Src activity is commonly observed in tumors and Src has become an established therapeutic target (reviewed in Rosel et al., 2013).

[1]Department of Cell Biology, Charles University in Prague, Viničná 7, Prague, 12843, Czech Republic. [2]Department of Cell Biology, Biotechnology and Biomedicine Centre of the Academy of Sciences and Charles University (BIOCEV), Průmyslová 595, Vestec u Prahy 25242, Czech Republic. [3]Department of Cell and Developmental Biology, Vanderbilt University School of Medicine, Nashville, TN 37232, USA.
*Present address: Center for Molecular Medicine, Maine Medical Center Research Institute, Scarborough, ME 04074, USA.
‡These authors contributed equally to this work

§Author for correspondence (rosel@natur.cuni.cz)

D.R., 0000-0001-7221-8672

Received 13 September 2016; Accepted 26 May 2017

Src plays an essential role in cell migration through regulation of cytoskeletal organization and adhesion dynamics. 'SYF' fibroblasts (from mice lacking the Src-family kinases Src, Yes and Fyn) or fibroblasts ectopically expressing kinase-inactive Src exhibit impaired migration and large peripheral adhesions with reduced turnover (Fincham and Frame, 1998; Klinghoffer et al., 1999). In agreement, elevated Src activity is associated with the disruption of actin stress fibers followed by disassembly of focal adhesions (Fincham et al., 1999; Frame et al., 2002; Webb et al., 2004).

Src can regulate focal adhesion dynamics through distinct pathways. A well-studied pathway involves focal adhesion kinase (FAK, also known as PTK2) (reviewed in Hanks et al., 2003). Upon integrin receptor activation, FAK autophosphorylates tyrosine 397 to create a binding site for the Src SH2 domain, resulting in Src recruitment to nascent focal adhesions. FAK phosphorylation at tyrosine 925 by Src results in activation of Erk proteins via the Grb2/SOS/Ras pathway (Schlaepfer et al., 1994) and subsequently the activation of MLCK (also known as MYLK), which is important for actin dynamics at lamellipodia (Cheresh et al., 1999). The FAK–Src complex phosphorylates p130Cas and paxillin (Hanks et al., 2003; Nojima et al., 1995), resulting in recruitment of the Rac-specific GEFs DOCK180 and β-PIX to focal adhesions (Kiyokawa et al., 1998; ten Klooster et al., 2006). Elevated activity of Rac promotes membrane ruffling, lamellipodium formation, and further formation of nascent focal adhesions by acting on the WASP and WAVE (also known as WAS and WASF) family of Arp2/3 complex activators to stimulate actin polymerization (Eden et al., 2002; Klemke et al., 1998; Miki et al., 2000; Welch and Mullins, 2002). Src can also affect cytoskeletal organization by direct regulation of the activity of Rho GTPases. For example, the FAK–Src complex downregulates RhoA activity through Src-mediated tyrosine phosphorylation of p190RhoGAP (also known as ARHGAP35), thereby elevating its RhoGAP activity (Arthur et al., 2000; Bass et al., 2008). Downregulation of RhoA leads to upregulation of Rac, which in turn results in increased lamellipodial activity and focal adhesion dynamics (Huveneers and Danen, 2009; Ren et al., 2000).

Although many Src substrates have been identified, there is still much to learn about the multiple roles of Src in regulating cell behavior and transformation. Previously, we employed a proteomics approach to acquire a global view of the impact of oncogenic Src on the phosphotyrosine proteome of mouse embryonic fibroblasts (Luo et al., 2008). Among the novel putative Src substrates identified in that study was a then uncharacterized protein annotated as 'similar to oligophrenin-1'. The 'similar to oligophrenin-1' protein has subsequently been described as 'Rho GTPase-activating protein 42', encoded by the mouse gene *Arhgap42* (UniProtKB/Swiss-Prot accession number B2RQE8), and is a fourth mammalian member of a family of RhoGAPs that have N-terminal tandem Bin/amphiphysin/Rvs (BAR) and pleckstrin homology (PH) domains. In the present study, we have further characterized this protein

Journal of Cell Science

Journal of Cell Science (2017) 130, 2382-2393 doi:10.1242/jcs.197434

(herein designated as ARHGAP42) in order to gain insight into its cellular function and regulation. We show that ARHGAP42 localizes to stress fibers and focal adhesions, and possesses GAP activity towards RhoA, which is autoinhibited by its BAR domain. Moreover, we show that Src-mediated phosphorylation of ARHGAP42 tyrosine 376 (Tyr-376) stimulates GAP activity to promote focal adhesion dynamics and cell motility.

RESULTS

The putative Src substrate ARHGAP42, a member of the BAR-PH RhoGAP family, associates with focal adhesions and actin stress fibers

To study ARHGAP42, we isolated a cDNA that encodes a full-length mouse protein of 875 amino acid residues (98.6 kDa). Mouse ARHGAP42 is highly similar throughout its length to human ARHGAP42 (Fig. S1). We noted that mouse ARHGAP42 encoded by our full-length cDNA is 34 residues longer than the predicted mouse ARHGAP42 from UniProtKB (accession number B2RQE8), due to the predicted mouse ARHGAP42 missing part of the BAR domain. We also obtained cDNAs encoding a variant of mouse ARHGAP42 that lacks the same 34 residues in the BAR domain, indicating that this may be a naturally occurring splice variant. In the present study, we examined mouse ARHGAP42 that contains the full BAR domain.

ARHGAP42 belongs to a RhoGAP family characterized by N-terminal tandem BAR and PH domains, followed by a central GAP domain (Fig. 1A). The other mammalian members of this BAR-PH RhoGAP family are oligophrenin-1, encoded by a gene mutated in X-linked mental retardation (Billuart et al., 1998), GTPase regulator associated with FAK (GRAF; also known as ARHGAP26) (Hildebrand et al., 1996), and PH and SH3 domain-containing RhoGAP protein (PSGAP; also known as GRAF2 or ARHGAP10) (Ren et al., 2001; Shibata et al., 2001). ARHGAP42 has alternatively been referred to as 'GRAF3' (Bai et al., 2013). Genes encoding BAR-PH RhoGAPs are also present in *Drosophila* (gene CG8948, encoding Dm Graf) and *C. elegans* (gene T04C9.1). ARHGAP42 contains a C-terminal SH3 domain, a feature common to all known BAR-PH family members with the exception of oligophrenin-1. However, if the SH3 domain is excluded, ARHGAP42 is overall most closely related to oligophrenin-1 (Fig. 1B). The mouse ARHGAP42 tyrosine residue corresponding to the phosphorylated tyrosine (pTyr) site identified in our phosphoproteomics study (Luo et al., 2008) is Tyr-376, which lies in the short linker region between the PH and GAP domains. This tyrosine residue is conserved in oligophrenin-1 and GRAF, but not in PSGAP. An *in vitro* assay of the isolated ARHGAP42 GAP domain demonstrated GAP activity toward RhoA and Cdc42, but not Rac1 (Fig. 1C), similar to the specificities reported for other members of the BAR-PH RhoGAP family (Billuart et al., 1998; Hildebrand et al., 1996; Ren et al., 2001).

To gain insight into cellular function, the subcellular localization of ARHGAP42 was examined. A GFP-tagged variant of ARHGAP42 was expressed in MEFs and cells were fixed and analyzed by fluorescence microscopy. Interestingly, GFP-ARHGAP42 localized prominently to both focal adhesions and actin stress fibers (Fig. 1D,E; Fig. S2). Further analysis indicated that the SH3 domain was indispensable for ARHGAP42 targeting to both actin stress fibers and focal adhesions (Fig. S2). These findings suggest a possible role for ARHGAP42 as a regulator of cell adhesion and actin cytoskeletal dynamics.

Src phosphorylates ARHGAP42 Tyr-376

In our phosphoproteomics study, ARHGAP42 pTyr-376 was readily detected in both Src-transformed mouse embryonic fibroblasts (MEFs) and counterpart nontransformed cells, a property indicative of biologically relevant Src substrates (Luo et al., 2008). The ability of Src to phosphorylate ARHGAP42 was further investigated; first using a COS-7 cell coexpression assay. To evaluate Tyr-376 as a site of phosphorylation, a variant of ARHGAP42 with Tyr-376 changed to phenylalanine (Y376F) was prepared. Wild-type (WT) or Y376F ARHGAP42 variants with an N-terminal GFP tag were expressed either alone or together with constitutively active mouse Src (Src-F529), after which ARHGAP42 tyrosine phosphorylation was assessed by immunoprecipitation with anti-GFP antibody and immunoblotting with either an anti-pTyr antibody or a phosphospecific antibody (pY376) directed against the phosphorylated Tyr-376 site. In COS-7 cells, GFP-ARHGAP42 expressed as a major band of expected size (~130 kDa) as well as a minor band that could be a degradation product. Src-F529 coexpression resulted in greatly elevated WT GFP-ARHGAP42 tyrosine phosphorylation, as detected by both pTyr and pY376 antibodies (Fig. 2A). By contrast, the Y376F variant was very poorly recognized by the pY376 antibody and recognition by the anti-pTyr antibody was much reduced in comparison to the WT (Fig. 2A, top panel; note the higher level of total Y376F versus WT in lanes 6 and 4, respectively). In a similar set of experiments carried out in MEFs, enhanced tyrosine phosphorylation of WT GFP-ARHGAP42 resulting from Src-F529 coexpression was again evident, and further shown to be sensitive to the Src inhibitor saracatinib (Fig. 2B). The ability of Src-F529 to directly phosphorylate ARHGAP42 Tyr-376 was further demonstrated by *in vitro* kinase assays of immunoprecipitates (Fig. 2C). Thus, Tyr-376 appears to be the major site of ARHGAP42 phosphorylation by Src.

The BAR and GAP domains of ARHGAP42 have mutually inhibitory properties

To further study ARHGAP42 function and regulation, GFP-tagged ARHGAP42 variants lacking either the BAR (ΔBAR), or GAP (ΔGAP) domains were expressed in MEFs. Immunoblot analysis using an antibody raised against ARHGAP42 showed that the variants were expressed to similar levels and gave rise to protein bands of expected sizes (Fig. 3A). When further assessing expression using fluorescence microscopy, it was apparent that the ΔBAR variant, in particular, caused a large fraction of the cells to take on an unusual dendritic-like arborized morphology characterized by a rounded cell body and numerous thin beaded extensions (Fig. 3B). In quantitative analysis, 56% of cells expressing GFP-ARHGAP42-ΔBAR were scored as having this arborized morphology, while only 8% of cells expressing GFP-ARHGAP42-WT took on this morphology (Fig. 3C). Such arborized cell morphology is characteristically observed when the RhoA/ROCK pathway is inhibited by various means (Omelchenko et al., 2002; Tatsis et al., 1998), including overexpression of different RhoGAP proteins such as p190RhoGAP or ARHGAP6 (Jiang et al., 2008; Prakash et al., 2000). Indeed, GFP-ARHGAP42-ΔGAP, which lacks the ability to inhibit RhoA, was unable to arborize cells (Fig. 3C). These observations suggest that the BAR domain of ARHGAP42 is autoinhibitory toward the GAP domain, such that GAP activity is elevated when the BAR domain is deleted. In a separate experiment, RhoA-GTP levels were assessed in MEFs stably expressing either ARHGAP42-WT or ARHGAP42-ΔBAR and, as predicted, RhoA-GTP levels were found to be significantly

Journal of Cell Science (2017) 130, 2382-2393 doi:10.1242/jcs.197434

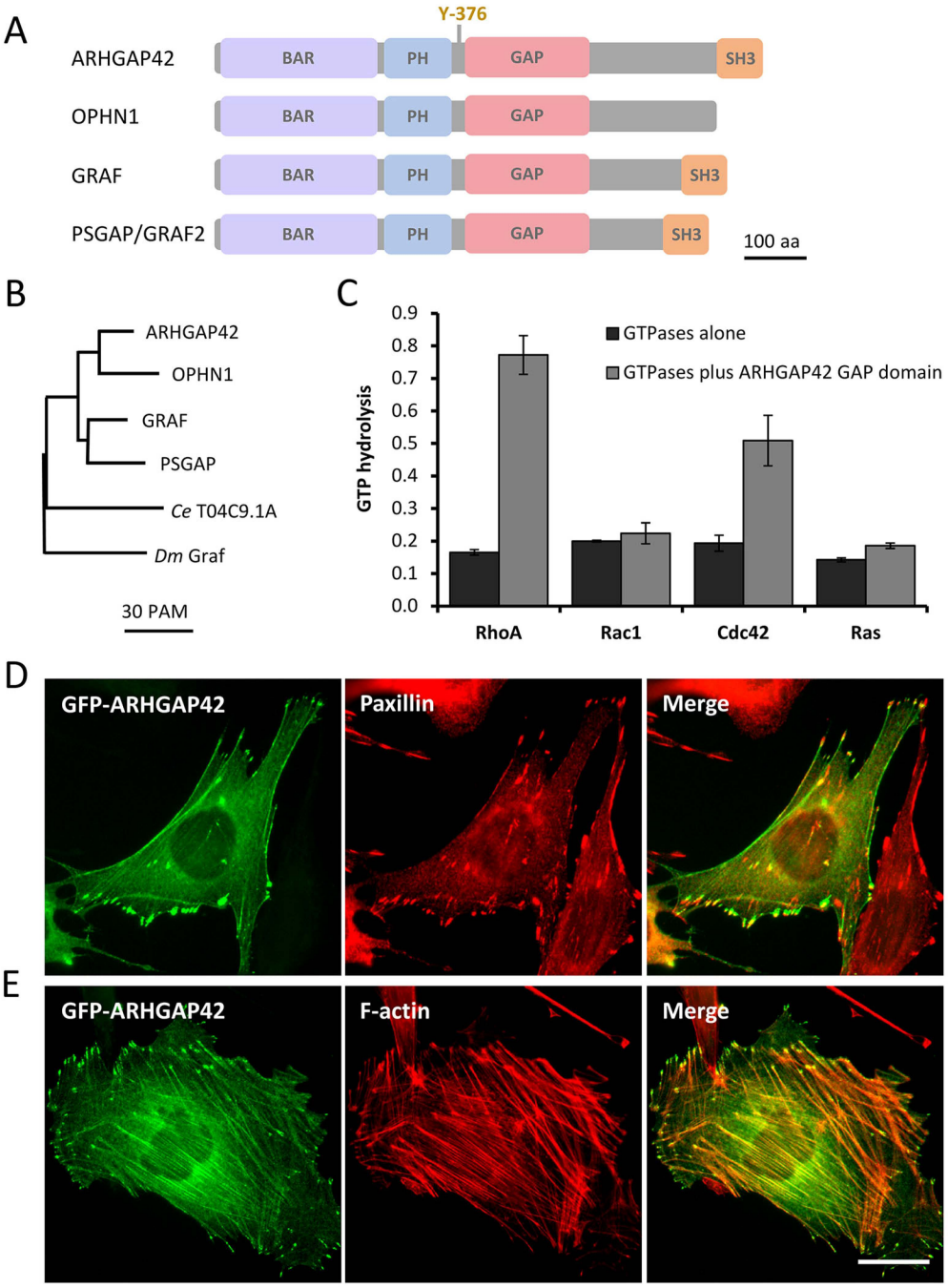

Fig. 1. Domain organization, phylogeny, substrate specificity and subcellular localization of ARHGAP42. (A) Domain organization of ARHGAP42 in comparison to the three other mammalian members of the BAR-PH RhoGAP family. For ARHGAP42, the position of the major site of Src-mediated phosphorylation, Tyr-376, is indicated. OPHN1, oligophrenin-1. (B) Phylogram showing evolutionary relationships among the mammalian BAR-PH RhoGAP family members and to more distant relatives predicted from *C. elegans* (*Ce* T04C9.1A) and *Drosophila* (*Dm* Graf) genomes. The phylogram was generated using Multalin software (Corpet, 1988). (C) ARHGAP42 is a GAP for RhoA and Cdc42, but not Rac1. The GAP domain of ARHGAP42 was bacterially expressed, recovered as a GST fusion protein, and assessed for its activity toward the Rho GTPases RhoA, Rac1 and Cdc42 by measuring the amount of phosphate released by GTP hydrolysis using an *in vitro* assay. Ras was included as a negative control. Values are mean±s.d. from triplicate assays. (D,E) MEFs were transfected with GFP-ARHGAP42 expression plasmid and viewed 24 h later by fluorescence microscopy of fixed cells. The cells were either immunostained with an antibody against paxillin to mark focal adhesions (D, red) or with phalloidin to mark F-actin (E, red). In the representative cell shown in D, GFP-ARHGAP42 is most prominently localized at the focal adhesions and actin stress fibers. In the representative cell shown in E, GFP-ARHGAP42 is more prominently observed in association with actin stress fibers, as well as in apparent focal adhesions. Scale bar: 30 µm.

lower in cells expressing the ΔBAR variant (Fig. 3D), indicative of elevated RhoGAP activity.

Tandem N-terminal BAR and PH domains are found not only in the members of the BAR-PH RhoGAP family but also in other proteins, including APPL1, APPL2 and centaurin α2 (also known as ADAP2), indicating that this organization has been evolutionarily conserved as a functional unit. Structural and biochemical studies have shown the BAR-PH module to form elongated crescent-shaped dimers that function in the sensing and induction of membrane curvature (Li et al., 2007; Peter et al., 2004; Zhu et al., 2007). The ability of the BAR-PH module to induce plasma membrane curvature can be observed as tubulovesicular membrane structures when expressed in cells (Lundmark et al., 2008; Peter et al., 2004). We employed this membrane tubulation assay to further examine the function and regulation of ARHGAP42. GFP-ARHGAP42-WT and -ΔGAP variants (and vector only control) were expressed in COS-7 cells (Fig. 4A) and analyzed 48 h later for membrane tubulation by fluorescence microscopy. The striking tubulovesicular membranes were apparent in many cells expressing GFP-ARHGAP42-WT and -ΔGAP (Fig. 4B,C), but were not observed in the vector only control cells. Notably, tubulovesicular membranes were observed in a significantly higher fraction of cells expressing GFP-ARHGAP42-ΔGAP (84%) as compared to cells expressing GFP-ARHGAP42-WT (27%) (Fig. 4C), even though the WT protein was expressed to a higher level. The finding that deletion of the ARHGAP42 GAP domain results in enhanced tubulovesicular membrane formation indicates that the GAP domain is also autoinhibitory to the BAR-PH module.

Journal of Cell Science (2017) 130, 2382-2393 doi:10.1242/jcs.197434

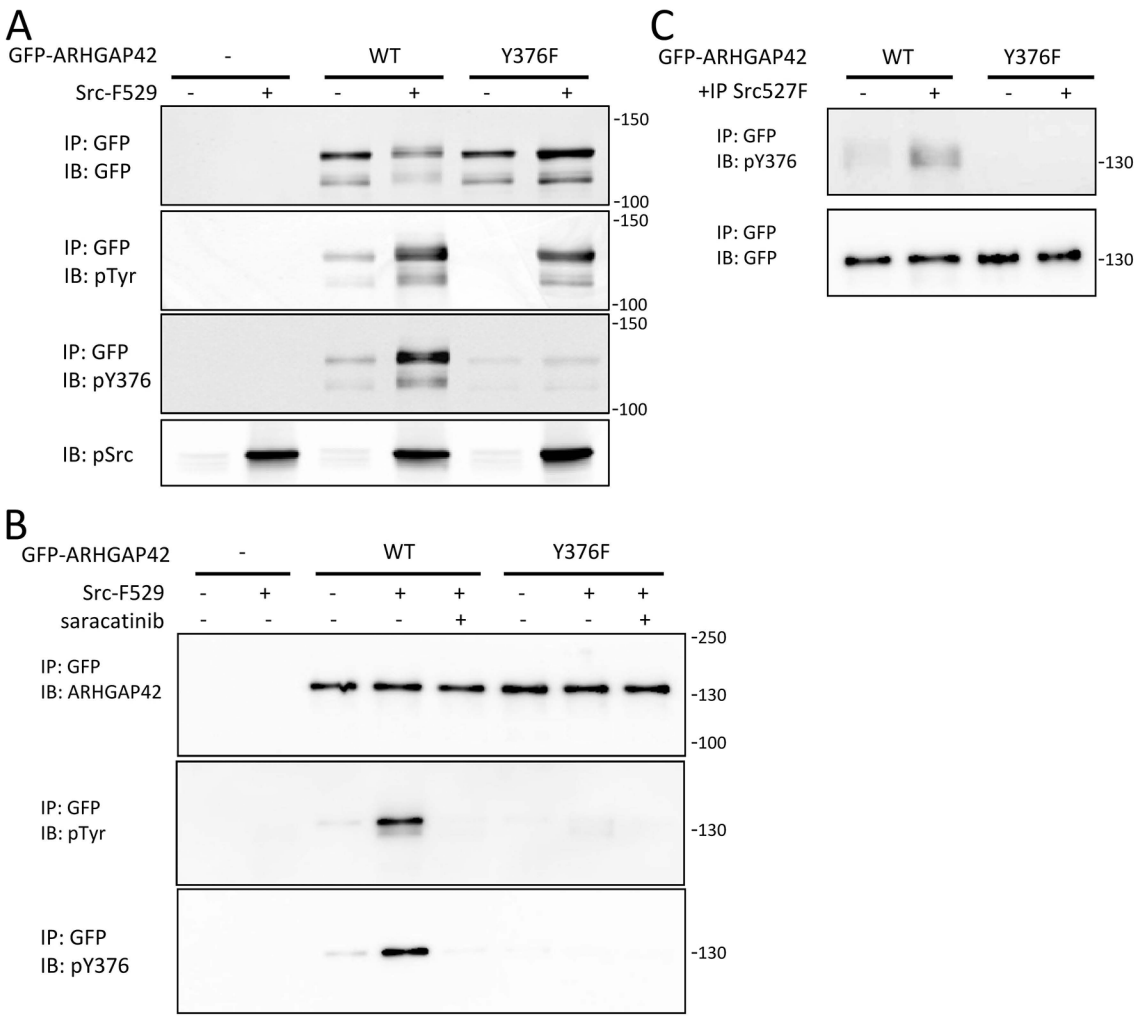

Fig. 2. Src promotes phosphorylation of ARHGAP42 Tyr-376. (A,B) Immunoblot analysis of GFP-ARHGAP42 phosphorylation. GFP-ARHGAP42 variants were transiently expressed in (A) COS-7 cells or (B) MEFs, either with or without constitutively active Src-F529, and ARHGAP42 tyrosine phosphorylation was assessed by immunoprecipitation (IP) with anti-GFP antibody followed by immunoblotting (IB) with general anti-pTyr (pTyr) or anti-pTyr376 (pY376) antibody. (B) Prior to immunoprecipitation in MEFs, Src activity was further manipulated by incubating the cells for 2 h in the presence or absence of 5 µM saracatinib. Src-F529 expression was confirmed by immunoblot analysis of total cell lysates with antibody against the Src autophosphorylation site (pSrc). (C) *In vitro* kinase assay. GFP-ARHGAP42 variants were individually expressed in MEFs and immunoprecipitated using anti-GFP antibody, eluted, and incubated with immunoprecipitated Src-F529. After the kinase reaction had been carried out for 1.5 h, levels of GFP-ARHGAP42 phosphorylation were assessed using a pY376 antibody. The numbers on the right indicate the positions of molecular size markers (kDa).

ARHGAP42-ΔBAR promotes focal adhesion dynamics and cell migration

Because RhoA is a known regulator of focal adhesion dynamics and cell migration (Lessey et al., 2012; Raftopoulou and Hall, 2004), it was of interest to further study ARHGAP42 by assessing these cellular properties in MEFs stably expressing either GFP-ARHGAP42-WT, GFP-ARHGAP42-ΔBAR or GFP-ARHGAP42-ΔGAP. Confocal immunofluorescence microscopy revealed that focal adhesion size is decreased in cells expressing GFP-ARHGAP42-ΔBAR as compared to cells expressing GFP-ARHGAP42-WT, whereas cells expressing the ΔGAP variant have significantly larger focal adhesions (Fig. 5A; Fig. S3A). Increased focal adhesion size could be caused by decreased focal adhesion turnover. To assess focal adhesion dynamics, the focal adhesion marker mCherry-zyxin was expressed in MEFs expressing ARHGAP42 variants and confocal live-cell microscopy was used to determine the percentage of adhesions that either assembled or disassembled during a 20 min time interval. As anticipated, the focal adhesion dynamics was highest in cells expressing the ΔBAR variant of ARHGAP42 and lowest in cells expressing the ΔGAP variant (Fig. 5B). To strengthen the observation of the effect of the ARHGAP42 variants on focal adhesion dynamics, we further investigated the exchange dynamics of vinculin within focal adhesions using fluorescence recovery after photobleaching (FRAP) experiments. Consistent with the above results, vinculin dynamics in focal adhesions was highest (slowest half-maximum recovery) in cells expressing the ΔBAR variant of ARHGAP42 and lowest in cells expressing the ΔGAP variant (Fig. 5C; Fig. S3B). Because adhesion dynamics are tightly interconnected with 2D cell migration (Kim and Wirtz, 2013; Webb et al., 2004), the influence of the ARHGAP42 variants on monolayer wound healing was assessed. Consistent with the results on focal adhesion size and turnover, MEFs expressing the ΔBAR variant healed the wounded area significantly faster than the cells expressing the other ARHGAP42 variants (Fig. 5D; Fig. S3C). Taken together, these data indicate that the elevated GAP activity of the ARHGAP42-

Journal of Cell Science (2017) 130, 2382-2393 doi:10.1242/jcs.197434

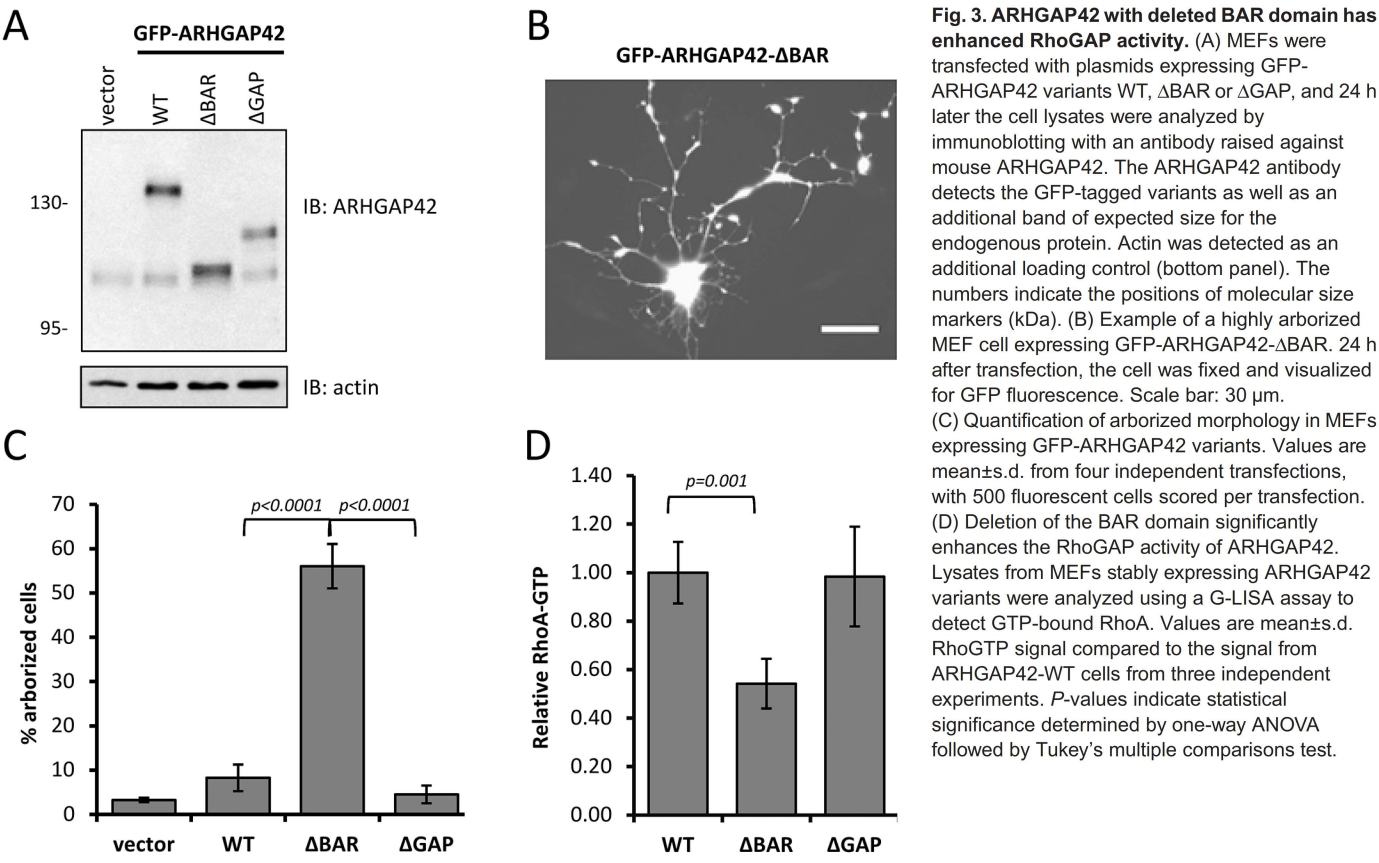

Fig. 3. ARHGAP42 with deleted BAR domain has enhanced RhoGAP activity. (A) MEFs were transfected with plasmids expressing GFP-ARHGAP42 variants WT, ΔBAR or ΔGAP, and 24 h later the cell lysates were analyzed by immunoblotting with an antibody raised against mouse ARHGAP42. The ARHGAP42 antibody detects the GFP-tagged variants as well as an additional band of expected size for the endogenous protein. Actin was detected as an additional loading control (bottom panel). The numbers indicate the positions of molecular size markers (kDa). (B) Example of a highly arborized MEF cell expressing GFP-ARHGAP42-ΔBAR. 24 h after transfection, the cell was fixed and visualized for GFP fluorescence. Scale bar: 30 µm. (C) Quantification of arborized morphology in MEFs expressing GFP-ARHGAP42 variants. Values are mean±s.d. from four independent transfections, with 500 fluorescent cells scored per transfection. (D) Deletion of the BAR domain significantly enhances the RhoGAP activity of ARHGAP42. Lysates from MEFs stably expressing ARHGAP42 variants were analyzed using a G-LISA assay to detect GTP-bound RhoA. Values are mean±s.d. RhoGTP signal compared to the signal from ARHGAP42-WT cells from three independent experiments. *P*-values indicate statistical significance determined by one-way ANOVA followed by Tukey's multiple comparisons test.

ΔBAR variant gives rise to enhanced focal adhesion dynamics and cell migration.

ARHGAP42 is activated by Src – requirement for the Tyr-376 phosphorylation site

The experiments described above showed that the GAP domain of ARHGAP42 can be activated by deletion of the BAR domain, and that GAP activity can be measured as changes in cell shape and dynamics. Similar approaches were undertaken to investigate the regulatory role of ARHGAP42 Tyr-376 phosphorylation. In initial experiments, either GFP-ARHGAP42-WT or GFP-ARHGAP42-Y376F was transiently expressed in v-Src-transformed versus nontransformed NIH-3T3 fibroblasts. Anti-pTyr antibody readily recognized GFP-ARHGAP42-WT expressed in the v-Src-transformed cells, but not GFP-ARHGAP42-Y376F (Fig. 6A). In the nontransformed cells, both WT and Y376F variants localized to stress fibers (Fig. 6C, left two panels). However, detailed analysis of its enrichment in longitudinal section through focal adhesions showed that GFP ARHGAP42 Y376F is mostly absent from the front side of the focal adhesions (Fig. S2B,D). Expression of the ARHGAP42 variants in the v-Src-transformed cells had a different outcome. When GFP-ARHGAP42-WT was expressed in v-Src-NIH-3T3, almost all cells (95%) took on the rounded arborized morphology (Fig. 6B,C), indicating that the GAP activity of ARHGAP42 was highly elevated in the presence of v-Src. In vector control cells expressing GFP only, 16% of the v-Src-transformed cells were scored as being rounded or arborized; a background value reflective of the classical v-Src-mediated fusiform morphology. Most notably, GFP-ARHGAP42-Y376F was unable to promote arborization in v-Src-NIH-3T3 cells above this background level (Fig. 6B). GFP-ARHGAP42-Y376F was observed to associate with structures reminiscent of podosome rosettes in in v-Src-NIH-3T3 cells (Fig. 6C, rightmost panel). These results indicate that Src-mediated phosphorylation of ARHGAP42 Tyr-376 acts as a mechanism to promote the GAP activity of ARHGAP42, resulting in RhoA inhibition and the arborized phenotype.

The effect of Src-mediated phosphorylation of ARHGAP42 Tyr-376 on RhoA activity was also analyzed in SYF cells, which are triple nulls for Src, Yes and Fyn, and thus lacking in endogenous Src-family kinase activity (Klinghoffer et al., 1999). Indeed, we found that RhoA-GTP levels are significantly lower in SYF cells stably expressing ARHGAP42-WT as compared to ARHGAP42-Y376F, but only when Src activity in the SYF cells was restored by expression of Src-F529 (Fig. 7A,B). To strengthen our observations that ARHGAP42 affects RhoA activity in a Tyr-376 phosphorylation-dependent manner, we performed a pull-down analysis with a bacterially expressed constitutively active form of RhoA (RhoA-CA), as described in García-Mata et al. (2006). We found that the ability of RhoA-CA to pull down ARHGAP42-WT, but not ARHGAP42-Y376F, is greatly enhanced in SYF cells expressing Src-F529 (Fig. 7C,D). This agrees with the decreased levels of RhoA-GTP in SYF+Src-F529 cells expressing GFP-ARHGAP42-WT, and strongly indicates that its GAP activity is responsible for the decrease.

The SYF cells were further employed to investigate the impact of Src-mediated phosphorylation of ARHGAP42 Tyr-376 on the regulation of focal adhesion dynamics and migration. Initially, focal adhesion size was analyzed in SYF versus SYF+Src-F529 cells transfected with GFP-ARHGAP42 variants. Analysis by confocal fluorescence microscopy revealed that the presence of Src activity (Src-F529) leads to decreased focal adhesion size in cells expressing

Journal of Cell Science (2017) 130, 2382-2393 doi:10.1242/jcs.197434

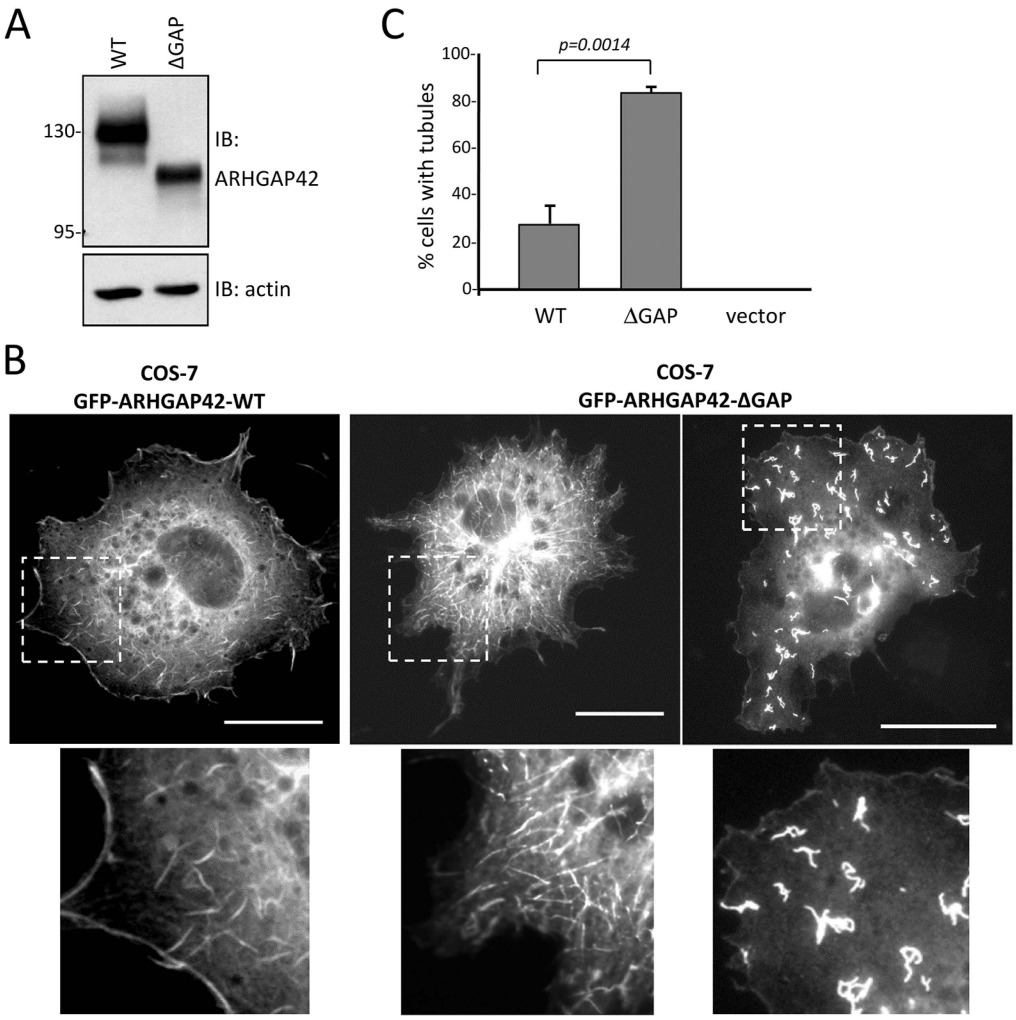

Fig. 4. Expression of ARHGAP42 promotes membrane tubulation that is enhanced by deletion of the GAP domain. Plasmids expressing GFP-ARHGAP42-WT versus -ΔGAP (or the empty vector) were transfected into COS-7 cells and the cells were analyzed 48 h later. (A) Immunoblot analysis of whole cell lysates shows expression levels of the ARHGAP42 variants, with actin as a control for equal loading. (B) Representative cells expressing GFP-ARHGAP42-WT (left) and GFP-ARHGAP42-ΔGAP (middle and right, exhibiting membrane tabulation). The cells were fixed and visualized for GFP fluorescence. The boxed regions in the upper panels are enlarged in the lower panels. Scale bars: 30 µm. (C) Quantitative analysis of membrane tubulation induced by ARHGAP42 variants. Values are mean±s.d. from four independent transfection experiments, with 500 cells scored per experiment. Statistical significance was determined by one-way ANOVA followed by Tukey's multiple comparisons test.

ARHGAP42-WT, but not in cells expressing ARHGAP42-Y376F (Fig. 8A). Expression of ARHGAP42-ΔBAR also gave rise to decreased focal adhesion size, but unlike ARHGAP42-WT, this was observed in both SYF and SYF+Src-F529 cells (Fig. 8A). These results indicate that Src-mediated phosphorylation of ARHGAP42 Tyr-376 results in activation of the GAP activity of ARHGAP42, similar to what is achieved by deletion of the BAR domain. The effect of ARHGAP42 GAP activity on focal adhesion dynamics was then assessed in these cells. Live-cell microscopy showed that Src activity resulted in increased focal adhesion dynamics in cells expressing ARHGAP42-WT and ARHGAP42-ΔBAR, but this was not the case for cells expressing ARHGAP42-Y376F (Fig. 8B; Fig. S4A). RhoA inhibition can lead to upregulation of Rac to stimulate lamellipodial dynamics (Cheresh et al., 1999; Ridley et al., 1992; Rottner et al., 1999; Sharma and Mayer, 2008). Therefore, we also analyzed the velocity of lamellipodial protrusions in SYF and SYF+SrcF cells expressing the ARHGAP42 variants. Kymograph analysis showed that the presence of Src activity in SYF+SrcF cells expressing ARHGAP42-WT and ARHGAP42-ΔBAR, but not ARHGAP42-Y376F, stimulated the velocity of lamellipodial protrusions (Fig. 8C; Fig. S4B). Taken together, these results indicate that phosphorylation of ARHGAP42 Tyr-376 by Src can play an important role in stimulation of focal adhesion dynamics, lamellipodial velocity and cell migration.

DISCUSSION

ARHGAP42 (also known as GRAF3) was first revealed to be a target of tyrosine phosphorylation by phosphoproteomics studies. In addition to our previous study that identified ARHGAP42 as one of 32 known or putative Src substrates of known or likely biological relevance (Luo et al., 2008), ARHGAP42 was also recognized as one of 13 hyperphosphorylated proteins in fibroblasts deficient in the protein tyrosine phosphatase PTP1B (also known as PTPN1) (Mertins et al., 2008). At the time of these studies, ARHGAP42 was called 'similar to oligophrenin-1'. In both studies, the site of ARHGAP42 phosphorylation was identified as Tyr-376. Now, according to the PhosphoSitePlus database (http://www.phosphosite.org), ARHGAP42 Tyr-376 has been detected in >200 independent mass spectrometry studies that analyzed various cancer cell lines and disease tissues. The PhosphoSitePlus database also documents the frequent identification of corresponding residues on GRAF (Tyr-371) and oligophrenin-1 (Tyr-370) as sites of phosphorylation. Despite this abundance of data, there have been no published studies addressing how these tyrosine phosphorylation events might impact signaling functions. The primary objective of the present study was to evaluate ARHGAP42 Tyr-376 as a site of phosphorylation by Src and to investigate its possible regulatory role. By expressing WT mouse ARHGAP42 versus mutational variants, we have characterized ARHGAP42 as a regulator of cell motility that can be activated by Src-mediated phosphorylation of Tyr-376.

Journal of Cell Science (2017) 130, 2382-2393 doi:10.1242/jcs.197434

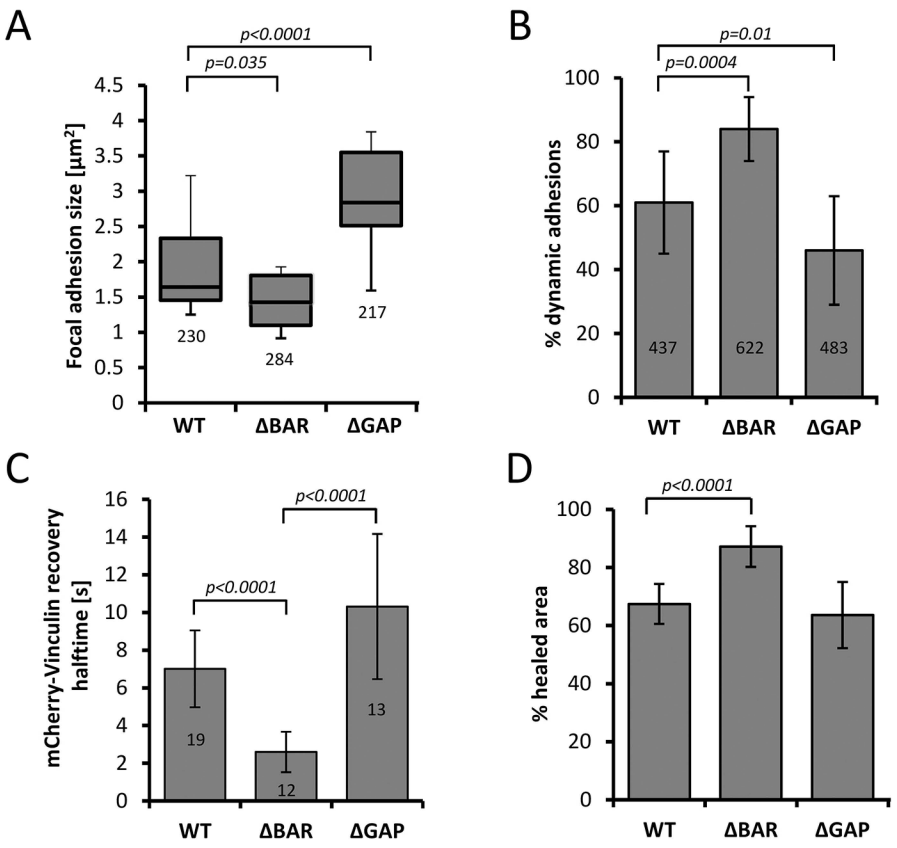

Fig. 5. Expression of ARHGAP42-ΔGAP increases focal adhesion size; expression of ARHGAP42-ΔBAR promotes focal adhesion turnover and cellular motility. (A) Quantification of focal adhesion size. MEFs expressing ARHGAP42 variants (WT, ΔBAR and ΔGAP) were grown on fibronectin-coated cover slips, fixed, immunostained with an antibody against paxillin, and focal adhesion size was analyzed by fluorescence microscopy. The box-and-whisker plot shows the range of size of focal adhesions. Center line shows the median, box limits indicate the first and third quartiles, whiskers extend to the minimum and maximum values. (B,C) MEFs were cotransfected with GFP-ARHGAP42 expression plasmids (WT, ΔBAR, ΔGAP) and (B) mCherry-zyxin or (C) mCherry-vinculin to mark focal adhesions. After transfection, cells were plated on fibronectin-coated glass bottom dishes and analyzed 48 h later by confocal live-cell microscopy. (B) The percentage of focal adhesions that either assembled or disassembled during a 20 min time interval. (C) FRAP analysis of mCherry-vinculin dynamics in focal adhesions, showing mean recovery halftimes. (A-C) The numbers in the histogram bars indicate the number of focal adhesions analyzed. (D) MEFs stably expressing GFP-ARHGAP42 variants (WT, ΔBAR, ΔGAP) were allowed to migrate for 24 h on a Petri dish and the healed area was subsequently determined by light microscopy followed by analysis using ImageJ software. Values are mean±s.d. Statistical significance was determined by one-way ANOVA followed by Tukey's post-hoc test.

ARHGAP42 is a member of a RhoGAP family characterized by N-terminal tandem BAR-PH domains followed by a central GAP domain with some specificity towards RhoA. In addition to BAR-PH and GAP domains, ARHGAP42 has an SH3 domain near the C-terminus. Of the three other mammalian members of this BAR-PH RhoGAP family, GRAF and PSGAP also have a C-terminal SH3 domain, but oligophrenin-1 does not. Nevertheless, phylogenetic analysis indicates that ARHGAP42 is more closely related to oligophrenin-1 than it is to GRAF and PSGAP, indicating that the loss of the oligophrenin-1 SH3 domain was a relatively recent evolutionary event.

By expressing GFP-tagged ARHGAP42 variants and detecting endogenous ARHGAP42 (Fig. S4C), we observed that ARHGAP42 localizes prominently in cells to actin stress fibers, which is consistent with a role for ARHGAP42 as an important regulator of actin cytoskeletal dynamics. The stress fiber localization requires the ARHGAP42 SH3 domain. Most likely the SH3 domain binds actin fibers indirectly through bridging proteins, such as is the case for the targeting of another BAR-GAP-SH3 protein, srGAP2, which binds via formin-like protein 1 (FMNL1) (Mason et al., 2011). In addition to stress fibers, ARHGAP42 was observed to variably localize to focal adhesions.

Previous *in vitro* studies demonstrated that the BAR domains of oligophrenin-1 and GRAF can interact directly, in *cis*, with their respective GAP domains to maintain the GAP domain in an autoinhibited state (Eberth et al., 2009). Our finding that expression of an ARHGAP42 variant with the BAR domain deleted gives rise to the arborized cell phenotype characteristic of RhoA/ROCK pathway inhibition indicates that the same autoinhibitory mechanism exists for ARHGAP42. With regard to this autoinhibitory function of the ARHGAP42 BAR domain, it is of interest that we obtained cDNAs encoding an alternate form of ARHGAP42 lacking 34 BAR domain residues (amino acids 129–162), but including much of the central BAR domain helix. It will be of interest for future studies to investigate the possibility that this alternative short form of ARHGAP42 has a constitutively active GAP domain.

We also presented evidence that the ability of the ARHGAP42 BAR-PH module to promote membrane tubulation in cells is enhanced when the GAP domain is deleted, suggesting that the GAP domain is also inhibitory to BAR-PH function. The apparent mutual inhibition of the BAR and GAP domains, however, stands in contrast to the findings of Eberth et al. (2009), showing that the BAR-PH domains of oligophrenin-1 and GRAF are not negatively impacted by the presence of the GAP domain. ARHGAP42 may have unique properties in this regard.

A role for the GAP activity of ARHGAP42 as a regulator of Rho-GTP levels and cytoskeletal or adhesion dynamics is evidenced by our findings that expression of the ARHGAP42 variant with the BAR domain deleted (and thus having elevated GAP activity) gives rise to increased focal adhesion dynamics, lamellipodial velocity and cell migration. These findings are in line with those of a recent study by Bai et al. (2013), which characterized ARHGAP42 as a RhoGAP expressed strongly in smooth muscle cells, and showed that depletion of the mouse *Arhgap42* gene resulted in a hypertensive phenotype with increased ROCK-dependent agonist-induced pressor responses.

To monitor the GAP activity of ARHGAP42, we employed two assays: a cell based assay analyzing arborized morphology induced by lowered RhoGTP levels, and a direct quantification of RhoGTP levels using a RhoGTP-pull-down approach. The effects of ARHGAP42 mutational variants were similar for both assays used, although their effects on arborized morphology were more prominent. However, similar results showing a mild decrease in

Journal of Cell Science (2017) 130, 2382-2393 doi:10.1242/jcs.197434

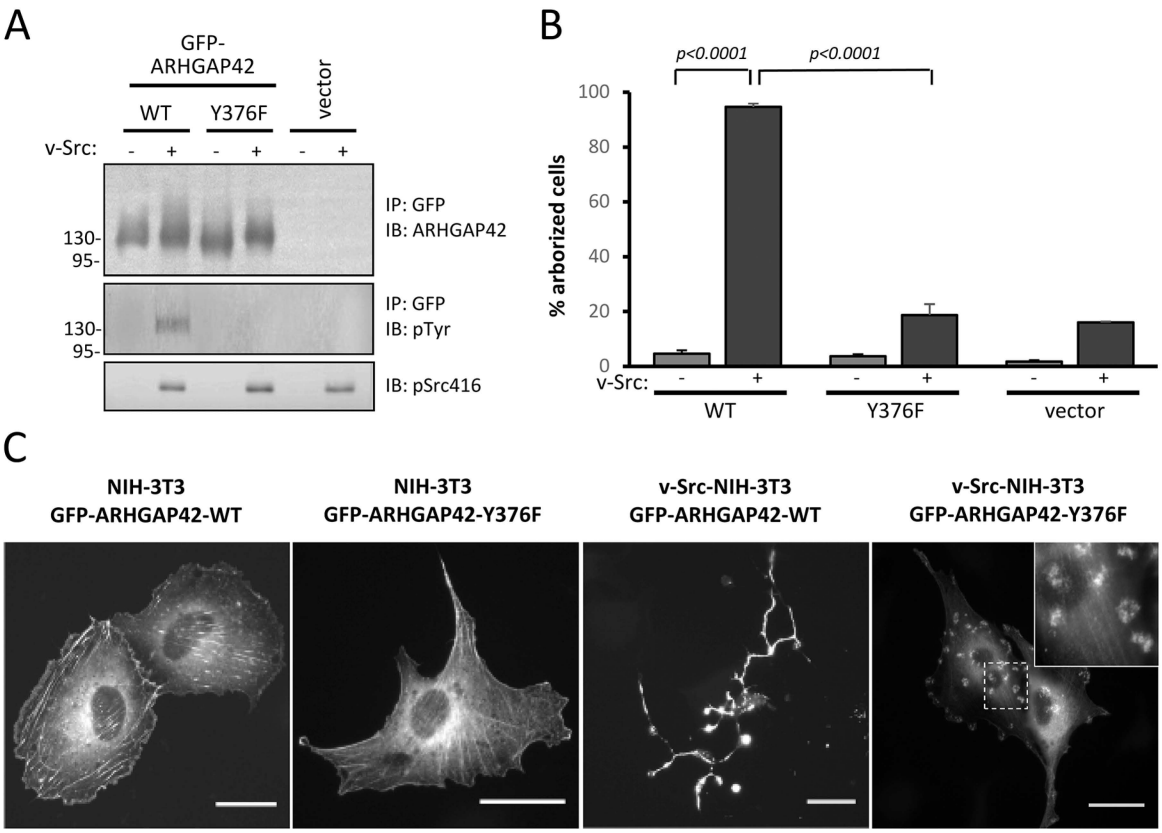

Fig. 6. Src activates the GAP activity of ARHGAP42, requiring the Tyr-376 phosphorylation site. GFP-ARHGAP42 variants, -WT versus -Y376F, were expressed in either nontransformed or v-Src-transformed NIH-3T3 fibroblasts and analyzed 24 h after transfection. (A) Expression and tyrosine phosphorylation of GFP-ARHGAP42 variants was assessed by IP using anti-GFP antibody, and IB with ARHGAP42 antibody (top panel) or anti-pTyr antibody (middle panel). Src activity is indicated by IB of whole cell lysates with antibody against the Src autophosphorylation site (bottom panel). (B) Quantitative analysis of the arborized morphology characteristic of RhoA inhibition in NIH-3T3 cells. Values are mean±s.d. from five independent transfection experiments, with 500 cells scored per experiment. Statistical significance was determined by one-way ANOVA followed by Tukey's post hoc test. (C) Subcellular localization of GFP-ARHGAP42 variants and cellular morphology were assessed by fluorescence microscopy of fixed cells. Representative nontransformed cells (left two panels) and v-Src-transformed cells (right two panels) are shown. The podosomal-like structures in the central region of a GFP-ARHGAP42-Y376F-expressing cell are shown in the inset. Scale bars: 30 µm.

RhoGTP levels leading to dramatic increase of the arborized phenotype have been observed (Noren et al., 2000). These could indicate that arborized morphology is induced only after some threshold level of RhoGTP is achieved.

We addressed the role of ARHGAP42 Tyr-376 phosphorylation as a critical regulator of ARHGAP42 activity by expressing WT versus Y376F variants of ARHGAP42 in cells with elevated Src activity, and monitoring the effects on cell shape and motility. In v-Src-transformed NIH-3T3 cells, expression of WT-ARHGAP42, but not Y376F-ARHGAP42, caused the cells to take on the highly arborized morphology indicative of elevated RhoGAP activity. In SYF cells that express Src-F529, the expression of WT-ARHGAP42, but not Y376F-ARHGAP42, resulted in decreased RhoA-GTP levels, while increasing focal adhesion dynamics, lamellipodial protrusion velocity, and cell migration. Notably, the effect of Tyr-376 phosphorylation mirrored the effect of the BAR domain deletion in promoting the GAP activity of ARHGAP42. Our findings add to a growing body of work documenting the role of protein phosphorylation in the regulation of BAR and F-BAR proteins (Ambroso et al., 2014; Quan et al., 2012; Roberts-Galbraith and Gould, 2010).

Our results suggest a phosphorylation model for the regulation of ARHGAP42 activity, whereby Src-mediated phosphorylation of ARHGAP42 Tyr-376 acts to disrupt the inhibitory effect of the BAR domain with the GAP domain, resulting in GAP domain activation, which reduces the levels of active GTP-bound RhoA and subsequently increases cell motility (Fig. S4D). In releasing the mutual inhibition of the BAR and GAP domains, Tyr-376 phosphorylation could also activate the membrane remodeling function for the ARHGAP42 BAR-PH domain.

MATERIALS AND METHODS

Mouse ARHGAP42 cDNA cloning and plasmids

A cDNA encoding full-length mouse ARHGAP42 was prepared from cultured MEFs using RT-PCR, with primers based on predicted N- and C-terminal coding regions. The forward primer (5′-AAGGTACC ATGGGGCTGCCCACTCTG-3′) incorporated a *KpnI* site prior to the start codon and the reverse primer (5′-GCGTCTAGATTAGAGGAAGAC AACGTAGTTTTCAGG-3′) incorporated an *XbaI* site following the stop codon. The amplified cDNA was then inserted into the *KpnI* and *XbaI* sites of cloning vector pBlueScript-SK+ for initial sequencing. For expression of mouse ARHGAP42 variants carrying an N-terminal GFP tag, vector pEGFP-C1 (Clontech) was used in the construction of plasmids pEGFP-C 1-mARHGAP42-WT, -ΔBAR, -ΔGAP, -ΔSH3, and -Y376F. Standard molecular methods were employed to introduce the individual deletions or point mutation. The three deletion variants lack amino acid residues 1–249 (ΔBAR), 388–576 (ΔGAP), or 819–875 (ΔSH3). For retroviral infection, the

Journal of Cell Science (2017) 130, 2382-2393 doi:10.1242/jcs.197434

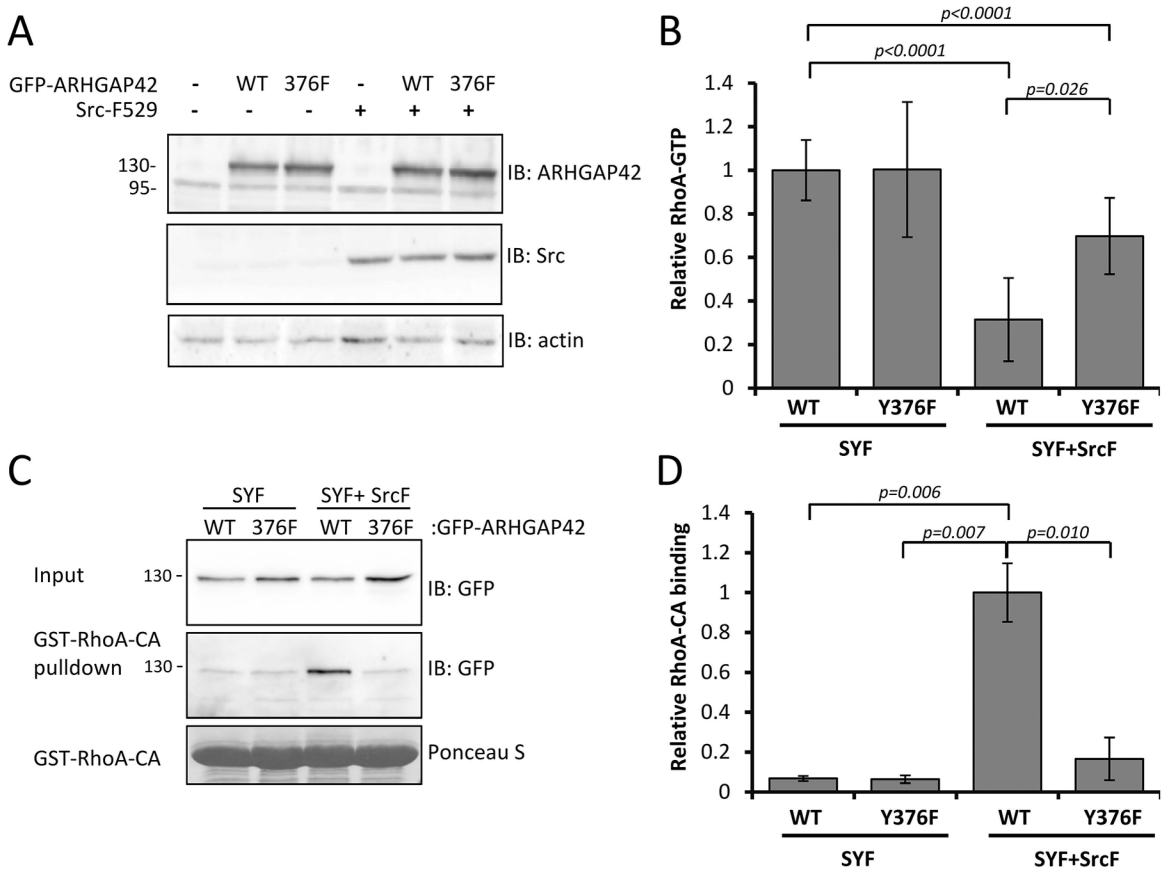

Fig. 7. Src phosphorylation on Tyr376 regulates ARHGAP42 activity. SYF cells or SYF cells expressing constitutively active Src-F529 (SrcF) were transfected to stably express GFP-ARHGAP42-WT versus -Y376F. (A) Expression of ARHGAP42 and Src was confirmed by IB, with actin (bottom) as a control for equal loading. The ARHGAP42 antibody detects the GFP-tagged variants as well as an additional band of expected size for the endogenous protein. (B) Relative RhoA-GTP levels were determined in cell lysates using the G-LISA assay. Values are mean±s.d. RhoA-GTP signal compared to the signal from ARHGAP42-WT-expressing cells, from three independent experiments performed in triplicate. (C) The ability of ARHGAP42 to bind RhoA-CA was analyzed using a GST-RhoA-CA pull-down assay and (D) quantified as a ratio of the amount of indicated GFP-ARHGAP42 variant pulled down with GST-RhoA-CA and the corresponding amount of GFP-ARHGAP42 in the input cell lysate. Statistical significance was determined by one-way ANOVA followed by Tukey's post-hoc test.

individual ARHGAP42 variants including the EGFP were PCR amplified from the corresponding pEGFP-C1 plasmids using a forward primer (5′-C TGCATGATCAGCCACCATGGTGAGCAAGGGC-3′) and a reverse primer (5′- CAGGTCAATTGTTAGAGGAAGACAACGTAGTT-3′). The amplified cDNAs were then cleaved with *BclI* and *MunI* and inserted into the *BglII* and *EcoRI* sites of pMSCV-puro vector. The resulting constructs were verified by sequencing. Plasmids pCMV-N2-mARHGAP42-HA-WT, -ΔBAR, -ΔSH3, and -Y376F were constructed for expression of mouse ARHGAP42 variants carrying a triple-HA epitope tag at their C-terminal ends; these plasmids were derived from vector pEGFP-N2 (Clontech), with the EGFP coding segment replaced with the sequence for the triple-HA tag. Plasmid pGEX-KG-mARHGAP42GAP was constructed for bacterial expression of the mouse ARHGAP42 GAP domain (amino acid residues 384–583). For construction of pMSCV-puro-Src-529F, Src-529F was recloned from source vector pBluescriptII-Src-529F (Brábek et al., 2002) using *NotI* (blunt ended) and *BamHI* restriction endonucleases, and the generated fragment was inserted to *HpaI* and *BglII* sites of pMSCV-puro vector. Plasmid mCherry-C1-zyxin was a gift from Irina Kaverina (Vanderbilt University, Nashville, TN).

Antibodies

A rabbit polyclonal antibody against mouse ARHGAP42 was custom made by Pacific Immunology (Ramona, CA) using a bacterially expressed immunogen-encompassing mouse ARHGAP42 (amino acid residues 580–820, a poorly conserved region between the GAP and SH3 domains) (at dilution 1:500). The monoclonal antibody against paxillin was from BD Transduction Laboratories (cat. no. 610051, 1:1,000) monoclonal antibodies against phospho-paxillin (cat. no. 07-1440, 1:1,000) and β actin (cat. no. A5316, 1:5,000) were from Sigma-Aldrich. The polyclonal anti-GFP antibody used for immunoblotting was from Thermo Fisher Scientific (cat. no. A-6455, 1:1,000), and the monoclonal anti-GFP 3E6 used for immunoprecipitation was from Invitrogen (cat. no. A-11120, 1:1,000). Anti-pTyr antibody 4G10 (cat. no. 05-321, 1:1,000) and v-Src antibody 327 (cat. no. OP07, 1:1,000) were from EMD Millipore. Rabbit monoclonal antibody against RhoA (cat. no. 2117, 1:1,000), and phosphospecific antibodies against Src-pTyr416 (cat. no. 6943, 1:1,000) and ARHGAP42-pTyr376 (cat. no. 5617, 1:1,000) were all obtained from Cell Signaling Technology.

Rho GTPase assay

The GAP domain of mouse ARHGAP42 was expressed from plasmid pGEX-KG-mARHGAP42GAP in bacterial strain BL21(DE3) as a GST-fusion protein and purified using glutathione agarose beads (Sigma-Aldrich). Protein was eluted from the beads using 0.25% glutathione and concentrated in 50 mM Tris-HCl, 50 mM NaCl and 5 mM EDTA (pH 7.5) to a final volume of 200 µl. Activity was assayed with a RhoGAP ASSAY, Biochem Kit (Cytoskeleton) according to the manufacturer's protocol. Briefly, 8 µg of protein was incubated in the presence of different recombinant GTPases, GTP and optimized buffer. The amount of released inorganic phosphate, the product of GTP hydrolysis, was measured by absorbance at 650 nm.

Cell culture and transfection

All cell lines were cultured in full DMEM (Life Technologies) with 4.5 g/l L-glucose, L-glutamine and pyruvate, supplemented with 10% fetal bovine serum (Sigma-Aldrich), 2% antibiotic–antimycotic (Life Technologies),

Journal of Cell Science (2017) 130, 2382-2393 doi:10.1242/jcs.197434

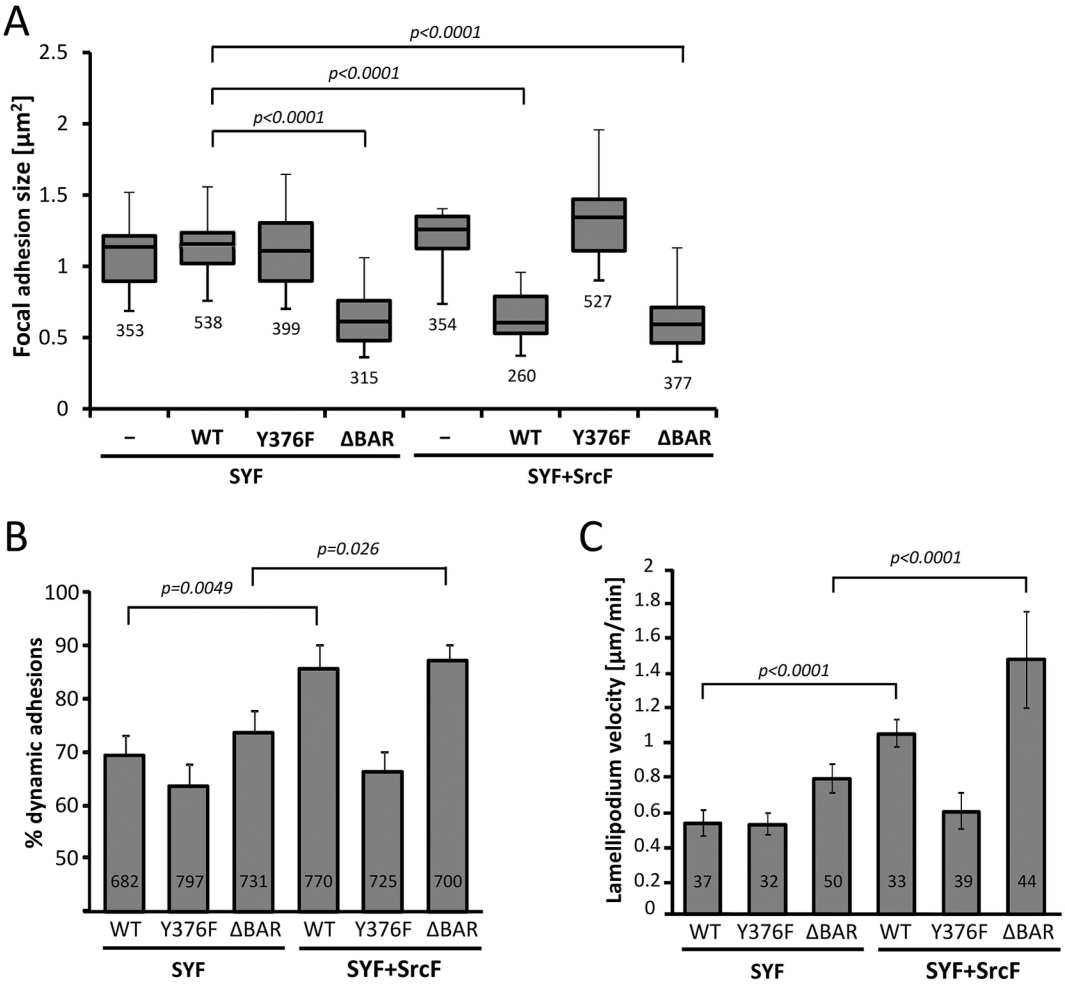

Fig. 8. Src phosphorylation of ARHGAP42 on Tyr376 regulates focal adhesion size and dynamics of lamellipodia and focal adhesions. SYF cells or SYF cells expressing constitutively active Src-F529 (SrcF) were cotransfected with GFP-ARHGAP42 expression plasmids (WT, Y376F and ΔBAR), and plated on fibronectin-covered glass bottom dishes. At 24 h, cells showing similar levels of GFP-ARHGAP42 fluorescence, judged using an integrated intensity value of the GFP signal per cell and acquired with same settings (exposure, laser power, detector gain, etc.) of the microscope, were analyzed by confocal cell microscopy. (A) Quantitative analysis of focal adhesion size. The box-and-whisker plot shows the range in size of focal adhesions marked by paxillin staining in fixed cells. (B) Quantitative analysis of focal adhesion dynamics in live cells. Values are mean±s.e.m. percentage of dynamic focal adhesions during a 10 min time interval. (A,B) The numbers in the indicate the number of focal adhesions analyzed. (C) Quantitative analysis of lamellipodia velocities. Values are mean±s.e.m. velocities of protruding lamellipodia. The numbers in the histogram bars indicate the number of cells analyzed. Statistical significance was determined by one-way ANOVA followed by Tukey's post-hoc test.

and 1% MEM nonessential amino acids (Life Technologies). Cell transfections were carried out using either Lipofectamine-2000 (Thermo Fisher Scientific) or Polyethylenimine-PEI (Sigma-Aldrich) according to the manufacturers' protocols. For some experiments, stable cell lines were prepared using plasmids pMSCV-puro-GFP-ARHGAP42-WT; -ΔBAR; -ΔGAP; -Y376F and the Phoenix retroviral packaging lineage, followed by fluorescence-activated cell sorting (FACS) for GFP. SYF fibroblasts stably expressing Src-529F were prepared via retrovirus infection using pMSCV-puro-Src-529F vector and Phoenix packaging lineage with subsequent puromycin selection.

Cell immunostaining and fluorescence microscopy

Transfected cells were seeded on coverslips coated with human fibronectin 10 µg/ml (Invitrogen), grown for 24–48 h, and subsequently fixed in 4% paraformaldehyde in 127 mM NaCl, 5 mM KCl, 1.1 mM NaH_2PO_4, 0.4 mM KH_2PO_4 and 20 mM HEPES (pH 7.1), permeabilized in 0.5% Triton X-100 in PBS, washed extensively with PBS, and blocked in 3% BSA in PBS. The cells were then sequentially incubated with the primary antibody against paxillin for 2 h, secondary antibody for 60 min and phalloidin Dy-405 (Dyomics) for 15 min, with extensive washing between each step. The secondary antibodies were anti-rabbit-IgG Alexa Fluor 546-conjugated antibody and anti-mouse-IgG Alexa Fluor 594- and Alexa Fluor 633-conjugated antibodies (Molecular Probes). Images were acquired by Leica TCS SP2 or TCS SP8 microscope systems equipped with a Leica 63×/1.45 NA oil objective.

Quantification of GFP-ARHGAP42 localization to focal adhesions

Focal adhesions indicated by paxillin staining were detected automatically using ImageJ according to Horzum et al., (2014). Focal adhesions were considered positive for GFP-ARHGAP42 if the GFP signal in focal adhesion was ≥20% higher than the average GFP signal in cytoplasm.

Immunoprecipitation and immunoblotting

Subconfluent cell cultures were washed with PBS and lysed in modified RIPA buffer [0.15 M NaCl, 50 mM Tris-HCl (pH 7.4), 1% Nonidet P-40, 0.1% SDS, 1% sodium deoxycholate, 5 mM EDTA and 50 mM NaF]. Protein concentrations in lysates were determined using the DC Protein Assay (Bio-Rad). Lysates equivalent to 20 µg protein were diluted in 2× Laemmli sample buffer [0.35 M Tris-HCl (pH 6.8), 10% SDS, 40% glycerol and 0.012% Bromophenol Blue] for immunoblot analysis of whole

cell extracts. Immunoprecipitations were carried out from 1 ml RIPA lysates containing equal amounts of total protein (200–500 µg). Lysates were incubated 4 h on ice with 1 µg primary antibody and immune complexes were collected by an additional 1 h incubation with protein G-Sepharose (20 µl 50% slurry). The immunoprecipitates were washed five times with 1 ml ice-cold RIPA buffer, resuspended in 2× SDS-PAGE sample buffer and processed for immunoblotting. For immunoblotting, samples were separated on SDS polyacrylamide gels (ranging from 7.5% to 15%), transferred to nitrocellulose membranes, and nonspecific activity was blocked by incubating the membranes for 90 min at room temperature in Tris-buffered saline containing 4% BSA. Membranes were then incubated overnight at 4°C with a primary antibody, washed extensively with Tris-buffered saline with Tween-20 (TTBS), incubated for 1 h at room temperature with HRP-conjugated secondary antibodies (Sigma-Aldrich) at 1:10,000 washed extensively in TTBS, and developed using either an Odyssey or Fuji LAS chemiluminescence imaging system. Western blot quantification was performed using ImageJ software (http://rsbweb.nih.gov/ij/).

Kinase assay

GFP-ARHGAP42 variants were immunoprecipitated from MEFs using anti-GFP antibody (Invitrogen), SrcF was immunoprecipitated from MEFs using v-Src antibody (EMD Millipore). The GFP-ARHGAP42 variants were eluted from the slurry using 0.1 M glycine pH 3.5 followed by neutralization with 1 M Tris-HCl pH 9.2 (1/20 of total volume). Precipitated GFP-ARHGAP42 variants were transferred to Src529F (bound on protein G-Sepharose) in kinase buffer (50 mM HEPES pH 7.4, 1% Triton X-100, 1 mM DTT, 6 mM $MgCl_2$, 6 mM $MnCl_2$, 100 µM ATP, 200 µM orthovanadate and protease inhibitors) and incubated on a rotator at 30°C for the indicated times (0.5, 1, 1.5 and 2 h). The reaction was stopped by adding 6× SDS-PAGE sample buffer and boiling for 5 min.

RhoA activation assay

Cells were grown to 70% confluency and then incubated overnight in serum-free medium. The cells were then serum stimulated by incubating for 3 min in DMEM containing 10% FBS, then washed in ice-cold PBS. Lysis buffer (G-LISA RhoA Activation Assay, Cytoskeleton) was added, and immediately the cells were scraped and lysates were centrifuged for 2 min at 9,300 ***g***. Aliquots for estimating protein concentration were collected, and the remaining lysates were snap-frozen in liquid nitrogen prior to being assessed for RhoA activity using the G-LISA assay according to the manufacturer's protocol.

RhoA pull-down assay

A constitutively active form of RhoA (RhoA-CA, G14V) was PCR amplified with a forward primer encoding *BamHI* (5′-ATTGGATCCCGG ATGGCTG-3′) and a reverse primer encoding *EcoRI* site (5′-GCAG AATTCCTCACAAGACCAG-3′) and subcloned into pGEX-2T bacterial expression vector via *BamHI* and *EcoRI* sites. GST-fused RhoA-CA was expressed in *E. coli* BL21(DE3) strain and affinity purified using Pierce Glutathione Agarose (Thermo Fisher Scientific). The RhoA pull-down assay was performed as described in García-Mata et al. (2006). Briefly, cells were washed twice with ice-cold HBS (20 mM HEPES pH 7.5, 150 mM NaCl) and lysed in HBS containing 1% Triton X-100, 5 mM $MgCl_2$ and 1 mM DTT supplied with inhibitors of proteases (Mix M, SERVA) and phosphatases (Mix-II, SERVA). The lysates were equalized for the total amount of GFP-ARHGAP42. Agarose-bound RhoA-CA (15 µg) was added to each lysate and rotated for 1 h at 4°C. The beads were then washed three times in lysis buffer and resuspended in SDS-PAGE sample buffer. The samples were resolved and analyzed by immunoblotting as described above.

Live-cell microscopy

MEFs were cotransfected with pEGFP-C1-mARHGAP42 variants and mCherry-C1-zyxin (focal adhesion marker), and 24 h later were transferred to glass bottom dishes (Ibidi). Cells were kept in Phenol Red-free DMEM supplemented with 10% FBS and 2% antibiotics-antimycotics mix. Motile cells were observed in red fluorescence channel for focal adhesion dynamics experiments, or using internal reflection microscopy mode for lamellipodial dynamics experiments at 37°C and 5% CO_2. Images were taken at 30 s intervals for a total of 20 min using a Leica TCS SP2 microscope system equipped with a Leica 63×/1.45 NA oil objective and a Zeiss LSM 880 confocal microscope, equipped with a Zeiss 63×/1.45 NA oil objective. Focal adhesion dynamics analysis was performed according to Webb et al. (2004). For kymograph analysis, ImageJ software was used to draw three lines (1 pixel wide, 0.22 mm) per lamellipodium in the direction of the protrusion. The lamellipodium velocities were calculated from kymographs using the kymograph plugin for ImageJ (J. Rietdorf, FMI Basel, and A. Seitz, EMBL Heidelberg; https://www.embl.de/eamnet/html/body_kymograph.html).

FRAP

FRAP experiments were performed on a Leica SP8 confocal microscope with a 63×/1.2 NA water immersion objective. Cells were cotransfected with mCherry-vinculin and GFP-ARHGAP42 variants. After 2 days, cells were transferred to 35 mm dishes (MatTek) and cultured overnight, and then used for FRAP analysis. A 584 nm white light laser was used for mCherry excitation and bleaching was performed with simultaneous excitation using 576 nm and 584 set on 100% of the fluorescence intensity for 5 s. The image acquisition started 3 s before bleaching and continued for approximately 60 s (one frame every 1.048 s). The recovery curves of the bleached regions were calculated from extracted image series, and the recovery halftime values were calculated from the FRAP curves as described in Tolde et al. (2012).

Wound healing assay

Cells were grown to full confluency and a wound was made in the confluent monolayer using a plastic 1 ml pipette tip. Immediately after the wounding, and again after 24 h in culture, ≥15 images of different areas were acquired using a Nikon Eclipse TE2000-S (10×/0.25 NA Plan Fluor objective). Cell-free areas were measured using ImageJ software and quantified.

Acknowledgements

We thank Professor Jan Černý for valuable discussions and comments.

Competing interests

The authors declare no competing or financial interests.

Author contributions

Conceptualization: R.J., J.B., S.K.H., D.R.; Formal analysis: W.L., R.J., O.T., L.M.R., L.K., M.D., S.K.H., D.R.; Investigation: W.L., R.J., O.T., L.M.R., L.K., M.D.; Resources: J.B., S.K.H., D.R.; Writing - original draft: W.L., R.J., O.T., L.M.R., J.B., S.K.H., D.R.; Writing - review & editing: W.L., R.J., O.T., J.B., S.K.H., D.R.; Visualization: W.L., R.J., O.T., S.K.H., D.R.; Supervision: J.B., S.K.H., D.R.; Project administration: J.B., S.K.H., D.R.; Funding acquisition: J.B., S.K.H., D.R.

Funding

This work was funded by the National Institutes of Health (R01-GM049882), Vanderbilt-Ingram Cancer Center (5P30-CA068485), Grantová Agentura České Republiky (Czech Science Foundation) (15-07321S), and Ministerstvo Školství, Mládeže a Tělovýchovy (Ministry of Education, Youth and Sports of the Czech Republic), within the LQ1604 National Sustainability Program II (Project BIOCEV-FAR) and the project BIOCEV (CZ.1.05/1.1.00/02.0109 and LM2015062, Czech-BioImaging). Deposited in PMC for release after 12 months.

Supplementary information

Supplementary information available online at
http://jcs.biologists.org/lookup/doi/10.1242/jcs.197434.supplemental

References

Ambroso, M. R., Hegde, B. G. and Langen, R. (2014). Endophilin A1 induces different membrane shapes using a conformational switch that is regulated by phosphorylation. *Proc. Natl. Acad. Sci. USA* **111**, 6982-6987.

Arthur, W. T., Petch, L. A. and Burridge, K. (2000). Integrin engagement suppresses RhoA activity via a c-Src-dependent mechanism. *Curr. Biol.* **10**, 719-722.

Bai, X., Lenhart, K. C., Bird, K. E., Suen, A. A., Rojas, M., Kakoki, M., Li, F., Smithies, O., Mack, C. P. and Taylor, J. M. (2013). The smooth muscle-selective RhoGAP GRAF3 is a critical regulator of vascular tone and hypertension. *Nat. Commun.* **4**, 2910.

Bass, M. D., Morgan, M. R., Roach, K. A., Settleman, J., Goryachev, A. B. and Humphries, M. J. (2008). p190RhoGAP is the convergence point of adhesion signals from alpha 5 beta 1 integrin and syndecan-4. *J. Cell Biol.* **181**, 1013-1026.
Billuart, P., Bienvenu, T., Ronce, N., des, P. V., Vinet, M. C., Zemni, R., Carrie, A., Beldjord, C., Kahn, A., Moraine, C. et al. (1998). Oligophrenin 1 encodes a rho-GAP protein involved in X-linked mental retardation. *Pathol. Biol. (Paris)* **46**, 678.
Brábek, J., Mojžita, D., Novotný, M., Půta, F. and Folk, P. (2002). The SH3 domain of Src can downregulate its kinase activity in the absence of the SH2 domain-pY527 interaction. *Biochem. Biophys. Res. Commun.* **296**, 664-670.
Cheresh, D. A., Leng, J. and Klemke, R. L. (1999). Regulation of cell contraction and membrane ruffling by distinct signals in migratory cells. *J. Cell Biol.* **146**, 1107-1116.
Corpet, F. (1988). Multiple sequence alignment with hierarchical clustering. *Nucleic Acids Res.* **16**, 10881-10890.
Eberth, A., Lundmark, R., Gremer, L., Dvorsky, R., Koessmeier, K. T., McMahon, H. T. and Ahmadian, M. R. (2009). A BAR domain-mediated autoinhibitory mechanism for RhoGAPs of the GRAF family. *Biochem. J.* **417**, 371-379.
Eden, S., Rohatgi, R., Podtelejnikov, A. V., Mann, M. and Kirschner, M. W. (2002). Mechanism of regulation of WAVE1-induced actin nucleation by Rac1 and Nck. *Nature* **418**, 790-793.
Fincham, V. J. and Frame, M. C. (1998). The catalytic activity of Src is dispensable for translocation to focal adhesions but controls the turnover of these structures during cell motility. *EMBO J.* **17**, 81-92.
Fincham, V. J., Chudleigh, A. and Frame, M. C. (1999). Regulation of p190 Rho-GAP by v-Src is linked to cytoskeletal disruption during transformation. *J. Cell Sci.* **112**, 947-956.
Frame, M. C. (2004). Newest findings on the oldest oncogene; how activated src does it. *J. Cell Sci.* **117**, 989-998.
Frame, M. C., Fincham, V. J., Carragher, N. O. and Wyke, J. A. (2002). v-Src's hold over actin and cell adhesions. *Nat. Rev. Mol. Cell Biol.* **3**, 233-245.
García-Mata, R., Wennerberg, K., Arthur, W. T., Noren, N. K., Ellerbroek, S. M. and Burridge, K. (2006). Analysis of activated GAPs and GEFs in cell lysates. *Methods Enzymol.* **406**, 425-437.
Hanks, S. K., Ryzhova, L., Shin, N. Y. and Brabek, J. (2003). Focal adhesion kinase signaling activities and their implications in the control of cell survival and motility. *Front. Biosci.* **8**, d982-d996.
Hildebrand, J. D., Taylor, J. M. and Parsons, J. T. (1996). An SH3 domain-containing GTPase-activating protein for Rho and Cdc42 associates with focal adhesion kinase. *Mol. Cell Biol.* **16**, 3169-3178.
Horzum, U., Ozdil, B. and Pesen-Okvur, D. (2014). Step-by-step quantitative analysis of focal adhesions. *MethodsX.* **1**, 56-59.
Huveneers, S. and Danen, E. H. J. (2009). Adhesion signaling-crosstalk between integrins, Src and Rho. *J. Cell Sci.* **122**, 1059-1069.
Jiang, W., Betson, M., Mulloy, R., Foster, R., Levay, M., Ligeti, E. and Settleman, J. (2008). p190A RhoGAP is a glycogen synthase kinase-3-beta substrate required for polarized cell migration. *J. Biol. Chem.* **283**, 20978-20988.
Kim, D.-H. and Wirtz, D. (2013). Focal adhesion size uniquely predicts cell migration. *FASEB J.* **27**, 1351-1361.
Kiyokawa, E., Hashimoto, Y., Kobayashi, S., Sugimura, H., Kurata, T. and Matsuda, M. (1998). Activation of Rac1 by a Crk SH3-binding protein, DOCK180. *Genes Dev.* **12**, 3331-3336.
Klemke, R. L., Leng, J., Molander, R., Brooks, P. C., Vuori, K. and Cheresh, D. A. (1998). CAS/Crk coupling serves as a "molecular switch" for induction of cell migration. *J. Cell Biol.* **140**, 961-972.
Klinghoffer, R. A., Sachsenmaier, C., Cooper, J. A. and Soriano, P. (1999). Src family kinases are required for integrin but not PDGFR signal transduction. *EMBO J.* **18**, 2459-2471.
Lessey, E. C., Guilluy, C. and Burridge, K. (2012). From mechanical force to RhoA activation. *Biochemistry* **51**, 7420-7432.
Li, J., Mao, X., Dong, L. Q., Liu, F. and Tong, L. (2007). Crystal structures of the BAR-PH and PTB domains of human APPL1. *Structure* **15**, 525-533.
Lundmark, R., Doherty, G. J., Howes, M. T., Cortese, K., Vallis, Y., Parton, R. G. and McMahon, H. T. (2008). The GTPase-activating protein GRAF1 regulates the CLIC/GEEC endocytic pathway. *Curr. Biol.* **18**, 1802-1808.
Luo, W., Slebos, R. J., Hill, S., Li, M., Brábek, J., Amanchy, R., Chaerkady, R., Pandey, A., Ham, A.-J. L. and Hanks, S. K. (2008). Global impact of oncogenic Src on a phosphotyrosine proteome. *J. Proteome. Res.* **7**, 3447-3460.
Mason, F. M., Heimsath, E. G., Higgs, H. N. and Soderling, S. H. (2011). Bi-modal regulation of a formin by srGAP2. *J. Biol. Chem.* **286**, 6577-6586.
Mertins, P., Eberl, H. C., Renkawitz, J., Olsen, J. V., Tremblay, M. L., Mann, M., Ullrich, A. and Daub, H. (2008). Investigation of protein-tyrosine phosphatase 1B function by quantitative proteomics. *Mol. Cell Proteomics.* **7**, 1763-1777.
Miki, H., Yamaguchi, H., Suetsugu, S. and Takenawa, T. (2000). IRSp53 is an essential intermediate between Rac and WAVE in the regulation of membrane ruffling. *Nature* **408**, 732-735.
Nojima, Y., Morino, N., Mimura, T., Hamasaki, K., Furuya, H., Sakai, R., Sato, T., Tachibana, K., Morimoto, C., Yazaki, Y. et al. (1995). Integrin-mediated cell adhesion promotes tyrosine phosphorylation of p130Cas, a Src homology 3-containing molecule having multiple Src homology 2-binding motifs. *J. Biol. Chem.* **270**, 15398-15402.
Noren, N. K., Liu, B. P., Burridge, K. and Kreft, B. (2000). p120 catenin regulates the actin cytoskeleton via Rho family GTPases. *J. Cell Biol.* **150**, 567-580.
Omelchenko, T., Vasiliev, J. M., Gelfand, I. M., Feder, H. H. and Bonder, E. M. (2002). Mechanisms of polarization of the shape of fibroblasts and epitheliocytes: separation of the roles of microtubules and Rho-dependent actin-myosin contractility. *Proc. Natl. Acad. Sci. USA* **99**, 10452-10457.
Peter, B. J., Kent, H. M., Mills, I. G., Vallis, Y., Butler, P. J., Evans, P. R. and McMahon, H. T. (2004). BAR domains as sensors of membrane curvature: the amphiphysin BAR structure. *Science* **303**, 495-499.
Prakash, S. K., Paylor, R., Jenna, S., Lamarche-Vane, N., Armstrong, D. L., Xu, B., Mancini, M. A. and Zoghbi, H. Y. (2000). Functional analysis of ARHGAP6, a novel GTPase-activating protein for RhoA. *Hum. Mol. Genet.* **9**, 477-488.
Quan, A., Xue, J., Wielens, J., Smillie, K. J., Anggono, V., Parker, M. W., Cousin, M. A., Graham, M. E. and Robinson, P. J. (2012). Phosphorylation of syndapin I F-BAR domain at two helix-capping motifs regulates membrane tubulation. *Proc. Natl. Acad. Sci. USA* **109**, 3760-3765.
Raftopoulou, M. and Hall, A. (2004). Cell migration: Rho GTPases lead the way. *Dev. Biol.* **265**, 23-32.
Ren, X. D., Kiosses, W. B., Sieg, D. J., Otey, C. A., Schlaepfer, D. D. and Schwartz, M. A. (2000). Focal adhesion kinase suppresses Rho activity to promote focal adhesion turnover. *J. Cell Sci.* **113**, 3673-3678.
Ren, X.-R., Du, Q.-S., Huang, Y.-Z., Ao, S.-Z., Mei, L. and Xiong, W.-C. (2001). Regulation of CDC42 GTPase by proline-rich tyrosine kinase 2 interacting with PSGAP, a novel pleckstrin homology and Src homology 3 domain containing rhoGAP protein. *J. Cell Biol.* **152**, 971-984.
Ridley, A. J., Paterson, H. F., Johnston, C. L., Diekmann, D. and Hall, A. (1992). The small GTP-binding protein rac regulates growth factor-induced membrane ruffling. *Cell* **70**, 401-410.
Roberts-Galbraith, R. H. and Gould, K. L. (2010). Setting the F-BAR: functions and regulation of the F-BAR protein family. *Cell Cycle* **9**, 4091-4097.
Rosel, D., Brabek, J., Vesely, P. and Fernandes, M. (2013). Drugs for solid cancer: the productivity crisis prompts a rethink. *Onco. Targets. Ther.* **6**, 767-777.
Rottner, K., Hall, A. and Small, J. V. (1999). Interplay between Rac and Rho in the control of substrate contact dynamics. *Curr. Biol.* **9**, 640-648.
Schlaepfer, D. D., Hanks, S. K., Hunter, T. and van der Geer, P. (1994). Integrin-mediated signal transduction linked to Ras pathway by GRB2 binding to focal adhesion kinase. *Nature* **372**, 786-791.
Sharma, A. and Mayer, B. J. (2008). Phosphorylation of p130Cas initiates Rac activation and membrane ruffling. *BMC. Cell Biol.* **9**, 50.
Shibata, H., Oishi, K., Yamagiwa, A., Matsumoto, M., Mukai, H. and Ono, Y. (2001). PKNbeta interacts with the SH3 domains of Graf and a novel Graf related protein, Graf2, which are GTPase activating proteins for Rho family. *J. Biochem.* **130**, 23-31.
Tatsis, N., Lannigan, D. A. and Macara, I. G. (1998). The function of the p190 Rho GTPase-activating protein is controlled by its N-terminal GTP binding domain. *J. Biol. Chem.* **273**, 34631-34638.
ten Klooster, J. P., Jaffer, Z. M., Chernoff, J. and Hordijk, P. L. (2006). Targeting and activation of Rac1 are mediated by the exchange factor beta-Pix. *J. Cell Biol.* **172**, 759-769.
Tolde, O., Rosel, D., Janostiak, R., Vesely, P. and Brabek, J. (2012). Dynamics and morphology of focal adhesions in complex 3D environment. *Folia Biol.* **58**, 177-184.
Webb, D. J., Donais, K., Whitmore, L. A., Thomas, S. M., Turner, C. E., Parsons, J. T. and Horwitz, A. F. (2004). FAK-Src signalling through paxillin, ERK and MLCK regulates adhesion disassembly. *Nat. Cell Biol.* **6**, 154-161.
Welch, M. D. and Mullins, R. D. (2002). Cellular control of actin nucleation. *Annu. Rev. Cell Dev. Biol.* **18**, 247-288.
Zhu, G., Chen, J., Liu, J., Brunzelle, J. S., Huang, B., Wakeham, N., Terzyan, S., Li, X., Rao, Z., Li, G. et al. (2007). Structure of the APPL1 BAR-PH domain and characterization of its interaction with Rab5. *EMBO J.* **26**, 3484-3493.

Supplemental Figure S1.

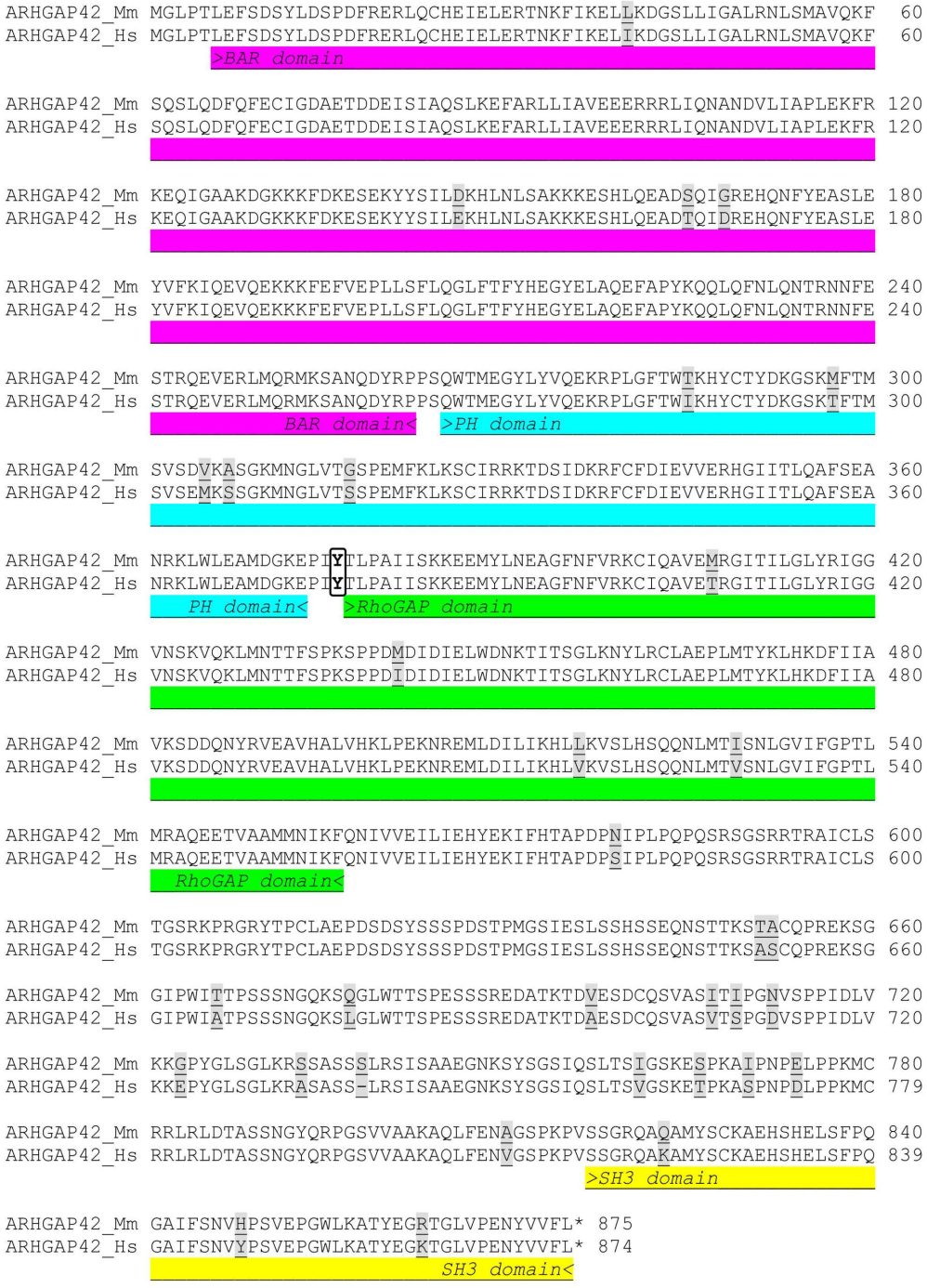

Supplemental Figure S1. Mouse *vs.* human ARHGAP42. Mouse ARHGAP42 (ARHGAP42_Mm) is shown aligned against the predicted human protein (ARHGAP42_Hs; UniProt accession number A6NI28). Non-identical residues are shaded. Asterisks indicate STOP codons. Numbers indicate amino acid position. Positions of BAR, PH, GAP, and SH3 domains are shown below the aligned sequences. The Tyr-376 phosphorylation site is in bold and indicated by a box. Note that the UniProt entry for mouse RhoGAP42 (accession number B2RQE8, not shown) is missing amino acid residues 129-162 within the BAR domain.

Supplemental Figure S2.

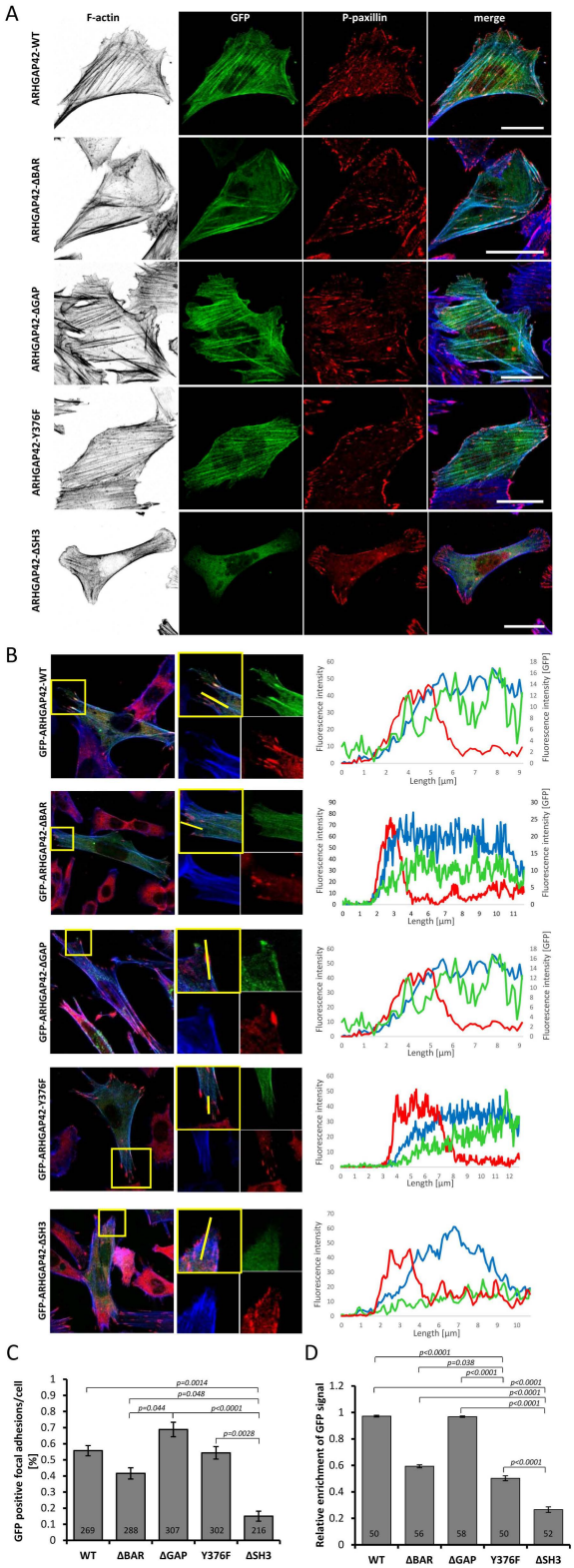

Supplemental Figure S2. Subcellular localization of ARHGAP42 mutational variants. (A) GFP-ARHGAP42 variants ΔBAR, ΔGAP, ΔSH3, and Y376F were expressed in MEFs and analyzed by fluorescence microscopy. The cells were immunostained with phalloidin to mark F-actin (in grey or blue), anti phospho-paxillin antibody to mark focal adhesions (in red) and GFP-ARHGAP42 variants were visualized by GFP fluorescence (in green). Scale bars are 30 µm. (B) Analysis of GFP-ARHGAP42 variants localization to focal adhesions. MEFs expressing indicated ARHGAP42 variants were prepared and immunostained as described above. Graphs on the right from the images show the fluorescence intensity profiles analyzed in a longitudinal section (indicated by the yellow line) through focal adhesion. (C) The bar graph shows the percentage of focal adhesions enriched in presence of indicated GFP-ARHGAP42 variant. (D) The bar graph shows statistical analysis of relative enrichment of indicated GFP-ARHGAP42 variants in longitudinal sections through focal adhesions. The relative enrichment was calculated as a ratio of length given by the presence of GFP signal in a longitudinal section through focal adhesion (as shown in B)) and length of the focal adhesion (defined by the P-paxillin signal). Only focal adhesions positive to GFP-ARHGAP42 signal were analyzed. (C, D) Numbers in the histogram bars indicate number of focal adhesions analyzed. Error bars represent standard errors. Statistical significances were determined by one-way ANOVA followed by Tukey's post-hoc test.

Supplemental Figure S3.

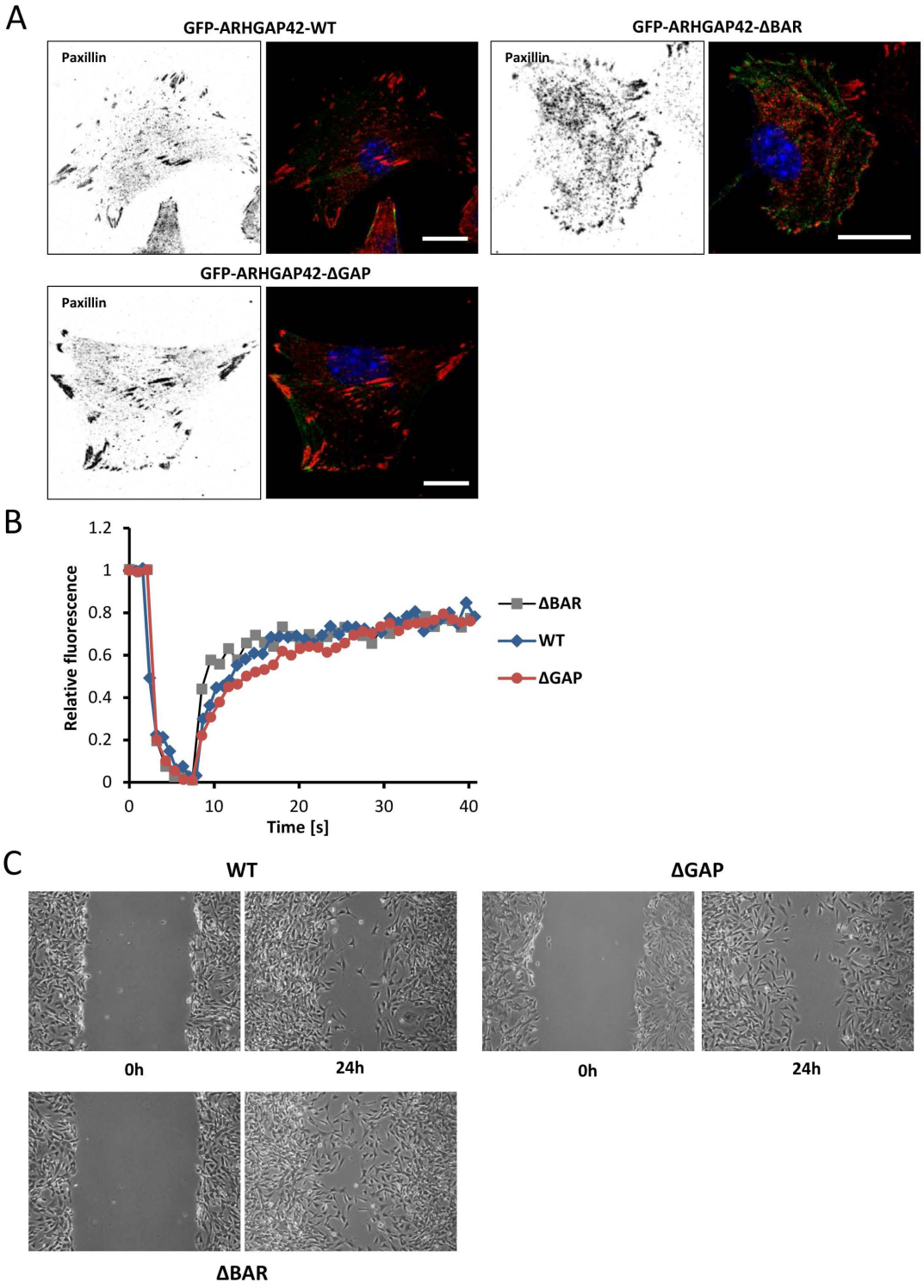

Supplemental Figure S3. Expression of ARHGAP42-ΔGAP increases the size of focal adhesions. MEFs stably expressing GFP-ARHGAP42 variants (WT, ΔBAR, ΔGAP) were grown on fibronectin-coated cover slips, fixed and focal adhesion size was analyzed by fluorescence microscopy. The cells were immunostained with an antibody against paxillin to mark focal adhesions. (A) Representative images showing focal adhesions stained by paxillin; left: greyscale signal of paxillin, right: merge (blue: DAPI, green: GFP, red: Paxillin). Scale bars are 20 µm. (B) Representative FRAP curves of mCherry-Vinculin dynamics in focal adhesions in MEFs expressing indicated variants of ARHGAP42. (C) Representative images of monolayer wound healing of MEFs expressing GFP-ARHGAP42 variants WT, ΔBAR, and ΔGAP.

Supplemental Figure S4.

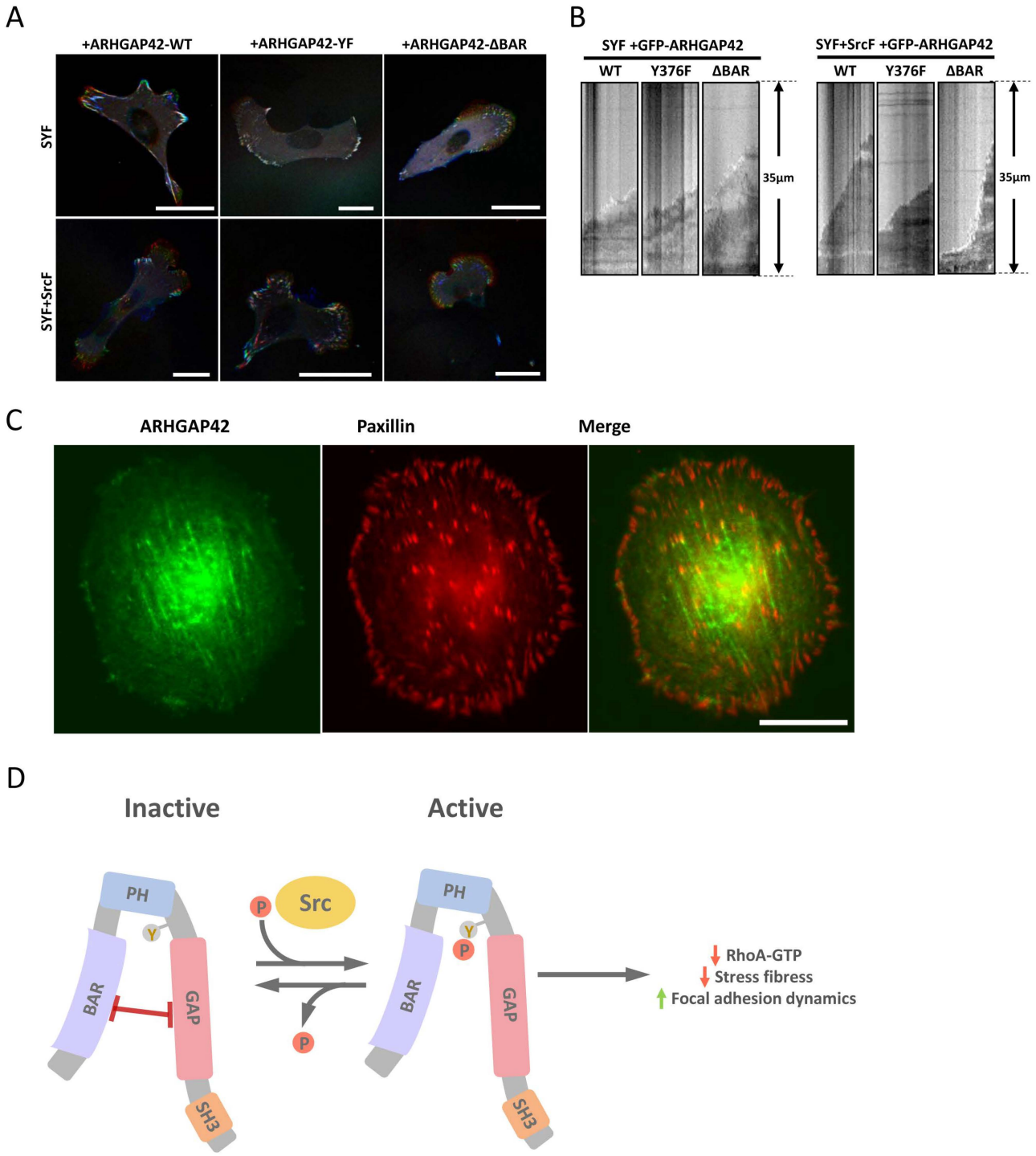

Supplemental Figure S4. (A, B) Src phosphorylation of ARHGAP42 on Tyr376 regulates focal adhesion and lamellipodial dynamics. SYF cells or SYF cells expressing constitutively active Src (SrcF) were co-transfected with GFP-ARHGAP42 expression plasmids (WT, Y376F, and ΔBAR). Cells were plated on fibronectin covered glass bottom dishes and after 24 hours cells showing similar levels of GFP-ARHGAP42 fluorescence, judged using an integrated intensity value of the GFP signal per cell and acquired with same settings (exposure, laser power, detector gain, etc.) of the microscope, were analyzed by confocal live cell microscopy. (A) Representative color-coded images of cell expressing ARHGAP42 variants observed for 10 min. Color coding: 0 min – blue, 5 min – green, 10 min – red; dynamic adhesions are colored and stable adhesions are white. (B) Representative kymographs of protruding lamellipodia showing increased lamellipodium velocity in cells with increased ARHGAP42 activity. **(C) Subcellular localization of endogenous ARHGAP42.** MEFs were immunostained with ARHGAP42 antibody (green, endogenous ARHGAP42) and anti-Paxillin (red) antibody to mark focal adhesions. Scale bars is 30 µm. **(D) Model showing ARHGAP42 activation by Src.** The BAR and GAP domains are inhibitory towards one another. Upon Src phosphorylation of Tyr-376 the inhibition is disrupted. Activation of the GAP domain leads to a decrease of RhoA-GTP levels and subsequently to lowering of acto-myosin tension, increased focal adhesion dynamics and loss of stress fibers.

4. Discussion

4.1. A screen for PKN3 substrates reveals an activating phosphorylation of ARHGAP18

Identification of novel putative PKN3 substrates

PKN3 kinase is an important effector kinase of small Rho GTPases. Despite its indisputable role in regulation of processes such as organization of cytoskeleton (Aleku et al., 2008), proliferation and promotion of tumor growth (Gemperle et al., 2019; Leenders et al., 2004; Unsal-Kacmaz et al., 2012), downstream signaling of PKN3 still remains largely understudied.

To identify the direct substrates of PKN3 we used a chemical-genetic approach based on the mutation of gatekeeper residue which would allow the kinase to use synthetic ATP analogs with bulky group in the N^6-position. To this end, we designed and created analog-sensitive (AS) PKN3 by substitution of Thr639 for glycine. It was observed in several kinases, such as Cdc5, MEKK1 or GRK2, that substitution of the gatekeeper residue, which is an important stabilizing amino acid in the hydrophobic spine of the kinases, led to a complete loss of the kinase activity. In these kinases, a second-site point mutations were introduced in the *N*-lobe of the kinase domain that partially rescued the activity of the AS kinases (Zhang et al., 2005). Importantly, in case of PKN3, substitution of the gatekeeper residue Thr639 for glycine had only a minor effect on PKN3 AS activity when compared to WT and no additional second-site mutations had to be introduced. We observed a slight decrease in PKN3 AS activity when assayed with ATPγS that could be explained by lower affinity of ATPγS to the enlarged ATP-binding pocket, which was most likely rescued in the presence of bulky N^6-Bn ATPγS. The rescue of kinase activity using bulky ATP analogs was nicely demonstrated in PINK1 (*PTEN-induced kinase 1*) kinase. A naturally occurring PINK1 mutation of Gly309 for aspartate results in about 70 % decrease in its kinase activity, which leads to mitochondrial defects associated with the early onset of Parkinson's disease. However, the use of bulky ATP analog, kinetin triphosphate, led to the rescue of PINK1 activity and Parkin recruitment to depolarized mitochondria (Hertz et al., 2013). In contrast with this, mutation of gatekeeper residue has also been previously connected with increased activity of BCR-ABL kinase. Moreover, this mutation conferred resistance to Imatinib treatment in patients with CML (Azam et al., 2008; Gorre et al., 2001).

In our screen performed in the lysate of MDA-MB-231 cell line we identified 281 new putative PKN3 substrate proteins with 418 phosphorylation sites. However, there are several factors that could have affected the results of the screen and should be taken into account when interpreting the data. First, since under normal conditions the ATP analog is not cell permeable, the screen was performed in cell lysate and not in intact cells. This most likely affected the spatial and temporal organization of PKN3 signaling and could have generated several

false-positive results. To overcome this limitation, mild detergents, such as digitonin, were used in various studies to permeabilize the membrane and facilitate the intake of ATP analogs preserving relatively physiological conditions. However, we did not use this approach since a huge amount of the expensive ATP analog is necessary for substrate thiophosphorylation in permeabilized cells to provide sufficient input material for LC-MS/MS analysis (Banko et al., 2011; Michowski et al., 2020). Hertz and colleagues suggested, that high overexpression of the studied AS kinase is necessary in order to ensure sufficient thiophosphorylation of target proteins and to identify also low-abundant substrates which could have remained undetected when assayed with endogenous levels of engineered kinase (Hertz et al., 2010). Overexpression of PKN3 AS in the cell lysate thus represents another factor potentially contributing to artifactual phosphorylation in our screen. Recently, a screen for Cdk1 (*cyclin-dependent kinase 1*) substrates has been performed in embryonic stem cells isolated from knock-in mice expressing AS Cdk1 suggesting endogenous AS kinase expression can also be sufficient to identify the most prominent substrates (Michowski et al., 2020).

The consensus phosphorylation motif of PKN3 was determined using peptide arrays in several studies (Browne et al., 2019; Collazos et al., 2011). Collazos and colleagues described the motif as X-R-X-Ne/Z-S/T-ϕ-X-X-X-Ne, where X means no preference for a specific amino acid, Ne represents neutral amino acids, Z marks the position where arginine residue is not tolerated and ϕ depicts hydrophobic amino acids (Collazos et al., 2011). It is notable that out of the 418 putative PKN3 phosphorylation sites identified in our phosphoproteomic screen only a relatively small number fits the predicted consensus motif when considering the strong preference of PKN3 for arginine residue in position -3 or hydrophobic residues in position +1. Moreover, when we tried to determine a consensus phosphorylation motif using the PKN3 phosphorylation sites identified in our screen we observed no strong preference towards any particular amino acids in these positions. The results of peptide arrays, however, represent only an "ideal substrate" motif and do not take into account other factors that could influence the phosphorylation of the full-length protein, such as docking interactions between the kinase and the substrate, a broader linear sequence context surrounding the phosphorylation site or its secondary structure. Interestingly, PKN3 as a member of PKC family of kinases is considered to be a "basophilic" kinase based on its preference for basic amino acids near the phosphoacceptor site (Miller and Turk, 2018). Indeed, most of the identified phosphosites exhibit basic residues either *N*- or *C*-terminally from the phosphorylated Ser/Thr, suggesting potential role of PKN3 in their phosphorylation.

Recently, a novel chemoproteomic approach, CITe-Id (*Covalent Inhibitor Target-site Identification*), was developed as a tool for accurate identification of covalently modified sites targeted by irreversible inhibitors. Using this approach, a new covalent inhibitor targeting Cys840 of PKN3, JZ128, was developed. However, several off-target protein kinases were identified to be bound by JZ128, such as TNK1, RIOK2, or RIPK2. Using this inhibitor, a phosphoproteomic screen identified 55 proteins as novel putative PKN3 substrates (Browne

et al., 2019). It is surprising, however. that proteins previously reported to be phosphorylated by PKN3, such as BCAR1, GRAF1 or GRAF2 (Gemperle et al., 2019; Shibata et al., 2001), were not identified in any of the screens. Similarly, absence of the known targets in the results of the AS screen for the AMPK kinase substrates suggests potential limitations when using AS kinase-based approaches (Banko et al., 2011). However, when we compared the results of the screen performed by Browne and colleagues with our phosphoproteomic data, three genes were identified in both datasets – LRRC16A, FAM21A and ARFGEF2.

LRRC16A (*F-actin-uncapping protein LRRC16A*), also known as CARMIL1, was identified as a high-affinity binding partner of actin capping protein, which is responsible for capping of actin barbed ends. LRRC16A was shown to localize to lamellipodia where it regulates actin polymerization rates and elongation of actin filaments (Liang et al., 2009; Yang et al., 2005). Its recruitment to lamellipodia was demonstrated to be mediated by the central part of the protein. Following this part, there is a so called C1 region, spanning from Arg962 to Lys1084, which mediates the interaction of LRRC16A with the capping protein (Yang et al., 2005). Interestingly, the putative PKN3 phosphorylation sites identified in our screen (Thr897 and Thr902) are located in the central part of LRRC16A in the close proximity of C1 region, suggesting their potential role in both the regulation of LRRC16A role in actin polymerization and interaction with the capping protein. Moreover, we have recently shown PKN3 localizes to lamellipodia, where it interacts with BCAR1 (Gemperle et al., 2019), further suggesting the possible PKN3-LRRC16A crosstalk.

Both FAM21A and ARFGEF2 are involved in regulation of endosomal signaling. FAM21A is a member of WASH (*Wiskott-Aldrich syndrome protein and SCAR homolog*) protein complex that plays a role in orchestration of cytoskeletal changes during endocytosis and endosomal sorting (Derivery et al., 2009; Gomez and Billadeau, 2009). On the other hand, ARFGEF2, also known as BIG2 (*brefeldin A-inhibited guanine nucleotide-exchange protein 2*), acts as a guanine nucleotide-exchange factor for ARF (*ADP-ribosylation factor*) family of small GTPases. It is essential for endosomal compartment integrity and promotes association of endosomal coat proteins with membrane (Boal and Stephens, 2010; Shinotsuka et al., 2002). Since RhoB-mediated activation of PKN1 kinase in endosomal compartment was already described in one of the earliest studies (Mellor et al., 1998) there might be a possible crosstalk of PKN3 with FAM21A and ARFGEF2 in the field of endosome-related signaling. Moreover, PKN3 is an interactor of GRAF1 and GRAF2 proteins which are known mediators of clathrin-independent endocytosis (Lundmark et al., 2008; Shibata et al., 2001). Nevertheless, phosphorylation of FAM21A and ARFGEF2 proteins by PKN3 could regulate their overall activity, localization or function.

Phosphorylation of ARHGAP18 and regulation of its activity

Among the putative PKN3 substrates identified in our phosphoproteomic screen we selected ARHGAP18 for further study and validation. Phosphorylation of two sites, Ser156 and Thr158, was detected in our data. However, in addition to these, we have focused also on potential phosphorylation of Thr154 since it matches the predicted PKN3 consensus motif, mainly given by the presence of preferred arginine in position -3. In a kinase reaction using either *N*-terminal part of ARHGAP18 or the full-length protein we confirmed PKN3 was able to phosphorylate all these residues *in vitro*. Moreover, in both cases the observed phosphorylation was highly specific since substitution of these three sites for unphosphorylatable alanine was sufficient to substantially reduce phosphorylation of ARHGAP18, even though there are 80 serine and threonine residues present in its 663 amino acids-long sequence. Still, the decrease in phosphorylation of the unphosphorylatable mutant of ARHGAP18 was not complete suggesting there might be additional sites potentially phosphorylated by PKN3.

We further examined whether PKN3 is able to interact with ARHGAP18. Indeed, using co-immunoprecipitation experiments with several truncated variants of ARHGAP18 we confirmed the two proteins can associate with one another. Interestingly, deletion of any part of ARHGAP18 following the first 200 amino acids led to a huge increase in interaction with PKN3 when compared with full-length ARHGAP18. Similarly, the interaction of ARHGAP18 N200 with PKN3 was substantially increased than in case of full-length protein, suggesting the accessibility of the *N*-terminal part of ARHGAP18 could be negatively regulated by a series of intramolecular interactions which are disrupted upon deletion of the regions following. Finally, we mapped the interaction interface to the first 25 amino acids in the sequence of ARHGAP18. Notably, this region is missing in ARHGAP18 Iso2 (isoform 2) which is translated from an alternative downstream start codon (Chang et al., 2014; Maeda et al., 2011) and, indeed, we observed no interaction of PKN3 with ARHGAP18 Iso2. In contrast, both isoforms were phosphorylated by PKN3 *in vitro* to a similar extent suggesting that docking interaction between the two proteins is not a prerequisite for ARHGAP18 phosphorylation. Moreover, only the phosphomimicking mutant of ARHGAP18 Iso1, and not Iso2, led to an increase of ARHGAP18 interaction with PKN3, suggesting that phosphorylation could lead to a partial disruption of intramolecular ARHGAP18 interactions leaving its *N*-terminal part more accessible for interaction with PKN3.

To date, phosphorylation of several Rho GAP proteins has been reported to regulate their activity, specificity or localization. For instance, attenuation of GAP activity was observed in case of p190A RhoGAP after phosphorylation by Rho-kinase or GSK3β (Jiang et al., 2008; Mori et al., 2009) or, similarly, change in specificity of MgcRacGAP from Rac to RhoA upon phosphorylation by Aurora B kinase (Minoshima et al., 2003). Moreover, phosphorylation of another Rho GAP protein, DLC1 (*Deleted in liver cancer 1*), was shown to stimulate the

binding of 14-3-3 proteins which leads to inhibition of DLC1 activity and nucleocytoplasmic shuttling (Scholz et al., 2009). In contrast, we found that phosphorylation of ARHGAP18 by PKN3 on Thr154, Ser156 and Thr158 leads to activation of its GAP activity and, therefore, to decrease in the levels of active RhoA. It is also surprising, that ARHGAP18 in its unphosphorylated state exhibited almost no GAP activity as judged by the results of both RhoA-GTP and GST-RhoA CA pull-down, suggesting that the GAP domain of unphosphorylated ARHGAP18 is not accessible for interaction with RhoA. These results further support our hypothesis that the activity of the GAP domain is negatively regulated by a series of intramolecular interactions which are at least partially disrupted after ARHGAP18 phosphorylation by PKN3.

Potential crosstalk of PKN3 and ARHGAP18 in endothelial signaling

Notably, PKN3 and ARHGAP18 share a lot of similar traits in the signaling of endothelial cells. Upon downregulation of either PKN3 or ARHGAP18 in endothelial cells, the cells lose their capacity of characteristic tube formation in both 2D and 3D conditions (Aleku et al., 2008; Coleman et al., 2010; Möpert et al., 2012). Recently, the role of ARHGAP18 has been extensively studied in the context of atherosclerosis, a chronic inflammatory disease of the arteries (Lusis, 2000), where ARHGAP18 was shown to act as an athero-protective and anti-inflammatory gene that facilitates the flow-responsive endothelial cell alignment via ARHGAP18/YAP axis (Coleman et al., 2020; Lay et al., 2019). Interestingly, PKN3 was identified in a subset of genes associated with trans-endothelial migration of leukocytes which leads to development of coronary artery disease (Hägg et al., 2009). Moreover, depletion of PKN3 was shown to attenuate the pro-inflammatory activation of endothelial cells caused by the defects in glycosylation of ICAM-1 adhesion molecules, suggesting its potential involvement in the promotion of atherosclerosis (Möpert et al., 2012; Mukai et al., 2016). Finally, PKN3 has been recently demonstrated to play a role in bone resorption downstream of non-canonical Wnt5a/Ror2 signaling cascade (Uehara et al., 2017, 2019) that has been linked with the regulation of the secretion of pro-inflammatory cytokines necessary for atherosclerosis development (Zhang et al., 2020). All these findings highlight a potential crosstalk of ARHGAP18 and PKN3 and should be considered in the future research.

Taken together, we performed a phosphoproteomic screen to identify novel direct PKN3 substrates and, based on our data, we characterized ARHGAP18 as a new substrate and interaction partner of PKN3. We showed that phosphorylation of ARHGAP18 by PKN3 leads to activation of its GAP domain and regulates the activity of small Rho GTPases. We also propose a model where ARHGAP18 in its unphosphorylated state exhibits low GAP activity and its *N*-terminus is potentially sterically blocked and, therefore, inaccessible for interactions.

We hypothesize this could be due to a series of inhibitory intramolecular interactions which are at least partially disrupted upon phosphorylation by PKN3 resulting in the activation of ARHGAP18 GAP domain and increased accessibility of its *N*-terminal region for interaction with PKN3. Moreover, our results strongly imply the existence of a negative feedback loop in the regulation of Rho GTPases via two separate pools of ARHGAP18 constituted by the individual isoforms. While ARHGAP18 Iso1 interaction with PKN3, which is stimulated upon phosphorylation, can regulate the activity of small Rho GTPases in direct association with PKN3 by formation of a ternary complex, activation of ARHGAP18 Iso2 by PKN3 could contribute to the regulation of the Rho GTPase activity in a broader cellular context (Figure 12.).

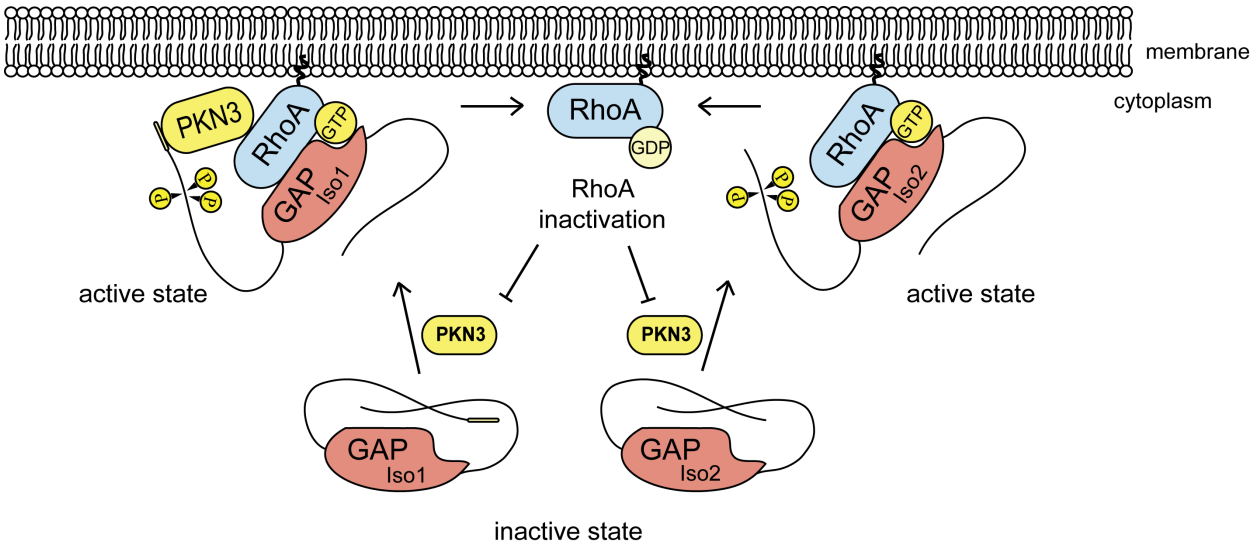

Figure 12. Model of ARHGAP18 regulation and activation. Based on the results from our co-immunoprecipitation experiments of individual ARHGAP18 deletion mutants with PKN3 we hypothesize, that in the unphosphorylated state ARHGAP18 adopts a conformation where the *N*-terminal part of ARHGAP18 is inaccessible for the interaction with PKN3. This could possibly be due to an existence of a series of intramolecular interactions that inhibit not only the ARHGAP18-PKN3 interaction, but also the activity of ARHGAP18 GAP domain. We believe, that upon PKN3-mediated phosphorylation of Thr154, Ser156 and Thr158 located in the *N*-terminal region of ARHGAP18, the inhibitory conformation of ARHGAP18 is at least partially disrupted, leading to both activation of ARHGAP18 GAP domain and increased interaction of ARHGAP18 Iso1 with PKN3. Moreover, our results strongly imply the existence of a negative feedback loop in the regulation of Rho GTPases via two separate pools of ARHGAP18 constituted by the individual isoforms. While ARHGAP18 Iso1 interaction with PKN3 can regulate the activity of small Rho GTPases in direct association with PKN3 by formation of a ternary complex, activation of ARHGAP18 Iso2 by PKN3 could contribute to the regulation of the Rho GTPase activity in a broader cellular context.

4.2. ARHGAP42 is activated by Src-mediated tyrosine phosphorylation to promote cell motility

ARHGAP42 tyrosine phosphorylation was first detected in a phosphoproteomic study performed in Src-transformed mouse embryonic fibroblasts (Luo et al., 2008). The study was focused on the identification of novel substrates of Src kinase, a non-receptor tyrosine kinase involved in signaling related to cell cycle or cell migration and invasion, such as regulation of cytoskeletal organization or regulation of cell adhesion (Guarino, 2010). ARHGAP42 was also identified as one of the 13 hyperphosphorylated proteins in fibroblasts deficient in PTP1B (*protein tyrosine phosphatase 1B*) tyrosine phosphatase (Mertins et al., 2008). To date, phosphorylation of Tyr376, which was identified in both of these studies, appeared in more than 200 phosphoproteomic screens from various tissues, cell lines or conditions (PhosphoSitePlus database, https://www.phosphosite.org/). Moreover, based on PhosphoSitePlus, phosphorylation of the corresponding site was detected also in other members of GRAF protein family (Tyr371 in GRAF1 and Tyr370 in OPHN1). Yet, the effect of this tyrosine residue phosphorylation on regulation of activity and signaling of these Rho GAPs was never examined. In our study, we aimed to characterize ARHGAP42 function and to describe the role of Tyr376 phosphorylation in its regulation.

In vitro studies of OPHN1 and GRAF1 demonstrated that the activation of their GAP domains is negatively regulated by intramolecular interaction with their respective BAR domains (Eberth et al., 2009). When we analyzed ARHGAP42 GAP activity in mouse embryonal fibroblasts expressing full-length ARHGAP42 we observed no difference in the levels of active RhoA when compared to cells expressing ARHGAP42 ΔGAP. However, expression of ARHGAP42 lacking the BAR domain led to a substantial GAP domain activation and a significant decrease in the levels of RhoA-GTP. Consistently, ARHGAP42 ΔBAR expressing cells exhibited a characteristic arborized cell phenotype previously connected with GAP domain hyperactivation (Lazarini et al., 2013) and subsequent inhibition of RhoA/ROCK pathway, suggesting ARHGAP42 BAR domain indeed acts as a negative regulator of the GAP domain activity. In this context it is interesting that an alternative form of ARHGAP42 with BAR domain lacking the 34 amino acids corresponding to exon5 has been described. Although we showed deletion of this region did not affect the membrane-associated functions of BAR domain, its ability to inhibit the GAP domain activity was fully compromised resulting in ARHGAP42 with constitutively active GAP domain (our unpublished results).

It was shown previously that dimers formed by BAR-PH domain module-containing proteins are implicated in sensing and induction of membrane curvature. When expressed in cells this effect can be observed as a formation of tubulovesicular membrane structures (Lundmark et al., 2008; Peter et al., 2004; Zhu et al., 2007). Indeed, overexpression of ARHGAP42 in COS-7 cell line resulted in formation of prominent membrane tubulations. This effect was further significantly elevated in cells expressing ARHGAP42 ΔGAP variant,

suggesting that the inhibitory effect of BAR domain and GAP domain is mutual, although BAR domain retains part of its function also in the autoinhibited state. In contrast with these results, studies of the intramolecular regulation of GRAF1 and OPHN1 showed that the function of BAR domain is not negatively impacted by GAP domain in these proteins (Eberth et al., 2009) suggesting that ARHGAP42 may exhibit unique properties in this regard.

We next focused on the role of ARHGAP42 GAP domain in regulation of cytoskeletal and adhesion dynamics in cells expressing ARHGAP42 lacking the BAR domain, therefore, with elevated GAP activity. We observed ARHGAP42 GAP activation led to an increase in focal adhesion dynamics, lamellipodial velocity and cell migration. These findings are in line with recently published study focused on the role of ARHGAP42 in nasopharyngeal carcinoma, where downregulation of ARHGAP42 expression resulted in significant inhibition of migration and invasion of these cells and, conversely, overexpression of ARHGAP42 led to stimulation of these processes (Hu et al., 2018).

Since phosphorylation of ARHGAP42 Tyr376 was detected in numerous phosphoproteomic studies (PhosphoSitePlus database) we hypothesized that phosphorylation of this residue by Src could have an effect on ARHGAP42 activity and function. We showed, that upon expression of ARHGAP42 WT in Src-transformed NIH-3T3 fibroblasts the vast majority of the cells adopted arborized phenotype indicative of elevated Rho GAP activity. However, this was not the case for cells expressing the unphosphorylatable mutant of ARHGAP42 with substitution of Tyr376 for phenylalanine (Y376F). Moreover, expression of ARHGAP42 WT, but not Y376F mutant, in SYF cells (mouse embryonal fibroblasts lacking the expression of Src kinases Src, Yes and Fyn) re-expressing the constitutively active Src kinase resulted in decrease in the levels of active RhoA, while increasing focal adhesion dynamics, lamellipodial protrusion velocity, and cell migration, similarly as observed in ARHGAP42 lacking the BAR domain. These results suggest phosphorylation of ARHGAP42 Tyr376 is sufficient to overcome the autoinhibitory conformation resulting in activation of the GAP activity.

Using the purified GAP domain of ARHGAP42 in an *in vitro* assay we showed activity of ARHGAP42 is specific towards RhoA and Cdc42, but not Rac1. It is surprising, however, that in a recent high-throughput proximity labeling screen focused on Rho signaling, ARHGAP42 was identified as a protein closely associated exclusively with the Rac subfamily of small GTPases and not with RhoA or Cdc42 (Bagci et al., 2020). There are several possible explanations for these conflicting findings. It was shown recently it is not a GAP domain that acts as a key determinant of Rho GAP specificity towards the individual Rho GTPases, but rather the influence of other protein domains, posttranslational modifications, intramolecular inhibitory interactions and the overall cellular context (Amin et al., 2016). However, although we used ARHGAP42 GAP domain alone to examine the Rho GAP specificity *in vitro*, it is unlikely it would negatively affect its specificity since we showed that also the full-length ARHGAP42 in its active state leads to decrease in the levels of RhoA-GTP. Moreover, we

observed a direct interaction of ARHGAP42 with constitutively active RhoA upon phosphorylation by Src, which is required for ARHGAP42 activation. Importantly, the proximity labeling screen was performed in HEK293 and HeLa cell lines where extremely low expression levels of Src have been documented (Kasahara et al., 2007; Yu et al., 2013). This would suggest that ARHGAP42 in its unphosphorylated and therefore inactive form might possibly interact with active Rac GTPases, or, alternatively, there might be other regulatory mechanisms influencing the ARHGAP42 specificity that remain to be discovered. It is notable in this context that nothing is known about ARHGAP42 phosphorylation on serine and threonine residues and its potential effect on ARHGAP42 activity. It was shown by Shibata and colleagues that PKN3 can directly interact with and phosphorylate both GRAF1 and GRAF2 (Shibata et al., 2001). We have recently confirmed there is also a direct interaction between PKN3 and ARHGAP42 which it is mediated by ARHGAP42 SH3 domain and polyproline region of PKN3 (our unpublished data). The specific phosphorylation sites, however, were not yet identified and the possible functional outcome of ARHGAP42 phosphorylation by PKN3, or any other Ser/Thr kinase, remains to be studied. Moreover, in this regard, by both detection of endogenous ARHGAP42 and expression of GFP-fused exogenous protein we observed a prominent SH3 domain-dependent localization of ARHGAP42 to stress fibers. Since we have recently shown the expression of PKN3 is important for stress fibers formation (Gemperle et al., 2019) it would be interesting to see whether the interaction of ARHGAP42 SH3 domain with PKN3 could play any stimulatory role in the regulation of ARHGAP42 localization. Alternatively, it could be likely mediated by a bridging interaction with other actin-interacting protein, similarly as observed in the case of another BAR, GAP and SH3-domain containing protein, srGAP2 (Mason et al., 2011).

Taken together, in this study we characterized the intramolecular mechanisms involved in the regulation of ARHGAP42 activity and its cellular functions. We propose a model, where ARHGAP42 in its unphosphorylated form adopts an autoinhibited conformation mediated by intramolecular interaction between BAR and GAP domain. The phosphorylation of Tyr376 is sufficient to disrupt the mutually inhibitory state and leads to activation of ARHGAP42 GAP domain resulting in the decrease of RhoA-GTP levels and subsequent increase in cell motility. Moreover, activation of the BAR domain could also lead to stimulation of its membrane remodeling function and increase in clathrin-independent endocytosis (Figure 13.).

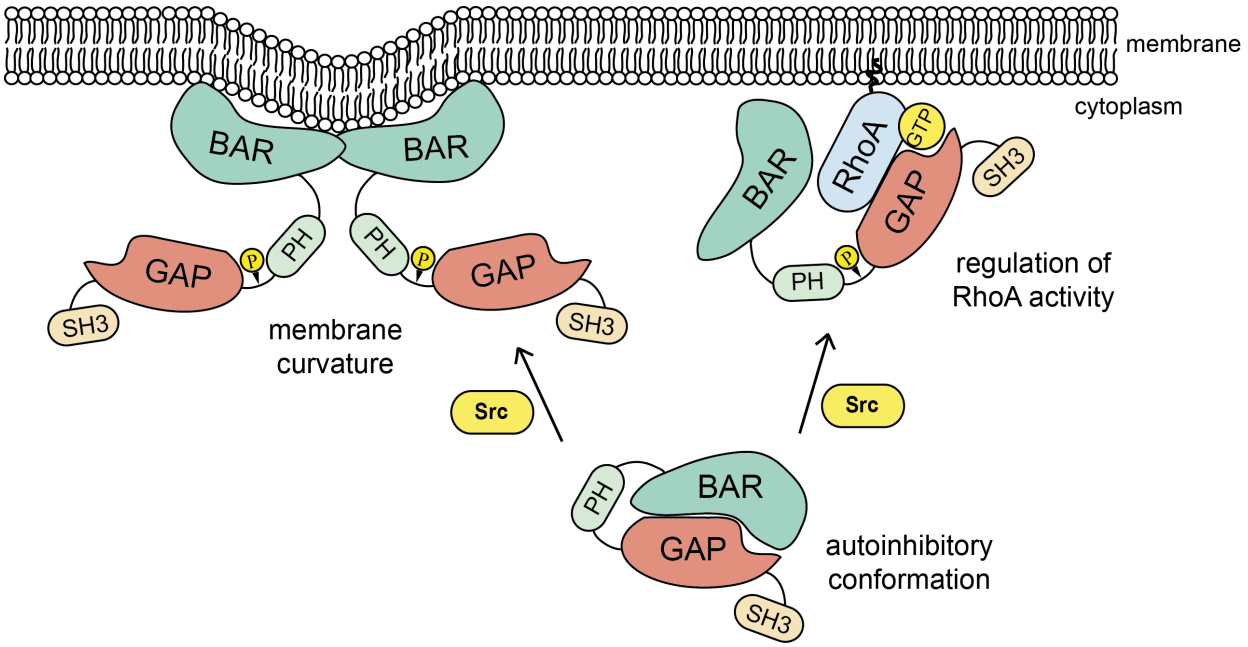

Figure 13. Model of ARHGAP42 regulation and function. In the unphosphorylated state ARHGAP42 adopts an autoinhibitory conformation which is mediated by mutual inhibition of BAR and GAP domains. While BAR domain retains a part of its function in shaping the membrane also in the autoinhibited state (not shown in the model), the function of ARHGAP42 GAP domain in regulation of RhoA activity is completely inhibited. Upon phosphorylation of Tyr376 by Src kinase the mutual inhibition is disrupted leading to both enhanced membrane-related function of the BAR domain and activation of GAP domain resulting in decrease of the levels of active RhoA.

5. Conclusions

- We have designed and created an analog-sensitive mutant of PKN3 kinase which we used to perform a phosphoproteomic screen to identify novel PKN3 substrates. We found 281 new putative PKN3 substrate proteins with 418 phosphorylation sites. By comparing our results with phosphoproteomic data by Browne et al., we suggest LRRC16A, FAM21A and ARFGEF2 as the most promising candidates for the future study of PKN3 downstream signaling.
- Among the newly identified putative PKN3 substrates we focused on ARHGAP18. We validated the results from our screen and confirmed PKN3 is able to phosphorylate ARHGAP18 on Thr154, Ser156 and Thr158 *in vitro*.
- We characterized the interaction between ARHGAP18 and PKN3 and mapped the interaction interface to the first 25 amino acids in the *N*-terminal region of ARHGAP18. This region is missing in ARHGAP18 Iso2 which does not interact with PKN3 although it is phosphorylated by PKN3 to a similar extent as ARHGAP18 Iso1.
- Substitution of Thr154, Ser156 and Thr158 for phosphomimicking aspartate leads to strengthening of the interaction between ARHGAP18 Iso1 and PKN3. Moreover, it leads to activation of ARHGAP18 GAP domain function which results in decrease of the levels of active RhoA. These results suggest that phosphorylation of ARHGAP18 by PKN3 could result in a formation of a negative feedback loop in control of the RhoA signaling.

- We characterized the localization of ARHGAP42 into stress fibers, focal adhesion complexes and podosomes. Localization of ARHGAP42 into stress fibers is SH3 domain-dependent.
- Using deletion mutants of ARHGAP42 lacking either GAP domain or BAR domain we studied the mutual autoinhibitory effect of these domains. Deletion of GAP domain resulted in an increased capacity of the BAR-PH domain module to form membrane tubulations. On the other hand, deletion of the BAR domain led to activation of ARHGAP42 GAP domain and resulted in decreased levels of active RhoA and induction of the arborized cell morphology.
- Phosphorylation of Tyr376 by Src kinase is sufficient to disrupt the autoinhibitory state of ARHGAP42 and to activate its GAP domain, similarly as in case of BAR domain deletion.
- Both deletion of BAR domain and phosphorylation of Tyr376 by Src leads to increase in focal adhesion dynamics, lamellipodial protrusion velocity and cell migration.

6. Publications and author contributions

Doctoral thesis contains the following publications:

Dibus, M., Brábek, J., & Rösel, D. (2020). A Screen for PKN3 Substrates Reveals an Activating Phosphorylation of ARHGAP18. International journal of molecular sciences, 21(20), E7769.

- all the experimental work in the paper was performed by the first author, as well as conceptualization of the project, visualization and writing of the original manuscript

Luo, W., Janoštiak, R., Tolde, O., Ryzhova, L. M., Koudelková, L., Dibus, M., Brábek, J., Hanks, S. K., & Rosel, D. (2017). ARHGAP42 is activated by Src-mediated tyrosine phosphorylation to promote cell motility. Journal of cell science, 130(14), 2382–2393.

- cloning and purification of GST-RhoA CA, RhoA activation assays, RhoGTP-ARHGAP42 binding assay

Accepted co-authored publications not included in the doctoral thesis:

Gemperle, J., Hexnerová, R., Lepšík, M., Tesina, P., Dibus, M., Novotný, M., Brábek, J., Veverka, V., & Rosel, D. (2017). Structural characterization of CAS SH3 domain selectivity and regulation reveals new CAS interaction partners. Scientific reports, 7(1), 8057.

Gemperle, J., Dibus, M., Koudelková, L., Rosel, D., & Brábek, J. (2019). The interaction of p130Cas with PKN3 promotes malignant growth. Molecular oncology, 13(2), 264–289.

Jorda, R., Magar, P., Hendrychová, D., Pauk, K., Dibus, M., Pilařová, E., Imramovský, A., & Kryštof, V. (2020). Novel modified leucine and phenylalanine dipeptides modulate viability and attachment of cancer cells. European journal of medicinal chemistry, 188, 112036.

Merta, L., Gandalovičová, A., Čermák, V., Dibus, M., Gutschner, T., Diederichs, S., Rösel, D., & Brábek, J. (2020). Increased Level of Long Non-Coding RNA MALAT1 is a Common Feature of Amoeboid Invasion. Cancers, 12(5), 1136.

Submitted manuscript not included in the doctoral thesis:

Li Q., Dibus M., Casey A., Yee Ch., Vargas S.O., Luo S., Rosen S.M., Madden J.A., Genetti C.A., Brabek J., Brownstein C.A., Kazerounian S., Raby B.A., Schmitz-Abe K., Kennedy J.C., Fishman M.P., Mullen M.P., Taylor J.M., Rosel D., Agrawal P.B. (202X). A homozygous stop-gain variant in ARHGAP42 is associated with childhood interstitial lung disease, systemic hypertension, and immunological findings. Submitted to PLOS Genetics.

……

doc. RNDr. Daniel Rösel , PhD.

Supervisor

7. References

Adam, K., and Hunter, T. (2018). Histidine kinases and the missing phosphoproteome from prokaryotes to eukaryotes. Lab. Investig. *98*, 233–247.

Aguilar-Rojas, A., Maya-Núñez, G., Huerta-Reyes, M., Pérez-Solis, M.A., Silva-García, R., Guillén, N., and Olivo-Marin, J.C. (2018). Activation of human gonadotropin-releasing hormone receptor promotes down regulation of ARHGAP18 and regulates the cell invasion of MDA-MB-231 cells. Mol. Cell. Endocrinol. *460*, 94–103.

Aleku, M., Schulz, P., Keil, O., Santel, A., Schaeper, U., Dieckhoff, B., Janke, O., Endruschat, J., Durieux, B., Röder, N., et al. (2008). Atu027, a liposomal small interfering RNA formulation targeting protein kinase N3, inhibits cancer progression. Cancer Res. *68*, 9788–9798.

Aleskandarany, M.A., Sonbul, S., Surridge, R., Mukherjee, A., Caldas, C., Diez-Rodriguez, M., Ashankyty, I., Albrahim, K.I., Elmouna, A.M., Aneja, R., et al. (2017). Rho-GTPase activating-protein 18: A biomarker associated with good prognosis in invasive breast cancer. Br. J. Cancer *117*, 1176–1184.

Allen, J.J., Li, M., Brinkworth, C.S., Paulson, J.L., Wang, D., Hübner, A., Chou, W.-H., Davis, R.J., Burlingame, A.L., Messing, R.O., et al. (2007). A semisynthetic epitope for kinase substrates. Nat. Methods *4*, 511–516.

Alonso-Rodríguez, E., Fernández-Piñar, P., Sacristán-Reviriego, A., Molina, M., and Martín, H. (2016). An analog-sensitive version of the protein kinase Slt2 allows identification of novel targets of the yeast cell wall integrity pathway. J. Biol. Chem. *291*, 5461–5472.

Amano, M., Ito, M., Kimura, K., Fukata, Y., Chihara, K., Nakano, T., Matsuura, Y., and Kaibuchi, K. (1996). Phosphorylation and activation of myosin by Rho-associated kinase (Rho- kinase). J. Biol. Chem. *271*, 20246–20249.

Amano, T., Tanabe, K., Eto, T., Narumiya, S., and Mizuno, K. (2001). LIM-kinase 2 induces formation of stress fibres, focal adhesions and membrane blebs, dependent on its activation by Rho-associated kinase-catalysed phosphorylation at threonine-505. Biochem. J. *354*, 149–159.

Amin, E., Jaiswal, M., Derewenda, U., Reis, K., Nouri, K., Koessmeier, K.T., Aspenström, P., Somlyo, A. V., Dvorsky, R., and Ahmadian, M.R. (2016). Deciphering the molecular and functional basis of RHOGAP family proteins: A systematic approach toward selective inactivation of RHO family proteins. J. Biol. Chem. *291*, 20353–20371.

Arencibia, J.M., Pastor-Flores, D., Bauer, A.F., Schulze, J.O., and Biondi, R.M. (2013). AGC protein kinases: from structural mechanism of regulation to allosteric drug development for the treatment of human diseases. Biochim. Biophys. Acta *1834*, 1302–1321.

Aspenstrom, P. (2018). BAR domain proteins regulate Rho GTPase signaling. Adv Exp Med Biol *5*.

Aspenström, P. (2020). Fast-cycling Rho GTPases. Small GTPases *11*, 248–255.

Azam, M., Seeliger, M.A., Gray, N.S., Kuriyan, J., and Daley, G.Q. (2008). Activation of tyrosine kinases by mutation of the gatekeeper threonine. Nat. Struct. Mol. Biol. *15*, 1109–1118.

Bagci, H., Sriskandarajah, N., Robert, A., Boulais, J., Elkholi, I.E., Tran, V., Lin, Z.Y., Thibault, M.P., Dubé, N., Faubert, D., et al. (2020). Mapping the proximity interaction network of the Rho-family GTPases reveals signalling pathways and regulatory mechanisms. Nat. Cell Biol. *22*, 120–134.

Bai, X., Lenhart, K.C., Bird, K.E., Suen, A.A., Rojas, M., Kakoki, M., Li, F., Smithies, O., MacK, C.P., and Taylor, J.M. (2013). The smooth muscle-selective RhoGAP GRAF3 is a critical regulator of vascular tone and hypertension. Nat. Commun. *4*, 1–8.

Bai, X., Mangum, K.D., Dee, R.A., Stouffer, G.A., Lee, C.R., Oni-Orisan, A., Patterson, C., Schisler, J.C., Viera, A.J., Taylor, J.M., et al. (2017). Blood pressure-associated polymorphism controls ARHGAP42 expression via serum response factor DNA binding. J. Clin. Invest. *127*, 670–680.

Bai, X., Mangum, K., Kakoki, M., Smithies, O., Mack, C.P., and Taylor, J.M. (2018). GRAF3 serves as a blood volume-sensitive rheostat to control smooth muscle contractility and blood pressure. Small GTPases *1248*, 1–10.

Banko, M.R., Allen, J.J., Schaffer, B.E., Wilker, E.W., Tsou, P.P., White, J.L., Villén, J., Wang, B., Kim, S.R., Sakamoto, K., et al. (2011). Chemical Genetic Screen for AMPKα2 Substrates Uncovers a Network of Proteins Involved in Mitosis. Mol. Cell *44*, 878–892.

Bartkowiak, B., Yan, C., and Greenleaf, A.L. (2015). Engineering an analog-sensitive CDK12 cell line using CRISPR/Cas. Biochim. Biophys. Acta - Gene Regul. Mech. *1849*, 1179–1187.

Bauer, A.F., Sonzogni, S., Meyer, L., Zeuzem, S., Piiper, A., Biondi, R.M., and Neimanis, S. (2012). Regulation of protein kinase C-related Protein Kinase 2 (PRK2) by an intermolecular PRK2-PRK2 interaction mediated by its N-terminal domain. J. Biol. Chem. *287*, 20590–20602.

Bernard, O. (2007). Lim kinases, regulators of actin dynamics. Int. J. Biochem. Cell Biol. *39*, 1071–1076.

Bhullar, K.S., Lagarón, N.O., McGowan, E.M., Parmar, I., Jha, A., Hubbard, B.P., and Rupasinghe, H.P.V. (2018). Kinase-targeted cancer therapies: Progress, challenges and future directions. Mol. Cancer *17*.

Bishop, A.C., Kung, C.Y., Shah, K., Witucki, L., Shokat, K.M., and Liu, Y. (1999). Generation of monospecific nanomolar tyrosine kinase inhibitors via a chemical genetic approach. J. Am. Chem. Soc. *121*, 627–631.

Bishop, A.C., Ubersax, J.A., Pøtsch, D.T., Matheos, D.P., Gray, N.S., Blethrow, J., Shimizu, E., Tsien, J.Z., Schultz, P.G., Rose, M.D., et al. (2000). A chemical switch for inhibitor-sensitive alleles of any protein kinase. Nature *407*, 395–401.

Boal, F., and Stephens, D.J. (2010). Specific functions of BIG1 and BIG2 in endomembrane organization. PLoS One *5*.

Browne, C.M., Jiang, B., Ficarro, S.B., Doctor, Z.M., Johnson, J.L., Card, J.D., Sivakumaren, S.C., Alexander, W.M., Yaron, T.M., Murphy, C.J., et al. (2019). A Chemoproteomic Strategy for Direct and Proteome-Wide Covalent Inhibitor Target-Site Identification. J. Am. Chem. Soc. *141*, 191–203.

Byrne, D.P., Clarke, C.J., Brownridge, P.J., Kalyuzhnyy, A., Perkins, S., Campbell, A., Mason, D., Jones, A.R., Eyers, P.A., and Eyers, C.E. (2020). Use of the Polo-like kinase 4 (PLK4) inhibitor centrinone to investigate intracellular signalling networks using SILAC-based phosphoproteomics. Biochem. J. *477*, 2451–2475.

Cardama, G.A., Gonzalez, N., Maggio, J., Lorenzano Menna, P., and Gomez, D.E. (2017). Rho GTPases as therapeutic targets in cancer (Review). Int. J. Oncol. *51*, 1025–1034.

Carlson, S.M., and White, F.M. (2012). Labeling and identification of direct kinase substrates. Sci. Signal. *5*, pl3.

Chang, G.H., Lay, A.J., Ting, K.K., Zhao, Y., Coleman, P.R., Powter, E.E., Formaz-Preston, A., Jolly, C.J., Bower, N.I., Hogan, B.M., et al. (2014). Arhgap18: An endogenous inhibitor of angiogenesis, limiting tip formation and stabilizing junctions. Small GTPases *5*.

Chen, X., Wei, S., Ji, Y., Guo, X., and Yang, F. (2015). Quantitative proteomics using SILAC: Principles, applications, and developments. Proteomics *15*, 3175–3192.

Cibrián Uhalte, E., Kirchner, M., Hellwig, N., Allen, J.J., Donat, S., Shokat, K.M., Selbach, M., and Abdelilah-Seyfried, S. (2012). In Vivo Conditions to Identify Prkci Phosphorylation Targets Using the Analog-Sensitive Kinase Method in Zebrafish. PLoS One *7*, e40000.

Cipak, L., Hyppa, R.W., Smith, G.R., and Gregan, J. (2012). ATP analog-sensitive Pat1 protein kinase for synchronous fission yeast meiosis at physiological temperature. Cell Cycle *11*, 1626–1633.

Cipak, L., Polakova, S., Hyppa, R.W., Smith, G.R., and Gregan, J. (2014). Synchronized fission yeast meiosis using an ATP analog-sensitive Pat1 protein kinase. Nat. Protoc. *9*, 223–231.

Coleman, P.R., Hahn, C.N., Grimshaw, M., Lu, Y., Li, X., Brautigan, P.J., Beck, K., Stocker, R., Vadas, M.A., and Gamble, J.R. (2010). Stress-induced premature senescence mediated by a novel gene, SENEX, results in an anti-inflammatory phenotype in endothelial cells. Blood *116*, 4016–4024.

Coleman, P.R., Lay, A.J., Ting, K.K., Zhao, Y., Li, J., Jarrah, S., Vadas, M.A., and Gamble, J.R. (2020). YAP and the RhoC regulator ARHGAP18, are required to mediate flow-dependent endothelial cell alignment. Cell Commun. Signal. *18*.

Collazos, A., Michael, N., Whelan, R.D.H., Kelly, G., Mellor, H., Pang, L.C.H., Totty, N., and Parker, P.J. (2011). Site recognition and substrate screens for PKN family proteins. Biochem. J. *438*, 535–543.

Coussens, L., Parker, P.J., Rhee, L., Yang-Feng, T.L., Chen, E., Waterfield, M.D., Francke, U., and Ullrich, A. (1986). Multiple, distinct forms of bovine and human protein kinase C suggest diversity in cellular signaling pathways. Science (80-.). *233*, 859–866.

Cox, J., Hein, M.Y., Luber, C.A., Paron, I., Nagaraj, N., and Mann, M. (2014). Accurate proteome-wide label-free quantification by delayed normalization and maximal peptide ratio extraction, termed MaxLFQ. Mol. Cell. Proteomics *13*, 2513–2526.

Dahmene, M., Quirion, L., and Laurin, M. (2020). High Throughput strategies Aimed at Closing the GAP in Our Knowledge of Rho GTPase Signaling. Cells *9*.

Decker, T.M., Forné, I., Straub, T., Elsaman, H., Ma, G., Shah, N., Imhof, A., and Eick, D. (2019). Analog-sensitive cell line identifies cellular substrates of CDK9. Oncotarget *10*, 6934–6943.

Derivery, E., Sousa, C., Gautier, J.J., Lombard, B., Loew, D., and Gautreau, A. (2009). The Arp2/3 Activator WASH Controls the Fission of Endosomes through a Large Multiprotein Complex. Dev. Cell *17*, 712–723.

Duarte, M.L., Pena, D.A., Ferraz, F.A.N., Berti, D.A., Sobreira, T.J.P., Costa-Junior, H.M., Baqui, M.M.A., Disatnik, M.H., Xavier-Neto, J., De Oliveira, P.S.L., et al. (2014). Protein folding creates structure-based, noncontiguous consensus phosphorylation motifs recognized by kinases. Sci. Signal. *7*, ra105–ra105.

Duong-Ly, K.C., and Peterson, J.R. (2013). The human kinome and kinase inhibition. Curr. Protoc. Pharmacol. *0 2*, Unit2.9.

Eberth, A., Lundmark, R., Gremer, L., Dvorsky, R., Koessmeier, K.T., McMahon, H.T., and Ahmadian, M.R. (2009). A BAR domain-mediated autoinhibitory mechanism for RhoGAPs of the GRAF family. Biochem. J. *417*, 371–377.

Edwards, D.C., Sanders, L.C., Bokoch, G.M., and Gill, G.N. (1999). Activation of LIM-kinase by Pak1 couples Rac/Cdc42 GTPase signalling to actin cytoskeletal dynamics. Nat. Cell Biol. *1*, 253–259.

Falk, M.D., Liu, W., Bolaños, B., Unsal-Kacmaz, K., Klippel, A., Grant, S., Brooun, A., and Timofeevski, S. (2014). Enzyme Kinetics and Distinct Modulation of the Protein Kinase N Family of Kinases by Lipid Activators and Small Molecule Inhibitors. Biosci. Rep.

Feng, J., Ito, M., Ichikawa, K., Isaka, N., Nishikawa, M., Hartshorne, D.J., and Nakano, T. (1999). Inhibitory phosphorylation site for Rho-associated kinase on smooth muscle myosin phosphatase. J. Biol. Chem. *274*, 37385–37390.

Fjorder, A.S., Rasmussen, M.B., Mehrjouy, M.M., Nazaryan-Petersen, L., Hansen, C., Bak, M., Grarup, N., Nørremølle, A., Larsen, L.A., Vestergaard, H., et al. (2019). Haploinsufficiency of ARHGAP42 is associated with hypertension. Eur. J. Hum. Genet. *27*, 1296–1303.

Floor, S.N., Barkovich, K.J., Condon, K.J., Shokat, K.M., and Doudna, J.A. (2016). Analog sensitive chemical inhibition of the DEAD-box protein DDX3. Protein Sci. *25*, 638–649.

Flynn, P., Mellor, H., Palmer, R., Panayotou, G., and Parker, J.P. (1998). Multiple Interactions of PRK1 with RhoA. FUNCTIONAL ASSIGNMENT OF THE HR1 REPEAT MOTIF. J. Biol. Chem. *273*, 2698–2705.

Flynn, P., Mellor, H., Casamassima, a, and Parker, P.J. (2000). Rho GTPase control of protein kinase C-related protein kinase activation by 3-phosphoinositide-dependent protein kinase. J. Biol. Chem. *275*, 11064–11070.

Fu, S., Fu, C., Zhou, Q., Lin, R., Ouyang, H., Wang, M., Sun, Y., Liu, Y., and Zhao, Y. (2020). Widespread arginine phosphorylation in human cells—a novel protein PTM revealed by mass spectrometry. Sci. China Chem. *63*, 341–346.

Gamblin, S.J., and Smerdon, S.J. (1998). GTPase-activating proteins and their complexes. Curr. Opin. Struct. Biol. *8*, 195–201.

Gemperle, J., Hexnerová, R., Lepšík, M., Tesina, P., Dibus, M., Novotný, M., Brábek, J., Veverka, V., and Rosel, D. (2017). Structural characterization of CAS SH3 domain selectivity and regulation reveals new CAS interaction partners. Sci. Rep. *7*, 8057.

Gemperle, J., Dibus, M., Koudelková, L., Rosel, D., and Brábek, J. (2019). The interaction of p130Cas with PKN3 promotes malignant growth. Mol. Oncol. *13*, 264–289.

Gomez, T.S., and Billadeau, D.D. (2009). A FAM21-Containing WASH Complex Regulates Retromer-Dependent Sorting. Dev. Cell *17*, 699–711.

Gorre, M.E., Mohammed, M., Ellwood, K., Hsu, N., Paquette, R., Rao, P.N., and Sawyers, C.L. (2001). Clinical Resistance to STI-571 Cancer Therapy Caused by BCR-ABL Gene Mutation or Amplification. Science (80-.). *293*, 876–880.

Gregan, J., Zhang, C., Rumpf, C., Cipak, L., Li, Z., Uluocak, P., Nasmyth, K., and Shokat, K.M. (2007). Construction of conditional analog-sensitive kinase alleles in the fission yeast schizosaccharomyces pombe. Nat. Protoc. *2*, 2996–3000.

Gressel, S., Schwalb, B., Decker, T.M., Qin, W., Leonhardt, H., Eick, D., and Cramer, P. (2017). CDK9-dependent RNA polymerase II pausing controls transcription initiation. Elife *6*.

Guarino, M. (2010). Src signaling in cancer invasion. J. Cell. Physiol. *223*, 14–26.

Hägg, S., Skogsberg, J., Lundström, J., Noori, P., Nilsson, R., Zhong, H., Maleki, S., Shang, M.M., Brinne, B.R., Bradshaw, M., et al. (2009). Multi-organ expression profiling uncovers a gene module in coronary artery disease involving transendothelial migration of leukocytes and LIM domain binding 2: The Stockholm Atherosclerosis Gene Expression (STAGE) study. PLoS Genet. *5*, e1000754.

Harashima, H., Dissmeyer, N., Hammann, P., Nomura, Y., Kramer, K., Nakagami, H., and Schnittger, A. (2016). Modulation of plant growth in vivo and identification of kinase substrates using an analog-sensitive variant of CYCLIN-DEPENDENT KINASE A;1. BMC Plant Biol. *16*.

Hashimoto, T., Mukai, H., and Kawamata, T. (1998). Localization of PKN mRNA in the rat brain. Mol. Brain Res.

Hertz, N.T., Wang, B.T., Allen, J.J., Zhang, C., Dar, A.C., Burlingame, A.L., and Shokat, K.M. (2010). Chemical Genetic Approach for Kinase-Substrate Mapping by Covalent Capture of Thiophosphopeptides and Analysis by Mass Spectrometry. Curr Protoc Chem Biol *2*, 15–36.

Hertz, N.T., Berthet, A., Sos, M.L., Thorn, K.S., Burlingame, A.L., Nakamura, K., and Shokat, K.M. (2013). A neo-substrate that amplifies catalytic activity of parkinson's-disease- related kinase PINK1. Cell *154*, 737–747.

Hiles, I.D., Otsu, M., Volinia, S., Fry, M.J., Gout, I., Dhand, R., Panayotou, G., Ruiz-Larrea, F., Thompson, A., Totty, N.F., et al. (1992). Phosphatidylinositol 3-Kinase: Structure and Expression of the 110 kd Catalytic Subunit.

Hodge, R.G., and Ridley, A.J. (2016). Regulating Rho GTPases and their regulators. Nat. Rev. Mol. Cell Biol. *17*, 496–510.

Holst, M.R., Vidal-Quadras, M., Larsson, E., Song, J., Hubert, M., Blomberg, J., Lundborg, M., Landström, M., and Lundmark, R. (2017). Clathrin-Independent Endocytosis Suppresses Cancer Cell Blebbing and Invasion. Cell Rep. *20*, 1893–1905.

Hu, Q., Lin, X., Ding, L., Zeng, Y., Pang, D., Ouyang, N., Xiang, Y., and Yao, H. (2018). ARHGAP42 promotes cell migration and invasion involving PI3K/Akt signaling pathway in nasopharyngeal carcinoma. Cancer Med. *7*, 3862–3874.

Humphries, B., Wang, Z., Li, Y., Jhan, J.R., Jiang, Y., and Yang, C. (2017). ARHGAP18 downregulation by miR-200b suppresses metastasis of triple-negative breast cancer by enhancing activation of RhoA. Cancer Res. *77*, 4051–4064.

Hunter, T. (2009). Tyrosine phosphorylation: thirty years and counting. Curr. Opin. Cell Biol. *21*, 140–146.

Hunter, T., and Sefton, B.M. (1980). Transforming gene product of Rous sarcoma virus phosphorylates tyrosine. Proc. Natl. Acad. Sci. U. S. A. *77*, 1311–1315.

Hutchinson, C.L., Lowe, P.N., McLaughlin, S.H., Mott, H.R., and Owen, D. (2011). Mutational analysis reveals a single binding interface between RhoA and its effector, PRK1. Biochemistry *50*, 2860–2869.

Hutchinson, C.L., Lowe, P.N., McLaughlin, S.H., Mott, H.R., and Owen, D. (2013). Differential binding of RhoA, RhoB, and RhoC to protein kinase C-related kinase (PRK) isoforms PRK1, PRK2, and PRK3: PRKs have the highest affinity for RhoB. Biochemistry *52*, 7999–8011.

Jiang, K., Liu, P., Xu, H., Liang, D., Fang, K., Du, S., Cheng, W., Ye, L., Liu, T., Zhang, X., et al. (2020). SASH1 suppresses triple-negative breast cancer cell invasion through YAP-ARHGAP42-actin axis. Oncogene *39*, 5015–5030.

Jiang, W., Betson, M., Mulloy, R., Foster, R., Lévay, M., Ligeti, E., and Settleman, J. (2008). P190A RhoGAP is a glycogen synthase kinase-3-β substrate required for polarized cell migration. J. Biol. Chem. *283*, 20978–20988.

Jurcik, J., Sivakova, B., Cipakova, I., Selicky, T., Stupenova, E., Jurcik, M., Osadska, M., Barath, P., and Cipak, L. (2020). Phosphoproteomics Meets Chemical Genetics: Approaches for Global Mapping and Deciphering the Phosphoproteome. Int. J. Mol. Sci. *21*, 7637.

Kasahara, K., Nakayama, Y., Sato, I., Ikeda, K., Hoshino, M., Endo, T., and Yamaguchi, N. (2007). Role of Src-family kinases in formation and trafficking of macropinosomes. J. Cell. Physiol. *211*, 220–232.

Ke, M., Chu, B., Lin, L., and Tian, R. (2017). SH2 domains as affinity reagents for phosphotyrosine protein enrichment and proteomic analysis. In Methods in Molecular Biology, (Humana Press Inc.), pp. 395–406.

Kimura, K., Ito, M., Amano, M., Chihara, K., Fukata, Y., Nakafuku, M., Yamamori, B., Feng, J., Nakano, T., Okawa, K., et al. (1996). Regulation of myosin phosphatase by Rho and Rho-associated kinase (Rho- kinase). Science (80-.). *273*, 245–248.

Knopf, J.L., Lee, M.H., Sultzman, L.A., Kriz, R.W., Loomis, C.R., Hewick, R.M., and Bell, R.M. (1986). Cloning and expression of multiple protein kinase C cDNAs. Cell *46*, 491–502.

Kretsinger, R.H., Uversky, V.N., and Permyakov, E.A. (2013). Encyclopedia of Metalloproteins (Springer New York).

Kühn, S., and Geyer, M. (2014). Formins as effector proteins of rho GTPases. Small GTPases *5*, 1–16.

Lachmann, S., Jevons, A., De Rycker, M., Casamassima, A., Radtke, S., Collazos, A., and Parker, P.J. (2011). Regulatory domain selectivity in the cell-type specific PKN-dependence of cell migration. PLoS One *6*, e21732.

Lammers, M., Meyer, S., Kühlmann, D., and Wittinghofer, A. (2008). Specificity of interactions between mDia isoforms and Rho proteins. J. Biol. Chem. *283*, 35236–35246.

Lauffenburger, D.A., and Horwitz, A.F. (1996). Cell migration: A physically integrated molecular process. Cell *84*, 359–369.

Lay, A.J., Coleman, P.R., Formaz-Preston, A., Ka Ting, K., Roediger, B., Weninger, W., Schwartz, M.A., Vadas, M.A., and Gamble, J.R. (2019). ARHGAP18: A flow-responsive gene that regulates endothelial cell alignment and protects against atherosclerosis. J. Am. Heart Assoc. *8*.

Lazarini, M., Traina, F., Machado-Neto, J.A., Barcellos, K.S.A., Moreira, Y.B., Brandão, M.M., Verjovski-Almeida, S., Ridley, A.J., and Saad, S.T.O. (2013). ARHGAP21 is a RhoGAP for RhoA and RhoC with a role in proliferation and migration of prostate adenocarcinoma cells. Biochim. Biophys. Acta - Mol. Basis Dis. *1832*, 365–374.

Leenders, F., Möpert, K., Schmiedeknecht, A., Santel, A., Czauderna, F., Aleku, M., Penschuck, S., Dames, S., Sternberger, M., Röhl, T., et al. (2004). PKN3 is required for malignant prostate cell growth downstream of activated PI 3-kinase. EMBO J. *23*, 3303–3313.

Leitner, A. (2016). Enrichment strategies in phosphoproteomics. In Methods in Molecular Biology, (Humana Press Inc.), pp. 105–121.

Li, X., Tao, Y., Wang, X., Wang, T., and Liu, J. (2020). Advanced glycosylation end products (AGEs) controls proliferation, invasion and permeability through orchestrating ARHGAP18/RhoA pathway in human umbilical vein endothelial cells. Glycoconj. J. *37*, 209–219.

Li, Y., Ji, S., Fu, L., Jiang, T., Wu, D., and Meng, F. (2018). Over-expression of ARHGAP18 suppressed cell proliferation, migration, invasion, and tumor growth in gastric cancer by restraining over-activation of MAPK signaling pathways. Onco. Targets. Ther. *11*, 279–290.

Liang, Y., Niederstrasser, H., Edwards, M., Jackson, C.E., and Cooper, J.A. (2009). Distinct roles for CARMIL isoforms in cell migration. Mol. Biol. Cell *20*, 5290–5305.

Lim, W.A., and Pawson, T. (2010). Phosphotyrosine Signaling: Evolving a New Cellular Communication System. Cell *142*, 661–667.

Liu, Y., Shah, K., Yang, F., Witucki, L., and Shokat, K.M. (1998). A molecular gate which controls unnatural ATP analogue recognition by the tyrosine kinase v-Src. Bioorganic Med. Chem. *6*, 1219–1226.

Liu, Y., Bishop, A., Witucki, L., Kraybill, B., Shimizu, E., Tsien, J., Ubersax, J., Blethrow, J., Morgan, D.O., and Shokat, K.M. (1999). Structural basis for selective inhibition of Src family kinases by PP1. Chem. Biol. *6*, 671–678.

Lovelace, M.D., Powter, E.E., Coleman, P.R., Zhao, Y., Parker, A., Chang, G.H., Lay, A.J., Hunter, J., McGrath, A.P., Jormakka, M., et al. (2017). The RhoGAP protein ARHGAP18/SENEX localizes to microtubules and regulates their stability in endothelial cells. Mol. Biol. Cell *28*, 1066–1078.

Lundmark, R., Doherty, G.J., Howes, M.T., Cortese, K., Vallis, Y., Parton, R.G., and McMahon, H.T. (2008). The GTPase-Activating Protein GRAF1 Regulates the CLIC/GEEC Endocytic Pathway. Curr. Biol. *18*, 1802–1808.

Luo, W., Slebos, R.J., Hill, S., Li, M., Brábek, J., Amanchy, R., Chaerkady, R., Pandey, A., Ham, A.J.L., and Hanks, S.K. (2008). Global impact of oncogenic src on a phosphotyrosine proteome. J. Proteome Res. *7*, 3447–3460.

Lusis, A.J. (2000). Atherosclerosis. Nature *407*, 233–241.

Maas, N.L., Singh, N., and Diehl, J.A. (2014). Generation and characterization of an analog-sensitive PERK allele. Cancer Biol. Ther. *15*, 1106–1111.

Maeda, M., Hasegawa, H., Hyodo, T., Ito, S., Asano, E., Yuang, H., Funasaka, K., Shimokata, K., Hasegawa, Y., Hamaguchi, M., et al. (2011). ARHGAP18, a GTPase-activating protein for RhoA, controls cell shape, spreading, and motility. Mol. Biol. Cell *22*, 3840–3852.

Maesaki, R., Ihara, K., Shimizu, T., Kuroda, S., Kaibuchi, K., and Hakoshima, T. (1999a). The structural basis of Rho effector recognition revealed by the crystal structure of human RhoA complexed with the effector domain of PKN/PRK1. Mol. Cell *4*, 793–803.

Maesaki, R., Shimizu, T., Ihara, K., Kuroda, S., Kaibuchi, K., and Hakoshima, T. (1999b). Biochemical and crystallographic characterization of a Rho effector domain of the protein serine/threonine kinase N in a complex with RhoA. J. Struct. Biol. *126*, 166–170.

Manning, G., Whyte, D.B., Martinez, R., Hunter, T., and Sudarsanam, S. (2002). The protein kinase complement of the human genome. Science (80-.). *298*, 1912–1934.

Mason, F.M., Heimsath, E.G., Higgs, H.N., and Soderling, S.H. (2011). Bi-modal regulation of a formin by srGAP2. J. Biol. Chem. *286*, 6577–6586.

Mellor, H., Flynn, P., Nobes, C.D., Hall, A., and Parker, P.J. (1998). PRK1 is targeted to endosomes by the small GTPase, RhoB. J. Biol. Chem. *273*, 4811–4814.

Mertins, P., Eberl, H.C., Renkawitz, J., Olsen, J. V., Tremblay, M.L., Mann, M., Ullricht, A., and Daubt, H. (2008). Investigation of protein-tyrosine phosphatase 1B function by quantitative proteomics. Mol. Cell. Proteomics *7*, 1763–1777.

Michowski, W., Chick, J.M., Chu, C., Kolodziejczyk, A., Wang, Y., Suski, J.M., Abraham, B., Anders, L., Day, D., Dunkl, L.M., et al. (2020). Cdk1 Controls Global Epigenetic Landscape in Embryonic Stem Cells. Mol. Cell *78*, 459-476.e13.

Miki, H., Suetsugu, S., and Takenawa, T. (1998). WAVE, a novel WASP-family protein involved in actin reorganization induced by Rac. EMBO J. *17*, 6932–6941.

Miller, C.J., and Turk, B.E. (2018). Homing in: Mechanisms of Substrate Targeting by Protein Kinases. Trends Biochem. Sci. *43*, 380–394.

Minoshima, Y., Kawashima, T., Hirose, K., Tonozuka, Y., Kawajiri, A., Bao, Y.C., Deng, X., Tatsuka, M., Narumiya, S., May, W.S., et al. (2003). Phosphorylation by Aurora B converts MgcRacGAP to a RhoGAP during cytokinesis. Dev. Cell *4*, 549–560.

Modha, R., Campbell, L.J., Nietlispach, D., Buhecha, H.R., Owen, D., and Mott, H.R. (2008). The Rac1 polybasic region is required for interaction with its effector PRK1. J. Biol. Chem. *283*, 1492–1500.

Möpert, K., Löffler, K., Röder, N., Kaufmann, J., and Santel, A. (2012). Depletion of protein kinase N3 (PKN3) impairs actin and adherens junctions dynamics and attenuates endothelial cell activation. Eur. J. Cell Biol. *91*, 694–705.

Mora, A., Komander, D., van Aalten, D.M.F., and Alessi, D.R. (2004). PDK1, the master regulator of AGC kinase signal transduction. Semin. Cell Dev. Biol. *15*, 161–170.

Mori, K., Amano, M., Takefuji, M., Kato, K., Morita, Y., Nishioka, T., Matsuura, Y., Murohara, T., and Kaibuchi, K. (2009). Rho-kinase contributes to sustained RhoA activation through phosphorylation of p190A RhoGAP. J. Biol. Chem. *284*, 5067–5076.

Mukai, H., and Ono, Y. (1994). A novel protein kinase with leucine zipper-like sequences: its catalytic domain is highly homologous to that of protein kinase C. Biochem. Biophys. Res. Commun.

Mukai, H., Muramatsu, A., Mashud, R., Kubouchi, K., Tsujimoto, S., Hongu, T., Kanaho, Y., Tsubaki, M., Nishida, S., Shioi, G., et al. (2016). PKN3 is the major regulator of angiogenesis and tumor metastasis in mice. Sci. Rep. *6*, 18979.

Müller, A.C., Giambruno, R., Weißer, J., Májek, P., Hofer, A., Bigenzahn, J.W., Superti-Furga, G., Jessen, H.J., and Bennett, K.L. (2016). Identifying Kinase Substrates via a Heavy ATP Kinase Assay and Quantitative Mass Spectrometry. Sci. Rep. *6*, 1–10.

Nalefski, E.A., and Falke, J.J. (1996). The C2 domain calcium-binding motif: structural and functional diversity. Protein Sci. *5*, 2375–2390.

Needham, E.J., Parker, B.L., Burykin, T., James, D.E., and Humphrey, S.J. (2019). Illuminating the dark phosphoproteome. Sci. Signal. *12*, 8645.

Neilson, K.A., Ali, N.A., Muralidharan, S., Mirzaei, M., Mariani, M., Assadourian, G., Lee, A., Van Sluyter, S.C., and Haynes, P.A. (2011). Less label, more free: Approaches in label-free quantitative mass spectrometry. Proteomics *11*, 535–553.

Nishioka, T., Nakayama, M., Amano, M., and Kaibuchi, K. (2012). Proteomic screening for Rho-kinase substrates by combining kinase and phosphatase inhibitors with 14-3-3ζ affinity chromatography. Cell Struct. Funct. *37*, 39–48.

Nishizuka, Y. (1988). The molecular heterogeneity of protein kinase C and its implications for cellular regulation. Nature *334*, 661–665.

Nobes, C.D., and Hall, A. (1995). Rho, Rac, and Cdc42 GTPases regulate the assembly of multimolecular focal complexes associated with actin stress fibers, lamellipodia, and filopodia. Cell *81*, 53–62.

Oishi, K., Mukai, H., Shibata, H., Takahashi, M., and Ona, Y. (1999). Identification and characterization of PKNβ, a novel isoform of protein kinase PKN: expression and arachidonic acid dependency are different from those of PKNα. Biochem. Biophys. Res. *814*, 808–814.

Owen, D., Lowe, P.N., Nietlispach, D., Brosnan, C.E., Chirgadze, D.Y., Parker, P.J., Blundell, T.L., and Mott, H.R. (2003). Molecular dissection of the interaction between the small G proteins Rac1 and RhoA and protein kinase C-related kinase 1 (PRK1). J. Biol. Chem. *278*, 50578–50587.

Parri, M., and Chiarugi, P. (2010). Rac and Rho GTPases in cancer cell motility control. Cell Commun. Signal. *8*, 23.

Pearce, L.R., Komander, D., and Alessi, D.R. (2010). The nuts and bolts of AGC protein kinases. Nat. Rev. Mol. Cell Biol. *11*, 9–22.

Perin, M.S., Fried, V.A., Mignery, G.A., Jahn, R., and Südhof, T.C. (1990). Phospholipid binding by a synaptic vesicle protein homologous to the regulatory region of protein kinase C. Nature *345*, 260–263.

Peter, B.J., Kent, H.M., Mills, I.G., Vallis, Y., Butler, P.J.G., Evans, P.R., and McMahon, H.T. (2004). BAR Domains as Sensors of Membrane Curvature: The Amphiphysin BAR Structure. Science (80-.). *303*, 495–499.

Polat, A.N., Karayel, Ö., Giese, S.H., Harmanda, B., Sanal, E., Hu, C.K., Renard, B.Y., and Özlü, N. (2015). Phosphoproteomic analysis of aurora kinase inhibition in monopolar cytokinesis. J. Proteome Res. *14*, 4087–4098.

Porazinski, S., Wang, H., Asaoka, Y., Behrndt, M., Miyamoto, T., Morita, H., Hata, S., Sasaki, T., Krens, S.F.G., Osada, Y., et al. (2015). YAP is essential for tissue tension to ensure vertebrate 3D body shape. Nature *521*, 217–221.

Quilliam, A.L., Lambert, Q.T., Mickelson-Young, L.A., Westwick, J.K., Sparks, A.B., Kay, B.K., Jenkins, N.A., Gilbert, D.J., Copeland, N.G., and Der, C.J. (1996). Isolation of a NCK-associated Kinase, PRK2, an SH3-binding Protein and Potential Effector of Rho Protein Signaling. J. Biol. Chem. *271*, 28772–28776.

Ren, X.R., Du, Q.S., Huang, Y.Z., Ao, S.Z., Mei, L., and Xiong, W.C. (2001). Regulation of CDC42 GTPase by proline-rich tyrosine kinase 2 interacting with PSGAP, a novel pleckstrin homology and Src homology 3 domain containing rhoGAP protein. J. Cell Biol. *152*, 971–983.

Rhee, S.G., Suh, P.G., Ryu, S.H., and Lee, S.Y. (1989). Studies of inositol phospholipid - Specific phospholipase C. Science (80-.). *244*, 546–550.

Rikova, K., Guo, A., Zeng, Q., Possemato, A., Yu, J., Haack, H., Nardone, J., Lee, K., Reeves, C., Li, Y., et al. (2007). Global Survey of Phosphotyrosine Signaling Identifies Oncogenic Kinases in Lung Cancer. Cell *131*, 1190–1203.

Rimel, J.K., Poss, Z.C., Erickson, B., Maas, Z.L., Ebmeier, C.C., Johnson, J.L., Decker, T.M., Yaron, T.M., Bradley, M.J., Hamman, K.B., et al. (2020). Selective inhibition of CDK7 reveals high-confidence targets and new models for TFIIH function in transcription. Genes Dev. *34*, 1452–1473.

Rittinger, K., Walker, P.A., Eccleston, J.F., Nurmahomed, K., Owen, D., Laue, E., Gamblin, S.J., and Smerdon, S.J. (1997). Crystal structure of a small G protein in complex with the GTPase- activating protein rhoGAP. Nature *388*, 693–697.

Rizo, J., and Sudhof, T.C. (1998). C2-domains, structure and function of a universal Ca2+-binding domain. J. Biol. Chem. *273*, 15879–15882.

Ross, P.L., Huang, Y.N., Marchese, J.N., Williamson, B., Parker, K., Hattan, S., Khainovski, N., Pillai, S., Dey, S., Daniels, S., et al. (2004). Multiplexed protein quantitation in Saccharomyces cerevisiae using amine-reactive isobaric tagging reagents. Mol. Cell. Proteomics *3*, 1154–1169.

Salzer, U., Kostan, J., and Djinović-Carugo, K. (2017). Deciphering the BAR code of membrane modulators. Cell. Mol. Life Sci. *74*, 2413–2438.

Schaefer, A., Reinhard, N.R., and Hordijk, P.L. (2014). Toward understanding RhoGTPase specificity: Structure, function and local activation. Small GTPases *5*, 1–11.

Scheffzek, K., Ahmadian, M.R., and Wittinghofer, A. (1998). GTPase-activating proteins: Helping hands to complement an active site. Trends Biochem. Sci. *23*, 257–262.

Scholz, R.P., Regner, J., Theil, A., Erlmann, P., Holeiter, G., Jähne, R., Schmid, S., Hausser, A., and Olayioye, M.A. (2009). DLC1 interacts with 14-3-3 proteins to inhibit RhoGAP activity and block nucleocytoplasmic shuttling. J. Cell Sci. *122*, 92–102.

Schultheis, B., Strumberg, D., Santel, A., Vank, C., Gebhardt, F., Keil, O., Lange, C., Giese, K., Kaufmann, J., Khan, M., et al. (2014). First-in-human phase I study of the liposomal RNA interference therapeutic Atu027 in patients with advanced solid tumors. J. Clin. Oncol. *32*, 4141–4148.

Schultheis, B., Strumberg, D., Kuhlmann, J., Wolf, M., Link, K., Seufferlein, T., Kaufmann, J., Feist, M., Gebhardt, F., Khan, M., et al. (2020). Safety, Efficacy and Pharcacokinetics of Targeted Therapy with The Liposomal RNA Interference Therapeutic Atu027 Combined with Gemcitabine in Patients with Pancreatic Adenocarcinoma. A Randomized Phase Ib/IIa Study. Cancers (Basel). *12*, 3130.

Shah, K., and Shokat, K.M. (2002). A chemical genetic screen for direct v-Src substrates reveals ordered assembly of a retrograde signaling pathway. Chem. Biol. *9*, 35–47.

Sharma, K., D'Souza, R.C.J., Tyanova, S., Schaab, C., Wiśniewski, J.R., Cox, J., and Mann, M. (2014). Ultradeep Human Phosphoproteome Reveals a Distinct Regulatory Nature of Tyr and Ser/Thr-Based Signaling. Cell Rep. *8*, 1583–1594.

Shibata, H., Mukai, H., Inagaki, Y., Homma, Y., Kimura, K., Kaibuchi, K., Narumiya, S., and Ono, Y. (1996). Characterization of the interaction between RhoA and the amino-terminal region of PKN. FEBS Lett. *385*, 221–224.

Shibata, H., Oishi, K., Yamagiwa, A., Matsumoto, M., Mukai, H., and Ono, Y. (2001). PKNbeta interacts with the SH3 Domains of Graf and a Novel Graf Related Protein , Graf 2 , Which Are GTPase Activating Proteins for Rho. J. Biochem. *31*, 23–31.

Shinotsuka, C., Waguri, S., Wakasugi, M., Uchiyama, Y., and Nakayama, K. (2002). Dominant-negative mutant of BIG2 an ARF-guanine nucleotide exchange factor specifically affects membrane trafficking from the trans-Golgi network through inhibiting membrane association of AP-1 and GGA coat proteins. Biochem. Biophys. Res. Commun. *294*, 254–260.

Shirataki, H., Kaibuchi, K., Sakoda, T., Kishida, S., Yamaguchi, T., Wada, K., Miyazaki, M., and Takai, Y. (1993). Rabphilin-3A, a putative target protein for smg p25A/rab3A p25 small GTP-binding protein related to synaptotagmin. Mol. Cell. Biol. *13*, 2061–2068.

Tcherkezian, J., and Lamarche-Vane, N. (2007). Current knowledge of the large RhoGAP family of proteins. Biol. Cell *99*, 67–86.

Thompson, A., Schäfer, J., Kuhn, K., Kienle, S., Schwarz, J., Schmidt, G., Neumann, T., and Hamon, C. (2003). Tandem mass tags: A novel quantification strategy for comparative analysis of complex protein mixtures by MS/MS. Anal. Chem. *75*, 1895–1904.

Uehara, S., Udagawa, N., Mukai, H., Ishihara, A., Maeda, K., Yamashita, T., Murakami, K., Nishita, M., Nakamura, T., Kato, S., et al. (2017). Protein kinase N3 promotes bone resorption by osteoclasts in response to Wnt5a-Ror2 signaling. Sci. Signal. *10*, 1–12.

Uehara, S., Udagawa, N., and Kobayashi, Y. (2019). Regulation of osteoclast function via Rho-Pkn3-c-Src pathways. J. Oral Biosci. *61*, 135–140.

Unsal-Kacmaz, K., Ragunathan, S., Rosfjord, E., Dann, S., Upeslacis, E., Grillo, M., Hernandez, R., Mack, F., and Klippel, A. (2012). The interaction of PKN3 with RhoC promotes malignant growth. Mol. Oncol. *6*, 284–298.

Vautrin-Glabik, A., Botia, B., Kischel, P., Ouadid-Ahidouch, H., and Rodat-Despoix, L. (2018). IP3R3 silencing induced actin cytoskeletal reorganization through ARHGAP18/RhoA/mDia1/FAK pathway in breast cancer cell lines. Biochim. Biophys. Acta - Mol. Cell Res. *1865*, 945–958.

Watanabe, N., Madaule, P., Reid, T., Ishizaki, T., Watanabe, G., Kakizuka, A., Saito, Y., Nakao, K., Jockusch, B.M., and Narumiya, S. (1997). p140mDia, a mammalian homolog of Drosophila diaphanous, is a target protein for Rho small GTPase and is a ligand for profilin. EMBO J. *16*, 3044–3056.

Watanabe, N., Kato, T., Fujita, A., Ishizaki, T., and Narumiya, S. (1999). Cooperation between mDia1 and ROCK in Rho-induced actin reorganization. Nat. Cell Biol. *1*, 136–143.

Wei, L., Surma, M., Shi, S., Lambert-Cheatham, N., and Shi, J. (2016). Novel Insights into the Roles of Rho Kinase in Cancer. Arch. Immunol. Ther. Exp. (Warsz). *64*, 259–278.

Wong, S., McLaughlin, J., Cheng, D., Zhang, C., Shokat, K.M., and Witte, O.N. (2004). Sole BCR-ABL inhibition is insufficient to eliminate all myeloproliferative disorder cell populations. Proc. Natl. Acad. Sci. U. S. A. *101*, 17456–17461.

Yang, C., Pring, M., Wear, M.A., Huang, M., Cooper, J.A., Svitkina, T.M., and Zigmond, S.H. (2005). Mammalian CARMIL inhibits actin filament capping by capping protein. Dev. Cell *9*, 209–221.

Yu, L., Thakur, S., Leong-Quong, R.Y., Suzuki, K., Pang, A., Bjorge, J.D., Riabowol, K., and Fujita, D.J. (2013). Src Regulates the Activity of the ING1 Tumor Suppressor. PLoS One *8*, e60943.

Zhang, C., Kenski, D.M., Paulson, J.L., Bonshtien, A., Sessa, G., Cross, J. V., Templeton, D.J., and Shokat, K.M. (2005). A second-site suppressor strategy for chemical genetic analysis of diverse protein kinases. Nat. Methods *2*, 435–441.

Zhang, C.J., Zhu, N., Liu, Z., Shi, Z., Long, J., Zu, X.Y., Tang, Z.W., Hu, Z.Y., Liao, D.F., and Qin, L. (2020). Wnt5a/Ror2 pathway contributes to the regulation of cholesterol homeostasis and inflammatory response in atherosclerosis. Biochim. Biophys. Acta - Mol. Cell Biol. Lipids *1865*, 158547.

Zhu, G., Chen, J., Liu, J., Brunzelle, J.S., Huang, B., Wakeham, N., Terzyan, S., Li, X., Rao, Z., Li, G., et al. (2007). Structure of the APPL1 BAR-PH domain and characterization of its interaction with Rab5. EMBO J. *26*, 3484–3493.

Zong, H., Raman, N., Mickelson-Young, L.A., Atkinson, S.J., and Quilliam, L.A. (1999). Loop 6 of RhoA confers specificity for effector binding, stress fiber formation, and cellular transformation. J. Biol. Chem. *274*, 4551–4560.